

# **For Reference**

---

**NOT TO BE TAKEN FROM THIS ROOM**

Ex LIBRIS  
UNIVERSITATIS  
ALBERTAEENSIS













THE UNIVERSITY OF ALBERTA

BOUNDARY SHEAR STRESS DISTRIBUTION  
IN OPEN CHANNEL FLOW

by



Albert Bill Hollingshead


A THESIS

SUBMITTED TO THE FACULTY OF GRADUATE STUDIES AND RESEARCH  
IN PARTIAL FULFILMENT OF THE REQUIREMENTS FOR THE DEGREE  
OF DOCTOR OF PHILOSOPHY

DEPARTMENT OF CIVIL ENGINEERING

EDMONTON, ALBERTA

SPRING, 1972



Digitized by the Internet Archive  
in 2019 with funding from  
University of Alberta Libraries

<https://archive.org/details/Hollingshead1972>

Thesis  
1972  
321

UNIVERSITY OF ALBERTA  
FACULTY OF GRADUATE STUDIES AND RESEARCH

The undersigned certify that they have read, and recommend to the Faculty of Graduate Studies and Research, for acceptance, a thesis entitled "BOUNDARY SHEAR STRESS DISTRIBUTION IN OPEN CHANNEL FLOW" submitted by Albert Bill Hollingshead in partial fulfilment of the requirements for the degree of Doctor of Philosophy.



## ABSTRACT

The requirements for detailed knowledge of the distribution of boundary shear stress are apparent in a number of problems encountered with flow in open channels.

The objectives of the present study were to find a suitable method for measuring boundary shear stress in open channels including boundaries with large roughness, to determine shear stress distributions for various channel shapes and flow conditions, and to explore the possibility of a general solution to the distribution of boundary shear stress.

A shear meter was constructed to measure the boundary shear stress directly. The use of the logarithmic velocity equation and measured velocities to determine local boundary shear stress was investigated. The Preston technique utilizing a total head tube in contact with the boundary was extended for use on rough boundaries, and tube calibrations were performed.

The Preston technique was found to be a suitable method for measuring boundary shear stress distributions in open channel flow including boundaries with large uniform roughness. An analytical method for estimating the ratio of tube pressure to local shear stress was established by using the logarithmic velocity equation and Nikuradse's constants. Shear stress distributions were measured for a large range of flow conditions and roughnesses in both rectangular and trapezoidal





channels. A series of diagrams presents the relationships between boundary shear stress, channel aspect ratio, and relative roughness. These diagrams can be used to estimate the local shear stress on the boundary for a large range of flow conditions and roughnesses for the selected channel shapes.

It is shown that the logarithmic velocity equation with Nikuradse's constants can be used for normals to both the bed and walls in rectangular and trapezoidal channels providing it is limited to the appropriate region of flow. For channels with equal bed and wall roughness the corner angle bisector is suitable for separation of these regions.



## ACKNOWLEDGEMENTS

This study was initiated while the author was employed by the Highway and River Engineering Division, Research Council of Alberta. Research Council of Alberta employees, Mr. Grant Gehmlich and Mr. Vinod Arora carried out some of the early measurements and assisted with data conversion and computing respectively. This assistance is gratefully acknowledged.

All of the staff of the Hydraulics Laboratory, Department of Civil Engineering were most cooperative throughout the course of the study. Mr. Ladislav Ferenczi assisted with the measurements and Mr. Roy Gitzel designed several of the electrical components and maintained the data acquisition system. Mr. Arthur Charbonneau provided technical assistance and reviewed portions of the manuscript.

Dr. Thomas Blench and Professor John Nuttall provided assistance throughout the study. Thesis supervisor, Dr. N. Rajaratnam provided the initial interest in this topic through his excellent lecture series. The author wishes to thank Dr. N. Rajaratnam for guidance during the course of the experimental work and suggestions during review of the manuscript.

Support from the Department of Energy, Mines and Resources through a grant to Dr. N. Rajaratnam is acknowledged.

Finally, the author wishes to thank the estate of Izaak Walton Killam for financial support throughout the period of study.



## TABLE OF CONTENTS

	Page
TITLE PAGE .....	i
ABSTRACT .....	iii
ACKNOWLEDGEMENTS .....	v
TABLE OF CONTENTS .....	vi
LIST OF TABLES .....	x
LIST OF FIGURES .....	xii
 CHAPTER I. INTRODUCTION .....	 1
1.1. General .....	1
1.2. Objectives .....	4
 CHAPTER II. METHODS OF DETERMINING SHEAR STRESS .....	 5
2.1. General .....	5
2.2. Momentum Techniques .....	5
2.3. Reynolds Stresses .....	6
2.4. Velocity Profile Method .....	8
2.5. Preston Tube Technique .....	13
2.6. Shear Meter Method .....	19
2.7. Laminar Flow Solution for Boundary Shear Stress .....	20
2.8. Membrane Analogy for Boundary Shear Stress ....	21
2.9. Summary .....	22



## TABLE OF CONTENTS

CHAPTER IV - (Cont'd.)	Page
4.10. Data Acquisition System .....	50
4.11. Test Method .....	51
CHAPTER V. EXPERIMENTAL RESULTS .....	53
5.1. Data Handling .....	53
5.2. Preliminary Data Processing .....	53
5.3. Primary Analysis .....	55
5.4. Estimates of Experimental Errors .....	56
5.5. Presentation of Results .....	57
5.5.1. Velocity Distribution .....	58
5.5.2. Non-Dimensional Velocity Profiles .....	60
5.5.3. Boundary Shear Stress Distribution .....	64
CHAPTER VI. ANALYSIS .....	69
6.1. Rough Boundary Datum .....	69
6.2. Pitot Tube Displacement at the Boundary .....	71
6.3. The Effect of Tube Position with Respect to the Roughness Elements on Measured Pressures .....	73
6.4. Equivalent Roughness and Limits for the Logarithmic Velocity Equations .....	74
6.5. Channel Resistance .....	81
6.6. Three Dimensional Velocity Distributions .....	83
6.7. Preston Tube Calibration .....	89
6.8. Comparison of Methods of Measuring Boundary Shear Stress at the Channel Centerline .....	98
6.9. Comparisons of Average Boundary Shear Stress ...	100





## TABLE OF CONTENTS

CHAPTER VI - (Cont'd.)	Page
6.10. Distribution of Boundary Shear Stress .....	105
6.11. Maximum Boundary Shear Stress .....	108
6.12. Discussion of Results .....	113
CHAPTER VII. CONCLUSIONS AND RECOMMENDATIONS .....	117
7.1. Summary .....	117
7.2. Conclusions .....	117
7.3. Recommendations .....	120
LIST OF REFERENCES .....	122
APPENDIX A. NOTATION	
APPENDIX B. SAMPLE CALCULATIONS	
APPENDIX C. EXPERIMENTAL DATA	
APPENDIX D. VELOCITY MEASUREMENTS	
APPENDIX E. DIMENSIONLESS VELOCITY PROFILES	
APPENDIX F. SHEAR STRESS DISTRIBUTIONS	



## LIST OF TABLES

	Page
 CHAPTER IV	
4-1      Details of Roughness .....	40
4-2      Preston Tube Dimensions .....	43
 CHAPTER V	
5-1      Range of Variables for All Tests .....	58
 CHAPTER VI	
6-1      Location of Datum for Rough Boundaries .....	71
6-2      Effect of Wall Displacement Correction on Calculated Shear Stress .....	72
6-3      Equivalent Sand Grain Roughness .....	78
6-4      Comparison of Pressure : Shear Ratios for Preston Tubes on Fully Rough Boundary .....	94
 APPENDIX B	
B-1      Data for Normal to the Bed After Preliminary Processing .....	B4
B-2      Regression for Sample Data of TABLE B-1 ....	B6
B-3      Local Boundary Shear Stresses and Coordinates from Velocity Profiles, Test 3.60 .....	B8
B-4      Mean Velocity for Each Velocity Profile Normal to the Bed, Test 3.60 .....	B9
B-5      Data from Boundary Tube 1 After Preliminary Processing .....	B12
B-6      Boundary Shear Stresses and Coordinates from Preston Tube Data, Test 3.61 .....	B14



## LIST OF TABLES

APPENDIX B - (Cont'd.)		Page
B-7	Estimated Experimental Errors for Tests 3.60 and 3.61 .....	B15
APPENDIX C		
C-1 to C-9	Experimental Data, Series 1 to 9 .....	C2 to C15



## LIST OF FIGURES

	Page
 CHAPTER I	
1-1      Definition Sketch for Average Boundary Shear Stress .....	3
 CHAPTER II	
2-1      Distribution of Shear Stress Normal to the Boundary .....	7
2-2      Pressure-Shear Ratio for Rough Boundaries (Analytical) (Hwang and Laursen, 1963) .....	18
2-3      Principle of Shear Meter .....	20
 CHAPTER III	
3-1      Average Boundary Shear Stress (Cruff, 1965) ..	25
3-2      Variation of Maximum Boundary Shear Stress with Aspect Ratio (Kantha and Leutheusser, 1970) ...	27
3-3      Comparison of Dimensionless Shear Stress Distributions .....	35
 CHAPTER IV	
4-1      No. 36 Wet-or-Dry, Aluminum Oxide Cloth .....	38
4-2      Details of Roughness Nos. 2 and 3 .....	39
4-3      Boundary Tubes Used with Preston's Technique ..	43
4-4      Details of Bed Shear Meter .....	45
4-5      Shear Meter Calibration .....	46
4-6      Pendulum Technique for Shear Meter Static Calibration .....	47
4-7      Data Acquisition System .....	48





## LIST OF FIGURES

CHAPTER IV - (Cont'd.)		Page
4-8	Data Acquisition and Processing System .....	49
CHAPTER V		
5-1	Velocity Distribution Normal to the Boundaries, Test 3.60 .....	59
5-2	Isovel-Plot of Velocity Distribution, Test 3.60 .....	61
5-3	Dimensionless Velocity Profiles Normal to the Bed, Test 3.60 .....	62
5-4	Dimensionless Velocity Profiles Normal to the Bed, Test 3.60 .....	63
5-5	Distribution of Boundary Shear Stress .....	65
5-6	Distribution of Boundary Shear Stress .....	66
5-7	Distribution of Boundary Shear Stress .....	68
CHAPTER VI		
6-1	Selection of Rough Boundary Datum .....	70
6-2	Dimensionless Velocity Profiles .....	76
6-3	Dimensionless Velocity Profiles .....	77
6-4	Variation of B with $u_*k/\nu$ .....	79
6-5	Variation of $B_s$ with $u_*k_s/\nu$ , Nikuradse's Equivalent Sand Grain Roughness .....	80
6-6	Friction Factor Diagram .....	82
6-7	Dimensionless Velocity Profiles, $u_*$ from Equation 2-20, $A = 5.75$ .....	86
6-8	Dimensionless Velocity Profiles, $u_*$ from Preston Tube Measurements .....	86



# LIST OF FIGURES

## CHAPTER VI - (Cont'd.)

	Page
6-9 Dimensionless Velocity Profiles, $u_*$ from Equation 2-20, $A = 5.75$ .....	88
6-10 Dimensionless Velocity Profiles, $u_*$ from Preston Tube Measurements .....	88
6-11 Preston Tube Calibration with Analytical Solution .....	90
6-12 Preston Tube Calibration with Analytical Solution .....	90
6-13 Comparison of Estimated and Measured Pressure : Shear Ratios .....	93
6-14 Variation of $\Delta p/\tau_0$ with $d/k_s$ .....	93
6-15 Preston Tube Calibration Analytical Solution with Other Experimental Data .....	96
6-16 Comparison of Boundary Shear at the Channel Centerline .....	99
6-17 Comparison of Measurements of Average Boundary Shear Stress, Rectangular Channel .....	101
6-18 Comparison of Measurements of Average Boundary Shear Stress, Trapezoidal Channel .....	101
6-19 Ratio of Average Bed Shear Stress to Average Boundary Shear Stress for Various Aspect Ratios and Roughness .....	103
6-20 Variation of Average Wall to Average Bed Shear Stress with Aspect Ratio and Roughness, Rectangular Channels .....	104
6-21 Variation of Average Wall to Average Bed Shear Stress with Aspect Ratio and Roughness, Trapezoidal Channels .....	104
6-22 Wall Shear Stress Diagrams, Rectangular Channels .....	109



## LIST OF FIGURES

CHAPTER VI - (Cont'd.)		Page
6-23	Wall Shear Stress Diagrams, Trapezoidal Channels .....	109
6-24	Variation of Maximum Boundary Shear Stress, Rectangular Channels .....	110
6-25	Variation of Maximum Boundary Shear Stress, Trapezoidal Channels .....	111
6-26	Average Curves Showing the Distribution of Bed Shear Stress .....	115
APPENDIX D		
D-1 to D-9	Velocity Measurements, Series 1 to 9 .....	D2 to D17
APPENDIX E		
E-1 to E-6	Dimensionless Velocity Profiles, Series 3 and 5 to 9 .....	E2 to E7
APPENDIX F		
F-1 to F-6	Shear Stress Distributions, Series 3 and 5 to 9 .....	F2 to F8
F-7 to F-12	Shear Stress Diagrams, Series 3 and 5 to 9 .....	F9 to F14



## CHAPTER I

### INTRODUCTION

#### 1.1. General

In many types of hydraulic engineering problems the use of gross flow characteristics such as average velocity or total resistance is not sufficient. The need for detailed velocity and boundary shear stress distributions becomes apparent in a large number of problems associated with scour, bed and bank protection, sediment transport and the design of hydraulic structures.

A channel running in alluvial material may erode its banks, may remain stable or may silt up its section depending upon whether or not the shear stress at the boundary is sufficient to cause the material to move. The distribution of shear stress is therefore needed for the design of unlined channels that are to remain stable. In sediment transport, applying an average bed shear stress criterion to the entire channel cross section is not realistic, since the average value may indicate no transport while high local values of shear and therefore high transport rates may occur over some portion of the boundary. The selection of riprap sizes for the protection of guide banks and aprons should properly be based on knowledge of local shear stress values.





Generally used hydraulic formulas are based on the assumption that the boundary shear stress is uniformly distributed over the wetted perimeter and therefore do not provide for the calculation of local values of shear stress. Popular river engineering and open channel flow text books such as Leliavsky (1955), Chow (1959), Henderson (1966), and Raudikivi (1967) provide some discussion on the distribution of boundary shear stress and all present the semi-analytical results from the membrane analogy for laminar flow with particular channel shapes and flow conditions. The tractive force design procedures of Lane (1952) are described in these texts. None of these texts present experimental shear stress measurements for turbulent flow by other methods nor do they give any general analytical solutions to the distribution of boundary shear stress in open channel flow. Goncharov (1964) gives an analytical development for boundary shear stress distribution in rectangular channels, compares the equations with measurements and includes a discussion of the three dimensional boundary layer problem.

The concept of average boundary shear stress in balance with the component of the gravity force of the flow is attributed to du Boys in 1879, however it was used by Brahms as early as 1754. The average shear on the channel bottom  $\bar{\tau}_o$  is derived by dividing the total force  $\gamma A L \sin \theta$  by the boundary area  $P L$  or

$$\bar{\tau}_o = \frac{\gamma A L \sin \theta}{P L} = \gamma R S \quad \dots\dots\dots 1-1$$



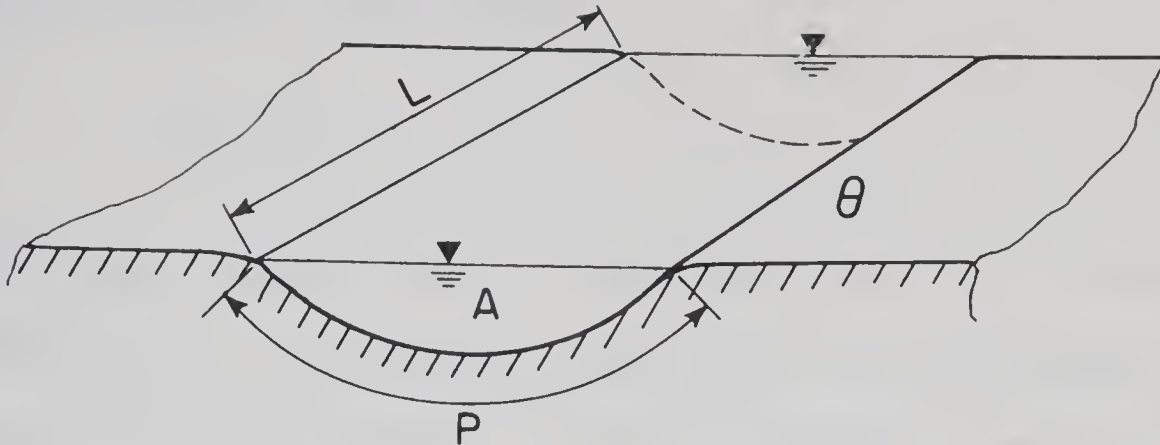


FIGURE 1-1. DEFINITION SKETCH FOR AVERAGE BOUNDARY SHEAR STRESS

where  $\bar{\tau}_0$  is the average boundary shear stress

$\gamma$  is the unit weight of fluid

$A$  is the flow section area

$L$  is the length of the element

$S$  is  $\tan \theta$ , the slope of the energy gradient, equal to the bed slope for uniform flow

$P$  is the wetted perimeter

$R$  is the hydraulic radius  $A/P$

If this force is equated to a resisting force per unit area proportional to the square of the mean velocity, the resulting equation is that given by Chezy in 1769:

$$V = C \sqrt{R S} \quad \dots\dots\dots 1-2$$

where  $V$  is the mean velocity of flow, and

$C$  is the Chezy resistance coefficient.

This is the first known uniform flow formula.



For very wide open channels the hydraulic radius is nearly equal to the depth of flow  $h$ , and therefore

$$\overline{\tau}_O \approx \tau_O = \gamma h S \quad \dots\dots\dots 1-3$$

the uniform wide - channel value. Except for uniform wide open channels and closed pipe flow, the boundary shear stress is not uniformly distributed along the wetted perimeter. There is therefore a need to be able to calculate or measure local boundary shear stress in open channel flow.

## 1.2. Objectives

The objects of this study were:

1. to find a suitable method of measuring boundary shear stress in open channel flow including those with large roughness,
2. to determine boundary shear stress distributions for various common channel shapes with a number of flow conditions and different boundary roughnesses, and
3. to explore the possibility of a general solution to boundary shear stress distributions in open channel flow.

The basic methods of determining boundary shear stress are reviewed in CHAPTER II. A few studies have been conducted to specifically measure the distribution of shear stress in open channel flow and these are reviewed in CHAPTER III.



## CHAPTER II

### METHODS OF DETERMINING SHEAR STRESS

#### 2.1. General

The following sections describe commonly used methods of determining shear stress. In particular, those methods thought to be most adaptable to rough boundaries in open channel flow have been selected for review. Discussion of a number of methods not described here, such as dye traces, heat transfer, Stanton tubes, and boundary layer fences can be found in the fluid mechanics literature (Brown and Joubert, 1969).

Boundary shear stresses are often of small magnitude and accurate measurements are generally difficult. Unless otherwise stated all values of shear stress are time averages in the following discussion.

#### 2.2. Momentum Techniques

Momentum techniques include the momentum integral methods used for developing boundary layers as well as momentum balance for fully developed flow. For the developing boundary layer it is necessary to substitute measured values in the velocity and pressure terms of the momentum integral equation in order to solve for the local shear stress (Schlichting, 1968). This requires measurement of the total and static





pressure fields. The determination of derivatives of the slowly varying quantities of displacement thickness and momentum thickness require a high degree of accuracy in the measurements.

The application of momentum balance to fully developed flow is much simpler. For flow in a straight uniform duct, the momentum balance yields

$$\overline{\tau}_0 = \frac{A}{P} \frac{dp}{dx} \quad \dots\dots\dots 2-1$$

where  $dp/dx$  is the stream-wise pressure gradient in the duct and  $\overline{\tau}_0$  is the average shear stress on the wetted perimeter. For fully developed circular pipe flow the wall shear stress distribution is uniform, hence the method gives a value of local shear stress. For uniform open channel flow we have already noted the simple average value form

$$\overline{\tau}_0 = \gamma R S \quad \dots\dots\dots 1-1$$

where  $R$  is the hydraulic radius and  $\gamma S$  replaces  $dp/dx$  of equation 2-1 as the pressure gradient.

### 2.3. Reynolds Stresses

For an infinitely wide channel with uniform flow the total shear stress varies linearly in the direction normal to the boundary according to the equation

$$\tau = \gamma S h (1 - y/h) \quad \dots\dots\dots 2-2$$

as indicated in FIGURE 2-1. The shear stress value is  $\gamma h S$  at the boundary and zero at the free surface. This equation is valid for both



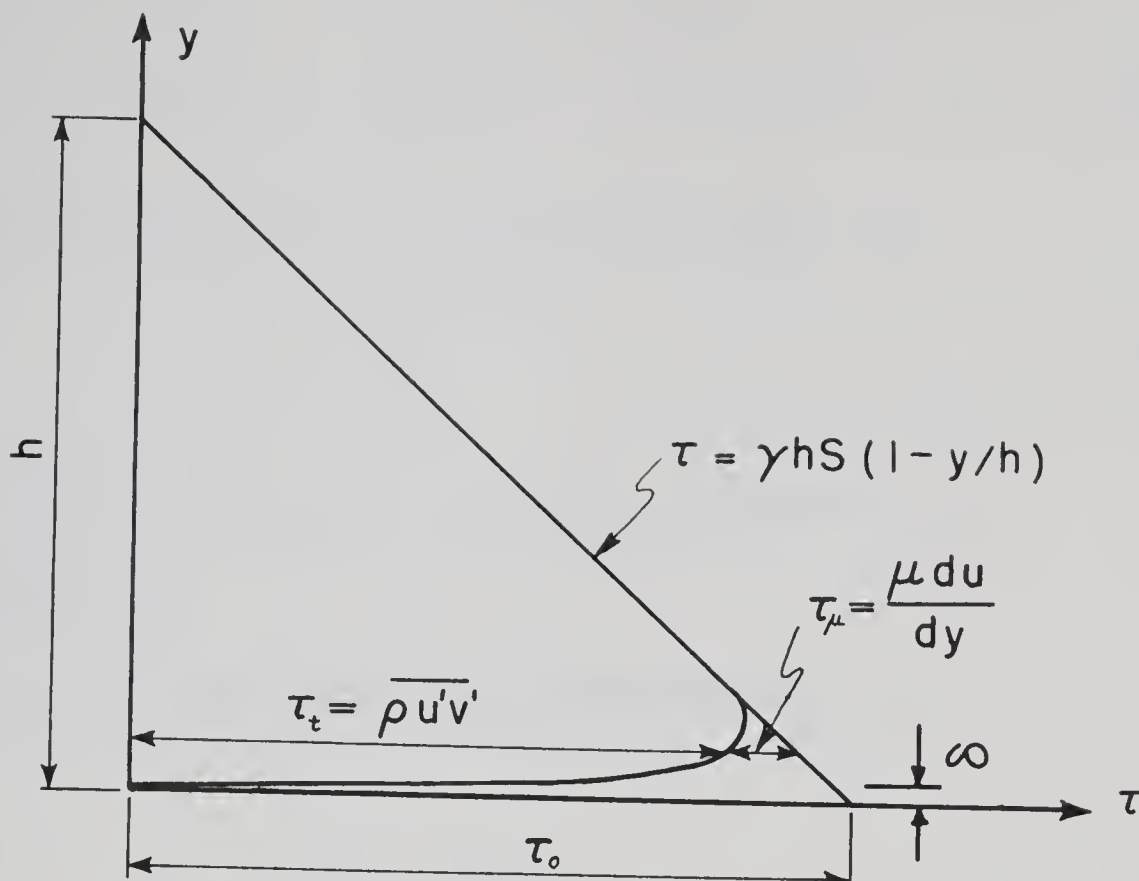


FIGURE 2-1. DISTRIBUTION OF SHEAR STRESS NORMAL TO THE BOUNDARY

laminar and turbulent flow. Within the turbulent region, that is in the region  $\delta < y < h$  where  $\delta$  is the thickness of the viscous sublayer, the shear stress is almost entirely due to momentum interchange.

That is,

$$\tau \approx \tau_t = -\rho \overline{u'v'} \quad \dots\dots\dots 2-3$$

where  $\tau_t$  represents the shear stress due to turbulence and  $u'$  and  $v'$  are the fluctuating velocity components in the  $x$  and  $y$  directions respectively. The term  $-\rho \overline{u'v'}$  is the Reynolds shear stress on the  $x - z$  plane. On the other hand, when the value of  $y$  is small ( $0 < y < \delta$ ), the shear stress is almost entirely due to viscosity such that  $\tau_t \approx 0$



and

$$\tau \approx \tau_{\mu} = \mu \frac{du}{dy} \dots\dots\dots 2-4$$

The thickness of the viscous sublayer can be shown to be

$$\delta = C \frac{\nu}{u_*} \dots\dots\dots 2-5$$

where  $u_* = \sqrt{\frac{\tau_o}{\rho}}$ . The constant C has been evaluated at 5.0 (Schlichting, 1968).

If  $\overline{u'v'}$  is measured near the boundary, but at  $y > \delta$  then

$$\tau_o \approx \tau_t = -\rho \overline{u'v'} \dots\dots\dots 2-6$$

and the boundary shear stress can be calculated. For a fully rough boundary with large roughness, that is  $k > \delta$ , the maximum value of the Reynolds stress on the x - z plane is a good approximation to the boundary shear stress.

Unfortunately, measurement of the turbulent components of flow or of  $\overline{u'v'}$  are difficult in open channel flow (Arndt and Ippen, 1970; McQuivey and Richardson, 1969; Blinco and Partheniades, 1971) and as a result this method has produced few useful measurements of boundary shear stress (Nece and Smith, 1970).

#### 2.4. Velocity Profile Method

Outside of the viscous sublayer ( $y > \delta$ ), the Prandtl - Von Karman logarithmic velocity equation describes the distribution of velocity for



wide open channels as shown by Keulegan (1938). This equation can be derived using Prandtl's concept of a "mixing length". The turbulent shear stress due to velocity fluctuations is

$$\tau_t = -\rho \overline{u'v'} \quad \dots\dots\dots 2-3$$

Using a mixing length  $l$ , the turbulent shear stress can be written in terms of the time average velocity as

$$\tau_t = \rho l^2 (du/dy)^2 \quad \dots\dots\dots 2-7$$

By assuming that this mixing length is proportional to the distance from the boundary in the region  $\delta < y \ll h$ ,

$$l = \kappa y \quad \dots\dots\dots 2-8$$

where  $\kappa$  is the "Von Karman constant". As described in the previous section, in the region  $\delta \leq y \ll h$  the boundary shear stress is approximately equal to the turbulent shear stress. That is:

$$\tau_t \simeq \tau_0, \quad (\text{i.e., } \tau_\mu \simeq 0) \quad \dots\dots\dots 2-9$$

Using the shear velocity  $u_* = \sqrt{\frac{\tau_0}{\rho}}$  and substituting Equations 2-8 and 2-9 into 2-7:

$$u_* = \kappa y (du/dy) \quad \dots\dots\dots 2-10$$

Integrating Equation 2-10 from  $y_0$  to  $y$

$$\frac{u}{u_*} = \frac{1}{\kappa} \ln \frac{y}{y_0} + \frac{u_0}{u_*} \quad \dots\dots\dots 2-11$$





where  $y_0$  is the minimum value of  $y$  which could be taken equal to  $\delta$  for  $k < \delta$  or  $k$  for  $k > \delta$ . In either case Equation 2-11 can be written as

$$\frac{u}{u_*} = \frac{1}{\kappa} \ln \frac{y}{k} + B \quad \dots\dots\dots 2-12$$

where  $B = f(\delta/k)$  or by using Equation 2-5,  $B = f(u_*k/\nu)$ . Nikuradse (1933) determined the functional relationship between  $B_s$  and  $u_*k_s/\nu$  in a set of experiments using pipes lined with uniform sand grains. The subscript 's' implies equivalent sand grain roughness.

These experiments indicated that for  $\frac{u_*k_s}{\nu} < 3.5$  where the boundary behaves as though it is hydraulically smooth

$$B_s = 5.75 \log \frac{u_*k_s}{\nu} + 5.5 \quad \dots\dots\dots 2-13$$

or from Equation 2-12

$$\frac{u}{u_*} = 5.75 \log \frac{u_*y}{\nu} + 5.5 \quad \dots\dots\dots 2-14$$

For values of  $\frac{u_*k_s}{\nu} \gtrsim 70$  the boundary behaves hydraulically rough and

$$B_s = 8.5 \quad \dots\dots\dots 2-15$$

or

$$\frac{u}{u_*} = 5.75 \log \frac{y}{k_s} + 8.5 \quad \dots\dots\dots 2-16$$

The value 5.75 in these equations results from a value of  $\kappa$  equal to 0.4 and the conversion from natural to common logarithms.

Nikuradse split the transition region ( $3.5 < \frac{u_*k_s}{\nu} < 70$ ) into three ranges and presented the following equations for  $B_s$  depending on the value of  $\frac{u_*k_s}{\nu}$ :



$$3.5 < \frac{u_* k_s}{\nu} \leq 7.1, \quad B_s = 3.5 \log \frac{u_* k_s}{\nu} + 6.59 \quad \dots\dots 2-17$$

$$7.1 < \frac{u_* k_s}{\nu} \leq 14.1, \quad B_s = 9.58 \quad \dots\dots 2-18$$

$$14.1 < \frac{u_* k_s}{\nu} < 70, \quad B_s = 11.5 - 1.62 \log \frac{u_* k_s}{\nu} \quad \dots\dots 2-19$$

Regardless of whether the boundary is acting hydraulically smooth, transitional, or rough the logarithmic equation can be written in the form

$$\sqrt{\frac{\tau_0}{\rho}} = u_* = \frac{1}{A} \frac{u_2 - u_1}{\log \frac{y_2}{y_1}} \quad \dots\dots\dots 2-20$$

where  $u_1$  and  $u_2$  are time average velocities measured at  $y_1$  and  $y_2$  respectively. The local shear stress on the boundary can therefore be calculated using two or more measured velocities within the region where the equation is valid. If the value of  $A = 5.75$  is accepted then  $u_*$  is obtained by evaluating the right hand quotient in Equation 2-20 which is the slope of the velocity profile plotted on semi-logarithmic paper. Using Equation 2-20 the values of  $B_s$  and  $k_s$  are not required and therefore there is no need to determine the functional relationship  $B = f(u_* k / \nu)$ .

In order to use this method it is necessary to determine the correct datum from which to measure  $y$  in order to plot  $y$  vs.  $u$ . This problem is not encountered for smooth boundaries, and when the roughness height is small compared with the minimum measurement distance  $y$ , the datum adjustment can be neglected. For large roughnesses the



datum selection can be made by trial and error by plotting  $y$  vs.  $u$  for various datum planes until the best fit logarithmic plot is obtained.

Nikuradse defined the origin from which to measure the wall distance as the surface of an imaginary cylinder having a volume equal to the measured volume of water contained in a known length of pipe. Schlichting (1936) plotted velocity profiles from this same hypothetical wall. On the other hand, in plotting the data of Bazin, Keulegan (1938) used the top of the roughness elements as the origin of  $y$ . Einstein and El-Samni (1949) found that for a surface consisting of closely packed hemispheres, the logarithmic velocity distribution law is valid if distances are measured from a hypothetical wall 0.2 diameters below the tops of the hemispheres. For this type of roughness the hypothetical wall located such that the volume of those portions of the roughness elements above it equals the volume of interstices below it is at nearly the same location. Reinius (1961) studied the flow in an open channel using closely packed 4.76 and 9.52 millimeter steel balls as bed roughnesses and found zero datum was 1.02 and 2.04 millimeters respectively below the sphere tops, or about 0.22 of the diameter. Blinco and Parentheniades (1971) found that the theoretical bed lies 0.27 times the average roughness diameter below the plane joining the tops of fairly uniform particles. Other investigators using natural gravel have adopted a datum plane located such that half its area lies within the particles. Taylor (1961) found that for non-spherical grains this method produced the same results as the trial and error best-fit method mentioned above.





A second problem encountered when determining the shear stress from velocities measured with pitot tubes is the determination of the pitot displacement effect when measuring near the wall. The displacement of the effective center from the geometric center of the pitot tube has been determined to be 0.18 times the tube diameter, for a tube resting on a smooth boundary (MacMillan, 1957; Daily and Hardison, 1964). For rough boundaries this displacement is open to question. A related problem is the limiting minimum value of  $y/k$  for which the logarithmic equation is valid. These problems are discussed in CHAPTER VI.

### 2.5. Preston Tube Technique

In 1954 Preston described a simple method of determining the local shear stress on a smooth boundary which utilized a round total head tube, with a square cut end, placed in contact with the boundary. The utilization of this technique is dependent on the existence of a region of similarity near the boundary. The original relation given by Preston was

$$\frac{(p - p_o)d^2}{\rho v^2} = f\left(\frac{\tau_o d^2}{\rho v^2}\right) \dots\dots\dots 2-21$$

where  $p$  is the pressure reading from the Preston tube

$p_o$  is the static pressure at the same point

$d$  is the tube outside diameter

$\rho$  is the mass density of the fluid

$v$  is the kinematic viscosity of the fluid.





Since this development a number of experiments have been carried out to check Preston's original calibration, to extend the use of the technique to developing boundary layers and to investigate the effect of pressure gradients (Hsu, 1955; Bradshaw and Gregory, 1958; Smith and Walker, 1958; Head and Rechenberg, 1962; Rajaratnam, 1965). Patel (1965) presented the following equations for Preston tubes on smooth boundaries:

$$\begin{aligned} \text{for } \log \tau_{o*} < 1.5 \\ \log \tau_{o*} &= \frac{1}{2} \log \Delta p_* + 0.037 \quad \dots\dots\dots 2-22 \end{aligned}$$

$$\begin{aligned} \text{for } 1.5 \leq \log \tau_{o*} < 3.5 \\ \log \tau_{o*} &= 0.829 - 0.138 \log \Delta p_* + 0.144 (\log \Delta p_*)^2 \\ &\quad - 0.006 (\log \Delta p_*)^3 \quad \dots\dots\dots 2-23 \end{aligned}$$

$$\begin{aligned} \text{for } 3.5 \leq \log \tau_{o*} < 5.3 \\ \log \Delta p_* &= \log \tau_{o*} + 2 \log (1.95 \log \tau_{o*} + 4.10) \quad 2-24 \end{aligned}$$

$$\text{where } \Delta p_* = \frac{\Delta p}{4} \frac{d^2}{\rho v^2} \quad \text{and} \quad \tau_{o*} = \frac{\tau_o}{4} \frac{d^2}{\rho v^2}$$

The numerous smooth boundary calibrations show differences of a few percent.

For fully rough boundaries Preston suggested the relation

$$\frac{p-p_o}{\tau_o} = f(d/k) \quad \dots\dots\dots 2-25$$



where  $k$  is the roughness height. This relationship can be derived through dimensional analysis as follows.

For the general case of two dimensional, steady, uniform flow over a rigid uniformly rough bed, the dynamic pressure measured by a boundary tube is a function of  $(\rho, \mu, u_*, k, d, a)$

$$\text{that is } \Delta p = f(\rho, \mu, u_*, k, d, a) \quad \dots\dots 2-26$$

where the parameter  $\rho$  is the mass density of the fluid

$\mu$  is the dynamic viscosity of the fluid

$u_*$  is the friction velocity

$k$  is the roughness height of the bed (dependent on the size, spacing, and shape of the roughness elements)

$a$  is the radius of the pitot opening

$d$  is the diameter of the pitot tube.

Using these parameters and dimensionless analysis, the following dimensionless groups can be obtained:

$$\frac{\Delta p}{\rho u_*^2} = f\left(\frac{u_* k}{\nu}, \frac{d}{k}, \frac{a}{d}\right) \quad \dots\dots\dots 2-27$$

which states that the pressure-shear ratio is a function of the roughness Reynolds number, the tube size to roughness ratio and a tube thickness ratio. Hsu (1955) shows the effect of the  $a/d$  ratio on the pressure-shear ratio is small for a surface pitot tube on a smooth boundary. Regardless of this effect, if this ratio is kept constant by using geometrically similar tubes then Equation 2-27 can be written

$$\frac{\Delta p}{\tau_o} = f\left(\frac{u_* k}{\nu}, \frac{d}{k}\right) \quad \dots\dots\dots 2-28$$



For fully rough flow, viscosity is no longer a characteristic parameter and the pressure to shear stress ratio can be expressed as a function of the tube size to roughness ratio only, i.e.,

$$\frac{\Delta p}{\tau_o} = f\left(\frac{d}{k}\right) \dots\dots\dots 2-29$$

as suggested by Preston. For a set of experiments in the fully rough phase with a fixed roughness and one tube size, this implies that

$$\frac{\Delta p}{\tau_o} = \text{constant} \dots\dots\dots 2-30$$

Equation 2-28 gives the functional form for the pressure to shear stress ratio for smooth, rough, and transitional boundaries, and can be rewritten as

$$\frac{\Delta p}{\tau_o} = f\left(\Delta p_*, \frac{d}{k}\right) \dots\dots\dots 2-31$$

The limiting case for a smooth boundary is then

$$\frac{\Delta p}{\tau_o} = f(\Delta p_*) \dots\dots\dots 2-32$$

which is evaluated in Equations 2-22, 2-23, 2-24. The limiting case for fully rough turbulent flow is given by Equation 2-29. This can be evaluated by using the logarithmic velocity Equation 2-16. The relationship given by Equation 2-31 is the basis for the experimental calibration which is discussed in detail in CHAPTER VI.

Ippen and Drinker (1962) used a pitot tube which was developed and calibrated for use on rough surfaces. For one tube with a fixed



bed roughness and a small range of depths the following equation was obtained

$$\frac{\Delta p}{\tau_o} = 47.6 \dots\dots\dots 2-33$$

A study by Hwang and Laursen (1963) indicated that the Preston technique was suitable for rough boundaries. They used the logarithmic velocity with Nikuradse's constants (Equation 2-16) integrated over the area of the opening of the stagnation tube

$$(p-p_o) \pi a^2 = \frac{\rho}{2} \int_{h-a}^{h+a} \left( 5.75 u_* \log 30 \frac{y}{k_s} \right)^2 \times \\ 2 \sqrt{a^2 - (y-h)^2} dy \dots\dots\dots 2-34$$

where  $h$  = the distance from the datum to the geometric center of the tube

$a$  = the inside tube radius.

The result is

$$\frac{p-p_o}{\tau_o} = 16.531 \left( \left[ \log \frac{30h}{k_s} \right]^2 - \log \frac{30h}{k_s} \left[ 0.25 \left( \frac{a}{h} \right)^2 \right. \right. \\ \left. \left. + 0.0833 \left( \frac{a}{h} \right)^4 + \dots\dots \right] \right. \\ \left. + \left[ 0.25 \left( \frac{a}{h} \right)^2 + 0.1146 \left( \frac{a}{h} \right)^4 + \dots\dots \right] \right) \dots\dots 2-35$$

This equation converges rapidly for small values of  $a/h$ . The pressure to shear ratio is given for values of the tube position  $(h-a)/k_s$  for various values of  $a/k_s$  in FIGURE 2-2.





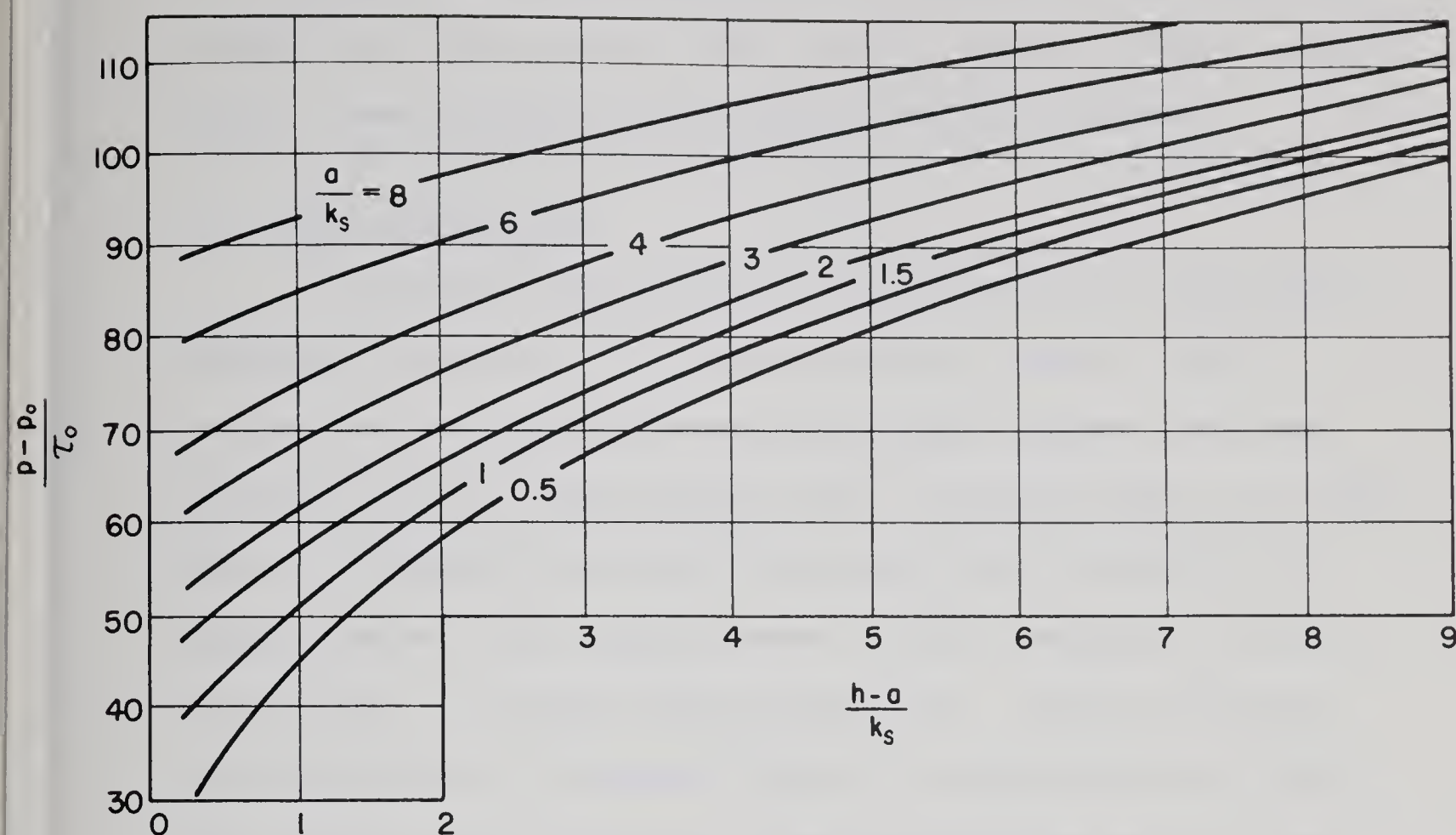


FIGURE 2-2. PRESSURE-SHEAR RATIO FOR ROUGH BOUNDARIES (ANALYTICAL)  
(Hwang and Laursen, 1963)

Hwang and Laursen conducted a series of pipe experiments using four different sand paper roughnesses and four sizes of Preston tubes with inside to outside diameter ratios of 0.64 to 0.78. Most of the measurements were taken in flows that were in the transition region and only a few measurements for the largest roughness size extended into the fully rough region as defined by  $(u_* k_s / \nu) \geq 70$ . The ratio of pressure to boundary shear as measured was compared to the pressure to shear ratio obtained analytically with a difference of about 12 percent.



Other studies using the Preston technique on rough boundaries include those of Rajaratnam (1965b), Bursali (1967), and Ghosh and Roy (1970). These studies are discussed in CHAPTERS III and VI.

## 2.6. Shear Meter Method

In 1929 Kempf measured the surface friction on a ship model by measuring the force on a flush-mounted surface element. Similar devices have been used by numerous researchers. Dhawan (1951) presented skin friction data obtained from a 'floating element' on a flat plate. In 1958 Smith and Walker carried out the calibration of a Preston tube on a flat plate by means of direct readings of the skin friction from a 'floating element dynamometer'. Bagnold (1955) describes the use of a 'suspended element' for measuring shear stress. More recently, Yalin and Russell (1966) reported the use of a 'bed-shear meter' to measure shear stresses due to long waves in an open channel. Bursali (1967) compared rough boundary shear stress measurements by 'shear plate' to those from Preston tubes and from velocity profiles. Brown and Joubert (1969) describe the use of a 'floating element device' in a two-dimensional boundary layer with pressure gradients. The last instrument mentioned was designed for measurement of shear stress in three-dimensional boundary layers. Petryk and Shen (1971) describe a 'shear meter' used in a flume.

All of these instruments were designed to measure the shear on a small element of the boundary by measuring directly the resisting force of the element supports. The principle of such instruments is indicated in FIGURE 2-3. The boundary shear stress is simply the



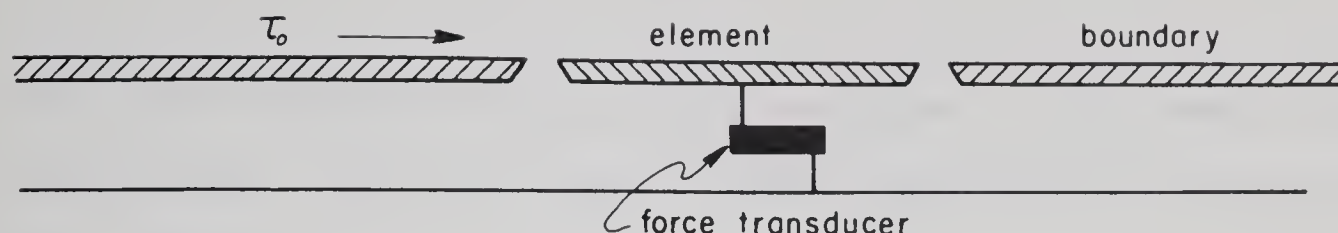


FIGURE 2-3. PRINCIPLE OF SHEAR METER

force  $F_x$  as measured by the transducer divided by the element area  $A_x$ .

$$\tau_o = \frac{F_x}{A_x} \dots\dots\dots 2-36$$

As the stresses involved are normally small, some elements are necessarily of considerable size, and the results therefore cannot be considered applicable to a single point. The instrumentation, although simple in principle, requires precise construction and careful use. Many of these instruments were fixed in one boundary location and thus could not be used to determine shear stress distributions.

## 2.7. Laminar Flow Solution for Boundary Shear Stress

A complete solution of the Reynolds equations for three-dimensional turbulent flow is beyond present analytical methods. Solution of the laminar flow equations has been carried out and assumed to give a simplified solution to the turbulent flow problem.

In 1952 Olsen and Florey presented a solution to Poisson's differential equation





$$\frac{\partial^2 \phi}{\partial z^2} + \frac{\partial^2 \phi}{\partial y^2} = \text{constant} \quad \dots\dots\dots 2-37$$

where  $\phi$  is a function of the velocity such that  $\phi = KV^n$ , where  $K$  and  $n$  are constants. The shear stress is taken proportional to the gradient of  $\phi$ , that is

$$\tau = -\mu \frac{\partial \phi}{\partial s} \quad \dots\dots\dots 2-38$$

with  $s$  the distance normal to the plane in question. Equation 2-37 is solved by combining an assumed particular integral  $F$  with a complementary function, such that

$$\phi = \psi + F, \quad \text{where} \quad \Delta^2 \psi = 0 \quad \dots\dots\dots 2-39$$

More recently the laminar flow differential equation has been solved using finite difference methods with the aid of computers. Replogle and Chow (1966) give details of this method. The velocity field for laminar flow can be adjusted to simulate turbulent flow and the velocity gradient normal to the channel boundaries is determined from the matrix of numerical values in order to determine the boundary shear stress.

These laminar flow solutions have produced shear stress distributions for particular channel shapes. In some cases they have been compared with experimental results and show some agreement.

## 2.8. Membrane Analogy for Boundary Shear Stress

The equation for the solution of the deformation of an elastic membrane is of the same form as the Poisson equation for laminar flow.





This analogy can be utilized by constructing an opening in a flat plate with boundary geometry corresponding to the channel cross section with symmetry about the free water surface. A thin rubber membrane is then stretched over the opening and a uniform pressure is applied to deform the membrane. The solution then involves measuring the elevation and slope of the membrane at selected grid points. The complete procedure is described by Olsen and Florey (1952) together with results and comparisons with the analytical solution.

## 2.9. Summary

After reviewing methods of determining boundary shear stress, it was decided that the following methods would probably be best suited to this study considering the time and resources available:

1. the use of measured velocities and the logarithmic velocity equation,
2. Preston's technique using total head tube measurements on the boundary,
3. the use of a floating element shear meter, and
4. the comparison of these methods with the boundary-average - value  $\gamma R S$ .

The equipment developed for these methods is described in CHAPTER IV.

A comparison of the results of each method is given in CHAPTER VI.



## CHAPTER III

### REVIEW OF STUDIES ON SHEAR STRESS DISTRIBUTION IN OPEN CHANNEL FLOW

#### 3.1. General

A number of investigations have been carried out to study the distribution of velocities within regular channels without explicitly measuring the distribution of boundary shear stress. In 1938 Keulegan presented formulas for the distribution of velocity in open channels based on the theoretical investigations of Prandtl and Karman and the experimental work of Nikuradse. Bazin's experimental data were used to evaluate the required constants and test the validity of these formulas. Using these formulas and measured velocities, the shear velocities and therefore shear stresses were calculated and presented for various boundary locations on rough rectangular channels. The results showed minimum values of shear stress at the corners and a maximum on the bed at mid channel. On the vertical walls the maximum shear was found at a point slightly below the water surface and with a value considerably less than the maximum shear stress on the bottom (Tables 8 and 9, Keulegan, 1938).

Tracy and Lester (1961) analyzed a number of velocity distributions in smooth rectangular channels to determine the effect of side walls. They found that the logarithmic form for velocity distribution



within the central region of flow is valid and plotted dimensionless velocity profiles using both the wide-channel boundary shear velocity  $\sqrt{g h S}$  and the average boundary shear velocity  $\sqrt{g R S}$ . Velocity plots were also presented for the wall region.

A more recent study by Yen (1968) attempted to generalize velocity distributions for straight smooth rectangular channels. This generalization can be shown providing the width of the wall affected zone is chosen as the characteristic length and the velocity is referred to the local maximum velocity. Velocity distribution data for rough rectangular channels, and for smooth sides with rough bottoms as well as rough sides with a smooth bottom, are presented but no generalized distributions are given for these cases.

An analytical solution was given by Lundgren and Jonsson (1964) for determining the boundary shear stress for shallow symmetrical channels with boundaries of small curvature. This involved a numerical solution of a differential equation derived using the area between orthogonals to the isovels and using a logarithmic velocity equation. This method is not suitable to shapes like rectangles and trapezoids because of the requirement for continuous small curvature throughout the boundary.

### 3.2. Shear Distributions in Rectangular Channels

#### 3.2.1. Smooth Boundary

Cruff (1965) extended the work of Tracy and Lester (1961) and presented shear distribution measurements for smooth rectangular channels with width to depth ratios from 4.7 to 40. Both the





logarithmic velocity formula and Preston's technique were used to determine shear stress. The average shear stress on the channel bottom was much larger than that for the walls at large width to depth ratios. The difference between these two averages diminishes as the width to depth ratio decreases. This is indicated in FIGURE 3-1 in which Cruff includes data from Keulegan (1938) and Leutheusser (1963). Leutheusser's data was obtained from a closed rectangular duct with air.

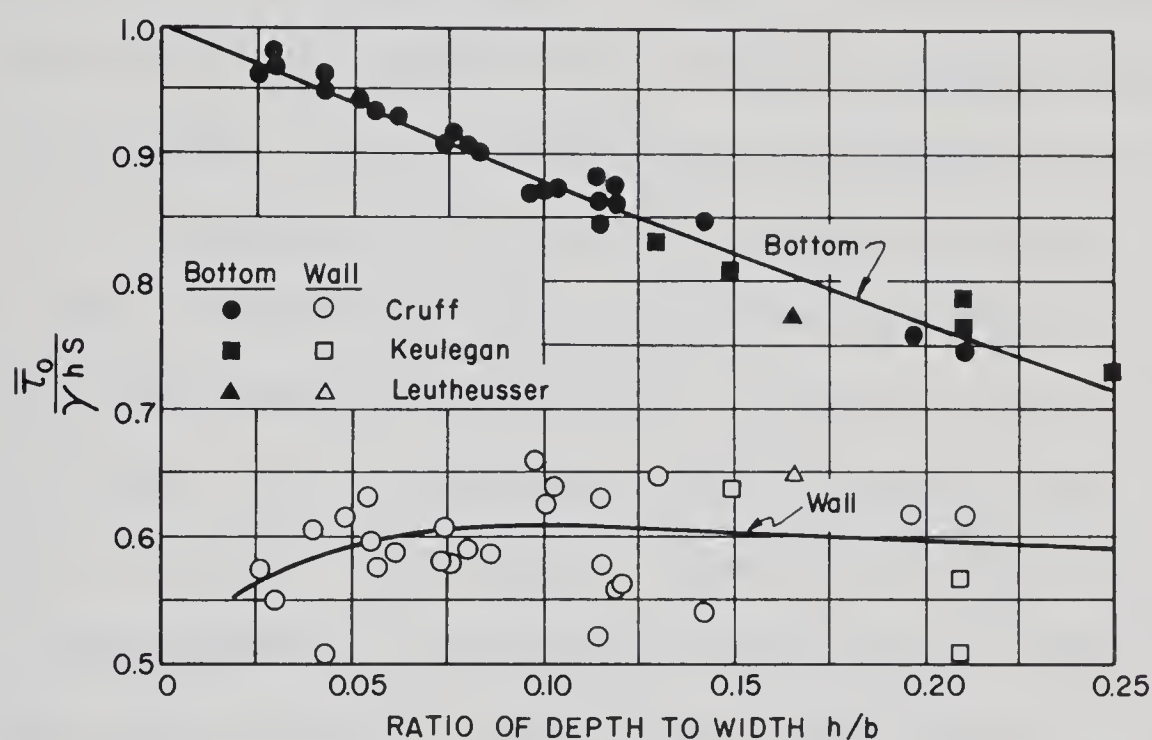


FIGURE 3-1. AVERAGE BOUNDARY SHEAR STRESS (Cruff, 1965)

Cruff found the maximum bed shear stress  $\tau_{b \text{ max.}}$  approximately equal to the wide channel value  $\gamma h S$  for width to depth ratios larger than about 12.5 and the maximum was located at mid-channel. The maximum shear stress on the wall  $\tau_{w \text{ max.}}$  was found to be 0.65 times the





wide-channel value for large aspect ratios and was located at 0.6 of the depth from the bed for all aspect ratios. Cruff also compared the maximum boundary shear stress values with the values given by Lane (1955). Lane's curves were taken from the solutions for laminar flow as given by Olsen and Florey (1952). For given width to depth ratios these curves give significantly higher values of maximum shear stress, both for the bed and walls, compared with Cruff's experimental results.

Rajaratnam and Muralidhar (1969) presented results from a series of tests on smooth rectangular channels with width to depth ratios from 0.83 to 20. Boundary shear stress was measured using the Preston tube method. It was determined that the maximum bed shear stress was at the channel centerline. The maximum wall shear stress occurred over a considerable length of wall and this length was greater for larger width to depth ratios. For small width to depth ratios (0.83 and 1.58) the maximum wall shear stress was larger than the maximum on the bed. These results compared with Cruff's show generally good agreement. The maximum bed shear stress reached the wide channel value for width to depth ratios greater than 15. It was concluded from this study that the distribution of boundary shear stress is dependent on the Reynolds number as well as the aspect ratios.

Kartha and Leutheusser (1970) presented shear stress distributions for smooth rectangular channels with width to depth ratios of 1.0 to 12.5. Measurements were made using Preston tubes and a smooth boundary calibration. Ratios of maximum to average boundary shear stress for a range of aspect ratios are indicated in FIGURE 3-2.



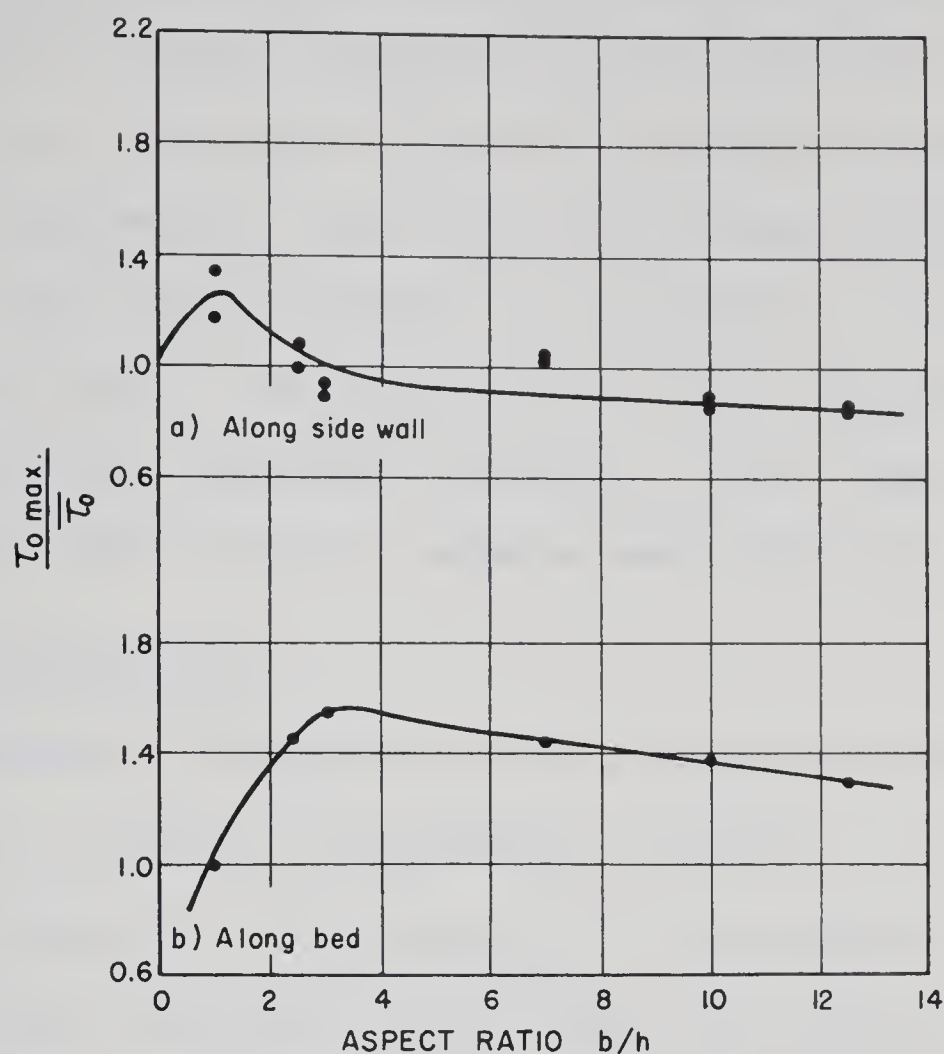


FIGURE 3-2. VARIATION OF MAXIMUM BOUNDARY SHEAR STRESS WITH ASPECT RATIO (Kantha and Leutheusser, 1970)

This figure indicates a maximum value for the maximum wall shear stress equal to 1.3 times the boundary average at a width to depth ratio of unity. The maximum for the bed is about 1.6 times the average for the boundary at a width to depth ratio of 3 and tends toward unity for an infinitely wide channel. This study showed that the actual shear distributions were very different from the analytical laminar flow solutions, however the ratios of maximum to average values of shear stress were represented quite well by the analytical solutions.



Ghosh and Roy (1970) presented data on the distribution of shear stress on smooth rectangular channels with width to depth ratios of 1.2 to 3.1. Local shear stress was calculated from measured velocity distributions, from Preston tube readings, and measured directly with a floating element on the boundary. All methods gave comparable results. The results indicated that the maximum bed shear stress occurred at the channel centerline. In all cases the maximum wall shear stress was the one measured nearest the free surface.

### 3.2.2. Rough Boundary

Because of the difficulty in measuring shear stress on rough boundaries, the number of measurements are fewer.

Rajaratnam (1970) carried out velocity distribution measurements in rough rectangular channels using two different roughnesses and width to depth ratios from 2 to 7. Boundary shear stress was determined from the velocity profiles after evaluating the constant in the logarithmic equation by equating the integrated local shear stresses with the boundary average  $\tau_{rs}$ . The bed shear stress was found to be maximum at the flume centerline and about 1.5 times the average for the boundary. The wall shear stress plots showed considerable scatter but indicated values nearly equivalent to the bed shear stress for the same dimensionless normal distance from the adjacent boundary.

Ghosh and Roy (1970) also presented boundary shear stress measurements on rough rectangular channels for different roughnesses and for width to depth ratios of 1 to 2. In contrast to the smooth boundary measurements, the three methods used (velocity profiles,





Preston tubes, and shear meter) did not yield similar distributions. Velocity profiles indicated the maximum bed shear stress at the flume centerline while the other methods located the maximum approximately mid-way between the centerline and the wall. Similarly, for the walls the velocity profiles continued to yield maximum shear stress near the free surface while the other methods indicated maximums at some depth on the wall. The shear stress when integrated over the boundary yielded average values by the three methods which were in quite good agreement. Ghosh and Roy relied on the accuracy of the direct shear measurements and preferred the Preston tube method to that of using measured velocity profiles. They concluded that the variation of boundary shear stress for varying depth is not simply related although there is a tendency for the distribution to be more uniform as depth is reduced and as roughness density is increased. They also reported that local values of Von Karman's coefficient vary with boundary location as a result of secondary flow.

### 3.2.3. Rough Bed with Smooth Sides

Rajaratnam (1970) presented velocity distributions and shear stress distributions in channels with rough beds and smooth walls. Shear stress was determined in the same manner as described in 3.2.2. The experiments were carried out for the limited range of width to depth from 4 to 9. For this situation the maximum bed shear stress was clearly displaced from the centerline towards the wall. The maximum wall shear stresses were about 0.5 times the boundary average and located 0.6 to 0.8 of the depth from the bed. This is a common





configuration for flume experiments on sediment transport and considerable effort has been taken in the past to separate the effect of smooth walls (Einstein, 1942; Vanoni and Brooks, 1957).

### 3.3. Shear Stress Distribution in Trapezoidal Channels

Because of the practical application of the trapezoidal channel shape in canal design, a number of studies are available that deal with the distribution of shear stress for both smooth and rough boundaries.

#### 3.3.1. Smooth Boundary

Ippen and Drinker (1962 ) described the distribution of boundary shear stress in concrete trapezoidal channels. These channels had widths of 1 and 2 feet with side slopes of 1 vertical and 2 horizontal. Width to depth ratios varied from 4 to 12 based on the bottom width. Local shear stress was measured using Preston's technique. The maximum boundary shear stress was about 1.2 times the boundary average and was displaced towards the wall from the channel centerline. From the maximums the shear stress decreased continuously along the boundary towards the free surface.

Rajaratnam and Muralidhar (1970) reported measurements on smooth trapezoidal channels with side slopes of 1 vertical to 1 horizontal. Using the bed width, width to depth ratios varied from 0.8 to 2.5. Shear stress was determined by integrating the local shear stress calculated from velocity profiles in terms of the constant A in Equation 2-20 and equating it to the average boundary shear stress  $\tau_R$ . The resulting A values were found equal to 5.75. For these



tests the bed shear stress was nearly uniform and the wall shear stress was equal to that on the bed near the bed and decreased towards the free surface.

### 3.3.2. Rough Boundary

In 1961 Enger performed a set of tests on a straight trapezoidal channel lined with a sand-gravel mixture. Local shear stress was calculated from two measured velocities after establishing the logarithmic velocity law valid throughout the uniform flow. The data exhibited considerable scatter but showed that the distribution of boundary shear stress was similar to the results from smooth boundaries but with less uniformity. The maximum local shear stress was 1.6 times the average and was located away from the centerline.

Ippen et al. (1962) carried out measurements with the channels described in the previous section covered with uniform roughness fabricated from lucite parallelepipeds. Width to depth ratios for these tests were 4.0 and 6.1 based on the bottom width. Shear stress was determined using a Preston tube calibrated on the rough boundary. The boundary shear stress distribution was similar to the smooth boundary data with slightly less uniformity. These shear distributions did not show a minimum value at the interior corner but rather a continuous decrease from the bed, along the wall to the free surface. The maximum local shear stress was about 1.3 times the average for the boundary and was offset from the channel centerline.

Rajaratnam and Muralidhar (1970) performed measurements on rough trapezoidal channels with 1 on 1 side slopes with a range of



width to depth ratios from 0.83 to 1.85. The boundaries were covered with rubber floor mats simulating saw-tooth and strip roughness. The constant A in Equation 2-20 was determined by equating the integrated values of shear stress calculated from velocity profiles to  $\gamma R S$ . Values of A equal to 7.0 and 6.3 were found and local shear stresses were then computed. Plots of the distribution of shear stress indicated a less uniform distribution than for the smooth boundary channels. In all cases a minimum value was found at the interior corner. The maximum local shear stress on the bed was at the channel centerline. The maximum local shear stress on the wall was in some cases larger than that on the bed and in all cases reached a maximum at some distance from the corner and then decreased towards the free surface.

Ghosh and Roy (1970) also presented data on the shear stress distribution in rough trapezoidal channels. Width to depth ratios based on bed width varied between 2 and 4. Each set of tests had the same boundary roughness and side slopes of 1 vertical to 1/2 horizontal, 1:1 and 1:1.5 were tested. Shear stress distributions were obtained from velocity profiles, from Preston tube measurements and from a direct shear meter. There were considerable differences in the distributions obtained by each method. Near the corners, results from velocity profiles and Preston tubes are in best agreement while near the flume centerline the Preston tube and direct shear meter results were nearly equal. The distributions were dissimilar to the previously mentioned results in that the wall maximum was pronounced and closer to the bed and the wall shear stress approached zero near the free surface.





### 3.4. Shear Stress Distributions in other Shapes of Channels

Replogle and Chow (1966) reported shear stress measurements carried out on the circular periphery of partially filled rough pipes. Measurements were obtained by Preston tubes which were calibrated in the pipes when flowing full. These measurements were used to confirm shear stresses calculated by a semi-analytical approach using a finite difference solution of the laminar flow equations. In all tests, the boundary shear stress decreased as the water surface was approached and was a maximum near the center of the wetted perimeter. This study concluded that a change in relative roughness alters the distribution of boundary shear stress, similar to the effects of changing the aspect ratio but the manner of this change was not established.

Studies to measure the distribution of shear stress on the boundary of more complex shapes of channels exist. Wright and Carstens (1970) reported measurements in rectangular conduits joined to represent overbank flow sections. Using a small tube on the boundary they showed the local value of shear stress tending to zero at the sharp interior corner. The maximum value of boundary shear stress was located at the obtuse ( $270^\circ$ ) corner. Ghosh and Jena (1971) carried out measurements on compound open channels with both smooth and rough boundaries. Their measurements confirmed the results found by Wright and Carstens and showed that both roughness and aspect ratio affect these complex shear stress distributions.





### 3.5. Summary of Present Knowledge on the Distribution of Boundary Shear Stress

The review of literature in this chapter shows a number of apparent differences in results of measured shear stress distributions. These differences are apparent for both smooth and rough boundaries and for various channel shapes. These studies show, without exception, the importance of channel shape and aspect ratio on the distribution of boundary shear stress. Some studies have indicated that shear stress distribution is dependent on the Reynolds number of the flow (Rajaratnam and Muralidhar, 1969). The relative roughness has been shown to be an important factor affecting the distribution but general relations have not been obtained (Ghosh and Roy, 1970). Secondary flow is commonly mentioned as having an affect on the distribution of boundary shear stress but methods to predict this effect are not available.

FIGURE 3-3 shows examples of data for similar flows, similar channel geometries, and similar roughnesses from different sources. This figure indicates apparent differences in distributions for similar flow conditions. Many of the differences noted in comparison of the preceding experimental studies may be due to different measuring methods, or different experimental techniques with the same method. Other differences probably result from the uniqueness of experimental channels and the resulting development of both primary and secondary flow conditions. Data from several of the studies reviewed, are included in the comparisons of results in CHAPTER VI and some of the most obvious discrepancies are discussed.



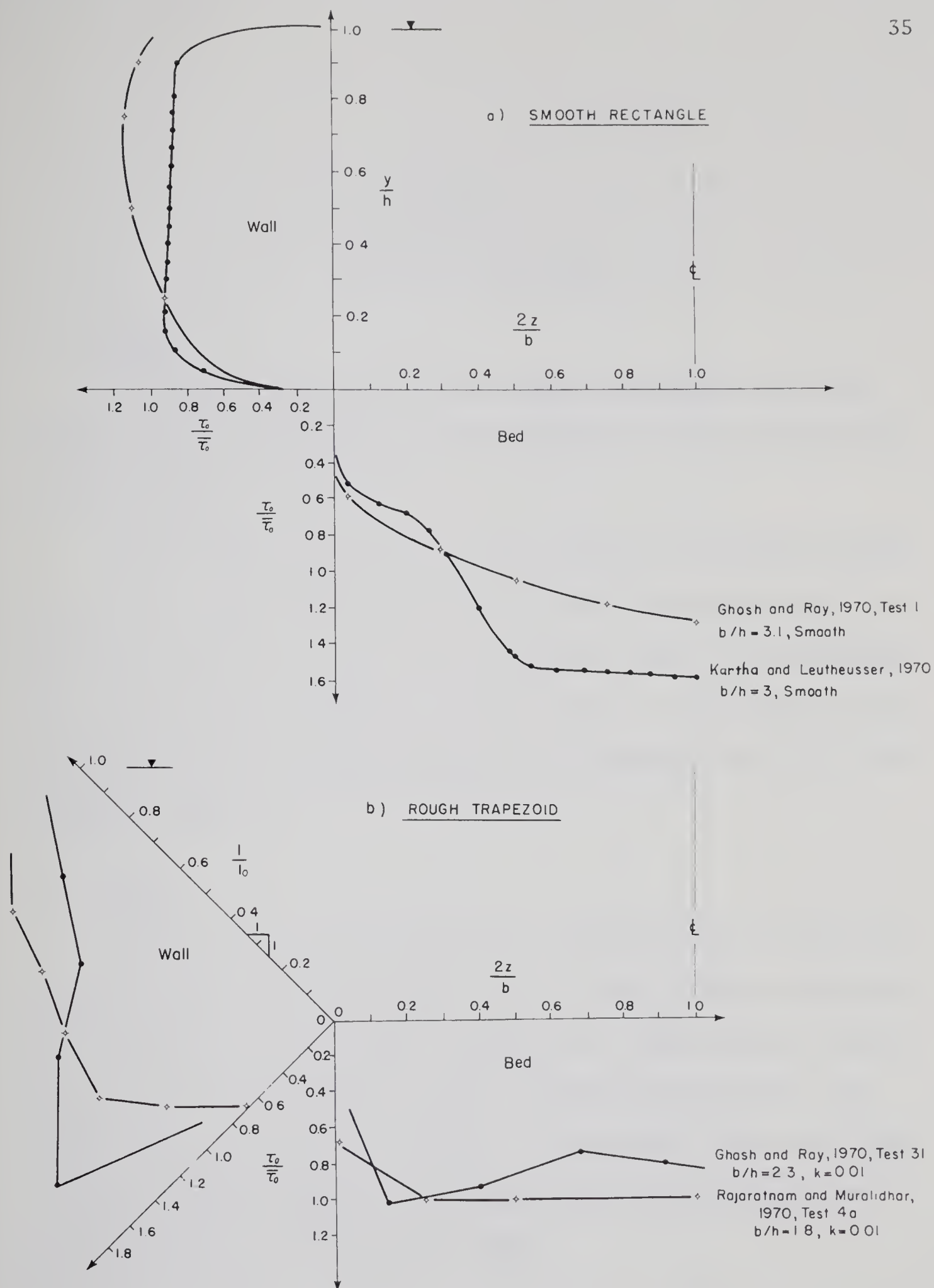


FIGURE 3-3. COMPARISON OF DIMENSIONLESS SHEAR STRESS DISTRIBUTIONS



## CHAPTER IV

### EQUIPMENT AND METHODS

#### 4.1. General

The experimental work for this study was carried out in the Graduate Hydraulics Laboratory of the Department of Civil Engineering at the University of Alberta.

The experimental facilities were modified and expanded during the period of study from 1969 to 1971 and those described in the following sections are either the configuration used for the majority of the measurements presented or the final form. Detail plans of all equipment developed during the course of the study are on file in the Hydraulics Laboratory.

#### 4.2. Flume

All tests were conducted using a tilting flume 4.0 feet wide and 60 feet long. The side walls of the rectangular flume were plexiglass and the floor was plywood covered with a smooth layer of fiberglass resin. The trapezoidal channel, constructed of plywood, was placed within the rectangular channel. Considerable effort was taken to ensure that the channels were uniform with level beds prior to adding roughness or to tilting the flume.



The flume was supported on three sets of synchronized screws which could be driven by an electric motor for slope adjustment. The flow was pumped from a storage sump into the flume head-tank through a 12 inch overhead pipe which was fitted with valves and flow measurement equipment. The flume was fitted with a tilting tailgate for depth control.

#### 4.3. Boundary Roughness

For most of the testing, the boundary was covered with a pre-fabricated uniform roughness. The roughnesses used were:

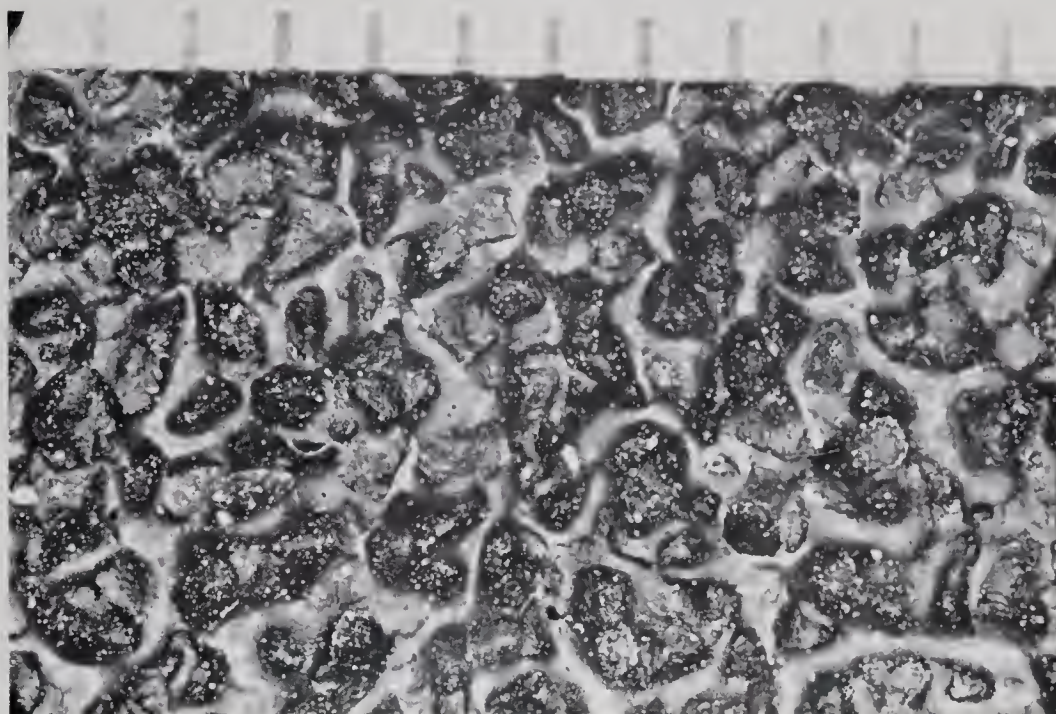
1. No. 36 aluminum oxide wet-or-dry cloth,
2. Half inch diameter hemispheres, closely packed,
3. One inch diameter hemispheres, closely packed.

Roughness 1 was a continuous strip of aluminum oxide cloth manufactured by the 3M Company. The grains on this cloth were quite angular as indicated in the photograph in FIGURE 4-1. The grains ranged in size from 0.00124 feet to 0.00230 feet with a median size of 0.00183 feet (0.56 mm). The grains were imbedded in a waterproof glue to varying depths.

Roughnesses 2 and 3 were fabricated from hard rubber into rectangular sheets using a steel mold. The elements were hemispheres placed in a close packed arrangement for maximum density as indicated in FIGURE 4-2. A small surface roughness was superimposed on each roughness element as a result of machining of the mold. This was relatively large (about 0.001 feet) for the smaller elements. The







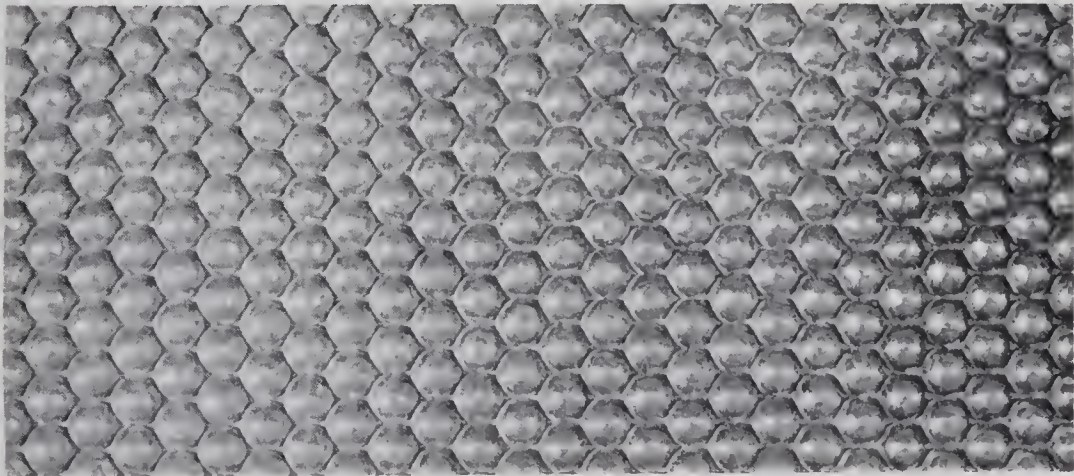
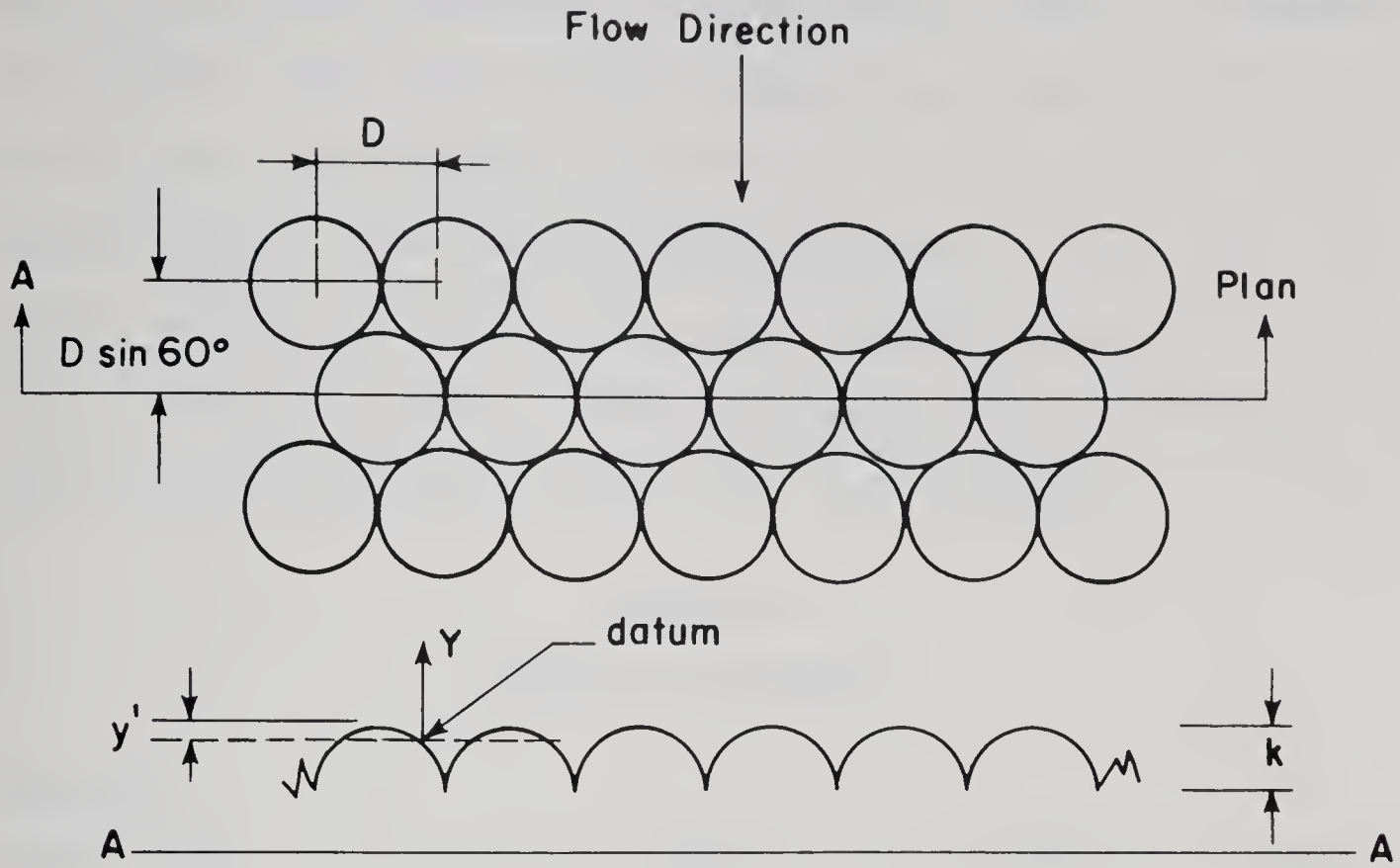
Plan View  
Scale in  
millimeters



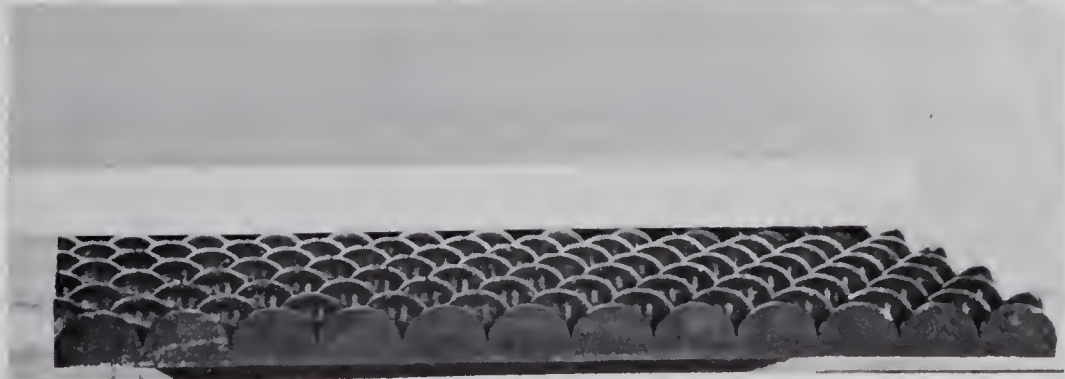
Section  
Scale in  
millimeters

FIGURE 4-1. NO. 36 WET-OR-DRY, ALUMINUM OXIDE CLOTH





Plan View  
1/2 inch  
diameter



Section  
1 inch  
diameter

FIGURE 4-2. DETAILS OF ROUGHNESS NOS. 2 and 3





mold for the larger elements was polished smooth. TABLE 4-1 summarizes the roughness sizes. The selected roughness sizes given in TABLE 4-1 are the median grain diameter for roughness 1 and the actual measured element heights in the case of roughnesses 2 and 3. In all cases the uniform roughness was placed over a flume length of at least 30 feet and the velocity and shear stress measurements were carried out at least 20 feet downstream from the start of the roughness.

TABLE 4-1  
DETAILS OF ROUGHNESS

Roughness	1	2	3
Nominal size	#36	1/2 inch	1 inch
Shape	angular grains	hemispheres	hemispheres
Median diameter, feet	0.00183	0.0410	0.0826
Selected roughness size, feet	0.00183	0.0208	0.0415

#### 4.4. Discharge and Temperature Measurements

Initially, discharges were calculated from the differential pressure measured across a 9 inch orifice plate in the supply line. This method was replaced by the use of an 8 inch Foxboro magnetic flow meter with a continuous recorder which proved to be more accurate and more useful for indicating fluctuations in discharge.

Water temperature was measured in order to determine the water viscosity. The temperature was taken at fixed time intervals during each test using a thermometer which was read to the nearest 0.1 degree



Fahrenheit. Water temperatures ranged from 59 degrees to 79 degrees F. and increased by as much as 3 degrees during a single test.

#### 4.5. Depth and Slope Measurements

Depths were determined from manual point gage readings of the water surface along the flume centerline at one foot intervals. These readings were referenced to a previously determined datum at the surface of the bed roughness. For subcritical flow conditions the tailgate was adjusted to establish uniform flow by a trial and error process. The bed slope was set and uniform flow conditions were approached by manipulating the tailgate while observing a ten-station inclined manometer indicating the static pressure along the flume wall. Water levels were continuously monitored at two stations, one upstream and one downstream of the test section. These measurements were made by electronic water level recorders and provided the water surface slope at all times during testing.

#### 4.6. Velocity Measurements

Velocity measurements were made using a 3 mm Prandtl type pitot static tube. The differential pressure was measured with a Pace model P 1 D variable reluctance differential pressure transducer with a 0.5 psid full scale diaphragm. Initially, readings were obtained from a direct reading Pace indicator (model CD 25). A multi-channel carrier-demodulator was developed to handle a number of pressure transducers, the output of which could be scanned using a data acquisition system.





Calibration consisted of applying static differential heads to the Prandtl tube and adjusting the demodulator for a linear output of zero to 10 volts with differential heads of zero to 10 inches of water. This method of calibration was checked by dynamic calibrations in a circular towing tank on several occasions.

Each channel of the demodulator was provided with variable damping circuits to reduce the frequency response of the output to a level suitable for input to the data acquisition system. This was necessary because of the relatively slow sample interval of the paper punch system. Differential pressures at this sample rate were converted to velocities without a turbulence correction and then averaged.

For one series of tests a multi-tube velocity rake was fabricated from a number of 3 mm Prandtl type pitot static tubes, each connected to a pressure transducer. These tubes were spaced at 0.03 feet center to center in the vertical direction which allowed the simultaneous recording of a number of dynamic pressures in the vicinity of the bed. The use of a velocity rake has the advantage of yielding simultaneous velocities but it requires a greater number of calibrations and was found to be less suitable than a single probe for this study.

#### 4.7. Preston Tubes

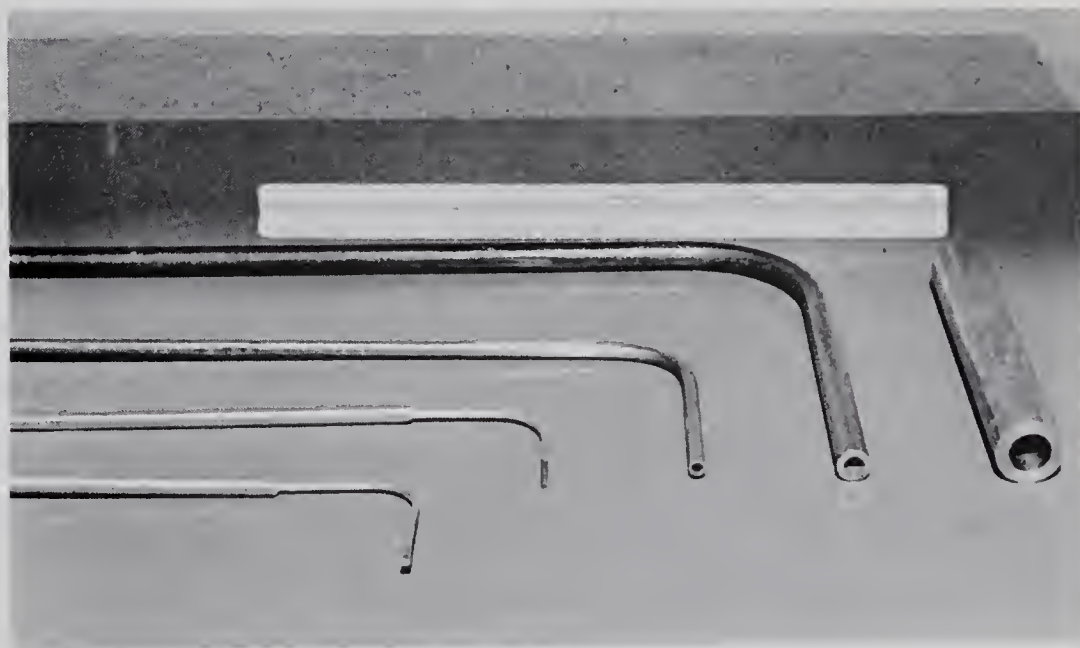
Total head boundary tube measurements were carried out using four tube sizes. Measurements were taken with the bottom of the tube resting on the smooth surface or on the tops of the roughness



elements. These Preston tubes were made from stainless steel tubing and were nearly geometrically similar in shape with nominal sizes from 3 mm to 1 inch. The exact dimensions are given in TABLE 4-2. The Preston tubes are shown in FIGURE 4-3.

TABLE 4-2  
PRESTON TUBE DIMENSIONS

Tube Number	Nominal Size	Measured size (in use)			I.D./O.D.
		O.D. feet	I.D. feet	t feet	
1	3 mm	0.00984	0.00392	0.00296	0.40
2	1/4 inch	0.0208	0.0146	0.0031	0.70
3	1/2 inch	0.0420	0.0256	0.0082	0.61
4	1 inch	0.0833	0.0523	0.0155	0.63



from left to right - 3 mm vertical screw driver probe,  
3 mm, 1/4 inch, 1/2 inch total  
head tubes, and 1 inch adapter

FIGURE 4-3. BOUNDARY TUBES USED WITH PRESTON'S TECHNIQUE



Simultaneously with the total head measurement, the static pressure was measured with a 3 mm vertical screw driver probe. This tube is described by Rajaratnam and Muralidhar (1968). The screw driver probe was positioned at an elevation equal to the geometric center of the total head tube, in the same relative location with respect to a roughness element as the total head tube, and at a traverse distance (z direction) of approximately ten times the diameter of the total head tube. Both the total head tube and the screw driver static tube were connected to a differential pressure transducer and the signal was handled in the same manner as the signal from the velocity measurements. The Preston tube together with the screw driver probe were mounted on an electric coordinate positioner which is described in Section 4.9.

#### 4.8. Shear Meter

The floating element shear meter was based on the Wallingford Hydraulics Research Station design as described by Yalin and Russell (1966). FIGURE 4-4 indicates the basic parts of the instrument. The floating element was about 1/2 square foot and was located on the flume centerline. The three stainless steel supporting strips were 0.5 inch wide and had thicknesses of 0.005, 0.007, and 0.010 inches depending on the range of shear stress expected. Displacements were a maximum of 0.010 inch and were measured with a Hewlett Packard linear variable differential transformer (LVDT-7DCDT-100). The transformer was connected to a 6 volt DC power supply and the DC output was recorded at a fixed time interval by the data acquisition system.





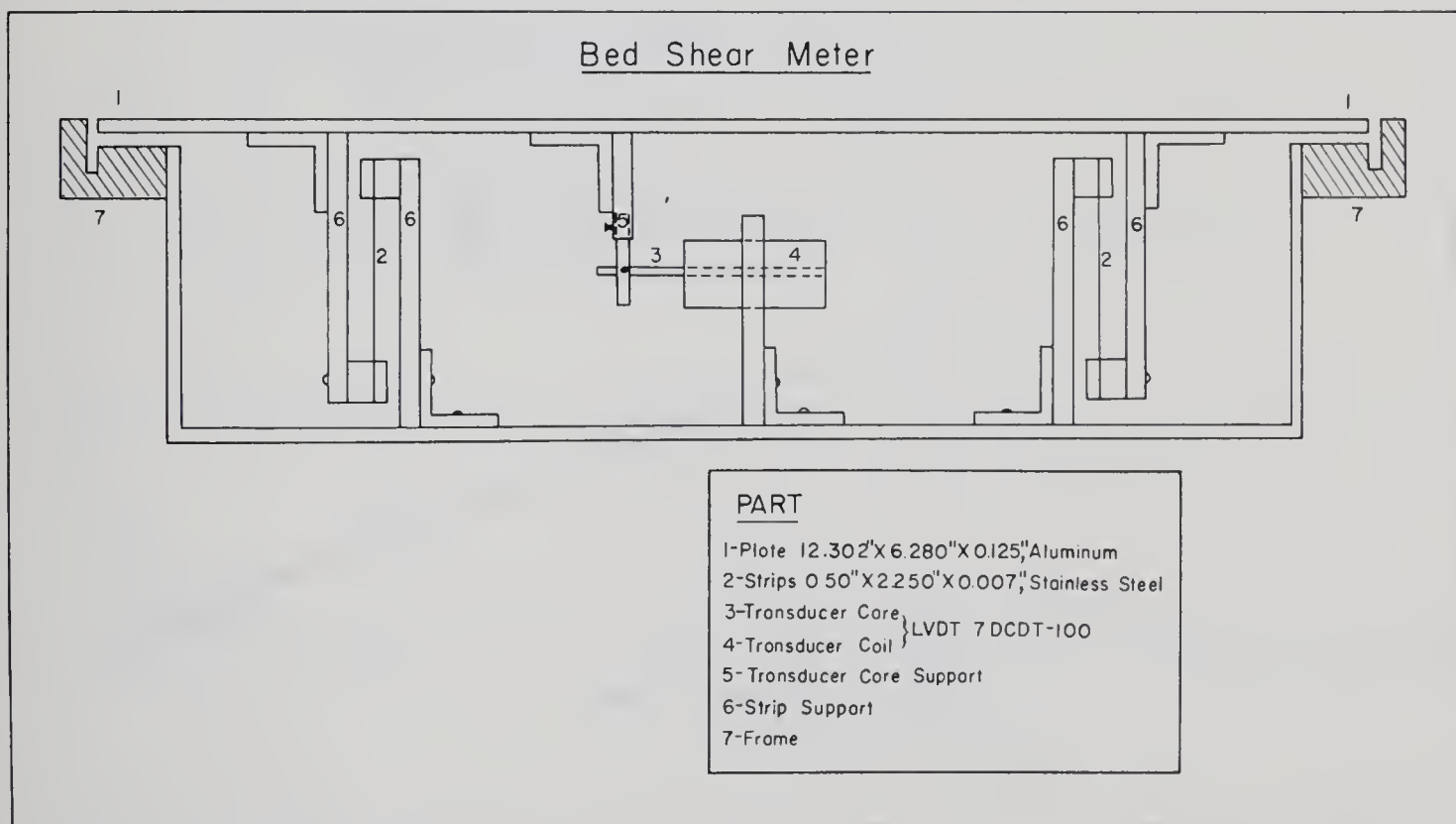


FIGURE 4-4. DETAILS OF BED SHEAR METER





Static calibration tests were carried out for the shear meter under various conditions. An example of the results of a calibration are given in FIGURE 4-5. The small horizontal forces required for this calibration were applied to a loading block attached to the centerline of the element using a simple pendulum technique. This method is illustrated in the sketch in FIGURE 4-6. To use this method it is only necessary to know the pendulum weight  $W$  and the length  $L$ , and to measure the displacement  $a$ . The force  $F_x$  is then calculated and calibrated with the transformer output.

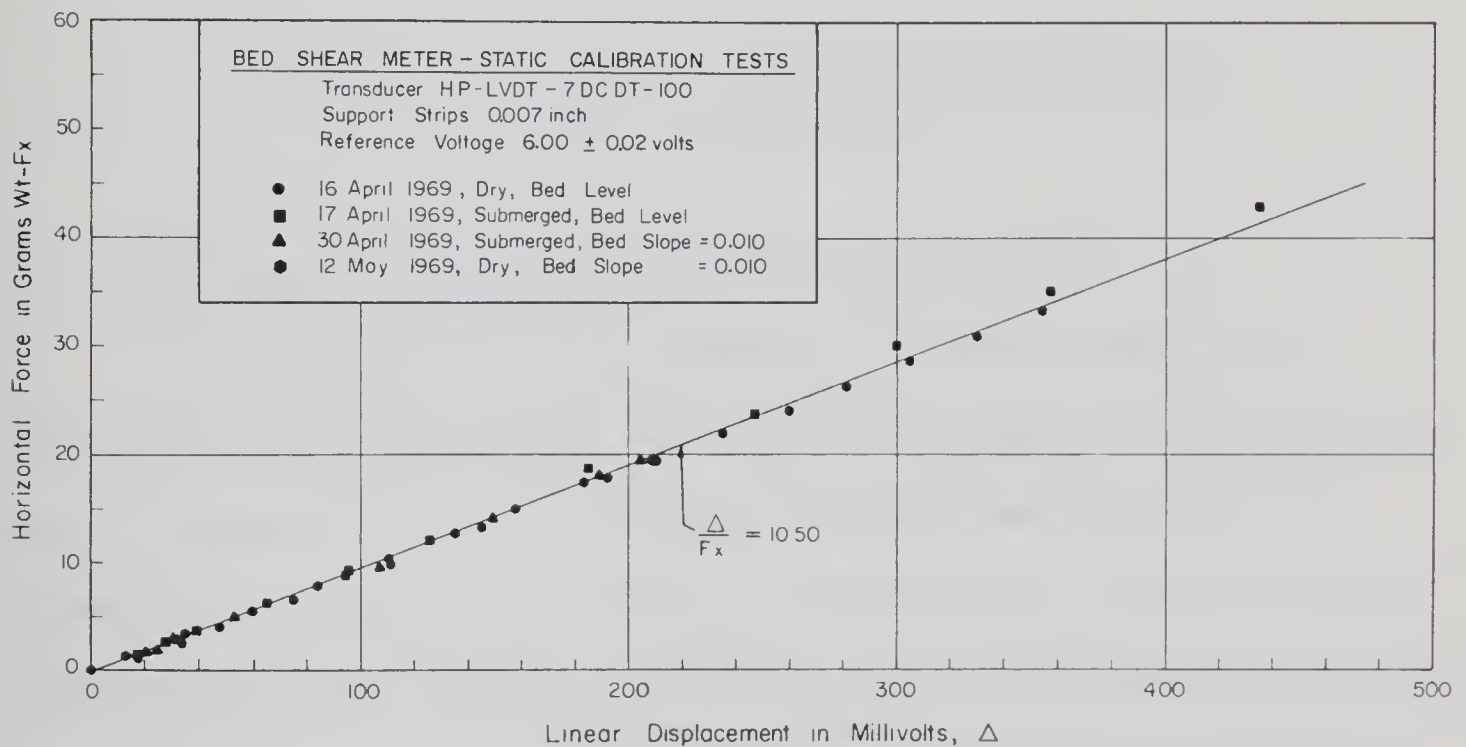


FIGURE 4-5. SHEAR METER CALIBRATION



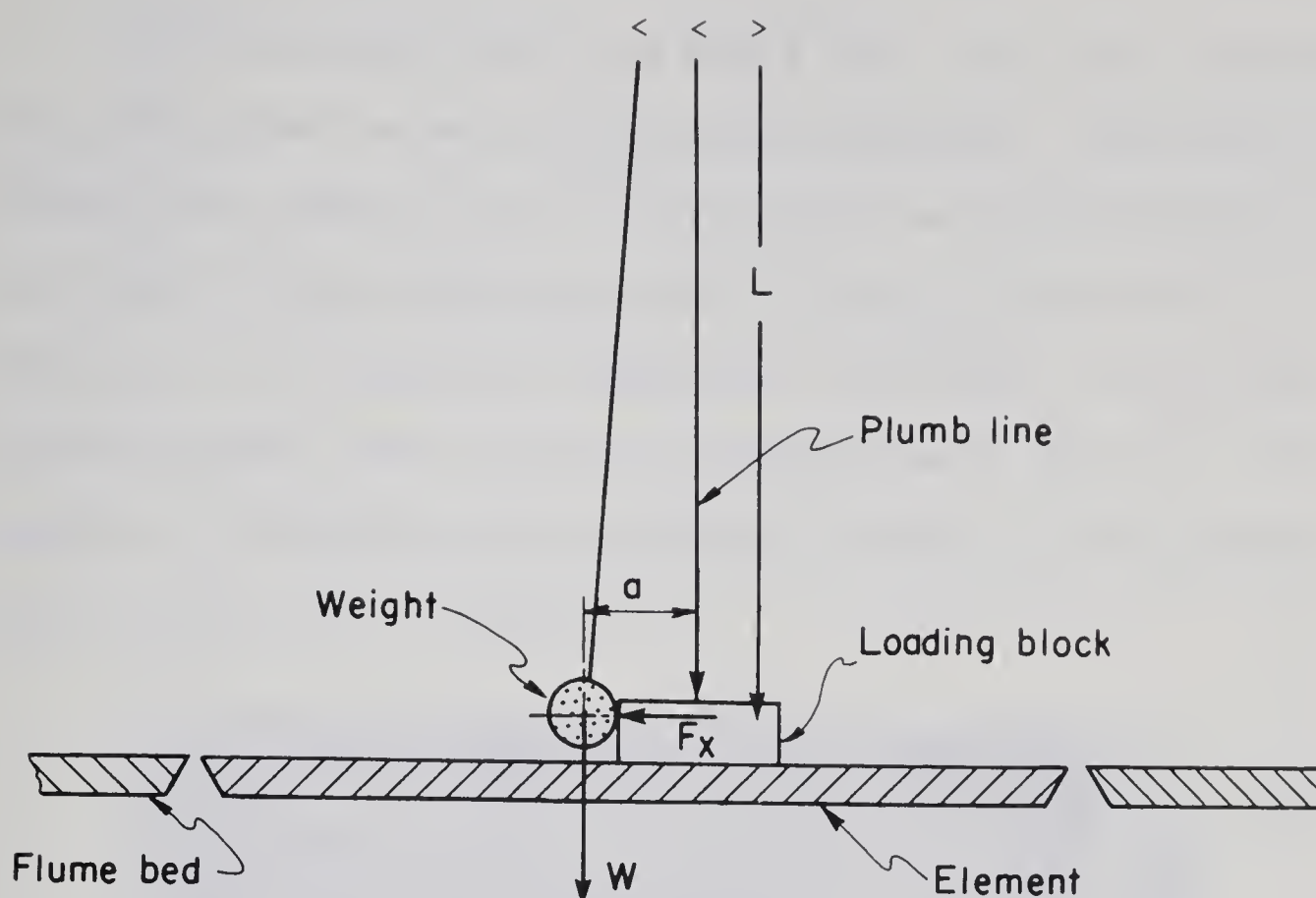


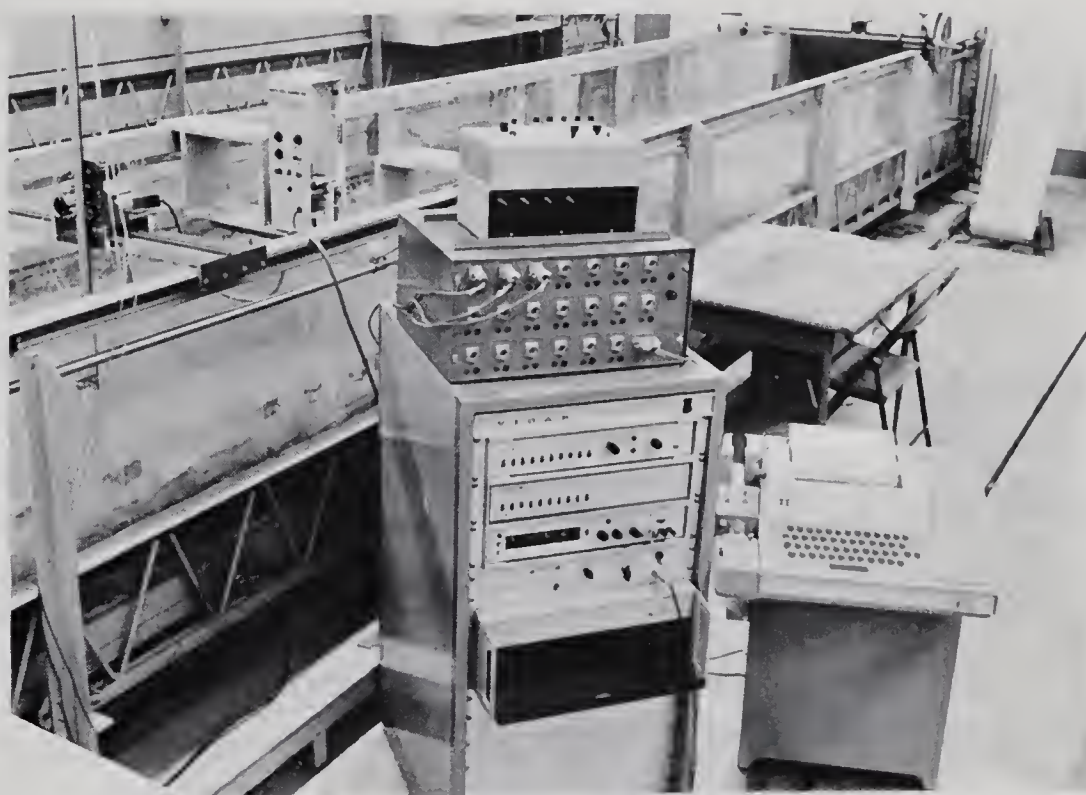
FIGURE 4-6. PENDULUM TECHNIQUE FOR SHEAR METER STATIC CALIBRATION

#### 4.9. Coordinate Positioner and Parameter Input Panel

The pitot static tube, velocity rake, total head boundary tubes, and screw driver probe were positioned within the flume section by a y-z electric coordinate system. The frame was manually positioned at the desired cross section (x coordinate). The tubes could then be positioned to any y-z coordinate by driving the mechanism with small DC electric motors. The coordinate voltages were zeroed with reference to the flume side and bed datum planes. The DC voltages representing the coordinates were then fed into the data acquisition system.



This system was controlled from a small panel where coordinate datum planes could be set and calibrations performed. The panel also provided for a number of small DC voltages which could be dialed into any channel of the acquisition system. In this way values for the discharge, the x coordinate, temperature, test number, or any other desired parameter were recorded for each portion of the test. This equipment is indicated in the photograph in FIGURE 4-7 and is represented schematically in FIGURE 4-8.



- |                       |                                     |
|-----------------------|-------------------------------------|
| at left in flume      | - Coordinate positioner             |
|                       | - Water level transmitter           |
| center, top to bottom | - Parameter input and control panel |
|                       | - Variable damping unit             |
|                       | - 20 Channel demodulator            |
|                       | - 20 Channel scanner                |
|                       | - Digital voltmeter                 |
|                       | - Scan counter                      |
|                       | - Data coupler                      |
| at right              | - Teleprinter                       |

FIGURE 4-7. DATA ACQUISITION SYSTEM



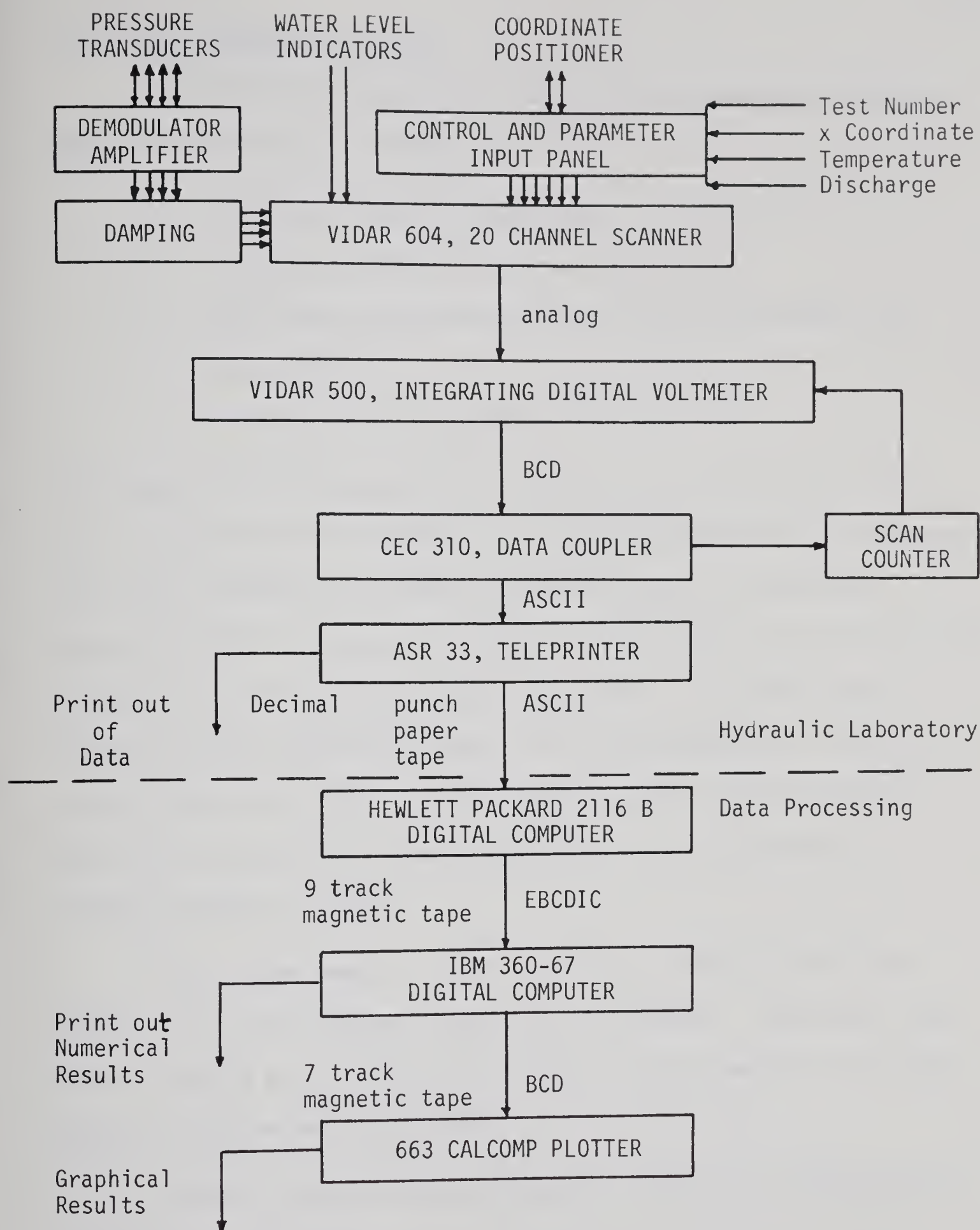


FIGURE 4-8. DATA ACQUISITION AND PROCESSING SYSTEM







#### 4.10. Data Acquisition System

The acquisition system was made up of the following elements, which are represented in FIGURE 4-8.

1. 20 channel Scanner (Vidar 604).
2. Integrating Digital Voltmeter (Vidar 500).
3. Data Coupler (Control Equipment Corporation Model 310).
4. Scan Counter.
5. Teleprinter (Teletype Model ASR 33).

All inputs for the data acquisition system were in the range zero to ten volts and each was assigned to a particular channel of the Scanner. The Scanner sequentially sampled selected channels, routing the analogue signals to the Digital Voltmeter where they were digitized and converted to a Binary Coded Decimal (BCD) code. The Data Coupler formatted the BCD signal and routed it to the Teleprinter. The Teleprinter outputs the data on punched paper tape in American Standard Code for Information Interchange (ASCII) as well as providing a decimal printout on paper.

The desired number of scan cycles was selected on the Scan Counter. The scan rate was selected on the Scanner. The upper limit was one reading per second as determined by the allowable teleprinter speed of 10 characters per second.

Further conversion and processing of the data is described in CHAPTER V.



#### 4.11. Test Method

The following procedure was normally carried out to complete a single test:

1. the channel shape and boundary roughness were selected,
2. the flume slope was set,
3. a discharge was selected,
4. uniform flow was established by measuring water depths, plotting the water surface, and adjusting the tailgate elevation,
5. final depths were measured, the water surface plotted, and slope determined,
6. the velocity distribution was measured by
  - (a) selecting the cross section (x coordinate),
  - (b) zeroing and calibrating the coordinate positioner (y and z coordinates), the water level recorders, and the pressure transducers,
  - (c) setting a value for discharge, temperature, test number, and x coordinate on the parameter input panel,
  - (d) selecting the scan rate,
  - (e) selecting the number of scan cycles,
  - (f) positioning the velocity probe, selecting the channels to be scanned, and starting the counter,
  - (g) repeating (f) for each selected point in the flow field (normally a matrix of about 13 x 13 was used for a rectangular section),



7. boundary tube measurements were then carried out by following the same procedure as above with each of the boundary tubes in turn, using only points on the boundary (this was normally about 20 points on the bed and 10 to 20 points on the wall).

A similar test procedure was followed for the trapezoidal channel shapes with the coordinate positioner and coordinates rotated when measuring normal to the sloping walls.



## CHAPTER V

### EXPERIMENTAL RESULTS

#### 5.1. Data Handling

The data acquisition system described in the previous chapter yielded a punched paper tape in American Standard Code for Information Interchange (ASCII). This data was transferred to a 9 track magnetic tape in Extended Binary Code (EBCDIC) using a Hewlett Packard 2116B digital computer with a 300 character per second paper tape reader. This service was provided by the Biomedical Engineering Department, University of Alberta.

The 9 track magnetic tape with a complete test series was then transferred to the University Computing Center. From here the tape could be called for under the Michigan Time Sharing System (MTS) using an International Business Machine (IBM) 360-67. All data processing and analysis was carried out using the IBM 360-67 and the results were plotted using a model 663 CalComp Plotter (see FIGURE 4-8).

#### 5.2. Preliminary Data Processing

Prior to analysis, the data for a complete test was processed by a series of programs which included the following.





1. The raw data was listed and checked for the correct number and type of readings.
2. The data was sorted into sub-tests with the following designations:
  - (0) velocity distribution,
  - (1) 3 mm boundary tube,
  - (2) 1/4 inch boundary tube,
  - (3) 1/2 inch boundary tube,
  - (4) 1 inch boundary tube.
3. Calibrations were applied to each reading to convert it to the desired measurement, i.e., for the pressure transducers, 1 volt equalled 1 inch differential head of water.
4. The measurements were then converted to the desired variables, i.e., differential head to velocity.
5. Sets of readings were then averaged (for velocity, discharge, and temperature, these were time averages for a given location; for the coordinates and depth both time wise and areal averaging were carried out).
6. The averaged values were then stored in matrices suitable for access during analysis.

An example of this processing is included in the sample calculations in APPENDIX B.



### 5.3. Primary Analysis

After preliminary data processing, the corrected and averaged data was read into a main program from which a number of sub-programs were called upon to carry out the basic analysis. The principal computations are outlined in the following list. A detailed sample calculation is contained in APPENDIX B.

1. The local shear velocity and boundary shear stress were calculated for each velocity profile using Equation 2-20 with  $A = 5.75$ . Prior to solving this equation, sub-programs were entered to do the following:
  - (a) locate the best datum from which to measure the normal distance,
  - (b) fit a regression line to the velocity profile using a least squares fit with the logarithms of the normal distance,
  - (c) eliminate data from the profiles normal to the bed in the zone where wall effects were obvious and similarly for the wall profiles where bed effects were obvious.
2. The local values of boundary shear stress calculated from velocity profiles were then integrated to yield mean values for the bed, the walls and the entire boundary.
3. The mean value of velocity for each normal to the bed was calculated using a trapezoidal rule.



4. The values calculated in 3 were then integrated to determine the mean value of velocity for the cross section.
5. Parameters required for the Preston tube calibration were calculated after a comparison of the resulting shear stress from the velocity profile on the flume centerline with the shear meter result.
6. Using a given Preston tube calibration curve, the boundary tube readings were then used to determine local boundary shear stress for each position on the boundary with each tube.
7. These local shear stress values were then integrated over the boundary to yield mean values for the bed, the walls and the entire boundary.

The remainder of the computer programs were used to compute parameter groups as given in the tables in APPENDIX C and to calculate and arrange the dimensionless parameters for plotting.

#### 5.4. Estimates of Experimental Errors

With each of the measurements there is an associated experimental error. Prior to discussing and comparing results, an assessment of the experimental errors is considered necessary. A complete list of the measured and calculated parameters with the estimated error is contained in APPENDIX B. These errors were estimated using the data from the example tests (3.60 and 3.61). The relative magnitude of these estimates should be applicable to all test results.



Of primary interest are the errors associated with the determination of boundary shear stress. For example, the wide-channel value of local boundary shear stress calculated from  $\gamma h S$  has an estimated error of  $\pm 15$  percent. The value calculated from a single measured velocity profile may be as much as  $\pm 20$  percent in error while the expected error for the shear meter result is given in TABLE B-7 as  $\pm 6$  percent. TABLE B-7 will be referred to in the following sections where results are compared.

#### 5.5. Presentation of Results

The results of primary analysis of the measurements for each test are presented in tables in APPENDIX C and figures in APPENDICES D, E, and F. There were a total of nine test series. The first six series were conducted using the four foot rectangular channel. Three of these included complete velocity and boundary shear stress distribution measurements (one series for each roughness; Series 3, 5 and 6). In Series 1, 2 and 4 measurements were limited to the central region of the channel and were conducted on a smooth boundary and the two smaller roughnesses respectively. Series 7, 8 and 9 were conducted using trapezoidal channels with side slopes with 1 unit vertical to 2 units horizontal and rough boundaries.

TABLE 5-1 summarizes the range of variables for all tests. Each table in APPENDIX C summarizes a set of parameters for each test series. The flow conditions for each test are completely defined by these tabulated values.





TABLE 5-1  
RANGE OF VARIABLES FOR ALL TESTS

Variable	Symbol	Units	Range
Slope	S		0.0008 to 0.012
Discharge	Q	c.f.s.	0.27 to 9.10
Depth	h	ft.	0.068 to 0.83
Kinematic Viscosity	$\nu \times 10^5$	ft. <sup>2</sup> /sec.	0.925 to 1.23
Breadth/Depth	b/h		4.75 to 59.1
Depth/Roughness	h/k		3.50 to 371
Mean Velocity	V	f.p.s.	0.98 to 5.90
Froude Number	$V^2/gh$		0.072 to 4.19
Reynolds Number	$VR/\nu$		9,680 to 198,000
Friction Factor	$8gRS/V^2$		0.0155 to 0.192
Roughness Reynolds Number	$u_*k/\nu$		2.5 to 1,520
Average Shear Stress	$\bar{\tau}_0$	lbs./ft. <sup>2</sup>	0.010 to 0.263

#### 5.5.1. Velocity Distribution

The velocity distribution within a selected channel cross section for each test is presented in the figures in APPENDIX D. These figures show the velocity plotted against the normal distance from a boundary for fixed distances from the adjacent boundary. A typical plot using the data from Test 3.60 is presented in FIGURE 5-1. This is the same test used for the sample calculations in APPENDIX B. One portion of the figure is for normals to the bed and the second



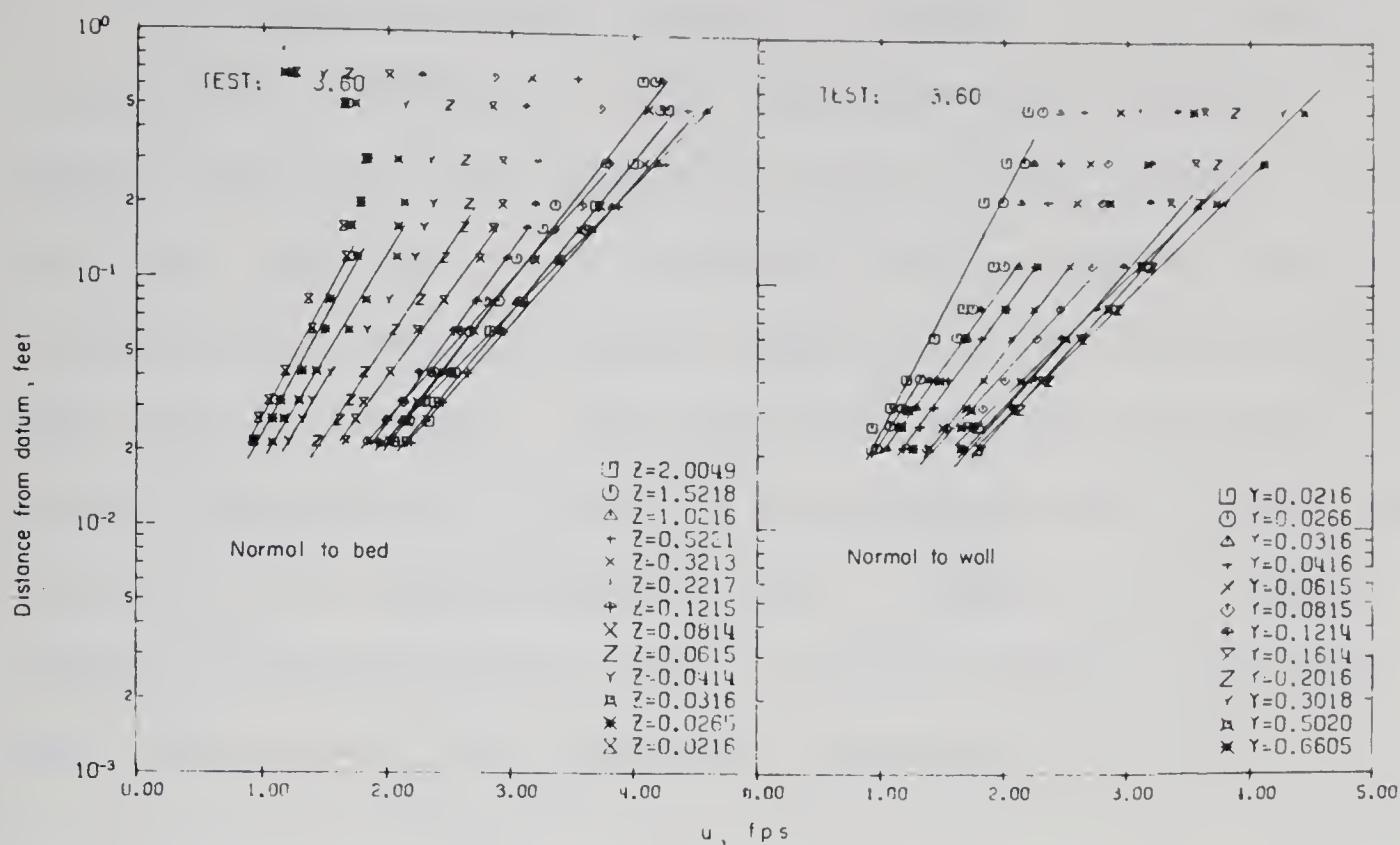


FIGURE 5-1. VELOCITY DISTRIBUTION NORMAL TO THE BOUNDARIES, TEST 3.60

portion is for normals to the wall. For each of these normals all measured velocities are given and a regression line is shown for that portion of the data from which the local shear stress was calculated. For normals to the bed the number of data points used in the regression generally decreases as the wall is approached. The minimum number of data points was arbitrarily limited to the four nearest the boundary. Similarly, for the normals to the wall, the number of data points used to give a least squares best fit regression line is variable. By noting the limiting regions for which these regression lines are given on the respective plots, zones of flow affected by the adjacent boundary can be inferred. This is discussed in detail in Section 6.6. Most normals clearly show some length over which a logarithmic formula provides a reasonably good fit.



An example isovel plot is given in FIGURE 5-2 for the same data presented in FIGURE 5-1. This figure gives the coordinate positions within the cross section for points of equal velocity. The points for a given isovel were determined from the velocity data by interpolating and extrapolating the logarithms of the normal distance using a two point formula. The isovels show the flow pattern and provide visualization of the zones of flow predominated by the bed, the wall and the free surface boundary layers. FIGURE 5-2 is a typical velocity distribution for the rough rectangular channels and clearly shows a high velocity cell between the centerline and the wall.

#### 5.5.2. Non-Dimensional Velocity Profiles

For each test with complete velocity distribution data, non-dimensional plots of the velocity profiles were prepared in several ways. In this section example plots are described and presented. Discussion of the data and further analysis is contained in CHAPTER VI.

FIGURE 5-3 presents the velocity data for Test 3.60 (see FIGURE 5-1) in dimensionless form, with the dimensionless velocity  $u/u_*$  plotted against the dimensionless distance  $y/k$ . The value of  $u_*$  was calculated from the regression lines shown in FIGURE 5-1 with the use of Equation 2-20 and  $A = 5.75$ . All measurements at distances from the boundary larger than the limit of the regression line have been removed. FIGURE 5-3 shows Nikuradse's Equation 2-16 for hydraulically rough flow with equivalent sand grain roughness. The value of  $B$  in

$$\frac{u}{u_*} = 5.75 \log \frac{y}{k} + B \quad \dots\dots\dots 5-1$$



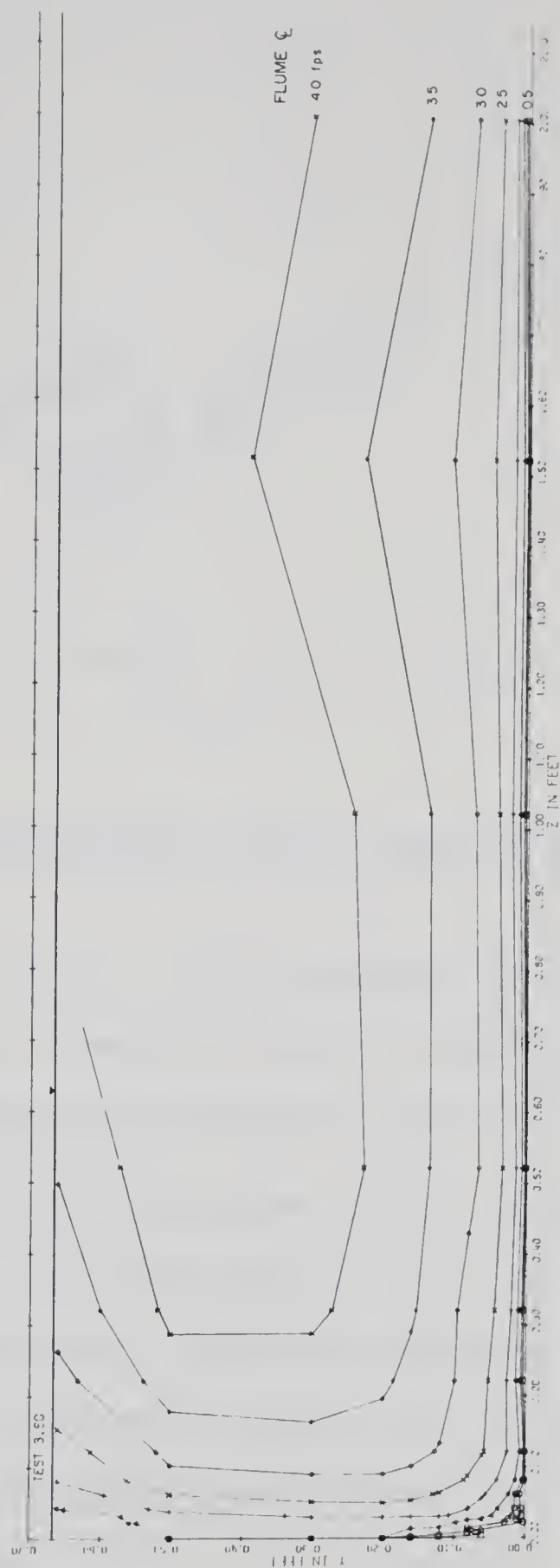


FIGURE 5-2. ISOVEL-PLOT OF VELOCITY DISTRIBUTION, TEST 3.60





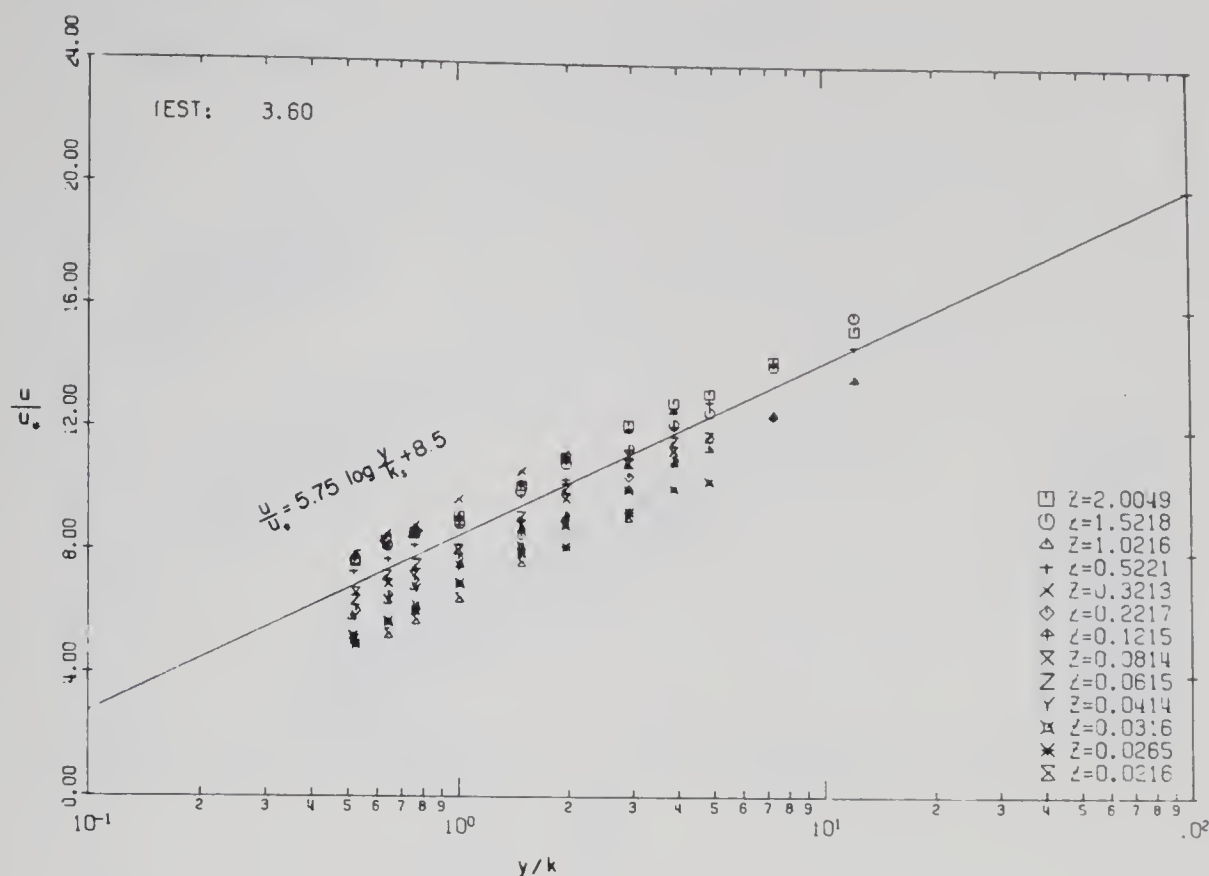


FIGURE 5-3. DIMENSIONLESS VELOCITY PROFILES NORMAL TO THE BED

is the intercept at  $y/k = 1$ . The variability of  $B$  as indicated in this figure along with the evaluation of  $k_s$  as required for use of Equations 2-13 to 2-19 is discussed in Sections 6.4 and 6.6.

FIGURE 5-4 is an alternative form for the dimensionless velocity profiles. By plotting  $u/u_*$  vs.  $yu_*/\nu$  the same data is shown with respect to the smooth, transitional and fully rough phases of flow at the boundary as described in Section 2.4. The limiting values for smooth and rough turbulent flow are indicated on this figure by the following equations:

$$\frac{u}{u_*} = 5.75 \log \frac{u_* y}{\nu} + 5.5 \quad \dots\dots\dots 2-14$$



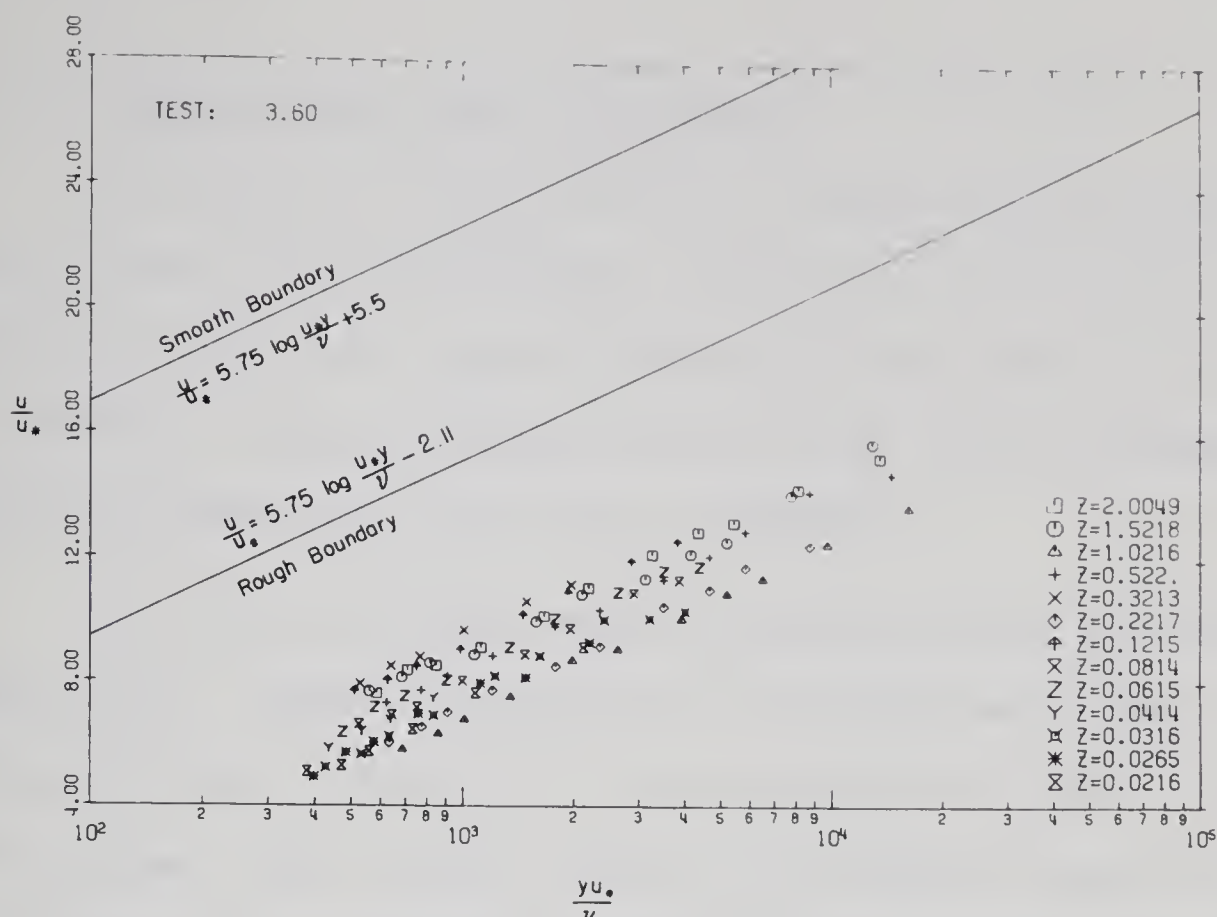


FIGURE 5-4. DIMENSIONLESS VELOCITY PROFILES NORMAL TO THE BED

$$\frac{u}{u_*} = 5.75 \log \frac{u_* y}{\nu} - 2.11 \quad \dots\dots\dots 5-2$$

Equation 2-14 is for smooth turbulent flow at the boundary as given by Nikuradse for  $u_* k_s / \nu \leq 3.5$ . Equation 5-2 is the equivalent of Equation 2-16 with the substitution  $u_* k_s / \nu = 70$  which is the lower limit for fully rough turbulent flow determined by Nikuradse. This type of representation of non-dimensional velocities has the advantage of being independent of the roughness size. It also clearly indicates changes in the boundary flow conditions, that is to say, whether or not the boundary is behaving hydraulically smooth, transitional or rough. An example is given in Section 6.4. Non-dimensional velocity plots for each test series are contained in APPENDIX E.



### 5.5.3. Boundary Shear Stress Distribution

The purpose of this section is to present the experimental results of shear stress measurements. Comparisons of the different measuring methods and a detailed analysis of the results are contained in CHAPTER VI. Mean and maximum values of bed, wall and boundary shear stress are summarized in the tables in APPENDIX C.

For each test various forms of the shear stress distribution were plotted. FIGURE 5-5 presents the non-dimensional boundary shear stress for Tests 3.60 and 3.61. The top portion of FIGURE 5-5 shows the local wall shear stress in terms of the boundary average value  $\tau_w/\bar{\tau}_0$  versus the dimensionless distance up the wall from the corner  $y/h$ . The bottom portion of this figure shows the local shear stress on the bed in terms of the boundary average  $\tau_b/\bar{\tau}_0$  versus the dimensionless distance along the bed from the corner to the channel centerline  $(2 z/b)$ . The different symbols indicate whether the results were calculated from velocity profiles or from Preston tube measurements. In all cases the average boundary values are those from the integration of local shear stress using the same measurement method. The local shear stress measurements for these tests are given in TABLES B-3 and B-6. Similar plots were prepared for each sub-test. In general the results from the Preston tube measurements show more continuity than those from velocity profiles. This is discussed in Section 6.10.

FIGURE 5-6 is a typical non-dimensional plot of the local wall and bed shear stress for a single test showing the results of all four Preston tubes. The parameters are identical to those used in FIGURE



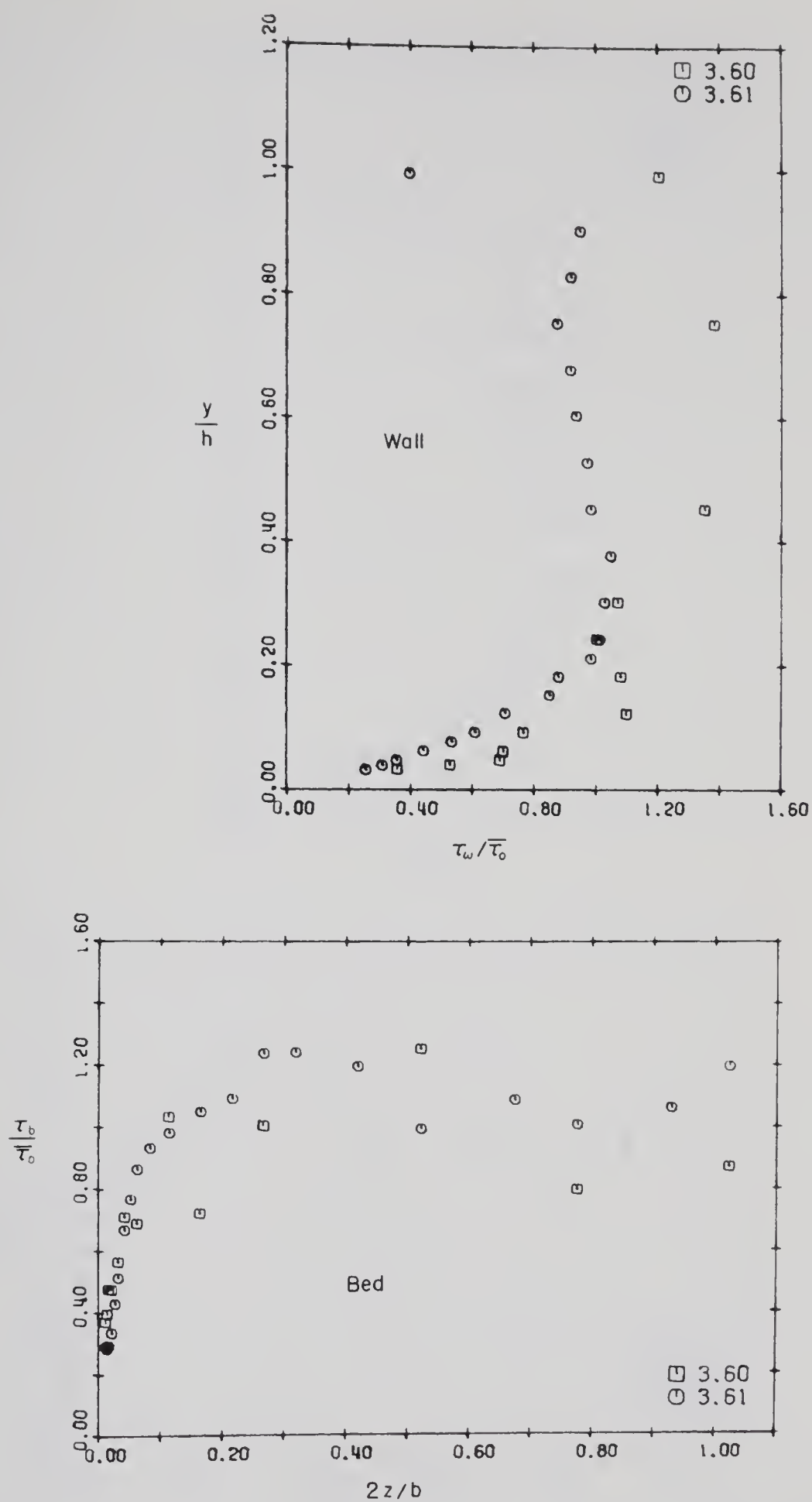


FIGURE 5-5. DISTRIBUTION OF BOUNDARY SHEAR STRESS





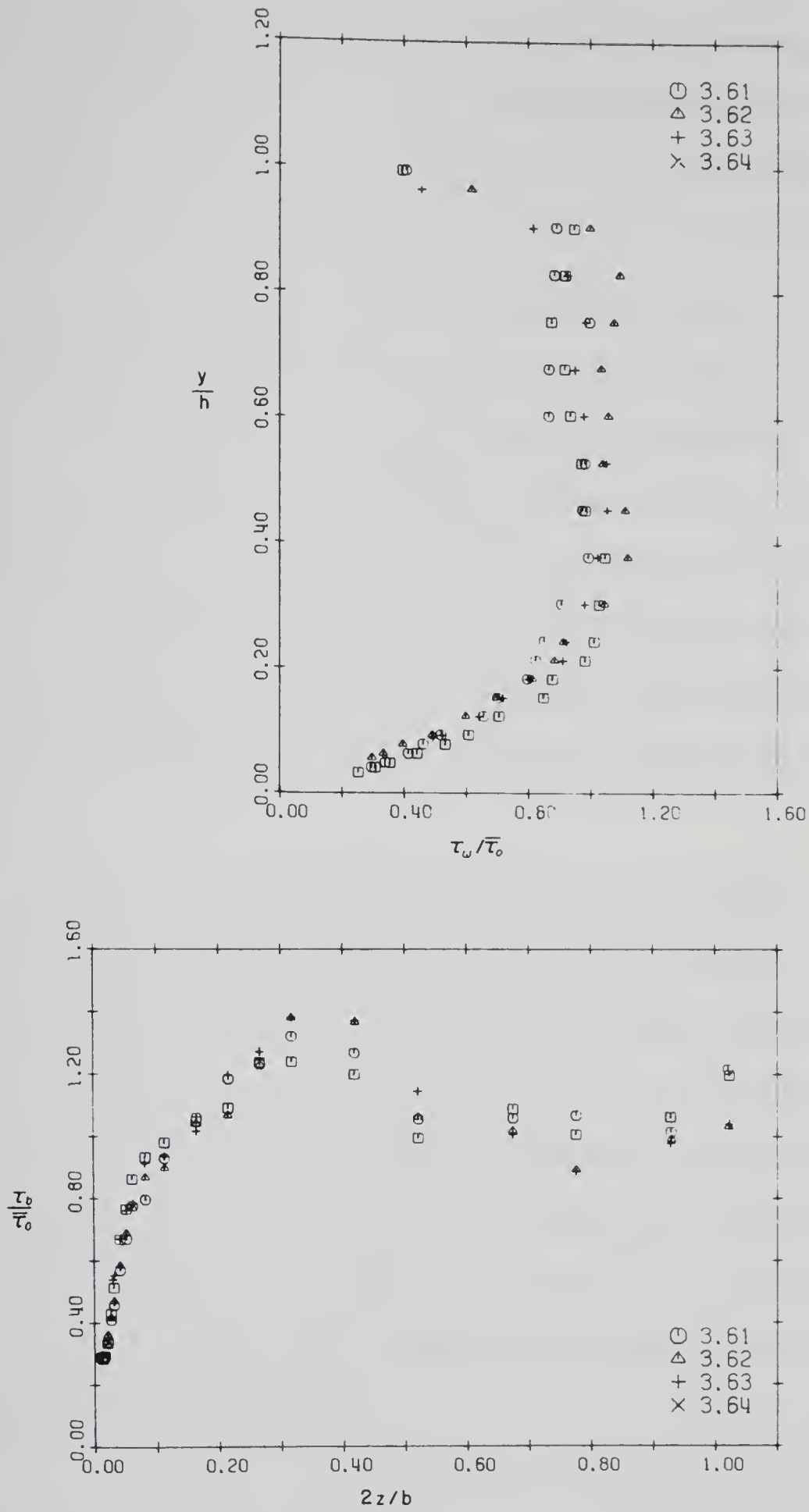


FIGURE 5-6. DISTRIBUTION OF BOUNDARY SHEAR STRESS



5-5. In all cases the results showed remarkable agreement, considering that each set of measurements were independent and each had a unique calibration. As a result of this agreement the measurements with the two largest Preston tubes were discontinued prior to Test Series 7.

The data from each test were also plotted with the local shear stress for the wall and the bed on a single plot for comparison. FIGURE 5-7 shows the local bed shear stress  $\tau_b$  versus the bed coordinate  $z$  together with the local wall shear stress  $\tau_w$  versus the wall coordinate  $y$ . The bottom portion of FIGURE 5-7 is based on the results from measured velocity profiles while the top portion uses the Preston tube data (Test 3.61). This figure clearly shows that the Preston tube results are more continuous than the velocity profile results.

Shear stress distributions in the form of FIGURE 5-7 using Preston tube data are presented for each test in APPENDIX F. Summary plots of the non-dimensional boundary shear stress distribution for each test series with one Preston tube size are also contained in APPENDIX F. For figures presenting the results of tests on trapezoidal channel shapes, the distance along the sloping wall from the corner is  $l$ , and the wall distance at the free surface is  $l_0$ . The non-dimensional wall distance  $l/l_0$  therefore replaces  $y/h$  which was used for the rectangular channels.



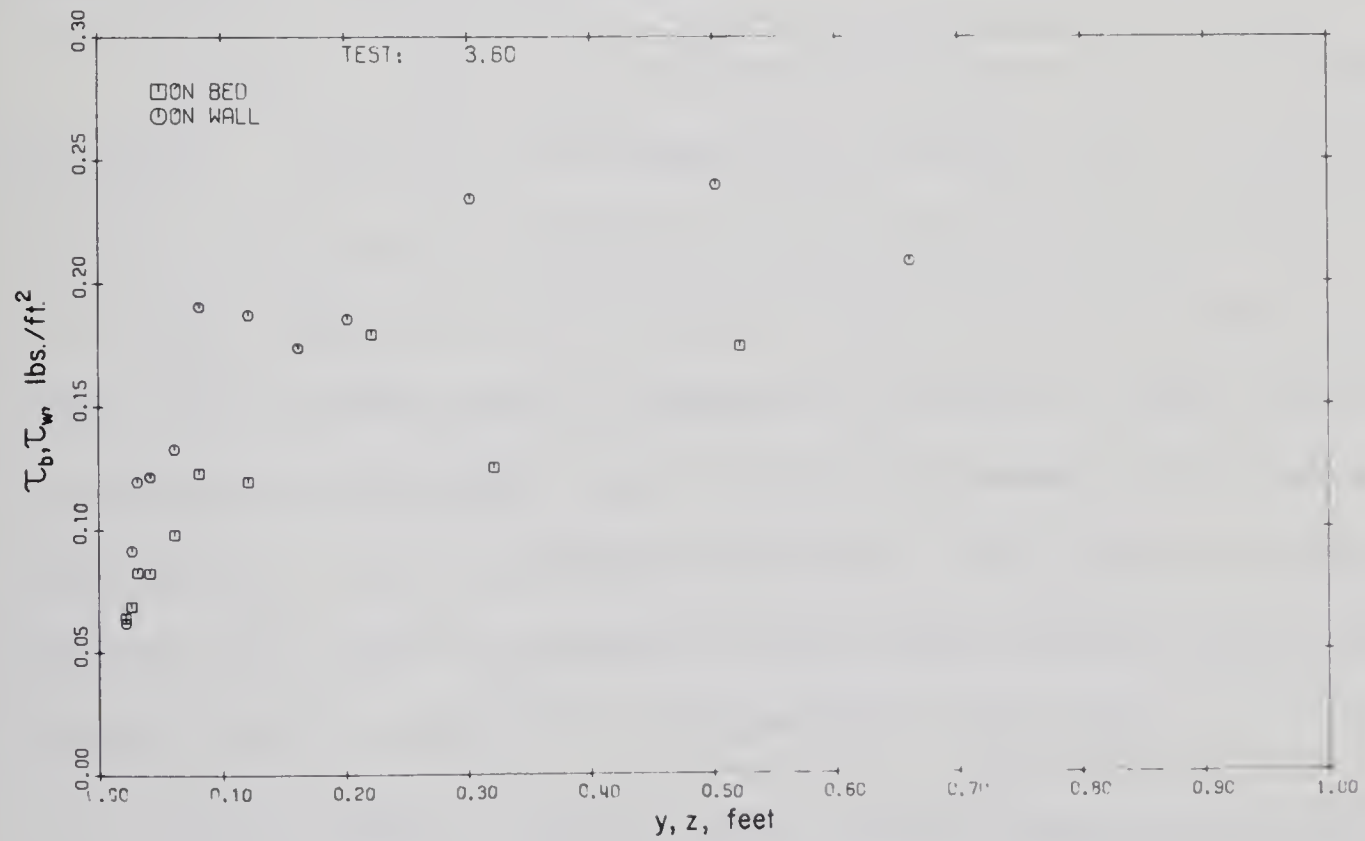
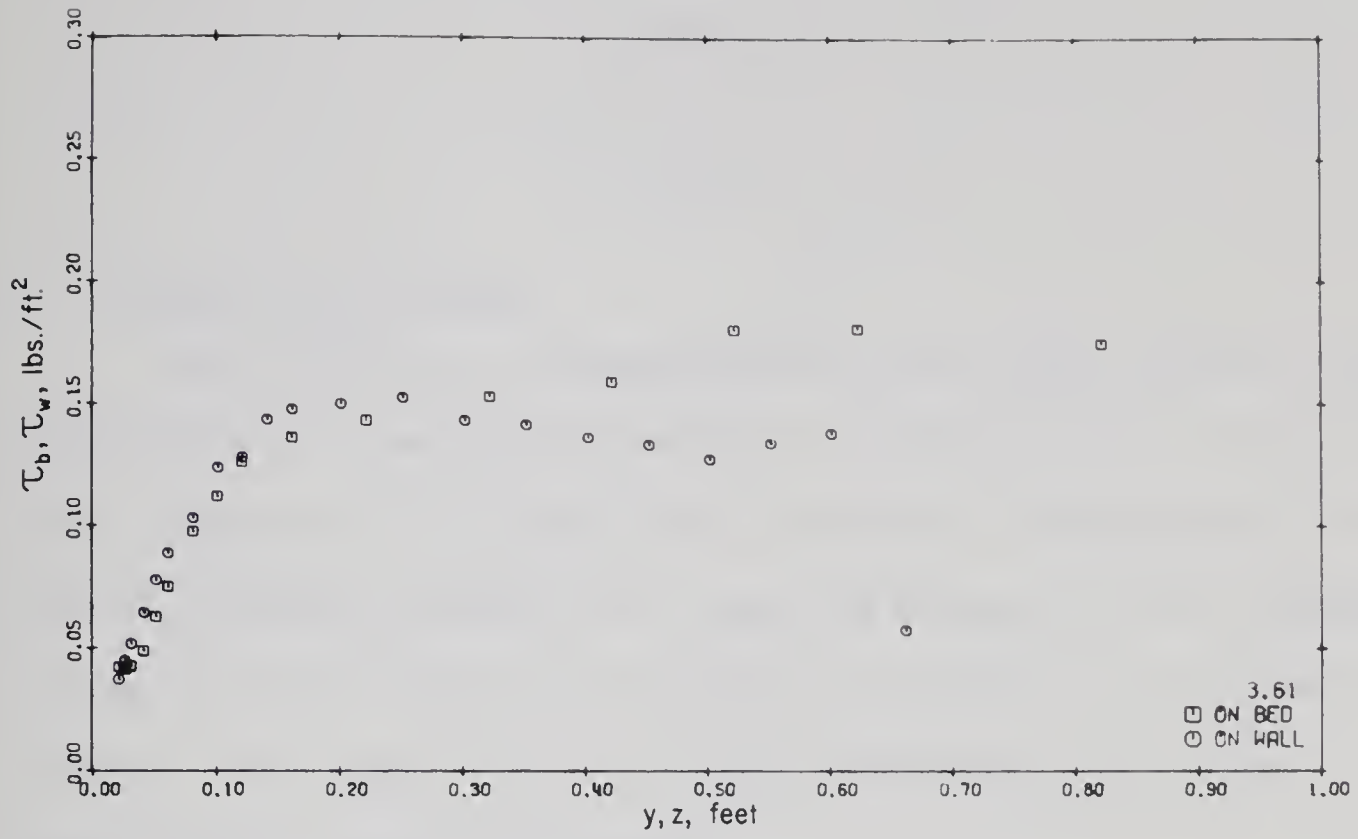


FIGURE 5-7. DISTRIBUTION OF BOUNDARY SHEAR STRESS



## CHAPTER VI

### ANALYSIS

#### 6.1. Rough Boundary Datum

The selection of a datum from which the normal distance from a rough boundary is measured was introduced in Section 2.4. For the two larger roughnesses ( $k = 0.0208$  and  $0.0415$  feet) a displacement of 0.4 times the roughness height or 0.2 times the diameter of the roughness elements below the top of the hemispherical elements was found most suitable. This agrees with the results of Einstein and El-Samni (1949), Reinius (1961), and others.

FIGURE 6-1 shows results from the procedure used to determine this datum. The velocity measurements were plotted using a variable datum and the datum was selected which gave the best least squares fit for a linear regression line using the logarithms of the normal distances. Two extreme cases are presented in FIGURE 6-1 along with the data plotted to the adopted datum. Only measurements on the channel centerline were used to determine this datum. This datum was determined for a few velocity profiles in each series and the value of 0.2 diameters was then adopted for the remainder of the tests.

For the smaller roughness this same datum location was used. In this case the adjustment is small compared to even the smallest





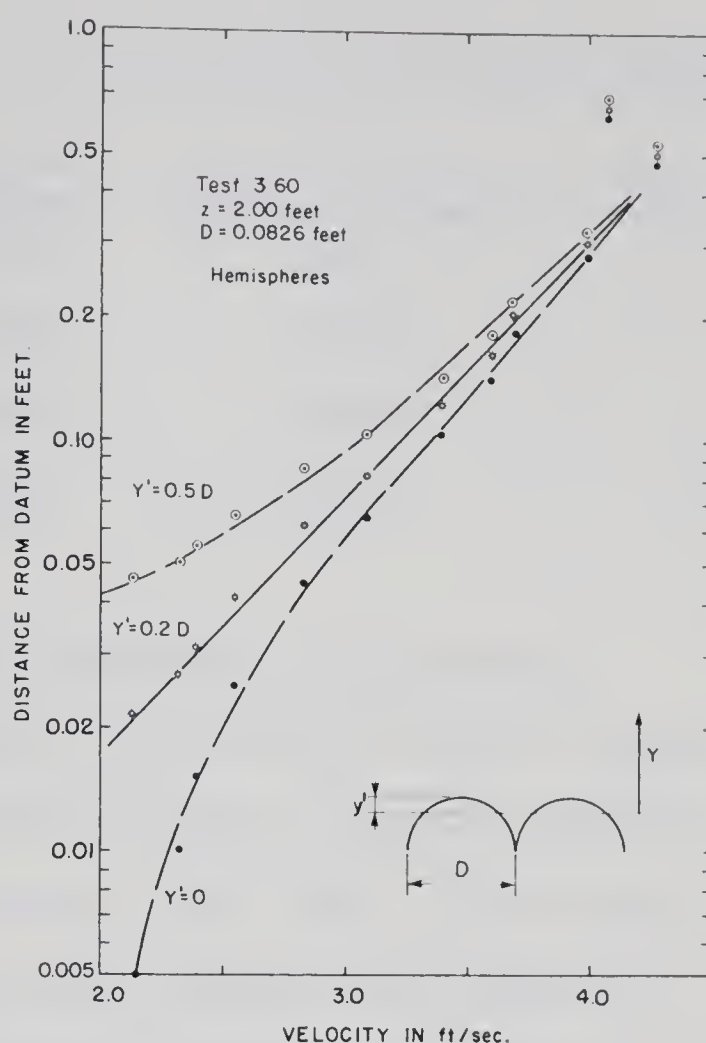


FIGURE 6-1. SELECTION OF ROUGH BOUNDARY DATUM

measured normal distance and therefore has a small effect on the results. The tops of the roughness elements are therefore at a distance of 0.2 diameters above the datum for all rough boundary tests. These positions and the distance from the datum to the geometric center of the 3 mm pitot static tube resting on the roughness are presented in TABLE 6-1.



TABLE 6-1  
LOCATION OF DATUM FOR ROUGH BOUNDARIES

Nominal Roughness	Roughness Diameter feet	Datum to Tops of Roughness Elements feet	Datum to Geometric Center of Pitot Static Tube feet
#36	0.0018	0.0004	0.0053
1/2 inch	0.0410	0.0082	0.0131
1 inch	0.0826	0.0165	0.0214

## 6.2. Pitot Tube Displacement at the Boundary

In a number of the velocity profiles presented in APPENDIX D, the measured velocity nearest the boundary is higher than that indicated by the regression line. This is most obvious for tests conducted on the smooth boundary (see FIGURE D-1). If a pitot displacement wall correction of 0.18 times the tube diameter (Daily and Hardison, 1964) or 0.00176 feet is applied to the measurements on the boundary, the agreement between boundary measurements and the regression line improves. This correction was not applied to the data plots for the smooth boundary. The velocity measurements nearest the boundary were not included in the determination of shear velocity for this series.

The effect of a pitot wall displacement for the pitot static tube resting on the smallest roughness ( $k = 0.0018$  feet) was also apparent (FIGURES D-2, D-5, and D-9). With this roughness height considerably less than the tube diameter some effect should be expected. The determination of the wall displacement effect is



dependent on the determination of the datum as discussed in Section 6.1. For the sand paper roughness a wall displacement correction of 0.18 tube diameters improves the fit of the regression line with the measurement at the wall. A wall displacement correction of 0.18 d was applied to the data in FIGURE D-2 and in Test 5.20 of FIGURE D-5 for comparison with the uncorrected data in Test 5.10. For measurements off the boundary no wall correction was made. The correction has a small effect on the calculated shear velocity as indicated in TABLE 6-2.

TABLE 6-2  
EFFECT OF WALL DISPLACEMENT CORRECTION ON  
CALCULATED SHEAR STRESS

Test 5.10  
k = 0.0018 feet  
z = 2.00 feet

	Without Displacement	With Wall Displacement
y coordinate of measurement at wall, feet	0.0053	0.0071
number of points in regression	10	10
correlation coefficient	0.9988	0.9991
calculated shear velocity, f.p.s.	0.3276	0.3440

For the larger roughnesses, the boundary measurements are made at a larger distance from the datum and no wall correction was considered necessary. For the largest roughness the smallest normal distance is more than twice the tube diameter and no wall effect



should exist. The difference between the measured velocities at the boundary and those given by the regression are probably affected more by the position with respect to the roughness elements and the use of an areal average datum.

### 6.3. The Effect of Tube Position with Respect to the Roughness Elements on Measured Pressures

For the smallest roughness ( $k = 0.0018$  feet) the effect of tube position with respect to individual grains on measured pressures was not assessed. With the tube size several times the roughness size this effect should be small.

For the larger roughnesses ( $k = 0.0208$  and  $k = 0.0415$  feet) the measurements near the boundary may have been affected by the tube position. This effect is dependent on the wall displacement and on the use of an average datum. The temporal average differential pressure measured with a pitot static tube at different points, with respect to the individual roughness elements, for a typical test varied by  $\pm 10$  percent of the spatial average at the boundary ( $y = 0.0214$  feet). At a normal distance of  $0.0264$  feet this variation was  $\pm 5$  percent for the same flow. The spatial average was determined from a grid of 12 points with spacing  $D/4$  in the  $z$  direction and  $1/3 D \sin 60$  in the  $x$  direction. At the boundary a trend was apparent for positions which read consistently high or consistently low but the determination of corrections for all positions was considered unwarranted. On the line where measurements were normally taken, that is from center to center of the elements at a constant  $x$  coordinate, the average determined was







within a few percent of the spatial average. For the average boundary shear stress determined from a number of point velocities the effect of tube position is therefore considered to be small.

With the smallest size Preston tube the variation of differential pressure with position on the largest roughness was less than that with the pitot static tube. Although the elevation of the geometric centers of these tubes was the same, the Preston tube had a smaller tube thickness which may account for some of the difference. The static pressure was measured at a different point with a screw-driver probe when using the Preston tubes and this may also have been a factor. In any case, the Preston tube readings were treated as if independent of position with respect to the roughness elements.

With the larger Preston tubes the effective tube centers are further removed from the effect of individual roughness elements and dependence on position was not apparent.

#### 6.4. Equivalent Roughness and Limits for the Logarithmic Velocity Equations

The constants in the logarithmic velocity equations presented in Section 2.4 are evaluated in this section. Limiting conditions of depth to roughness for use of these equations are also suggested.

The dimensionless velocity profiles with  $u/u_*$  vs.  $y/k$  were presented in Section 5.5.2 and indicated how the evaluation of the equivalent sand grain roughness  $k_s$  is performed. Prior to evaluating  $B$ , it must be determined if flow conditions are in fact fully rough



for that portion of the channel boundary from which measurements are used. This point is demonstrated in FIGURES 6-2 and 6-3. The dimensionless plot of  $u/u_*$  vs.  $yu_*/\nu$  for Test 9.10 indicates that the flow at the boundary is transitional ( $u_*k_s/\nu < 70$ ) and therefore B in the equation,

$$\frac{u}{u_*} = \frac{1}{\kappa} \ln \frac{y}{k} + B \quad \dots\dots\dots 2-12$$

is not expected to be a constant. When the same data is plotted with  $u/u_*$  vs.  $y/k$  the variation in B is apparent. Without a check, this variation might be taken as experimental scatter and an average B calculated. FIGURE 6-3 indicates that the flow conditions are fully rough for Test 9.30 since all dimensionless profiles fall below the line equivalent to  $u_*k_s/\nu = 70$ . This data replotted with  $u/u_*$  vs.  $y/k$  should then indicate a constant value of B which is the case.

The B values for each test in each series were calculated for each of the profiles in the central region of the channel. Profiles near the wall and on the wall were discarded at this time due to the uncertainty of the  $u_*$  values. This is discussed in Section 6.6. The B values were calculated from the regression equations for each profile. These were averaged for a single test and then all tests in a series were averaged. For the test data presented in FIGURE 6-3, B values vary from 6.32 to 6.93 and average 6.62. The averages for each series are presented in TABLE 6-3.

Equation 2-12 can be rewritten for Nikuradse's equivalent sand grain roughness,



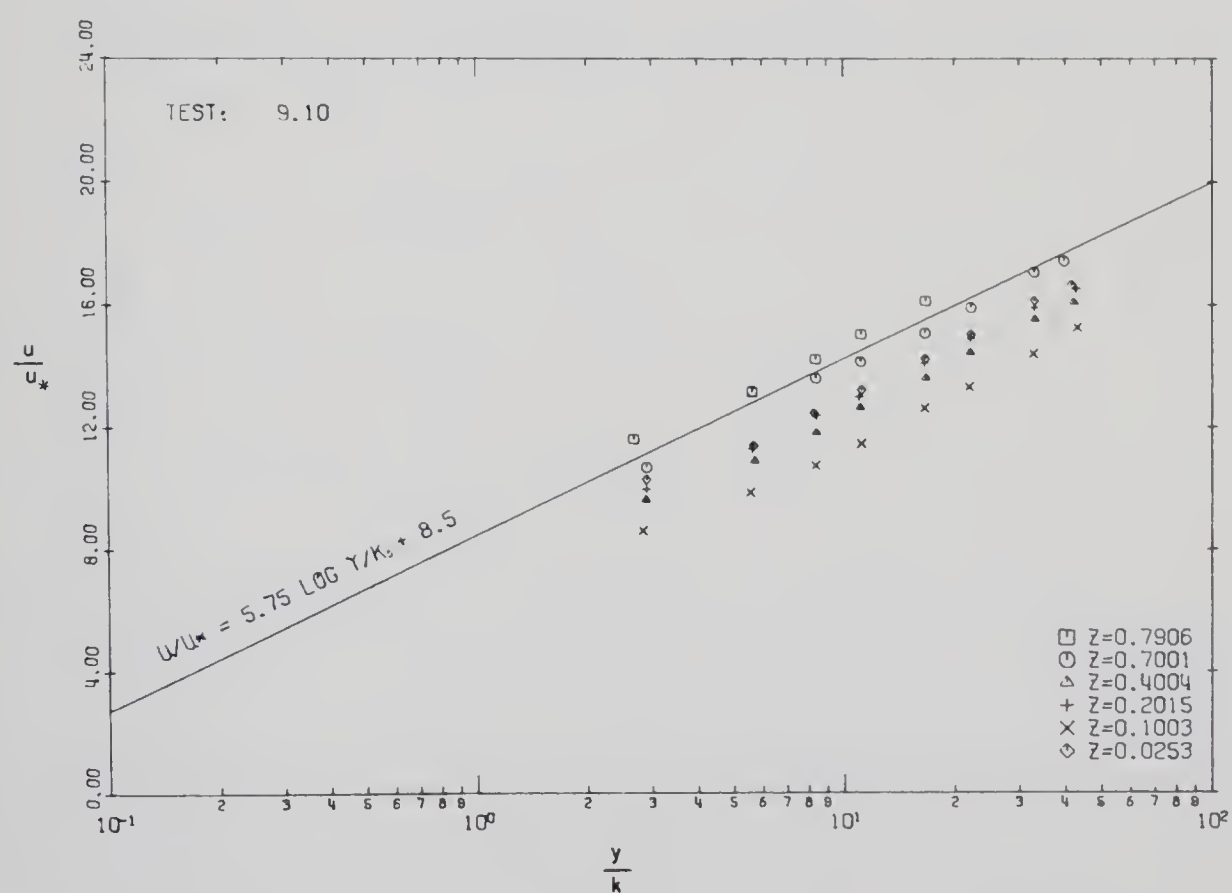
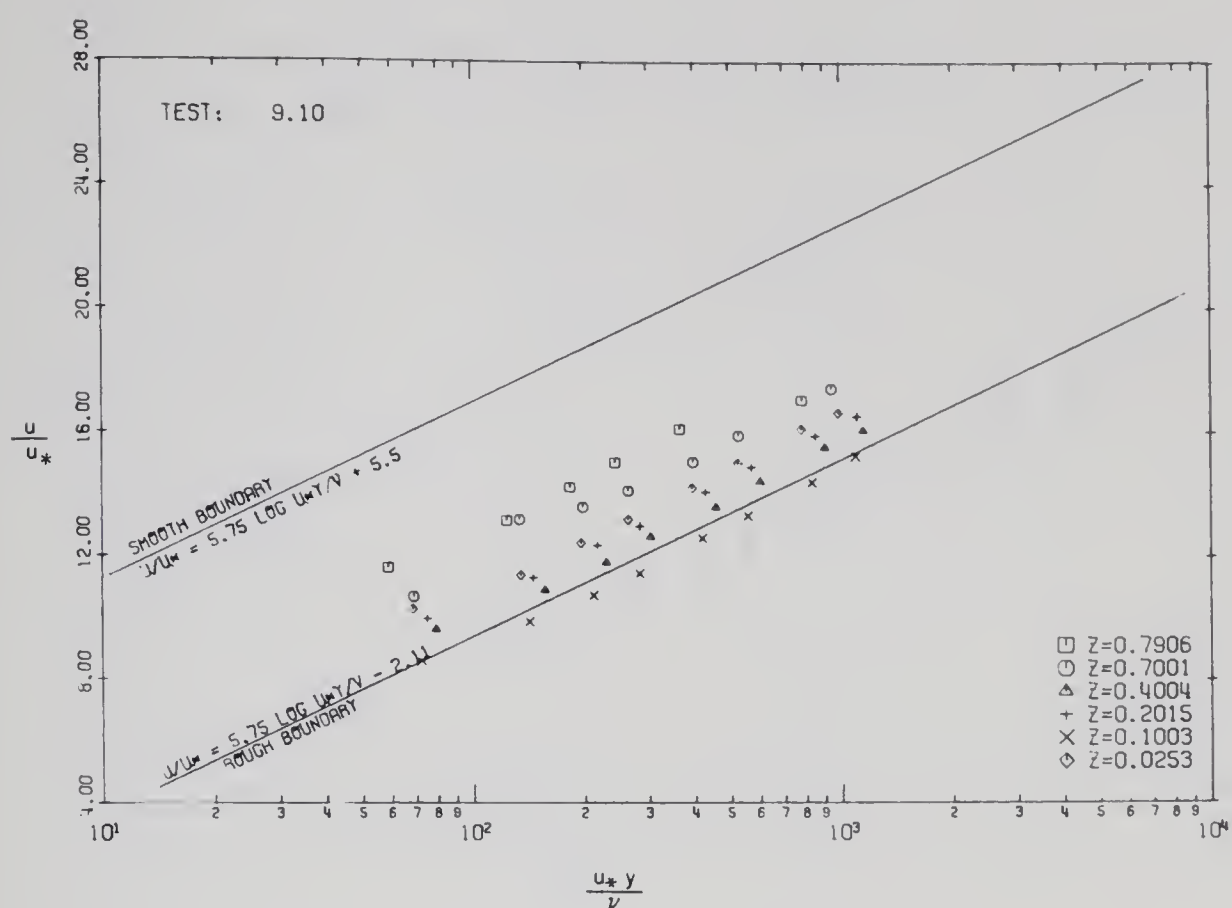


FIGURE 6-2. DIMENSIONLESS VELOCITY PROFILES



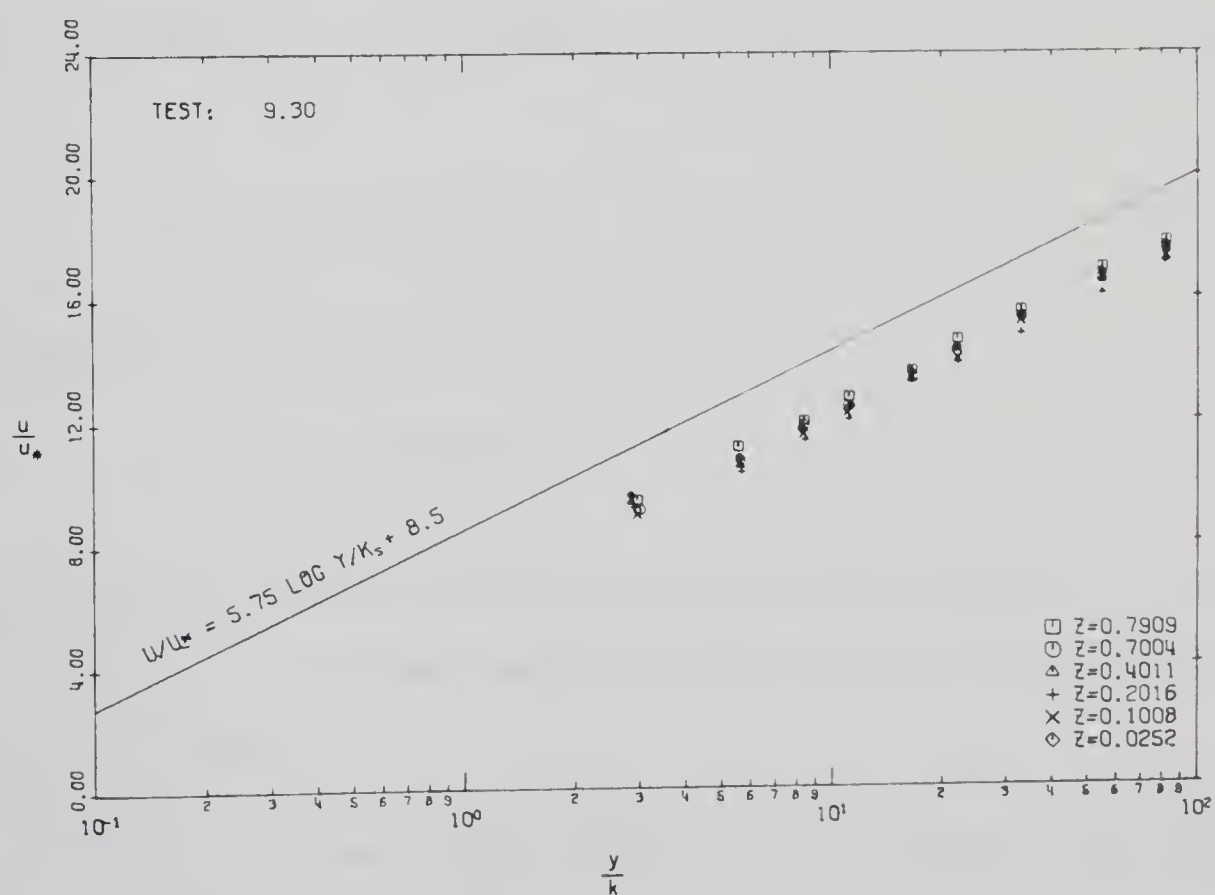
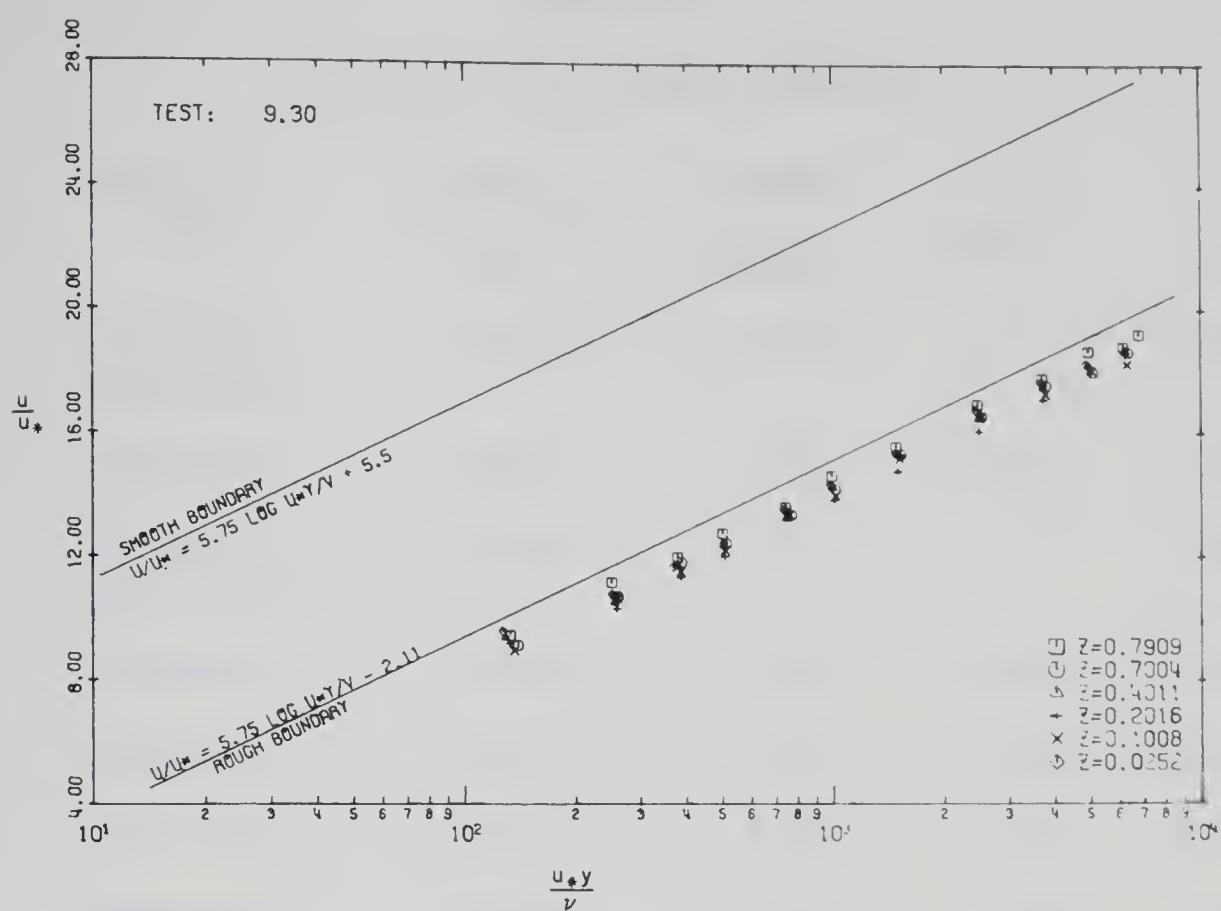


FIGURE 6-3. DIMENSIONLESS VELOCITY PROFILES





TABLE 6-3  
EQUIVALENT SAND GRAIN ROUGHNESS

Test Series	Channel Shape	Nominal Roughness feet	Average B On Bed	$k_s/k_{B_s=8.5}$	$k_s$ feet
2	Rectangular smooth walls	0.00183	5.50	3.32	0.00607
3	Rectangular	0.0415	8.50	1.00	0.0415
4	Rectangular smooth walls	0.0208	7.75	1.35	0.0281
5	Rectangular	0.00183	5.10	3.90	0.00713
6	Rectangular	0.0208	8.60	0.961	0.0200
7	Trapezoidal	0.0415	7.56	1.46	0.0606
8	Trapezoidal	0.0208	7.28	1.63	0.0339
9	Trapezoidal	0.00183	6.53	2.20	0.00402

$$\frac{u}{u_*} = \frac{1}{\kappa} \ln \frac{y}{k_s} + B_s \quad \dots\dots\dots 6-1$$

Using Equations 2-12 and 6-1 it follows that

$$\frac{k_s}{k} = e^{-\kappa(B-B_s)} \quad \dots\dots\dots 6-2$$

TABLE 6-3 presents the  $k_s/k$  ratios calculated from Equation 6-2 with  $\kappa = 0.4$  and  $B_s = 8.5$  for each series of tests and gives the equivalent sand grain roughness.

FIGURE 6-4 presents the average B values for each test versus the roughness Reynolds number  $u_*k/\nu$ . Considerable scatter exists between the average B values of tests in the same series. The tests in



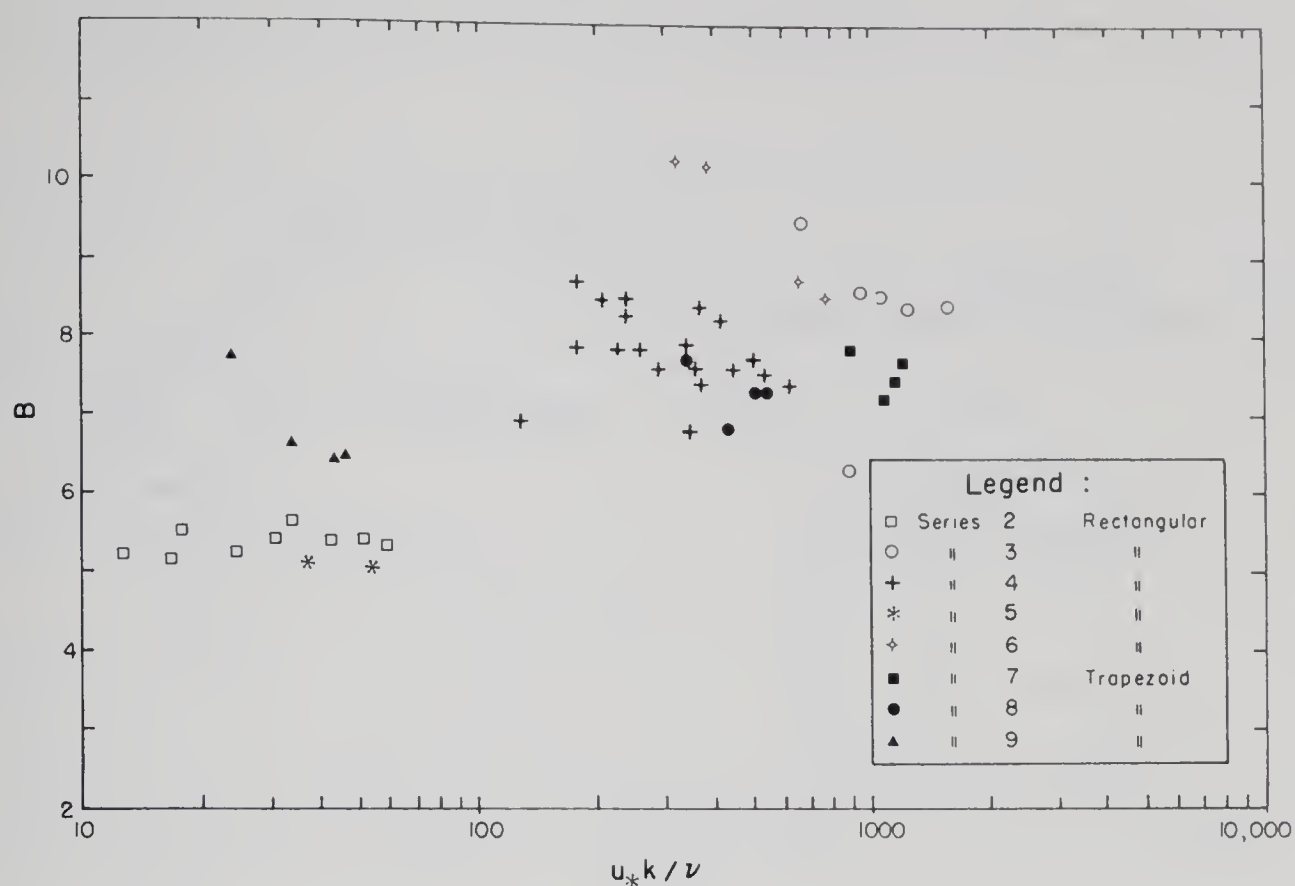


FIGURE 6-4. VARIATION OF  $B$  WITH  $u_*k/\nu$

Series 3, 6, 7 and 8 that deviate most from the respective series average all have small values of depth to roughness ratio ( $h/k < 5$ ) or large relative roughness (see TABLES C-1 to C-9). The scatter within Series 4 was expected since the  $B$  values were obtained from only one velocity profile. The high point in Series 9 is a result of transition flow at the boundary.

The data shown in FIGURE 6-4 is replotted in FIGURE 6-5 adjusted to equivalent sand grain roughness using the ratios of  $k_s/k$  presented in TABLE 6-3. Nikuradse's Equations 2-13 to 2-19 for  $B_s$  in terms of  $u_*k_s/\nu$  were used to plot the line shown.



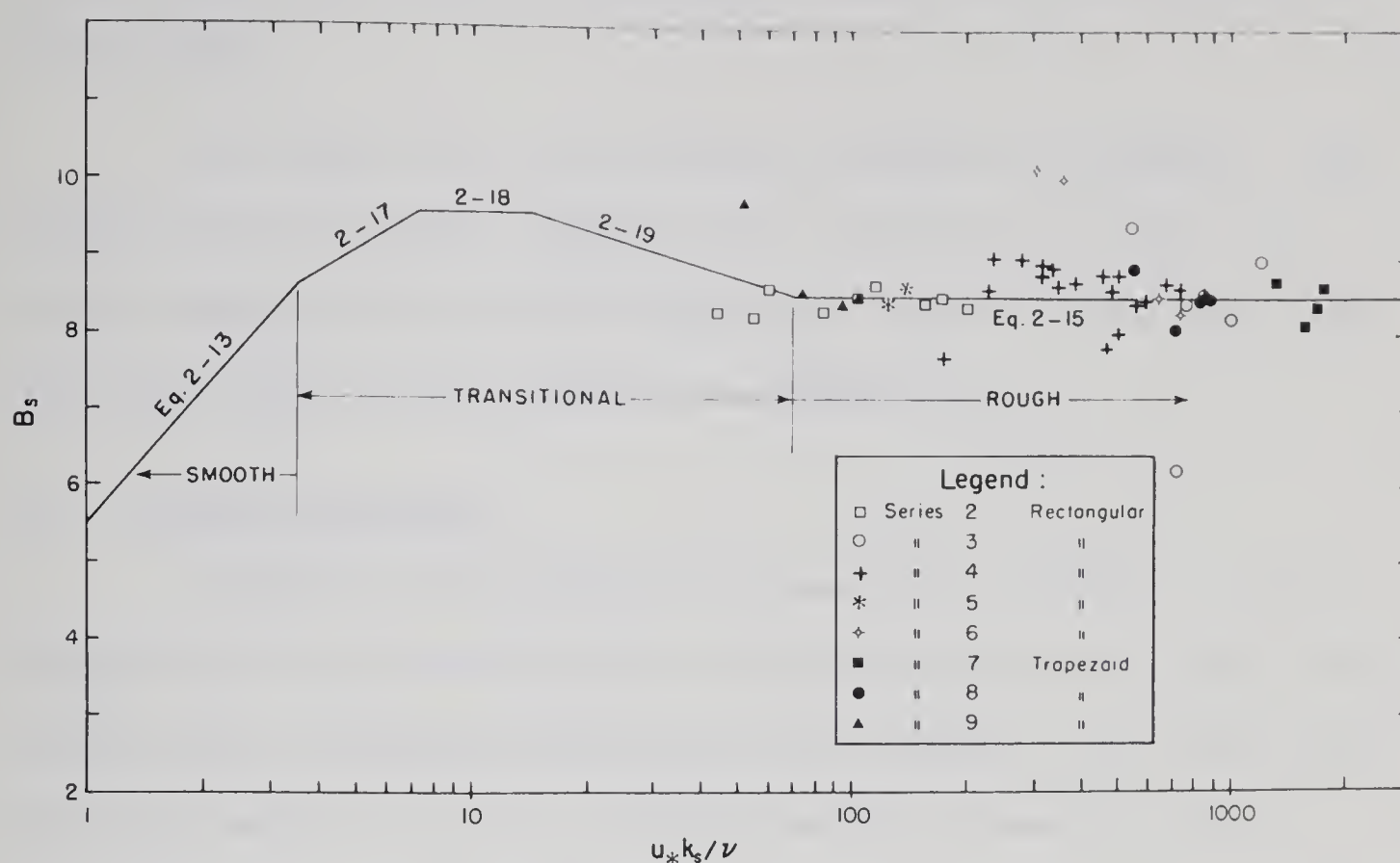


FIGURE 6-5. VARIATION OF  $B_s$  WITH  $u_* k_s / \nu$ , NIKURADSE'S EQUIVALENT SAND GRAIN ROUGHNESS

The difference in the  $k_s/k$  ratios for different series with the same nominal roughness can only be accounted for if channel shape, or wall roughness have an effect on the flow within the central portion of the channel. This is discussed in Sections 6.5 and 6.6. If the  $k_s/k$  ratios are averaged for each of the nominal roughnesses they indicate values of 3.1 for the #36 paper, 1.3 for the 1/2 inch hemispheres and 1.2 for the 1 inch hemispheres. These are equivalent to values of 3.1 D for the #36 paper and about 0.65 D for the hemispheres. Although the hemispheres were to be geometrically similar, the smaller size had larger surface roughness because the mould was left unpolished. This might account for the slightly higher ratio of  $k_s/k$ . The hemisphere



results agree with those of Schlichting (1936) and Einstein and El-Samni (1949).

The large ratio of  $k_s/k$  for the #36 paper was expected. The grains were very angular compared with sand grains and many of the grains appeared to have a long axis nearly twice the sieve size with this axis normal to the boundary (see FIGURE 4-1).

### 6.5. Channel Resistance

A friction factor diagram is presented in FIGURE 6-6. This diagram is of the Moody form with the friction factor  $f = 8gRS/V^2$  the ordinate and the Reynolds number  $4RV/\nu$  the abscissa. Four times the hydraulic radius was used to form the Reynolds number for direct comparison with the original diagram prepared for pipes. The indicated smooth boundary line was calculated from the Blasius equation for  $Re < 10^5$ ,

$$f = \frac{0.316}{Re^{1/4}} \dots\dots\dots 6-3$$

and from the Von Karman friction factor equation for  $Re > 10^5$ ,

$$\frac{1}{\sqrt{f}} = 2.0 \log \left( \frac{Re\sqrt{f}}{2.5} \right) \dots\dots\dots 6-4$$

For the fully rough region of the diagram, values of  $f$  have been calculated for a few values of the relative roughness  $R/k_s$  using the equation

$$\frac{1}{\sqrt{f}} = 2 \log \left( \frac{12R}{k_s} \right) \dots\dots\dots 6-5$$

This equation is recommended for use by the ASCE Task Force on Friction





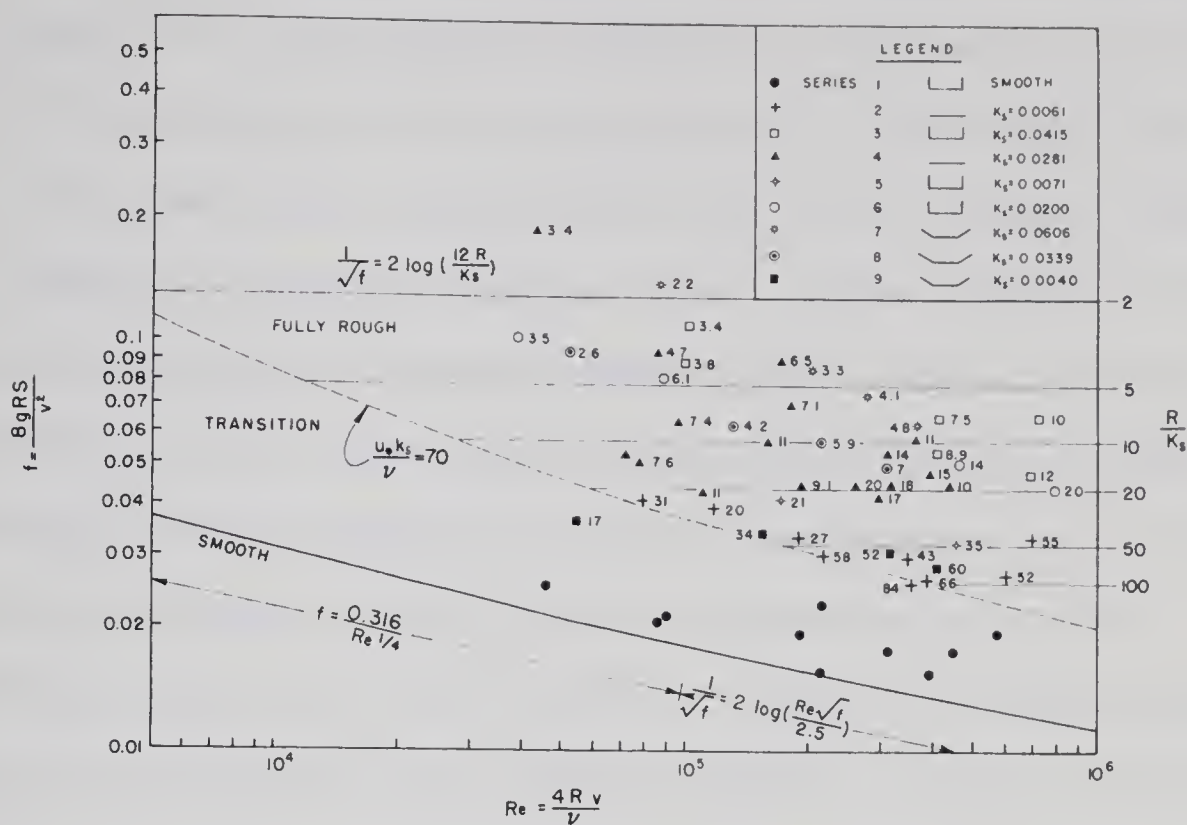


FIGURE 6-6. FRICTION FACTOR DIAGRAM

Factors in Open Channels (1963) and follows from the work of Keulegan (1938). The limit for the fully rough to transition regions is at  $u_* k_s / \nu = 70$  as suggested by Nikuradse. Within the transition region the friction factor can be evaluated using Nikuradse's Equations 2-13 to 2-19 or by using the modified Colebrook type of equation (ASCE Task Force, 1963)

$$\frac{1}{\sqrt{f}} = -2 \log \left( \frac{k_s}{12R} + \frac{2.5}{Re\sqrt{f}} \right) \quad \dots\dots\dots 6-6$$

This equation is suggested for surfaces such as wood, metal or concrete. Other values for the constants in this equation have been suggested depending on the channel shape and aspect ratio.



The data presented in FIGURE 6-6 are contained in TABLES C-1 to C-9. Values of  $k_s$  were taken from TABLE 6-3. The channel shape and portion of the boundary covered by roughness are indicated in the legend. The numeric given beside each point is the relative roughness  $R/k_s$ . FIGURE 6-6 indicates that the Series 1 tests were not in fact hydraulically smooth as defined by Equation 6-4. Most of the tests fall within the fully rough region of the friction factor diagram. The experimental results compared with the solution of Equation 6-5 indicate general agreement. The difference between analytical and experimental results can be attributed to variation in channel shape, variation in the portion of the channel boundary covered with roughness and a large range of aspect ratios. Experimental errors also contribute to the variability of the data. For the trapezoidal channels the friction factors tend to be lower than for rectangular channels with the same relative roughness. A small increase in the constant 12 in Equation 6-5 for trapezoidal channels would produce better agreement. This confirms the results of other investigations (ASCE Task Force, 1963).

#### 6.6. Three Dimensional Velocity Distributions

Velocity distributions were presented in Section 5.5 and detailed distributions for each test are plotted in APPENDIX D. Analysis of the data within the central region of the channel was contained in Section 6.4. In this section, the division of the wall and bed regions, and the use of the logarithmic equation in each region is discussed.



In Section 6.4 it was suggested that the shear velocities calculated from velocity profiles might be in error near the corners. This results from a set of conditions specified for the fit of the regression which does not specifically limit the zone from which measurements are taken. The minimum number of measurements was set at four in order to reduce the influence of a single measurement in error and this entailed a considerable minimum distance. On normals to the bed, velocities at a considerable distance from the bed were often included in the regression for extremely small wall distances. A similar situation occurs for normals to the wall near the bed. Many examples are apparent in the figures presented in APPENDIX D. Intuitively, it is unlikely that a velocity at 0.1 feet from the bed and on the wall should be included in the calculation of shear at the bed. As an example in Test 3.60 (FIGURE D-3) for  $z = 0.0216$  feet, if only the two points nearest the bed were used the resulting shear velocity would be considerably less. Similarly for the wall, with  $y = 0.0216$  feet the regression line extended to 0.5 feet whereas it should have been restricted to the zone near the wall. The shear velocities calculated from velocity profiles were compared with the results from Preston tubes and were found to be consistently higher in these corner regions. This comparison is fully discussed in Section 6.10. For the rectangular channels, if the normal distance for measurements included in the regression is limited to the distance from the adjacent boundary then the agreement of the resulting shear velocities with the Preston tube results improves.





The validity of the logarithmic velocity equation (Equation 2-12) is clearly demonstrated for the regions away from the corner and free surface of the channel by the dimensionless velocity plots presented in APPENDIX E. FIGURES E-1 to E-6 were constructed by removing the dimensionless profiles near adjacent boundaries and plotting the entire series on one figure. The bed normals are limited to  $z > 0.1$  feet and wall normals to  $(h-0.1) > y > 0.1$  feet in FIGURES E-1 to E-6. The variation in B values is greatly reduced from the case where all profiles are included. This also indicates probable error in the calculated shear velocities near the corners.

If the shear velocities from the Preston tube measurements are used rather than those calculated from velocity profiles, the variation in B is reduced further. FIGURE 6-7 shows all of the dimensionless profile data for normals to both the bed and the walls for Test 3.60, except the profile normal to the wall at the free surface. These same profiles are replotted in FIGURE 6-8 with  $u_*$  taken from the Preston tube measurements of Test 3.61. Using  $u_*$  from velocity profiles, B in Equation 5-1 averages 7.3 and has a standard deviation of 1.2 whereas using  $u_*$  from the Preston tube measurements, B averages 8.7 and the standard deviation is only 0.4. The average value of B determined in the central region of the channel for the series as a whole was 8.50. The data shown in FIGURE 6-8 indicates an A value of about 6.0 ( $\kappa = 0.385$ ) for the logarithmic velocity equation rather than 5.75. Test 3.60 is typical of the tests on rectangular channels.





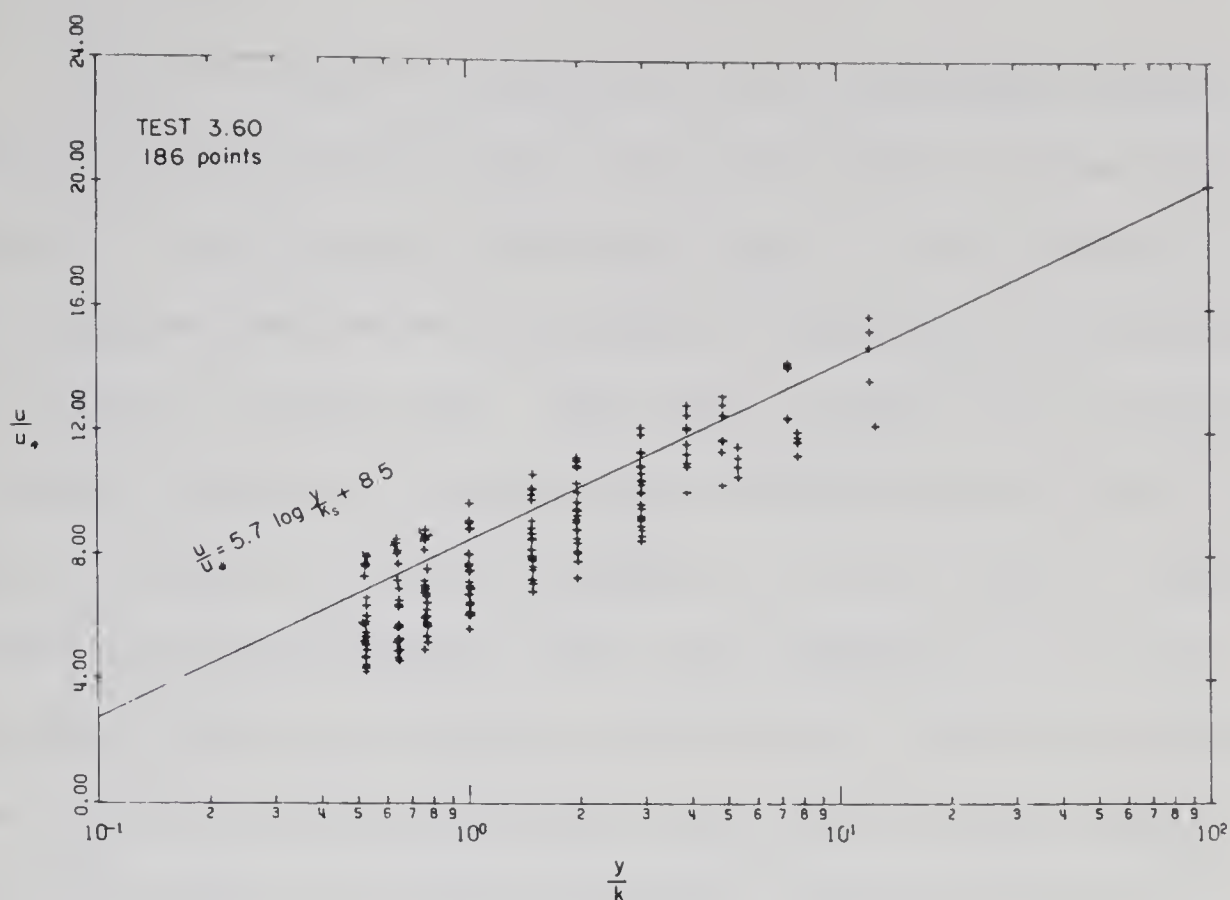


FIGURE 6-7. DIMENSIONLESS VELOCITY PROFILES,  
 $u_*$  FROM EQUATION 2-20,  $A = 5.75$

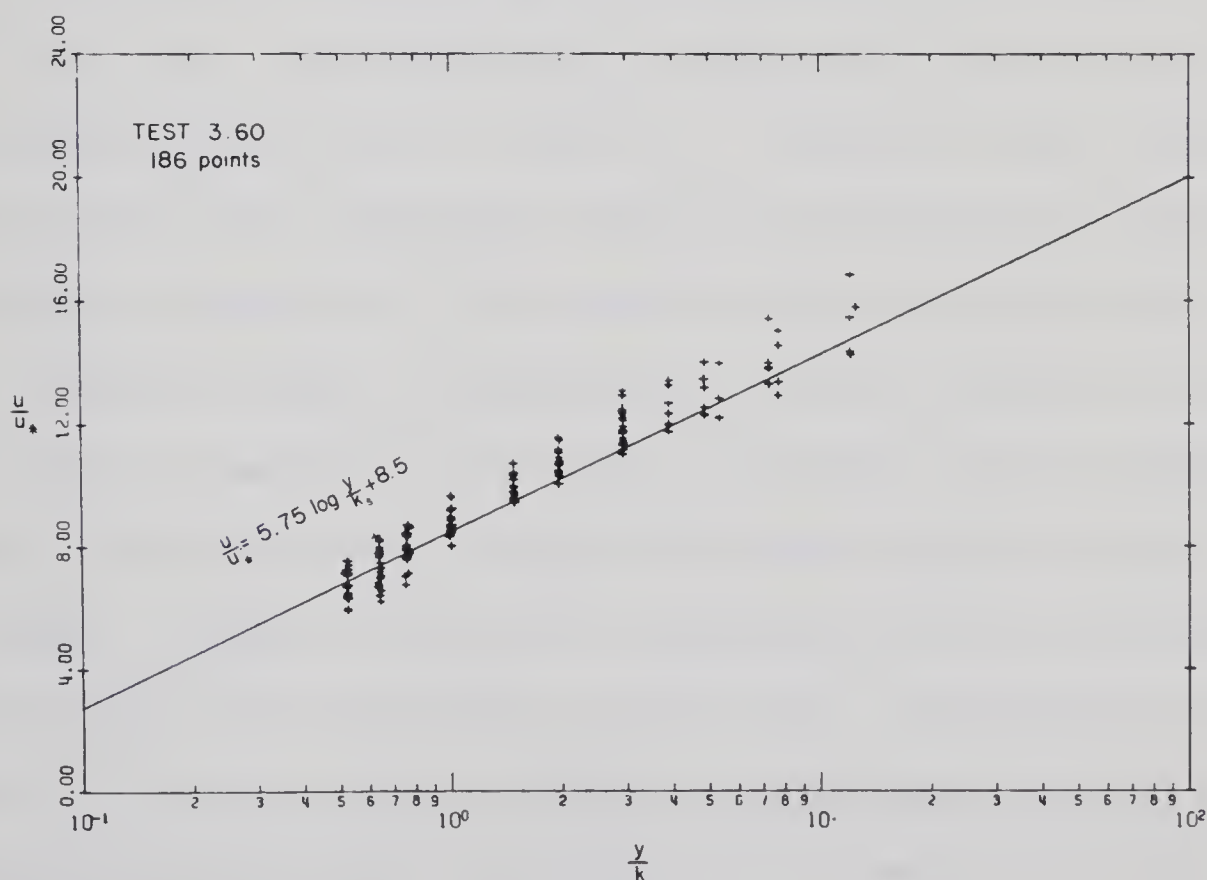


FIGURE 6-8. DIMENSIONLESS VELOCITY PROFILES,  
 $u_*$  FROM PRESTON TUBE MEASUREMENTS



The same situation is apparent for the trapezoidal channels. Because of the large obtuse angle, the corner effects are much less apparent. If the bisector of the corner angle is used to limit the normal distance from the bed from which the regression is determined, then  $y < 4.23 \times z$  is the limit. This limit is much less restrictive than for the rectangular channels where the corner angle bisector was suggested. Using Test 8.40 as an example, only the first  $u_*$  value at the corner would be affected by this limit (FIGURE D-8). The two measurements nearest the boundary at the corner, both for the wall and the bed, would obviously give smaller values for the local shear velocity and these are in better agreement with the Preston tube measurements.

The average B value in the central portion of the channels in Series 8 was 7.28. The dimensionless profiles with equivalent sand grain roughness are plotted in FIGURE E-4. The use of shear velocities from the Preston tube measurements reduces the variation of B and shows the validity of Equation 2-12 for normals to both the bed and the walls. FIGURE 6-9 shows the dimensionless velocity profiles for Test 8.40 for both the bed and the wall with  $u_*$  calculated from the velocity profiles. The profile normal to the wall nearest the free surface is not included. FIGURE 6-10 shows the same profiles with  $u_*$  calculated from the Preston tube measurements of Test 8.41. The variation of B is reduced. For the data shown in FIGURE 6-9, B averages 6.90 with a standard deviation of 0.76. In FIGURE 6-10, B averages 6.92 with a standard deviation of 0.36. The data in FIGURE 6-10 indicates an increase in A to about 6.0.



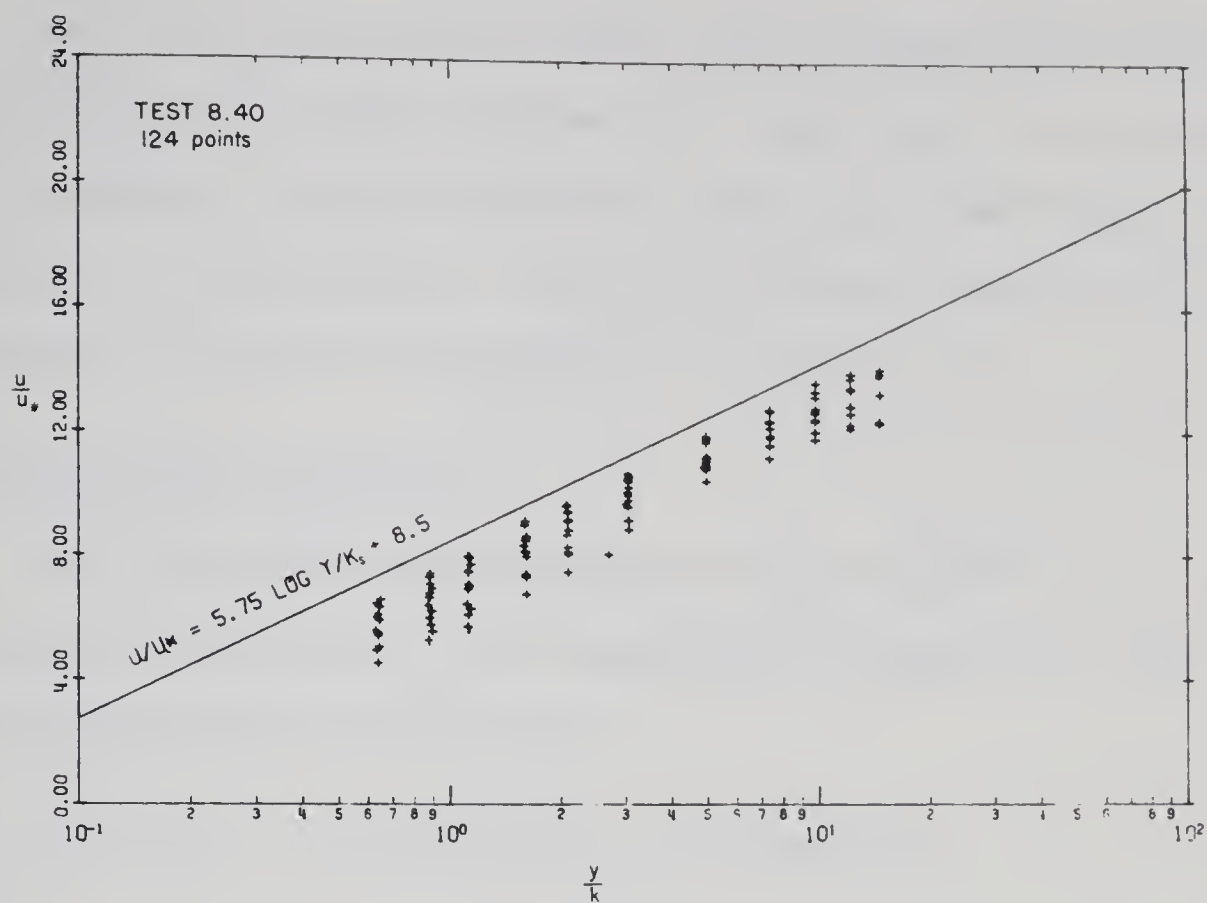


FIGURE 6-9. DIMENSIONLESS VELOCITY PROFILES,  
 $u_*$  FROM EQUATION 2-20,  $A = 5.75$

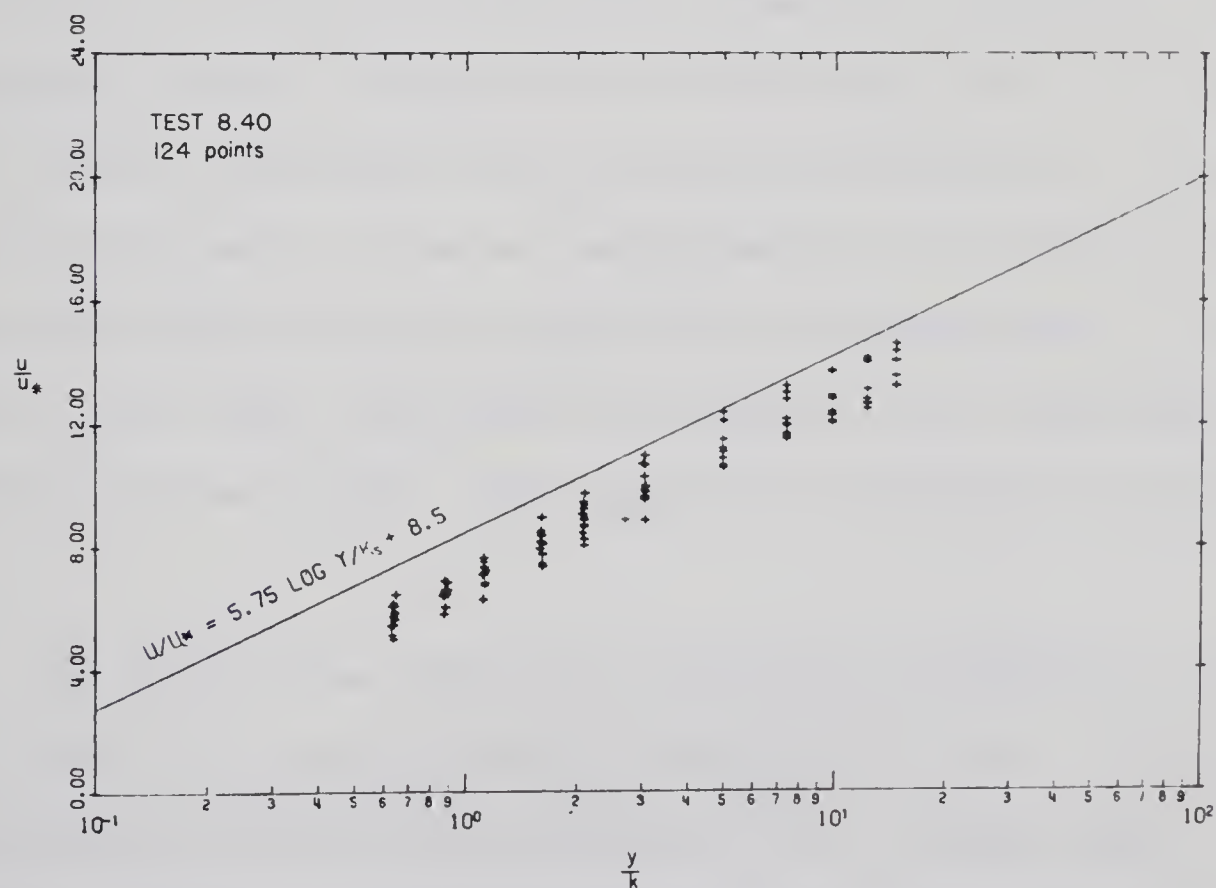


FIGURE 6-10. DIMENSIONLESS VELOCITY PROFILES,  
 $u_*$  FROM PRESTON TUBE MEASUREMENTS



The analysis presented in this section suggests that the use of Equation 2-12 with a single constant B for fully rough flow will provide the complete velocity distribution except for a small region near the wall at the free surface. This will be further discussed after presentation of the shear distributions in Section 6.10.

### 6.7. Preston Tube Calibration

The Preston tube technique for measuring boundary shear stress was outlined in Section 2.5. The experimental equipment for this method was described in Section 4.7.

Evaluation of the parameters in the equation,

$$\frac{\Delta p}{\tau_0} = f \left( \Delta p_*, \frac{d}{k} \right) \quad \dots\dots\dots 2-31$$

was carried out for each test in order to provide a calibration. Only measurements from the central portion of the channel where two dimensional flow was predominant were used for this calibration. The value of shear stress used, was the one calculated from the velocity profile at the same boundary location as the Preston tube measurement. These values of local shear stress were also compared to the value determined from the shear meter. This comparison is presented in Section 6.8.

The Preston tube calibrations are given in FIGURES 6-11 and 6-12. FIGURE 6-11 shows the results from Series 2, and 9. The calibration includes different  $d/k_s$  values each with a unique symbol. Similarly, FIGURE 6-12 shows the results of the Preston tubes on the





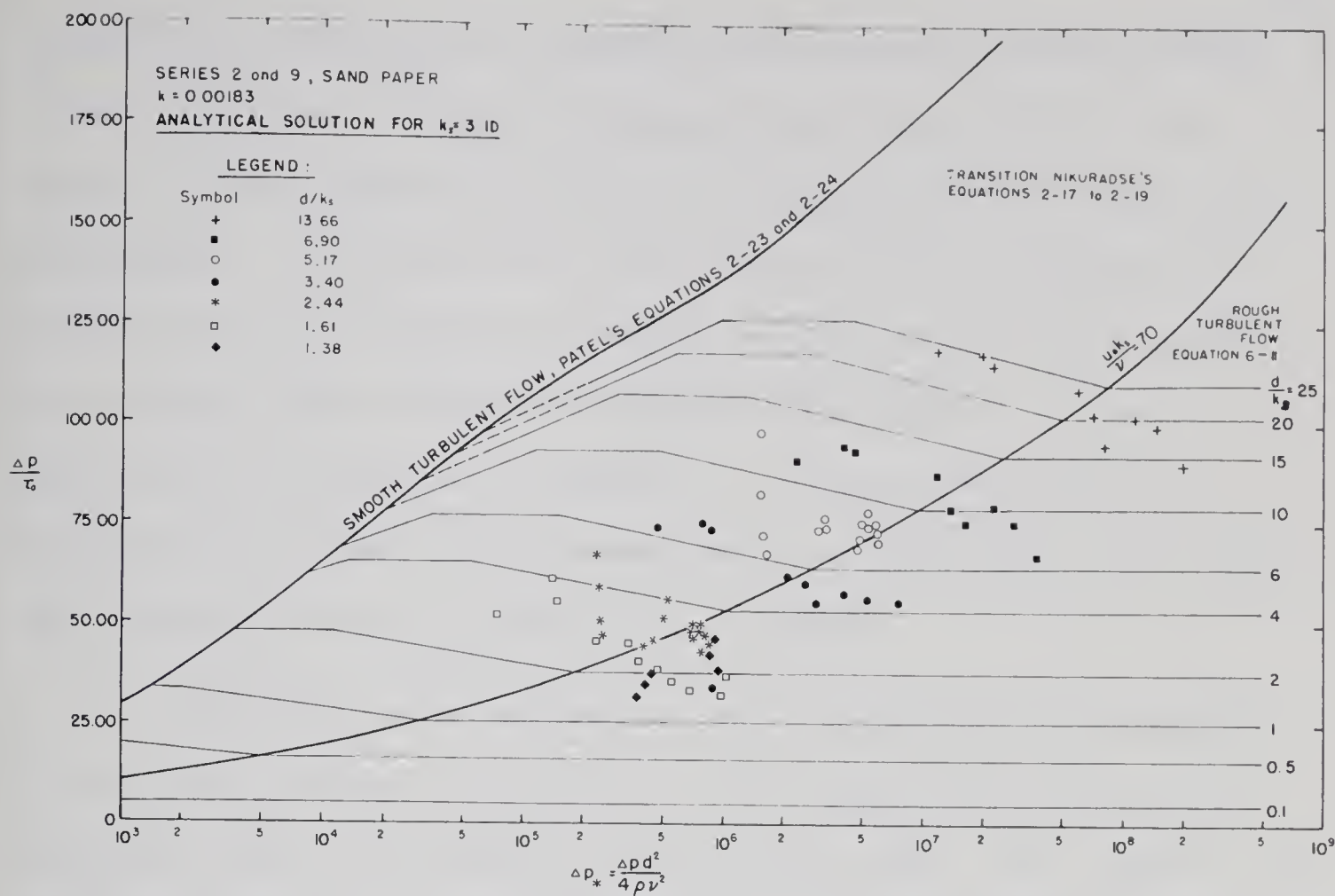


FIGURE 6-11. PRESTON TUBE CALIBRATION WITH ANALYTICAL SOLUTION

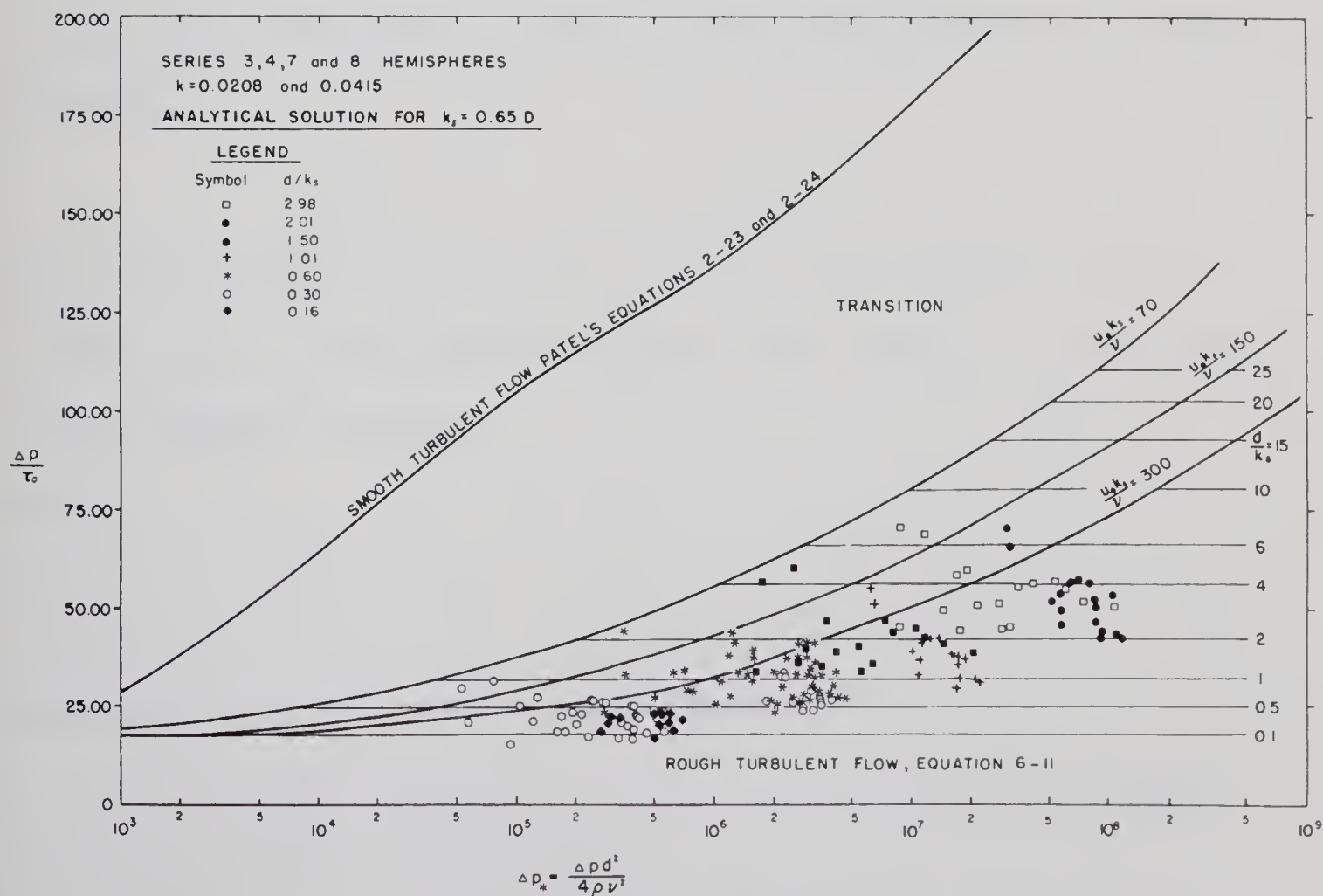


FIGURE 6-12 PRESTON TUBE CALIBRATION WITH ANALYTICAL SOLUTION



hemispherical roughnesses. A number of  $d/k_s$  values have been grouped in this figure and assigned an average value. The solid lines presented in these figures are an analytical solution which is described subsequently. The points for a given value of  $d/k_s$  were fitted with curves by eye to provide the necessary calibration from which Preston tube readings were converted to boundary shear stress. A detail calculation is presented in APPENDIX B. It was assumed that the calibration performed in the predominantly two dimensional flow region was applicable over all regions of the boundary.

The Preston tube calibration can be estimated by assuming that the measured pressure is equivalent to the stagnation pressure at an elevation equal to the geometric center of the tube. This neglects the wall displacement, the shear displacement, and the turbulence effects on the tube. The geometric center of the boundary tube is at a normal distance

$$y = \frac{d}{2} + y' \quad \dots\dots\dots 6-7$$

where  $d$  is the tube diameter and  $y'$  is the datum location discussed in Section 6.1. For the roughnesses used in this study  $y' = 0.2D$ , where  $D$  is the roughness diameter.

$$\text{With} \quad \Delta p = \frac{1}{2} \rho u^2 \quad \dots\dots\dots 6-8$$

$$\text{and} \quad \tau_o = \rho u_*^2 \quad \dots\dots\dots 6-9$$

the pressure to shear ratio can be written

$$\frac{\Delta p}{\tau_o} = \frac{1}{2} \left( \frac{u}{u_*} \right)^2 \quad \dots\dots\dots 6-10$$



Equation 6-10 can be evaluated using Equations 2-13 to 2-19.

For the fully rough region, defined by Nikuradse as  $u_* k_s / \nu \geq 70$ , Equation 2-16 can be used with Equations 6-10 and 6-7 such that,

$$\frac{\Delta p}{\tau_o} = \frac{1}{2} \left[ 5.75 \log \frac{1}{k_s} \left( \frac{d}{2} + y' \right) + 8.5 \right]^2 \quad \dots \quad 6-11$$

This is similar to the expression presented by Hwang and Laursen (1963) given as Equation 2-35. It replaces the integral by using the pressure at the geometric center which makes the use of the tube thickness unnecessary. Equations 2-35 and 6-11 have been evaluated for each of the experimental test conditions with  $y' = 0.2D$  and the results are compared with the measured values in TABLE 6-4. The values of  $k_s$  are taken from TABLE 6-3. These results are plotted in FIGURE 6-13. The comparison shows estimated and measured values agree fairly well with the exception of Series 6 and Test 2 in Series 9. Generally the estimates are low and those from Equation 2-35 are lower than those from Equation 6-11.

The measured results in TABLE 6-4 are replotted in FIGURE 6-14 without the Series 6 and 9 tests which were suspected of transducer calibration error. This figure shows the variation of  $\Delta p / \tau_o$  with  $d / k_s$  in the fully rough region. The curves presented were calculated from Equation 6-11. This figure shows a small difference in estimates for two values of  $k_s / D$  with  $y'$  fixed at  $0.2D$ . The values selected for  $k_s / D$  are the average value for hemispheres 0.65 and the average for grain roughness 3.1 (see TABLE 6-3).



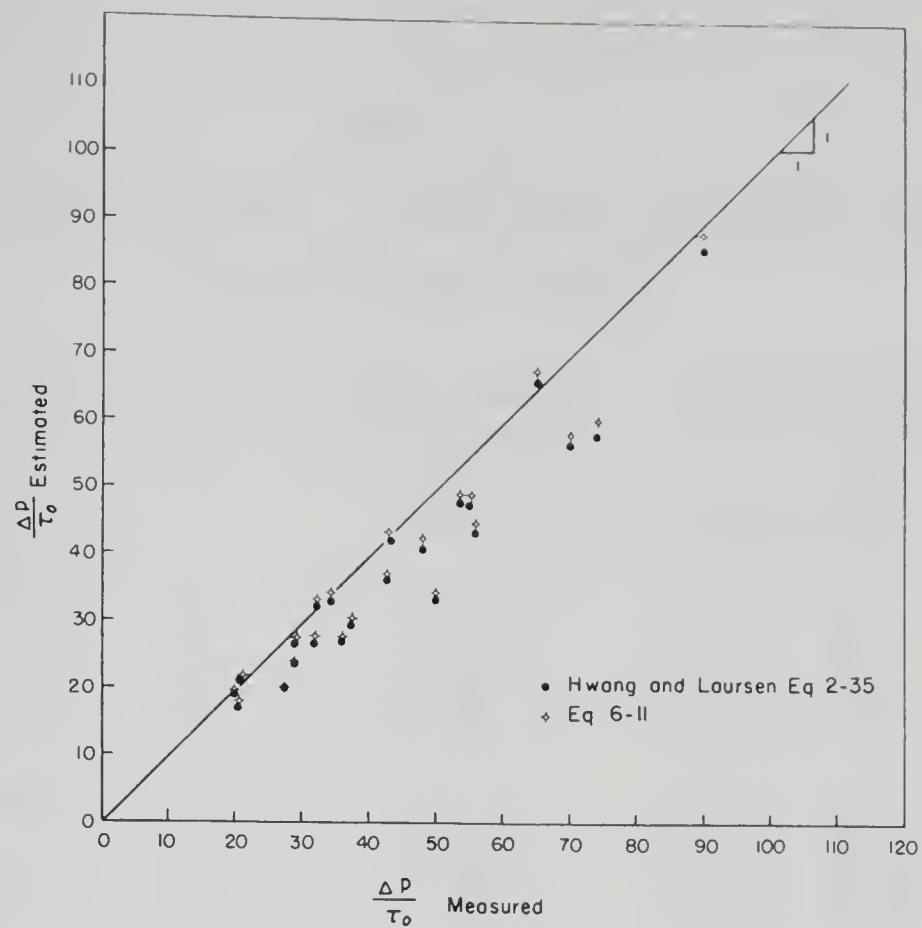


FIGURE 6-13. COMPARISON OF ESTIMATED AND MEASURED PRESSURE: SHEAR RATIOS

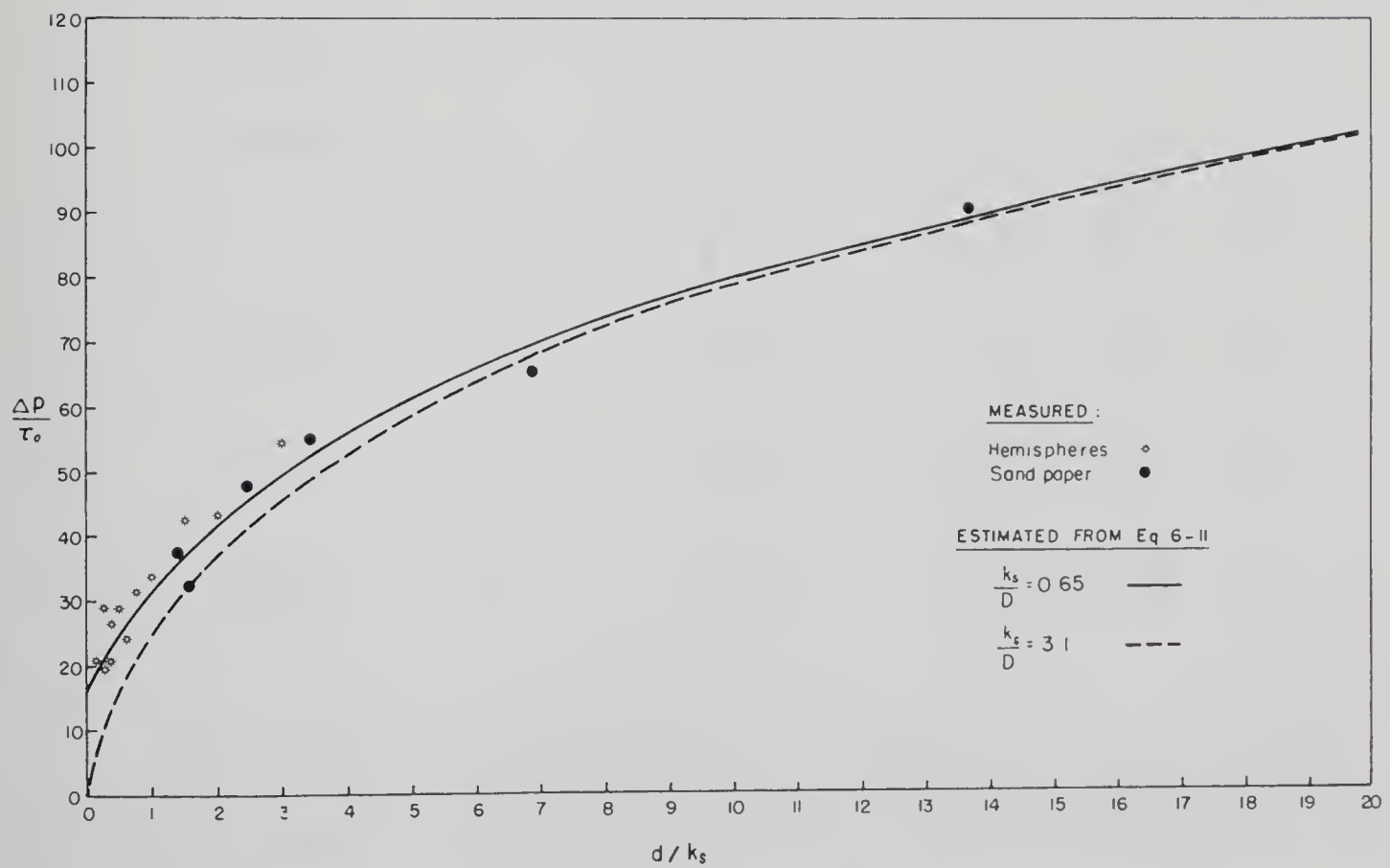


FIGURE 6-14. VARIATION OF  $\Delta p/\tau_0$  WITH  $d/k_s$





TABLE 6-4  
COMPARISON OF PRESSURE : SHEAR RATIOS FOR PRESTON TUBES  
ON FULLY ROUGH BOUNDARY

Series	Equivalent Roughness Size $k_s$ ft.	Preston Tube	Tube Diameter to Roughness Ratio $d/k_s$	Pressure : Shear Ratio $\Delta p/\tau_0$		
				Est. Eq.2-35	Est. Eq.6-11	Measured
2	0.0061	1	1.61	32.9	33.1	32.0
		2	3.40	47.7	49.1	55.0
		3	6.90	66.0	67.6	65.0
		4	13.66	86.3	88.6	90.0
3	0.0415	1	0.24	23.4	23.4	29.0
		2	0.50	27.4	27.5	29.0
		3	1.01	33.8	34.0	34.0
		4	2.01	43.0	43.6	43.0
4	0.0281	1	0.35	21.7	21.7	20.9
		2	0.74	27.7	27.8	31.7
		3	1.50	36.5	36.9	42.8
		4	2.97	48.4	49.3	54.2
5	0.0071	1	1.38	29.8	30.0	37.2
6	0.0200	1	0.49	27.7	27.7	36.0
		2	1.04	34.3	34.5	50.0
		3	2.10	44.1	44.6	56.0
		4	4.17	57.0	58.0	70.0
7	0.0606	1	0.16	17.4	17.4	20.8
		2	0.34	20.9	20.9	27.3
8	0.0339	1	0.29	18.7	18.7	20.7
		2	0.34	20.9	20.9	27.3
9	0.0040	1	2.44	41.7	42.0	47.9
		2	5.17	58.1	60.0	73.6

The analytical lines presented in FIGURES 6-11 and 6-12 were calculated using the equations and limits presented in Sections 2.4 and 2.5. The constant values of  $\Delta p/\tau_0$  in the fully rough region were



calculated using Equation 6-11 and have already been discussed. The difference between the two figures is apparent at the lower values of  $d/k_s$  and results from the use of different values of  $k_s/D$ . FIGURE 6-11 was constructed for the grain roughness with an average value of  $k_s/D = 3.1$  as compared to  $k_s/D = 0.65$  for the hemispheres in FIGURE 6-12. Lines indicating the lower limit of rough turbulent flow were calculated by substituting the limit  $u_* k_s/\nu = N$  into  $\Delta p_*$  such that,

$$\Delta p_* = \frac{1}{4} N^2 \frac{\Delta p}{\tau_o} \left( \frac{d}{k_s} \right)^2 \quad \dots\dots\dots 6-12$$

In FIGURE 6-11 this limit was set at  $N = 70$  as suggested by Nikuradse for sand grain roughness. Several values of  $N$  are indicated on FIGURE 6-12. The curves shown in the transition region of FIGURE 6-11 were calculated using,

$$\frac{\Delta p}{\tau_o} = \frac{1}{2} \left[ 5.75 \log \frac{1}{k_s} \left( \frac{d}{2} + y' \right) + B_s \right]^2 \quad \dots\dots 6-13$$

which is the form of Equation 6-11 into which Nikuradse's transition Equations 2-17, 2-18 and 2-19 can be substituted. The limiting values are determined by using Equation 6-12. The smooth boundary curve indicated on each of the figures was calculated using Patel's Equations 2-22, 2-23 and 2-24. Although the smooth boundary curve of Patel does not coincide identically with the limiting value of Nikuradse's transition curves at  $N = 3.5$ , the agreement is sufficient to show the trend. Those transition curves that crossed the smooth boundary curve in the lower portion of the figure ( $\Delta p_* < 10^4$ ) were terminated at Patel's curve.



The experimental data of Hwang and Laursen (1963) and Bursali (1970) are presented along with the analytical solution in FIGURE 6-15. This data also shows agreement in the fully rough region.

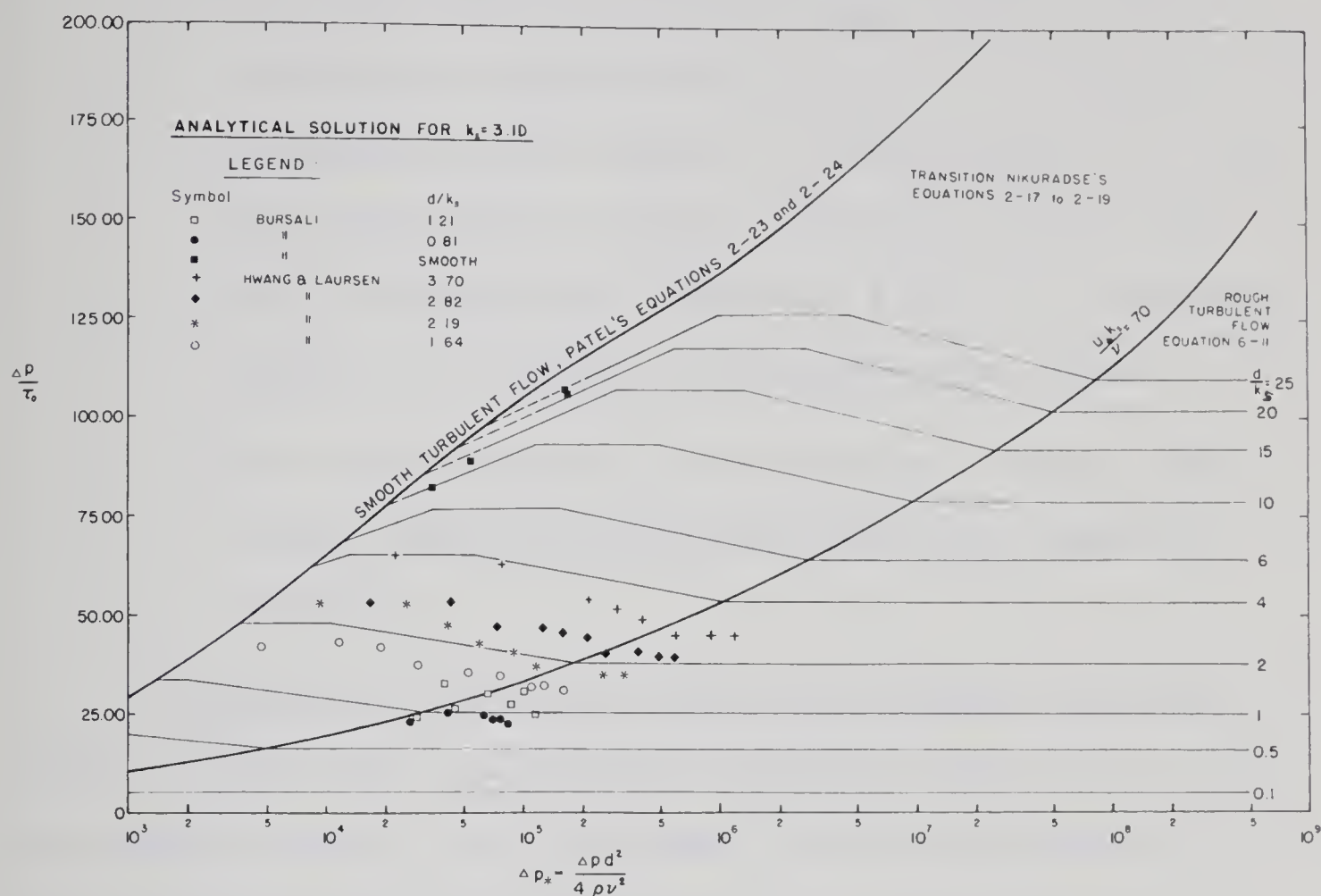


FIGURE 6-15. PRESTON TUBE CALIBRATION ANALYTICAL SOLUTION WITH OTHER EXPERIMENTAL DATA

The experimental data presented in FIGURES 6-11, 6-12 and 6-15 exhibit the following characteristics:

1. For large values of the roughness Reynolds number the measurements agree with the analytical solution developed using the logarithmic velocity equation to calculate the pressure at the geometric center of the Preston tube.



2. All data show an increase in the pressure-shear stress ratio as the dimensionless pressure decreases below some value of  $\Delta p_*$ .
3. The lower limit of the constant  $\Delta p/\tau_0$  region cannot be defined by a constant value of  $u_* k_s/\nu$ . For the grain roughness the limit appears to vary from about 70 to 200. The larger tube to roughness ratios have higher limits. For the hemispherical roughnesses a limit of around 300 appears to be useable for the smaller  $d/k_s$  values.
4. The increase in  $\Delta p/\tau_0$  in the transition region is much larger than that estimated from Nikuradse's transition equations.

Although the Preston tube calibrations display considerable scatter and the limits are apparently dependent on tube size as well as roughness geometry, it is considered to be an improvement on the use of a calculated constant value for  $\Delta p/\tau_0$  without regard for the possibility of approaching transition conditions. Some experimenters (Ghosh, 1970) have calculated a constant pressure shear ratio from a friction factor for the entire channel and then proceeded to use this value to determine the distribution of local boundary shear stress. Many of the measurements were made near corners where transitional flow conditions certainly prevailed. The usefulness of the Preston tube measurements are further discussed in the following sections where comparisons are made with other methods.







#### 6.8. Comparison of Methods of Measuring Boundary Shear Stress at the Channel Centerline

Methods of measuring shear stress were developed in CHAPTER II. The experimental equipment was described in CHAPTER IV. This section presents a comparison of the results obtained on the channel centerline by each method employed.

FIGURE 6-16 presents a comparison of boundary shear stress determined by the various methods. All test data in Series 1 to 4 are included in this figure. The abscissa in FIGURE 6-16 is the wide-channel value of shear stress calculated from slope and depth. The ordinate values are shear stresses calculated from the velocity profiles at the channel centerline or from the direct shear meter measurements at the channel centerline. The data presented in this figure are contained in APPENDIX C. The complete shear stress distributions for Series 5 to 9 are presented in the following section so have been excluded from this comparison.

If it is assumed that the maximum boundary shear stress is at the channel centerline, then for a wide channel the local value should be nearly equivalent to the value  $\gamma h S$ . Subsequent sections indicate that this assumption is not entirely valid. In FIGURE 6-16 the values calculated from velocity profiles agree reasonably well with the wide-channel values. For Series 1 tests, with the smooth boundary, shear meter alignment was simple and the results agree with the other methods. The shear meter results are consistently higher for Series 2 except for Test 2.9 which is in



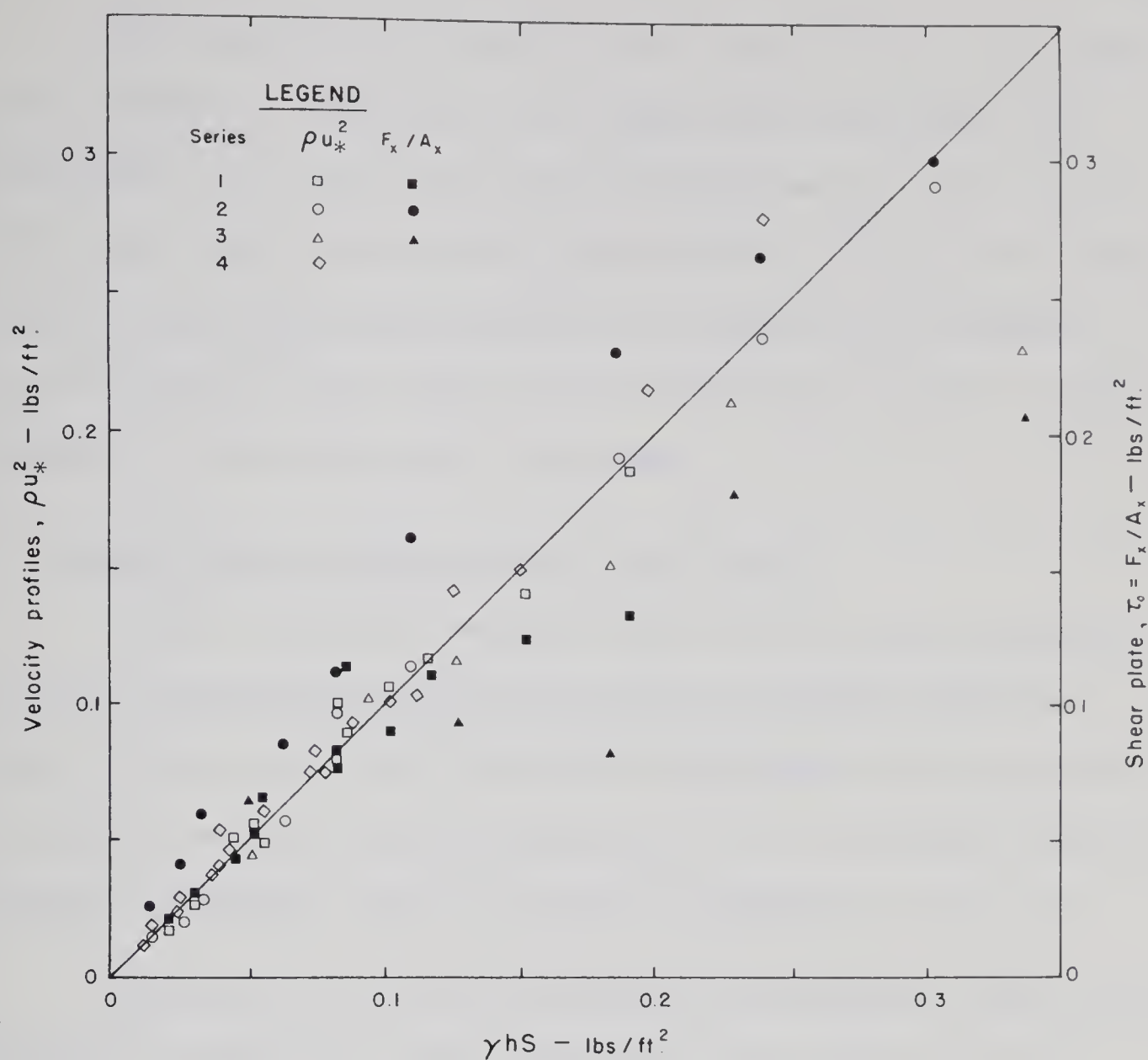


FIGURE 6-16. COMPARISON OF BOUNDARY SHEAR AT THE CHANNEL CENTERLINE

agreement with the result from the velocity profile. Prior to Test 2.9 the shear element was realigned with the channel bed surface and it is assumed that the high readings were caused by poor alignment. For the Series 3 tests, the shear meter results are generally lower than those from the other methods. Alignment of the element was complicated because of the attached roughness and this is considered to be the major cause of the difference.



After completion of the first four series of tests the experimental program was evaluated and the shear meter measurements were discontinued. This was mainly because of difficulties with alignment of the shear meter element and the unsuitability of the existing shear meter for determining shear stresses at all points on the boundary. Also, the success of the Preston tube calibrations provided a simpler alternative to the shear meter measurements.

#### 6.9. Comparisons of Average Boundary Shear Stress

In this section the average boundary shear stress determined from the integration of local shear stresses calculated from both velocity profiles and from Preston tube measurements are compared with the boundary average value calculated from  $\gamma_{RS}$ . The relevant data are contained in APPENDIX C and are plotted in FIGURES 6-17 and 6-18.

The results of all tests conducted on rectangular channels are presented in FIGURE 6-17. This figure shows the average boundary shear stress in terms of the wide-channel value versus the width to depth ratio. The calculated value for the average boundary shear stress  $\gamma_{RS}$  is indicated. Each method and tube size has a separate symbol. There is generally good agreement between the various measurements for a single test. The highest value is normally the one calculated from velocity profiles and this has been explained in Section 6.6. For those tests where the integrated values do not agree with  $\gamma_{RS}$  the slope measurement is generally the most suspect to error. However, for the tests in Series 6 which are all 10 to 20 percent below the value given by  $\gamma_{RS}$ , an error in the calculated shear velocities from velocity profiles is also suspected.



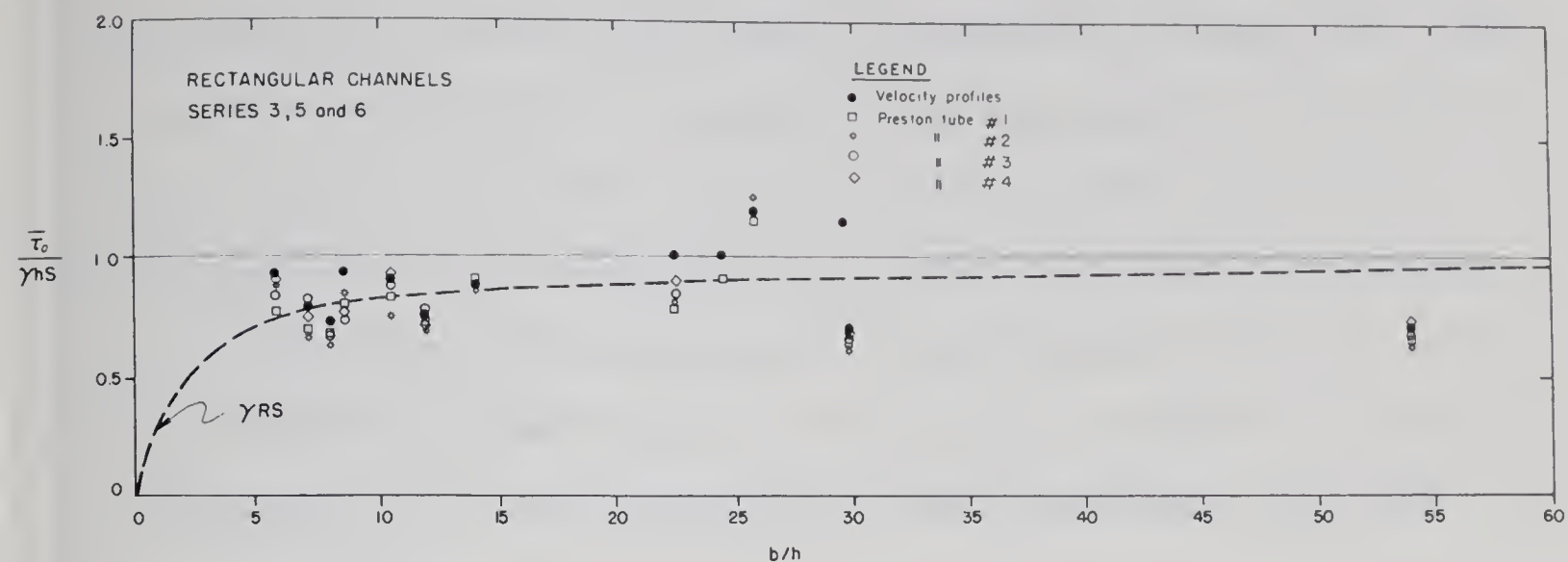


FIGURE 6-17. COMPARISON OF MEASUREMENTS OF AVERAGE BOUNDARY SHEAR STRESS, RECTANGULAR CHANNEL

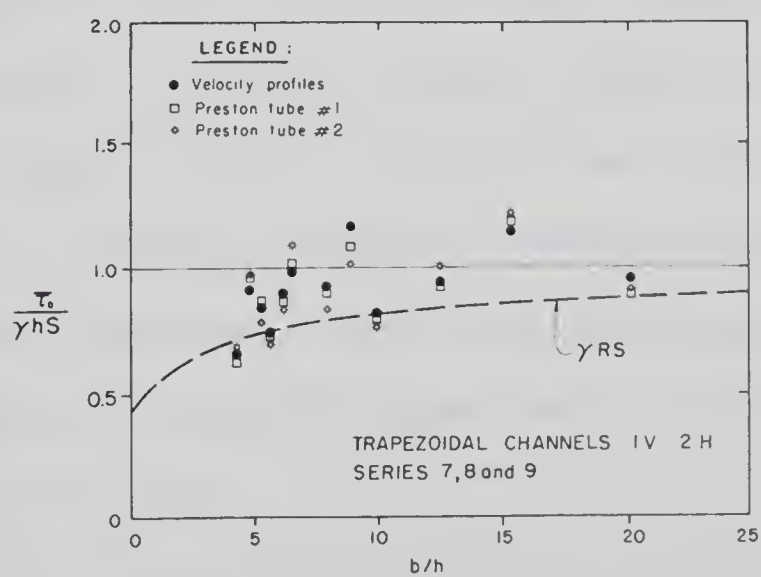


FIGURE 6-18. COMPARISON OF MEASUREMENTS OF AVERAGE BOUNDARY SHEAR STRESS, TRAPEZOIDAL CHANNEL





The results of tests conducted on trapezoidal channels with 2 horizontal to 1 vertical side slopes are presented in FIGURE 6-18. The breadth to depth ratio was calculated using the breadth at the channel bed. Only the two smaller Preston tubes were used for these series. A comparison of the measurements for a single test shows good agreement. All of the Series 8 test results plot about 20 percent above the value calculated from measured slope. The inaccurate measurement of slope is considered to be a major contributor to these differences (see error estimates, TABLE B-7).

The ratio of the average shear stress on the bed to the average shear stress on the entire boundary is presented in FIGURE 6-19. This figure presents the integrated measurements for both rectangular and trapezoidal channels. FIGURE 6-19 shows that for rectangular channels, the average bed shear stress is within 10 percent of the boundary average for aspect ratios greater than 2 and the ratio tends towards 1.0 as  $b/h$  increases. Relative roughness appears to have a small effect on this ratio and this is substantiated in the following analysis. As  $b/h$  decreases a change in roughness will be seen to be increasingly more important. The average line presented in FIGURE 6-19 has been extended to the smaller aspect ratios by using the results presented by Cruff (1965).

FIGURE 6-19 shows that for trapezoidal channels, the average bed shear stress in terms of the boundary average is considerably higher than for rectangular channels. After consideration of the effects of roughness and aspect ratio on the wall shear stress, and



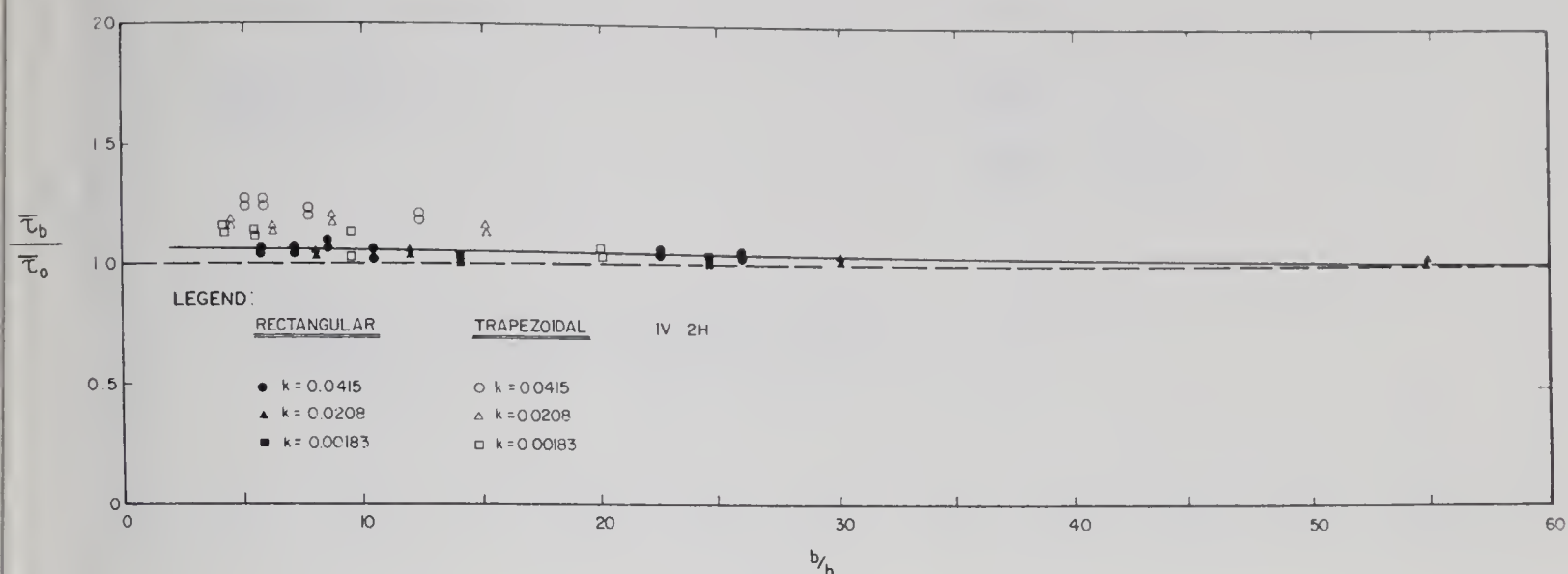


FIGURE 6-19. RATIO OF AVERAGE BED SHEAR STRESS TO AVERAGE BOUNDARY SHEAR STRESS FOR VARIOUS ASPECT RATIOS AND ROUGHNESSES

realizing that the walls make up a greater proportion of the wetted perimeter for trapezoidal channels, this difference becomes obvious. Similar to the rectangular case, the ratio of  $\bar{\tau}_b/\bar{\tau}_o$  decreases with increasing  $b/h$  tending towards 1.0 at large aspect ratios. The effect of roughness is apparent at the lower values of  $b/h$ .

The average shear stress on the wall relative to the average on the bed for the two channel shapes at various breadth to depth ratios are presented in FIGURES 6-20 and 6-21. Both figures show the same trends. The ratios of  $\bar{\tau}_w/\bar{\tau}_b$  decrease with increasing breadth to depth ratios. For smooth boundaries this ratio decreases to a value of 0.6 at  $b/h \approx 15$  and then remains nearly constant as indicated by the experimental curve from Cruff. These figures clearly show a decrease in  $\bar{\tau}_w/\bar{\tau}_b$  with an increase in roughness and this trend



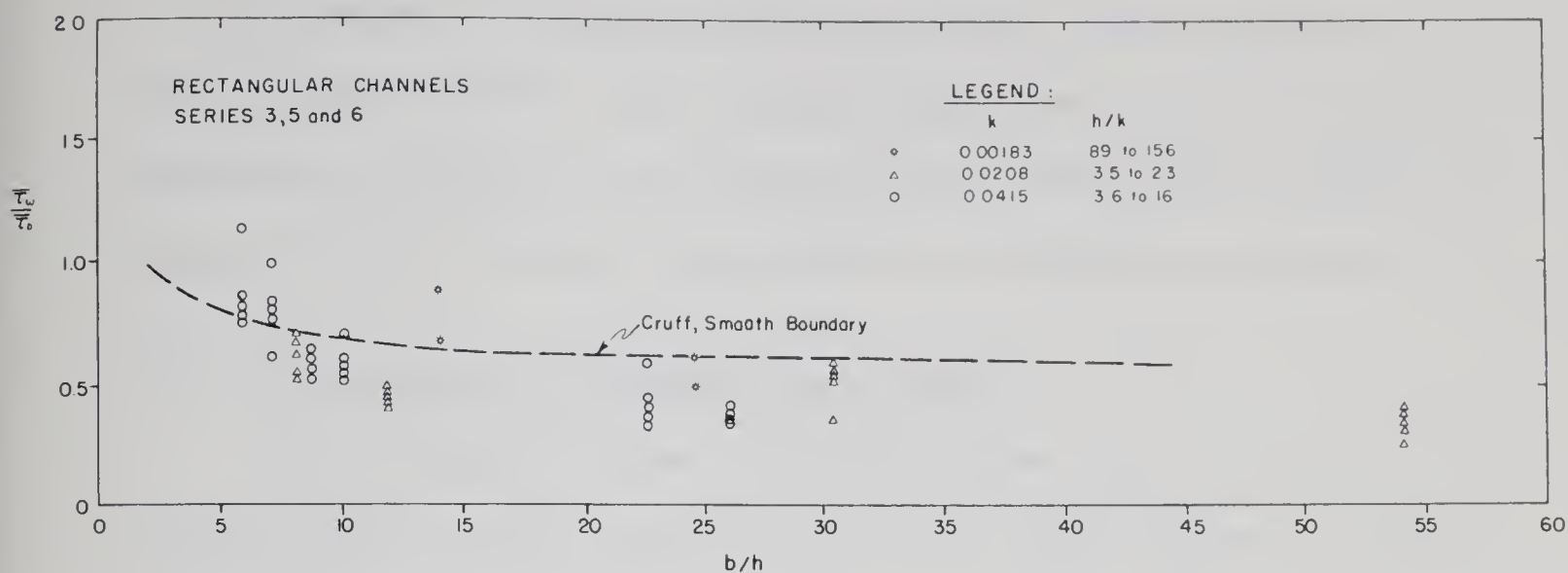


FIGURE 6-20. VARIATION OF AVERAGE WALL TO AVERAGE BED SHEAR STRESS WITH ASPECT RATIO AND ROUGHNESS, RECTANGULAR CHANNELS

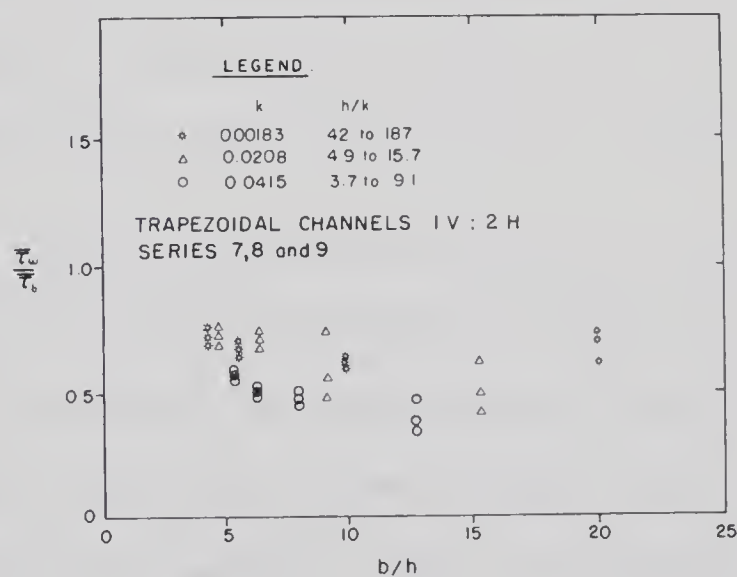


FIGURE 6-21. VARIATION OF AVERAGE WALL TO AVERAGE BED SHEAR STRESS WITH ASPECT RATIO AND ROUGHNESS, TRAPEZOIDAL CHANNELS



continues for aspect ratios greater than 15. The effect of roughness is less apparent at the smaller values of  $b/h$ . Since breadth was nearly constant for all tests in each figure, an increase in relative roughness is inherent in an increase in  $b/h$ . The relative effects of aspect ratio and roughness are treated in the following section.

#### 6.10. Distribution of Boundary Shear Stress

The integrated values of boundary shear stress obtained by the velocity profile method and the Preston tube method agreed favourably as pointed out in Section 6.9. The typical shear stress distributions presented in Section 5.5 show less agreement between these methods for values of local shear stress. The large differences between these methods are most apparent in corner regions and on the wall near the free surface. The main reason for the differences has been attributed to inaccurate calculation of shear velocities from velocity profiles in these areas. Many of the dimensionless shear distributions derived from velocity profiles showed large discontinuities and many indicated maximums near the corners which were obviously incorrect.

The shear stress distributions presented in APPENDIX F are therefore restricted to plots presenting Preston tube data. FIGURES F-1 to F-6 show the wall and bed shear stress distributions for each test. Since each of the Preston tubes yielded similar results, only measurements from the two smallest tubes are presented. The larger tubes generally displayed more continuous distributions but did not provide data as close to the adjacent boundary.







FIGURES F-1 to F-3 show that the shear stress on the bed and the shear stress on the wall are approximately equal for equal distances from the corners of rectangular channels up to a distance of at least  $2/3$  of the depth. The exact portion of the depth for this similarity is dependent on the roughness and increases as relative roughness decreases. This shows that the distribution of shear about a right angle corner with equivalent roughnesses is symmetrical. This substantiates the use of the bisector of the angle at the corner for separating the bed and wall regions for use of the logarithmic velocity equation. The non-uniform nature of the boundary shear stress is clearly indicated in these figures. Most bed distributions show more than one maximum and one minimum. The wall distributions are more continuous and generally show one maximum value.

For the trapezoidal channel data presented in FIGURES F-4 to F-6, the shear on the bed increases as the distance from the corner increases, while on the wall there is a small distance where the shear is equivalent to that on the bed and then it decreases continuously with distance from the corner. This also shows the suitability of using the corner angle bisector to divide the bed and wall zones. Generally the shear stresses on the bed and wall are equivalent for distances greater than  $0.24 h$  as stipulated for use of the bisector.

Boundary shear stress distributions are presented in non-dimensional form for each test in FIGURES F-7 to F-12. Since all Preston tube results were similar, the data in these figures are restricted to measurements with the smallest tube.



FIGURES F-7 to F-9 present the data for tests on rectangular channels. The bed shear stress ratios are nearly similar for each test. These ratios increase from a value near zero at the corner as distance from the corner increases. The maximums range from 1.1 to 1.4 in terms of the boundary average. The wall shear stress ratios are not similar. They are dependent on the breadth to depth ratio of the flow and the relative roughness. The wall shear stress ratios increase with distance from the corner to a maximum value and then decrease towards the free surface. The maximum values increase with a decrease in breadth to depth and range from 0.4 to 1.0 times the boundary average value. The location of the maximum is normally around  $y/h = 2/3$ .

FIGURES F-10 to F-12 present non-dimensional shear stress distributions for all tests on trapezoidal channels. The bed shear stress ratios are nearly similar for each test. These ratios, in terms of the boundary average, increase from a value of about 0.8 at the corner to a maximum of 1.2 to 1.4. These maximums occur between 0.1 and 1.0 of the distance to the centerline. The wall shear stress ratios show a small increase from the value near the corner and then decrease continuously towards the free surface. The wall maximums are affected by the width to depth ratio and reach a value of 1.2 times the boundary average for the larger depths of flow. The wall distributions tend toward zero near the free surface and the decrease is apparently affected by relative roughness.



In order to determine and separate the effect of aspect ratio from that of relative roughness on the distributions of wall shear stress, data were selected with nearly equivalent aspect ratios but different relative roughness. FIGURE 6-22 shows this data for the rectangular channels. Selected tests from the trapezoidal channels are presented in FIGURE 6-23. The data presented in these figures show the same general trends. For constant  $b/h$  values the average wall shear stress, in terms of either the bed or boundary average, decreases with an increase in relative roughness (decrease in  $h/k$ ). For constant relative roughness the average wall shear stress, in terms of either the bed or boundary average, decreases with increasing  $b/h$ . For the smaller aspect ratios (experimentally associated with smaller relative roughness) the variation in aspect ratio becomes more important. For larger aspect ratios (experimentally associated with larger relative roughness) the effect of relative roughness becomes predominant. These observations explain the results presented in FIGURES 6-20 and 6-21. The effect of roughness on the shape of the wall shear stress diagrams especially near the free surface is apparent in FIGURES 6-22 and 6-23.

#### 6.11. Maximum Boundary Shear Stress

The variation of maximum boundary shear stress with aspect ratio is presented in FIGURES 6-24 and 6-25. Both of these figures contain data from a number of independent studies as noted in the legends. Both smooth and rough boundary data are combined.

FIGURE 6-24 presents the data from rectangular channel tests. The maximum shear stress on the bed in terms of the boundary average is



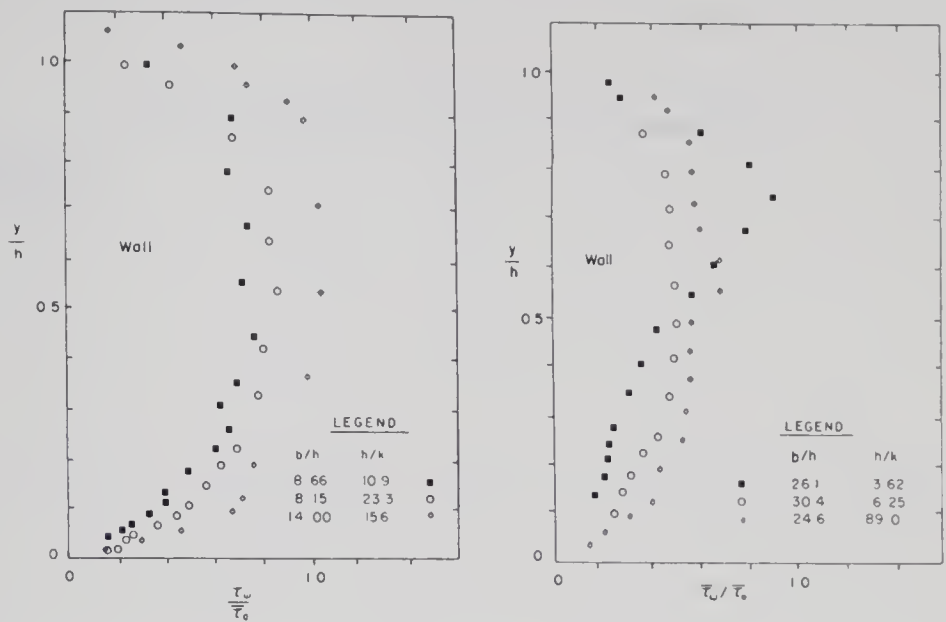


FIGURE 6-22. WALL SHEAR STRESS DIAGRAMS, RECTANGULAR CHANNELS

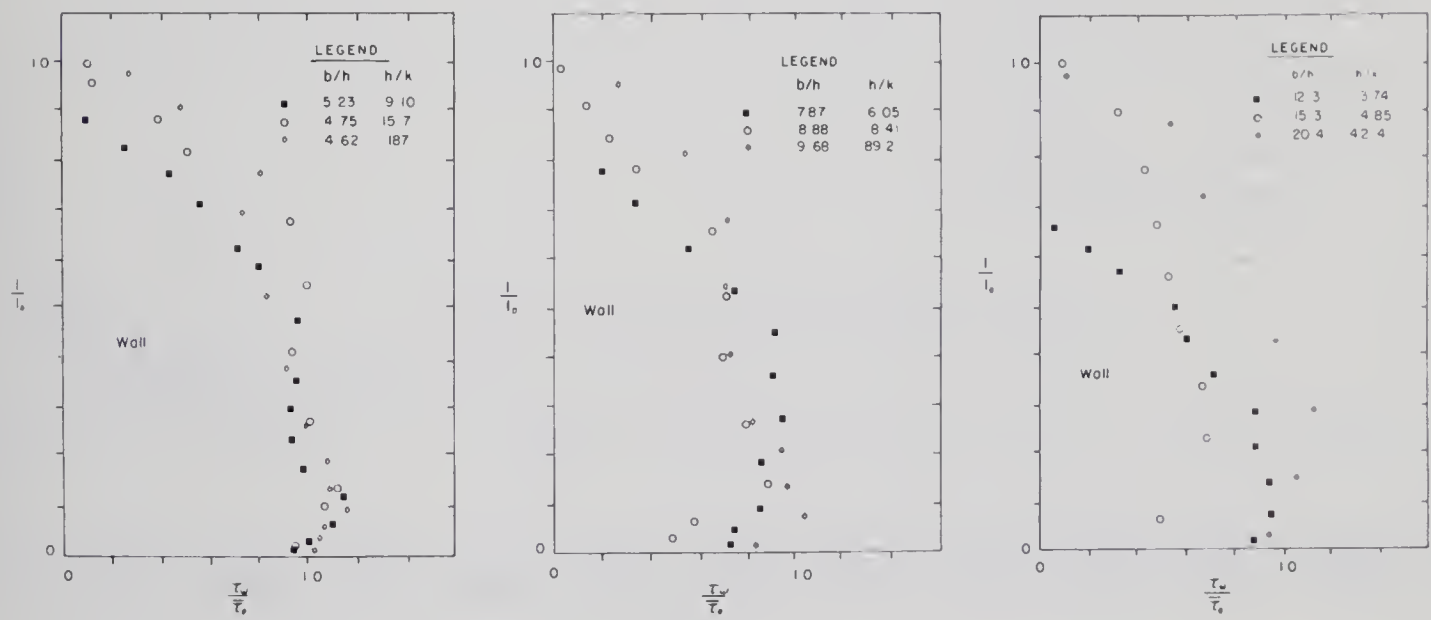


FIGURE 6-23. WALL SHEAR STRESS DIAGRAMS, TRAPEZOIDAL CHANNELS







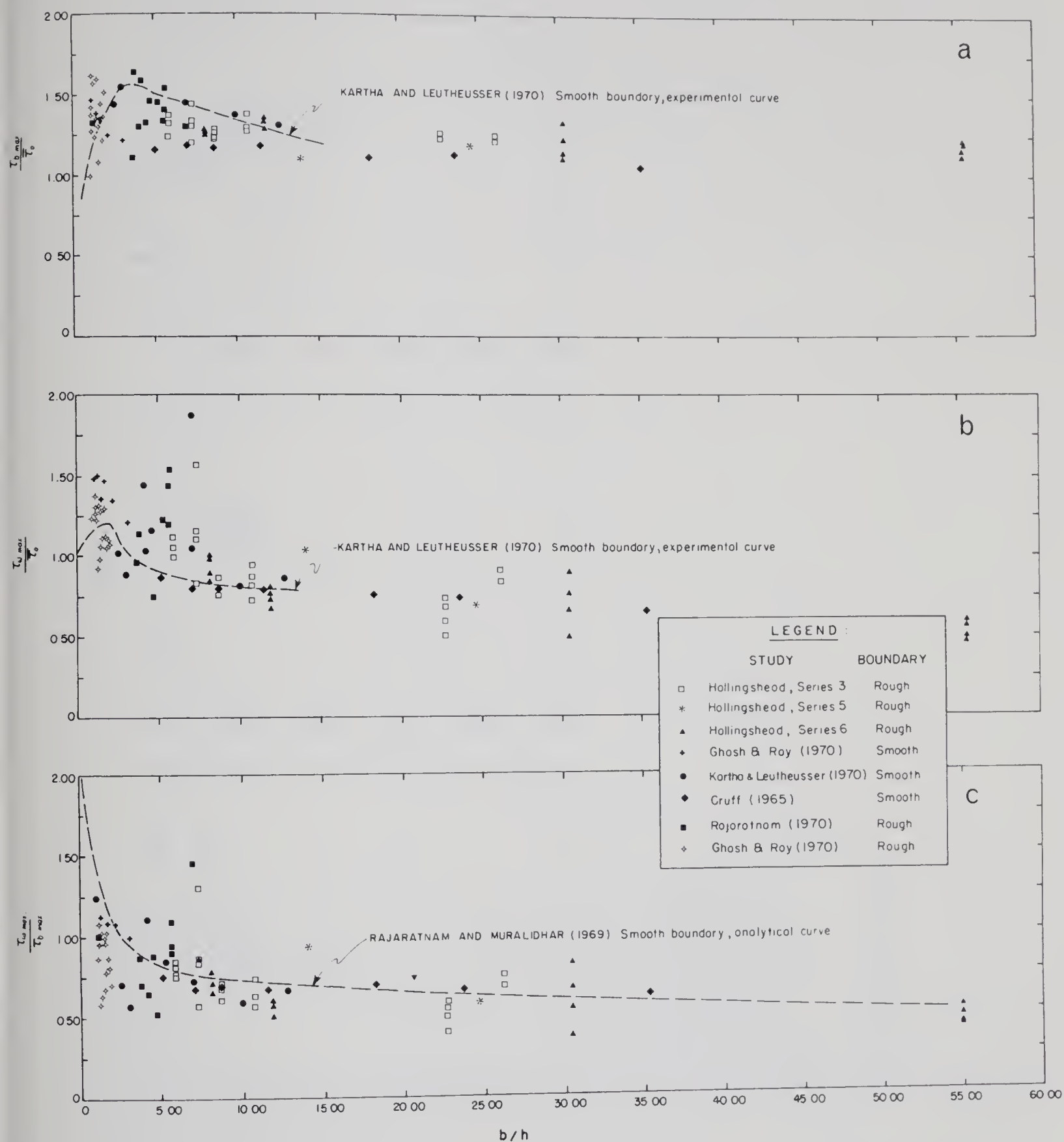


FIGURE 6-24. VARIATION OF MAXIMUM BOUNDARY SHEAR STRESS, RECTANGULAR CHANNELS



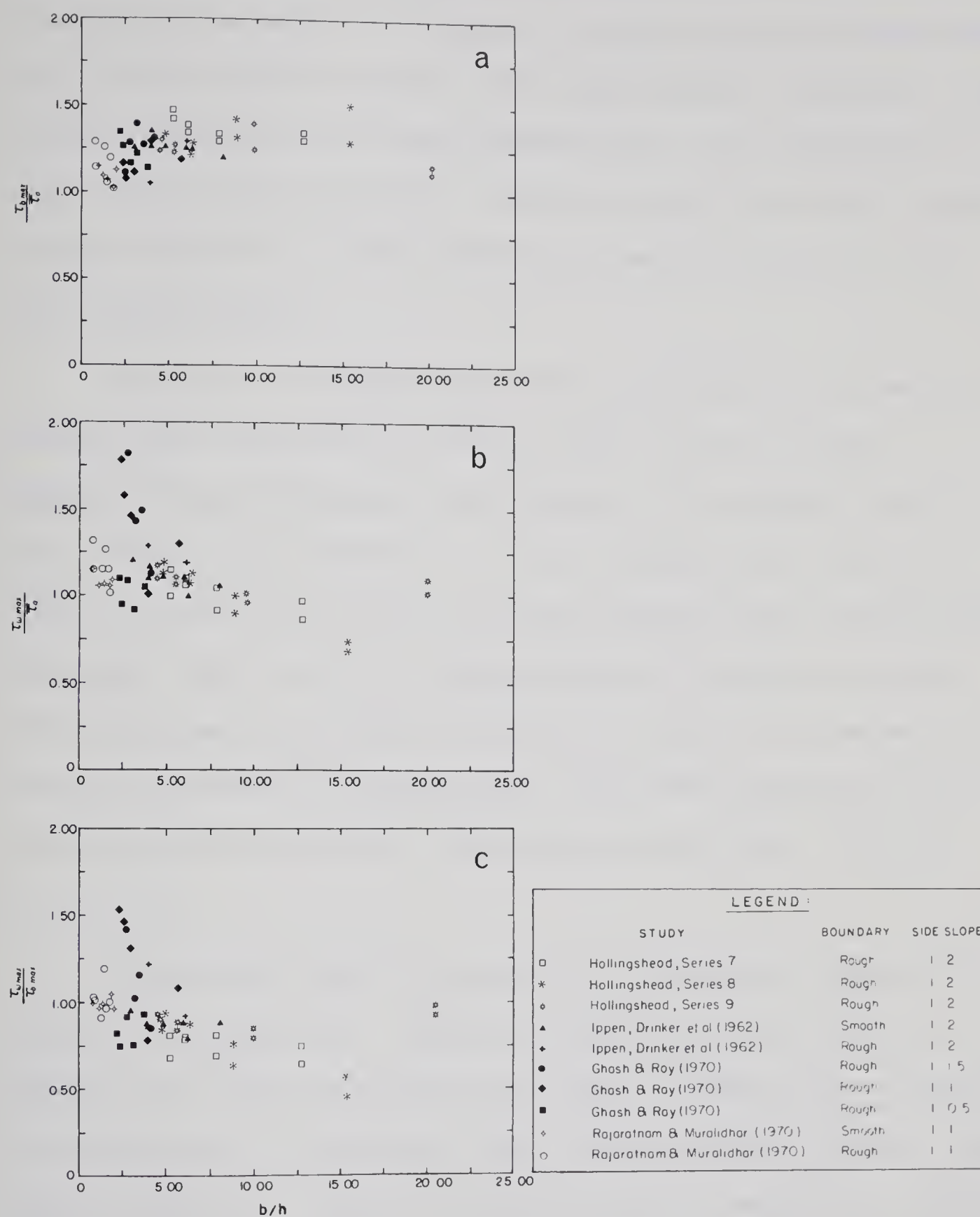


FIGURE 6-25. VARIATION OF MAXIMUM BOUNDARY SHEAR STRESS, TRAPEZOIDAL CHANNELS



shown in FIGURE 6-24(a). The scatter in these figures is not surprising since the points are based on a single boundary measurement and are taken from different sources. The rough boundary data agrees with the trend exhibited by the smooth boundary data. The maximum ratio is about 1.6 and occurs at  $b/h < 5$ . As  $b/h$  increases this ratio decreases to about 1.25 at  $b/h = 15$  and then remains nearly constant for much larger values of  $b/h$ .

The ratio of maximum shear stress on the wall to the boundary average value is presented in FIGURE 6-24(b). There is little difference between the smooth and rough data. The maximum ratio is about 1.5 and occurs for  $b/h < 5$ . As  $b/h$  increases this ratio decreases to about 0.75 at  $b/h = 15$  and then remains nearly constant for much larger values of  $b/h$ . A supplementary plot using the same data with the maximum shear stress on the wall in terms of the maximum on the bed is presented in FIGURE 6-24(c). The curve indicated on this plot was derived analytically (Rajaratnam and Muralidhar, 1969) for  $Re = 1 \times 10^5$ .

Similar data from tests conducted on trapezoidal channels are presented in FIGURE 6-25. This data includes tests with several different side slopes as noted in the legend. FIGURE 6-25(a) indicates the maximum ratio of maximum bed shear stress to average boundary shear stress is about 1.5. There is too much scatter to determine a definite trend but it appears that this ratio is about 1.25 at large aspect ratios ( $b/h > 15$ ). The ratio of maximum wall shear stress to average boundary shear stress is presented in FIGURE 6-25(b). This ratio



varies from 1.75 to 0.75 and generally decreases with an increase in aspect ratio. The highest values ( $\tau_{w \text{ max.}}/\tau_o > 1.3$ ) are all from Ghosh and Roy (1970) and were obtained with a shear meter. The measured maximums on the wall by this method were considerably higher than those obtained by Preston tube measurements. The lowest ratios in this figure are from those tests with large relative roughness ( $h/k < 5$ ).

The results presented in FIGURES 6-24 and 6-25 substantiate the trends shown in the preceding sections but also show the importance of the non-uniform nature of shear stress distributions resulting from secondary flow. The maximum bed shear stress normally was located at some distance from the centerline as shown in FIGURES F-7 to F-12. The location of the maximum bed shear stress was determined by the high velocity filaments associated with secondary flow. This is clearly shown by the isovels in FIGURE 5-2 which is typical of the rectangular channel tests. These high velocity filaments were not as apparent for the trapezoidal channel tests.

#### 6.12. Discussion of Results

FIGURES 6-19 to 6-25 show the effect of roughness and aspect ratio on the distribution of boundary shear stress for the two channel shapes selected for study. An estimate of the distribution of local shear stresses on the boundary can be made for these conditions. For a given value of the average boundary shear stress  $\gamma_{RS}$ , the average bed shear stress can be estimated from FIGURE 6-19 for particular geometry and aspect ratio. For the smaller aspect ratios the effect of roughness should be included especially for the trapezoidal channel





shape. FIGURE 6-26 can be used to roughly distribute the local shear stress on the bed. This figure was constructed using the data presented in FIGURES F-6 to F-12. An average curve is given for each shape which does not show the small variation of distribution for changes in aspect ratio or roughness. For the rectangular channel the wall shear stress can then be distributed by equating it to the value on the bed for equal distance from the corner up to about  $2/3 h$ , and then decreasing to zero at the free surface. For the trapezoidal channel shape the wall shear stress equals the bed shear stress at the corner and decreases to zero at the free surface. The shape of the wall shear stress diagram can be estimated from FIGURE 6-22 or 6-23. The estimated distribution can then be checked against FIGURE 6-20 or 6-21.

If one is interested in the maximum value of boundary shear, the use of values estimated from FIGURES 6-24 and 6-25 is considered to be more realistic. This data includes the maximums inherent in the non-uniform distributions found for most channels. Channel geometry plays a major role in the production of secondary flow which in turn influences the distribution of boundary shear stress and has a significant effect on the magnitude and position of maximum values. It should be noted that these maximums were measured in carefully controlled laboratory experiments and larger values could be expected for asymmetrical channels or where the flow is affected by irregularities upstream.



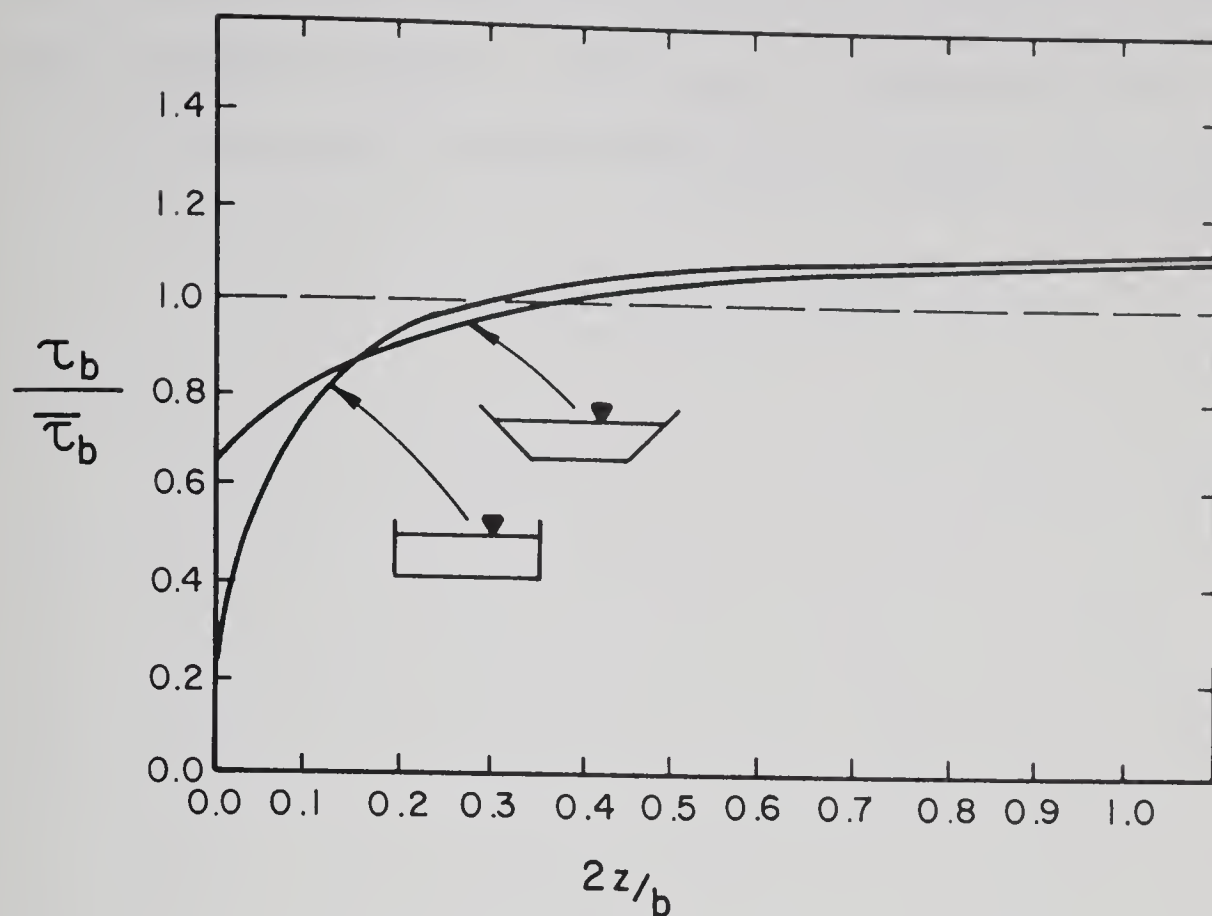


FIGURE 6-26. AVERAGE CURVES SHOWING THE DISTRIBUTION OF BED SHEAR STRESS

Until the three dimensional turbulent shear flow with a free surface boundary layer is completely solved, a satisfactory general analytical solution to the distribution of boundary shear stress in open channel flow is not possible. The simpler three dimensional turbulent boundary layer in a corner region is not fully solved (Bragg, 1969). A complete solution must necessarily include secondary flow. Measurements of the boundary shear stress in turbulent flow do not agree with the laminar flow solutions (Kantha and Leutheusser, 1970) nor do they agree with the simplified solutions for turbulent flow given by Chow (1959), Goncharov (1964), or Smutek (1970). In light of these difficulties, actual measurements of boundary shear



stress under various conditions provide the information required for proper hydraulic designs. This study has demonstrated the usefulness of the Preston tube to measure these local boundary shear stresses.



## CHAPTER VII

### CONCLUSIONS AND RECOMMENDATIONS

#### 7.1. Summary

The Preston technique was found to be a suitable method for measuring the distribution of boundary shear stress in open channel flow, including boundaries with large roughness. Boundary shear stress distributions were measured for a range of flow conditions in both rectangular and trapezoidal channels with three different boundary roughnesses. A series of figures show the relationships between boundary shear stress, aspect ratio and relative roughness for these tests. A method for estimating the local boundary shear stress for these channel shapes is described.

#### 7.2. Conclusions

For large hemispherical roughness elements that are closely packed, the best datum from which to measure normal distance for use in the logarithmic velocity equation is at a distance 0.2 times the roughness diameter below the top of the roughness elements. The hemispherical roughnesses have equivalent sand grain roughnesses equal to 0.65 D. The #36 wet-or-dry cloth has an equivalent sand grain roughness equal to 3.1 times the median grain diameter.





The logarithmic velocity equation with Nikuradse's equivalent sand grain roughness and constant  $B = 8.5$  is suitable for use in open channels with fully rough boundaries defined by  $u_* k_s / \nu > 70$ . This equation is not recommended for use when the relative roughness exceeds 0.2 ( $h/k < 5$ ). The logarithmic velocity equation can be used normal to the walls as well as the bed for both trapezoidal and rectangular channels except in a small region near the free surface. The bisector of the corner angle is suitable for division of the wall and bed regions for channels with the same roughness on the bed and walls. When calculating boundary shear stress from measured velocities and the logarithmic equation, measurements within the region controlled by the adjacent boundary should be discarded.

The use of Preston's technique with a total head tube resting on the boundary ensures that measurements are restricted to the appropriate region of flow. Preston tube calibrations were successfully carried out in the predominantly two dimensional region of flow using values calculated from velocity profiles and results from a bed shear meter. Total head tubes as large as 1 inch O.D. were used successfully on roughness elements up to 1 inch in diameter. The Preston tube calibrations agreed with analytical results calculated by using the logarithmic velocity equation to estimate the pressure at the geometric center of the boundary tube. For values of  $u_* k_s / \nu > 300$  (the exact limiting value is apparently dependent on roughness geometry and tube size) the pressure to shear stress ratios are constant. For smaller values of  $u_* k_s / \nu$  the measured pressure to shear stress ratios



increase and show the same trend as values calculated from Nikuradse's transition equations.

At the channel centerline where two dimensional flow is predominant the three methods of measuring local boundary shear stress (measured velocities in Equation 2-20, Preston tubes, and shear meter) agree reasonably well. The main difficulty encountered with the use of the shear meter was alignment. The shear meter was not suitable for measuring shear stress distribution. The Preston tube method required much less time than measuring velocity profiles and is considered to be better suited to measuring boundary shear stress distributions especially in corner regions.

The ratio of average wall to average bed shear stress for rough boundaries decreases with increasing aspect ratio similar to the trend exhibited for smooth boundaries. As the relative roughness increases there is a decrease in the wall to bed shear stress ratio. For rectangular channels the local shear stress on the bed and on the wall are approximately equal for equal distances from the corner, up to a distance of at least  $2/3$  of the depth. This substantiates the use of the corner angle bisector for separating the bed and wall regions. The boundary shear stress approaches zero at both the corner and the free surface. For the trapezoidal channels the local shear stress on the bed and on the wall are approximately equal for a small distance from the corner. The minimum measured shear stress at the corner is less pronounced than for the rectangular case. The boundary shear stress approaches zero at the free surface.



Diagrams of the non-dimensional shear stress show that aspect ratio has a very small effect on the bed shear stress ratios but a significant effect on the wall shear stress ratios. The wall shear stresses relative to the boundary average increase with decreasing breadth to depth ratios. Increasing the relative roughness of the boundaries has the same effect on the distribution of boundary shear stress as increasing the breadth to depth ratio.

Based on a number of independent studies on rectangular channels with both smooth and rough boundaries the maximum bed to average boundary shear stress ratio varies from about 1.6 at  $b/h < 5$  to 1.25 for  $b/h > 15$ . The maximum wall shear stress for similar aspect ratios varies from 1.5 to 0.75 times the boundary average. A similar survey of data from trapezoidal channels with various side slopes shows a considerable amount of variation. Until better data is available, the ratios of bed and wall local maximums in terms of the boundary average can be estimated by using the rectangular channel results for the same aspect ratios.

### 7.3. Recommendations

Based on the conclusions of this study and a review of other studies, the following recommendations should be considered in planning future research on the distribution of boundary shear stress.

1. Existing Preston tube calibrations should be supplemented and checked with various roughness types and tube sizes for transitional and fully rough boundary conditions in open channel flow.





2. A detailed study to determine the effects of tube size and roughness geometry on the limits of each region of the calibration should be considered.
3. A study to investigate the use of the Preston technique on boundaries with non-uniform roughness should be considered.
4. Regardless of the studies recommended in 2 and 3, local boundary shear stress measurements can easily be obtained by this method for a variety of conditions encountered in practical open channel flow problems. Various shapes of channels with varying roughness as encountered in bank and bed protection schemes can be investigated. Channel constrictions as encountered in bridge waterway openings with and without guide banks can be studied. Measurements of this type will provide the necessary information to improve upon existing design procedures for a wide range of river engineering problems.





## LIST OF REFERENCES



## LIST OF REFERENCES

- ASCE Task Force, "Friction Factor in Open Channels", Task Force Report, Proceedings ASCE, Hydraulics Division, March, 1963.
- Arndt, R.E.A. and Ippen, A.T., "Turbulence Measurements in Liquids Using an Improved Total Pressure Probe", IAHR, Journal of Hydraulic Research, Volume 8, No. 2, 1970.
- Bagnold, R.A., "Some Flume Experiments on Large Grains but Little Denser than the Transporting Fluid, and their Implications", Proceedings Inst. Civil Eng. 4, Part 3, 174, 1955.
- Blinco, P. and Partheniades, E., "Turbulence Characteristics in Free Surface Flows Over Smooth and Rough Boundaries", Journal of Hydraulic Research, Volume 9, No. 1, 1971.
- Bradshaw, P. and Gregory, N., "Calibration of Preston Tubes on a Flat Plate using Measurements of Local Skin Friction", Aeronautical Research Council 20, 1958.
- Bragg, G.M., "The Turbulent Boundary Layer in a Corner", Journal of Fluid Mechanics, Volume 36, Part 3, 1969.
- Brahms, A., "Anfangsgrunde der Deich - und Wasserbaukunst" (Elements of Dam and Hydraulic Engineering), Aurich, Germany, Volume 1, 1754.
- Brown, D.C. and Joubert, P.N., "The Measurement of Skin Friction in Turbulent Boundary Layers with Adverse Pressure Gradients", Journal of Fluid Mechanics, Volume 35, Part 4, 1969.
- Bursali, T.S., "Bottom Shear Measurements in an Open Channel Flow", Proceedings, 12th Congress IAHR, 1967.
- Chow, Ven Te., "Open-Channel Hydraulics", McGraw-Hill Book Co., 1959.
- Cruff, R.W., "Cross-Channel Transfer of Linear Momentum in Smooth Rectangular Channels", Geological Survey Water-Supply Paper 1592-B, Washington, 1965.



- Daily, J.W. and Hardison, R.L., "A Review of Literature Concerning Impact Probes Used in Steady Flows", MIT, Hydrodynamics Laboratory Report No. 67, April, 1964.
- Dhawan, S., "Direct Measurements of Skin Friction", National Advisory Committee for Aeronautics, Technical Memorandum 2567, 1951.
- du Boys, P., "Etudes du regime du Rhone et l'action exercee par les eaux sur un lit a fond de graviers indefiniment affouillable" (The Rhone and Streams with Movable Beds), Annales des ponts et chaussees, Volume 18, 1879.
- Einstein, H.A., "Formulas for the Transportation of Bed Load", Transactions, ASCE, Volume 107, 1942.
- Einstein, H.A. and El-Samni, A., "Hydrodynamic Forces on a Rough Wall", Rev. Mod. Phys. Volume 21, 1949.
- Enger, P.F., "Tractive Force Fluctuations Around an Open Channel Perimeter as Determined from Point Velocity Measurements", ASCE Convention, Phoenix, Arizona, April, 1961.
- Ghosh, S.N. and Roy, N., "Boundary Shear Distribution in Open Channel Flow", Proceedings ASCE, Hydraulics Division, HY4, April, 1970.
- Ghosh, S.N. and Jena, S.B., "Boundary Shear Distribution in Open Channel Compound", Proceedings Inst. Civil Eng. 7404, 1971.
- Goncharov, V.N., "Dynamics of Channel Flow", Translated from Russian, Israel Program for Scientific Translations, Jerusalem, 1964.
- Head, M.R. and Rechenberg, I., "The Preston Tube as a Means of Measuring Skin Friction", Journal of Fluid Mechanics, Volume 14, Part 1, 1962.
- Henderson, F.M. "Open Channel Flow", The MacMillan Company, New York, 1966.
- Hsu, E.Y., "The Measurement of Local Turbulent Skin Friction by Means of Surface Pitot Tubes", David W. Taylor Model Basin Report, No. 957, August, 1955.
- Hwang, L. and Laursen, M., "Shear Measurement Technique for Rough Surfaces", ASCE, Hydraulics Division, HY2, 1963.



- Ippen, A.T. and Drinker, P.A., "Boundary Shear Stress in Curved Trapezoidal Channels", Proceedings ASCE, HY5, September, 1962.
- Ippen, A.T., Drinker, P.A., Jobin, W.R. and Shemdin, O.H., "Stream Dynamics and Boundary Shear Distributions for Curved Trapezoidal Channels", Hydrodynamics Laboratory Massachusetts Institute of Technology, Report No. 47, 1962.
- Kartha, V.C. and Leutheusser, H.J., "Distribution of Tractive Force in Open Channels", Proceedings ASCE, Hydraulics Division, HY7, July, 1970.
- Kempf, G., "Neue Ergebnisse Der Widerstandsforschung" (New Resistance Investigation Results), Werft, Reederei, Hafen, 10, 1929.
- Keulegan, G.H., "Laws of Turbulent Flow in Open Channels", Journal of Research of National Bureau of Standards, Volume 21, 1938.
- Lane, E.W., "Progress Report on Results of Studies on Design of Stable Channels", U.S. Bureau of Reclamation Hyd. Lab. Report Hyd-352, 1952.
- Lane, E.W., "Design of Stable Channels", Transactions ASCE, Volume 120, 1955.
- Leighly, J.B., "Toward a Theory of the Morphologic Significance of Turbulence in the Flow of Water in Stream", University of California, Publications in Geography, Volume 6, No. 1, 1932.
- Leliavsky, S., "An Introduction to Fluvial Hydraulics", Constable and Company, Ltd., 1955.
- Leutheusser, H.J., "Turbulent Flow in Rectangular Ducts", Proceedings ASCE, Hydraulics Division, HY3, May, 1963.
- Lundgren, H. and Jonsson, I.G., "Shear and Velocity Distribution in Shallow Channels", Proceedings ASCE, Hydraulics Division, HY1, January, 1964.
- MacMillan, F.A., "Experiments on Pitot Tubes in Shear Flow", Aeronautical Research Council Reports and Memoranda No. 3028, 1957.
- Maggiolo, O.J., Guarga, R. and Borghi, J., "A New Method for Measuring Shear Stresses in a Hydraulically Rough Flow", Journal of Hydraulic Research, Volume 8, No. 2, 1970.





- McQuivey, R.S. and Richardson, E.V., "Some Turbulence Measurements in Open Channel Flow", Proceedings ASCE, Hydraulics Division, HY1, January, 1969.
- Ministry of Technology, "Hydraulics Research 1964", Report of Hydraulics Research Board, Wallingford, 1965.
- Munoz-Goma, R.J. and Gelhar, L.W., "Turbulent Pipe Flow with Rough and Porous Walls", Hydrodynamics Lab., MIT, Report No. 109, April, 1968.
- Nece, R.E. and Smith, J.D., "Boundary Shear Stress in Rivers and Estuaries", ASCE, Waterways and Harbors Division, May, 1970.
- Nikuradse, J., Translation "Laws of Flow in Rough Pipes", Technical Memorandum 1292, National Advisory Committee for Aeronautics, 1933.
- Olsen, O.J. and Florey, Q.L., (compilers), "Sedimentation Studies in Open Channels: Boundary Shear and Velocity Distribution and Membrane Analogy, Analytical and Finite-difference Methods", reviewed by McHenry, D. and Glover, R.E., U.S. Bureau of Reclamation, Laboratory Report Sp. 34, 1952.
- Patel, V.C., "Calibration of the Preston Tube and Limitations on its Use in Pressure Gradients", Journal of Fluid Mechanics, Volume 23, Part 1, 1965.
- Petryk, S. and Shen, H., "Direct Measurement of Shear Stress in a Flume", Proceedings ASCE, Hydraulics Division, HY6, June, 1971.
- Preston, J.H., "The Determination of Turbulent Skin Friction by Means of Pitot Tubes", Journal of Royal Aeronautical Society, Volume 58, 1954.
- Rajaratnam, N., "A Theoretical Calibration Curve for the Preston Tube on Smooth Boundaries for Large Reynolds Numbers", Journal of the Royal Aeronautical Society, 1965.
- Rajaratnam, N., "Plane Turbulent Wall Jets on Rough Boundaries", Dept. of Civil Engineering, University of Alberta, July, 1965.
- Rajaratnam, N., "An Experimental Study of Turbulent Flow in Rough Rectangular Open Channels", Department of Civil Engineering, University of Alberta, 1970.



- Rajaratnam, N. and Muralidhar, D., "Boundary Shear Stress Distribution in Rectangular Open Channels", La Houille Blanche, France, No. 6, 1969.
- Rajaratnam, N. and Muralidhar, D., "An Experimental Study of Turbulent Flow in Smooth and Rough Trapezoidal Channels", Department of Civil Engineering, University of Alberta, 1970.
- Raudkivi, A.J., "Loose Boundary Hydraulics", Pergamon Press Ltd., 1967.
- Reinius, E., "Steady Uniform Flow in Open Channels", Transactions Royal Society, Stockholm, 1961.
- Replogle, J.A. and Ven Te Chow, "Tractive Force Distribution in Open Channels", ASCE, Hydraulics Division, HY2, March, 1966.
- Richardson, E.V. and McQuivey, R.S., "Measurements of Turbulence in Water", Proceedings ASCE, Hydraulics Division, HY2, March, 1968.
- Schlichting, H., Translation, "Experimental Investigation of the Problem of Surface Roughness", Technical Memorandum 823, National Advisory Committee for Aeronautics, 1936.
- Schlichting, H., Translated by J. Kestin, "Boundary - Layer Theory", Sixth Edition McGraw-Hill Book Company, 1968.
- Smith, D.W. and Walker, J.H., "Skin Friction Measurements in Incompressible Flow", National Advisory Committee for Aeronautics, Technical Note No. 4231, 1958.
- Smutek, R., Discussion of "Distribution of Tractive Force in Open Channels" (Kantha and Leutheusser, 1970), ASCE, Hydraulics Division, April, 1971.
- Taylor, H.J., "Exploratory Studies of Open Channel Flow over Boundaries of Laterally Varying Roughness", California Institute of Technology, Report No. KH-R-4, July, 1961.
- Tracy, H.J. and Lester, C.M., "Resistance Coefficients and Velocity Distribution, Smooth Rectangular Channel", Geological Survey Water-Supply Paper 1592-A, Washington, 1961.



- Vanoni, V.A. and Brooks, N.H., "Laboratory Studies of the Roughness and Suspended Load of Alluvial Streams", California Institute of Technology, Report No. E-68, December, 1957.
- Wright, R.R. and Carstens, M.R., "Linear-Momentum Flux to Overbank Sections", ASCE, Hydraulics Division, September, 1970.
- Yalin, M.S. and Russell, R.C.H., "Shear Stress Due to Long Waves", Journal of Hydraulic Research, 4, 1966.
- Yen, Chin-lien, "Velocity-Distributions in Straight Rectangular Channels", Hydronautics, Incorporated, Technical Report 801-3, July, 1968.



## APPENDIX A

### NOTATION





## APPENDIX A

## NOTATION

Symbol		Dimensions
A	- area of channel flow section	$L^2$
	- constant in logarithmic velocity equation	
$A_x$	- area of shear meter	$L^2$
a	- inside radius of pitot tube	L
	- intercept of regression equation	
	- displacement of shear meter	L
B	- constant in logarithmic velocity equation	
$B_s$	- constant in logarithmic velocity equation for Nikuradse's equivalent sand grain roughness	
b	- width of channel bottom	L
	- slope of regression equation	
C	- general constant	
	- constant in logarithmic velocity equation	
	- Chezy's resistance coefficient	$L^{1/2}T^{-1}$
D	- roughness size, hemisphere diameter, median grain size	L
d	- outside diameter of pitot tube	L
F	- general force	F
$F_x$	- force on shear meter element	F



f	- general functional relation	
	- friction factor $8gRS/V^2$	
g	- acceleration due to gravity	LT <sup>-2</sup>
h	- depth of flow	L
	- distance from the datum to the geometric tube center	L
$\Delta h$	- differential head	L
K	- constant	
k	- height of roughness elements	L
$k_s$	- Nikuradse's equivalent sand grain roughness	L
L	- general length	L
	- distance along plumb line	L
	- length of channel section	L
$l$	- distance along sloping wall from bed $\sqrt{z^2+y^2}$	L
	- mixing length	L
$l_o$	- distance along sloping wall to free surface	L
N	- limit of $u_* k_s / \nu$	
	- number of points included in regression	
n	- number of points on bed or wall	
P	- length of wetted perimeter	L
p	- general pressure	FL <sup>-2</sup>
	- measured pressure with total head tube	FL <sup>-2</sup>



$p_o$	- measured pressure with static head tube	FL <sup>-2</sup>
$\Delta p$	- dynamic pressure ( $p-p_o$ )	FL <sup>-2</sup>
$\Delta p_*$	- dimensionless pressure parameter $\frac{\Delta p}{4\rho v^2} d^2$	
$Q$	- fluid discharge	L <sup>3</sup> T <sup>-1</sup>
$R$	- hydraulic radius $A/P$	L
$Re$	- Reynolds number $VR/\nu$	
$r$	- radius of roughness element	L
$S$	- slope of energy gradient, uniform flow	
$s$	- general normal distance	L
$T$	- temperature of fluid	°F
	- unit of time	T
$t$	- pitot tube wall thickness	L
$U_m$	- mean velocity on normal to bed	LT <sup>-1</sup>
$u$	- time average of local velocity in x direction	LT <sup>-1</sup>
$u_o$	- initial value of $u$	LT <sup>-1</sup>
$u'$	- turbulent velocity fluctuations in x direction	LT <sup>-1</sup>
$u_*$	- local shear velocity $\sqrt{\tau_o/\rho}$	LT <sup>-1</sup>
$V$	- mean velocity for cross section $Q/A$	LT <sup>-1</sup>
$V_m$	- mean velocity for cross section from integration	LT <sup>-1</sup>
$v'$	- turbulent velocity fluctuation in y direction	LT <sup>-1</sup>
$W$	- weight of pendulum	F



$x$	- coordinate in downstream direction	L
$y$	- coordinate direction normal to bed	L
$y_0$	- initial value of $y$	L
$y'$	- distance from datum to top of roughness	L
$z$	- coordinate direction normal to wall	L
$\gamma$	- unit weight of fluid	$FL^{-3}$
$\Delta$	- linear displacement of shear meter element	L
$\delta$	- thickness of viscous sublayer	L
$\kappa$	- Von Karmans coefficient	
$\mu$	- dynamic viscosity of fluid	$FTL^{-2}$
$\nu$	- kinematic viscosity of fluid	$L^2T^{-1}$
$\rho$	- mass density of fluid	$FT^2L^{-4}$
$\tau$	- time average value of shear stress	$FL^{-2}$
$\tau_0$	- shear stress at the boundary	$FL^{-2}$
$\overline{\tau}_0$	- average shear stress on the boundary	$FL^{-2}$
$\tau_{0 \text{ max.}}$	- maximum shear stress on the boundary	$FL^{-2}$
$\tau_0 *$	- dimensionless shear stress $\frac{\tau_0 d^2}{4\rho\nu^2}$	
$\tau_b$	- shear stress on the bed	$FL^{-2}$
$\tau_{b \text{ max.}}$	- maximum shear stress on the bed	$FL^{-2}$
$\overline{\tau}_b$	- average shear stress on the bed	$FL^{-2}$
$\tau_t$	- turbulent shear stress - $\rho \overline{u'v'}$	$FL^{-2}$





$\tau_w$	- shear stress on the wall	$FL^{-2}$
$\tau_w \text{ max.}$	- maximum shear stress on the wall	$FL^{-2}$
$\overline{\tau_w}$	- average shear stress on the wall	$FL^{-2}$
$\tau_\mu$	- viscous shear stress	$FL^{-2}$
$\phi$	- function of velocity	
$\psi$	- complementary function	



## APPENDIX B

### SAMPLE CALCULATIONS



## APPENDIX B

## SAMPLE CALCULATIONS

This appendix contains the details of a sample calculation. An outline of the analysis and presentation of the results is contained in CHAPTER V. The examples given are Tests 3.60 and 3.61. The first digit in these designations is the series number and the second is the test number. The final zero indicates velocity distribution data while the one indicates Preston tube data using the smallest tube.

B.1. Velocity Distribution Data

The following sections briefly describe the main computations carried out by a computer program for analysis of the velocity distribution measurements. A complete listing of this program is on file at the Hydraulics Laboratory.

B.1.1. Preliminary Processing

The raw data for Test 3.60 was comprised of 9412, 10 digit readings. For each 10 digit reading, digits 1 and 2 signified the channel number which in turn identified the variable, digit 3 was the sign code, digit 4 was blank, digits 5 to 8 were the 4 significant figures of the voltmeter measurement, digit 9 was blank, and digit 10 located the decimal place. These measurements included 20 readings of the velocity head and the coordinates at each of 12 points on 13 normals to the bed. Also included were 13 scans of the test number, the x-coordinate, the discharge and temperature. Preliminary



processing yielded the following type of data set for each of the normals.

The sample presented in TABLE B-1 is for the normal at the flume centerline. Each  $z$  and  $y$  coordinate are the average of 20 readings taken during the same scans as the velocity measurements. The  $y$  and  $z$  coordinates are from the bed and wall datum planes respectively to the geometric center of the pitot static tube. These datum planes were established in previous tests at 0.2 times the roughness diameter below the tops of the roughness elements. The first measurement at the boundary should therefore have a  $y$  coordinate equal to  $0.2D$  plus one half the tube diameter which equals 0.0214 feet.

The velocities are the average of 20 values which were calculated from the measured dynamic head on the pitot static tube without a turbulence correction using,

$$u = \sqrt{2 g \Delta h} \quad \text{.....} \quad \text{B-1}$$

where  $\Delta h$  is the dynamic head in feet of water. The pressure transducer calibrations were performed with measured heads of water.

#### B.1.2. Boundary Shear Stress

The data set given in TABLE B-1 was read by the main computer program along with data sets for each of the normals, and the average depth of flow for the test. The first sub-program eliminated data from the velocity profiles in the region obviously affected by the wall, or for normals to the wall that region affected by the bed and free surface boundaries. This program checked the velocity gradient





TABLE B-1  
DATA FOR NORMAL TO THE BED AFTER PRELIMINARY PROCESSING

Test Number	Discharge c.f.s.	Temp. °F	x Coord. ft.	z Coord. ft.	y Coord. ft.	Velocity ft/sec.
3.60	9.02	71.2	32.0	2.0035	0.0217	2.1286
				2.0060	0.0263	2.3385
				2.0045	0.0314	2.3844
				2.0075	0.0416	2.5477
				2.0065	0.0617	2.8325
				2.0035	0.0815	3.0923
				2.0050	0.1214	3.3971
				2.0035	0.1616	3.6008
				2.0040	0.2019	3.6873
				2.0045	0.3023	3.9928
				2.0055	0.5024	4.2764
				2.0045	0.6507	4.0701

and the assumption was made that if the gradient was continuously negative past some point away from the boundary, then those readings are in a zone affected by the adjacent boundary. This data was then eliminated from the computation of local boundary shear velocity. For the sample profile given in TABLE B-1 only the surface velocity was eliminated.

The next sub-program computed a linear regression line of velocity on the logarithm of normal distance using a least squares fit.



This program started with the four points nearest the boundary and continued by adding subsequent points away from the boundary. After each computation the program printed the slope and intercept of the regression line as well as the correlation coefficient. The following equations were used and a sample output is given in TABLE B-2. The regression equation is:

$$\log y = a + bu \quad \dots\dots\dots B-2$$

$$\text{with } b = \frac{N \sum u \log y - \sum u \sum \log y}{N \sum u^2 - (\sum u)^2} \quad \dots\dots\dots B-3$$

$$\text{and } a = \frac{1}{N} \sum \log y - \frac{b}{N} \sum u \quad \dots\dots\dots B-4$$

The correlation coefficient is:

$$r = \left( \frac{(N \sum u \log y - \sum u \sum \log y)^2}{(N \sum u^2 - (\sum u)^2) (N \sum (\log y)^2 - (\sum \log y)^2)} \right)^{1/2} \quad B-5$$

The best fit regression line was selected on the basis of the highest correlation. The final coefficient of determination ( $r^2$ ) indicates that 99.6% of the variance is explained by the computed regression equation. In this example the shear velocity was calculated from the final regression (11 points) using Equation 2-20 with  $A = 5.75$ :

$$\begin{aligned} u_* &= \frac{1}{A} \frac{u_2 - u_1}{\log y_2 / y_1} = \frac{1}{A} \times \frac{1}{b} = \frac{1}{5.75 \times 0.623} \\ &= 0.279 \text{ ft/sec.} \quad \dots \quad B-6 \end{aligned}$$

The local boundary shear stress is then,

$$\tau_0 = \rho u_*^2 = 1.937 \times (0.279)^2 = 0.151 \text{ lbs/ft.}^2 \quad B-7$$



TABLE B-2  
REGRESSION FOR SAMPLE DATA OF TABLE B-1

Number of Points	r	b	a
4	0.97327	0.67706	-3.12285
5	0.99083	0.67054	-3.10783
6	0.99309	0.62350	-2.99677
7	0.99556	0.60173	-2.94384
8	0.99711	0.59584	-2.92922
9	0.99746	0.60684	-2.95686
10	0.99817	0.61058	-2.96666
11	0.99823	0.62303	-3.00031
11	0.99823	0.62303	-3.00031

The calculated value was then stored for future integration.

After the local shear stress was calculated for all bed and wall normals, integrations were performed to find mean values for the boundary. The mean value on the bed was calculated using a trapezoidal rule. For  $n$  normals to the bed, starting at the wall,

$$\begin{aligned} \bar{\tau}_b = \frac{1}{z_n} & \left( \frac{\tau_{b1}}{2} (z_1) + \frac{\tau_{b1} + \tau_{b2}}{2} (z_2 - z_1) + \dots \right. \\ & \left. \dots + \frac{\tau_{b\ n-1} + \tau_{b\ n}}{2} (z_n - z_{n-1}) \right) \quad \dots\dots\dots B-8 \end{aligned}$$

For Test 3.60, the values of local shear stress are given in TABLE B-3. Using these values and assuming symmetry about the channel centerline,



Equation B-8 yields  $\bar{\tau}_b = 0.1635 \text{ lbs/ft.}^2$ . The mean value for the wall was calculated using the following equation, which starts at the bed.

$$\begin{aligned} \bar{\tau}_w = \frac{1}{h} & \left( \frac{\tau_{w1}}{2} (y_1) + \frac{\tau_{w1} + \tau_{w2}}{2} (y_2 - y_1) + \dots \right. \\ & \left. \dots + \frac{\tau_{wn-1} + \tau_{wn}}{2} (y_n - y_{n-1}) + \frac{\tau_{wn}}{2} (h - y_n) \right) \quad \text{B-9} \end{aligned}$$

In Equation B-9,  $h$  is the total depth of flow which equals 0.666 feet for the example. Using the values in TABLE B-3, Equation B-9 yields  $\bar{\tau}_w = 0.2029 \text{ lbs/ft.}^2$ . By assuming that the shear stress distribution about the channel centerline is symmetrical, the mean value for the entire wetted perimeter was calculated using,

$$\bar{\tau}_o = \left( \left( \bar{\tau}_b \times \frac{b}{2} \right) + (\bar{\tau}_w \times h) \right) \frac{1}{h + \frac{b}{2}} \quad \dots \quad \text{B-10}$$

For Test 3.60 with  $b = 3.923$  feet,  $\bar{\tau}_o = 0.1735 \text{ lbs/ft.}^2$ .

### B.1.3. Mean Velocity

The mean velocity for each normal to the bed was computed using all measured velocities. The trapezoidal rule was used assuming zero velocity at the boundary datum and the measured velocity nearest the surface for the surface interval. The equation used was,

$$\begin{aligned} U_m = \frac{1}{h} & \left( \frac{u_1}{2} (y_1) + \frac{u_1 + u_2}{2} (y_2 - y_1) + \dots \right. \\ & \left. \dots + \frac{u_{n-1} + u_n}{2} (y_n - y_{n-1}) + u_n (h - y_n) \right) \quad \dots \quad \text{B-11} \end{aligned}$$





TABLE B-3  
LOCAL BOUNDARY SHEAR STRESSES AND COORDINATES  
FROM VELOCITY PROFILES, TEST 3.60

ON BED			ON WALL		
Point	z Coordinate ft.	$\tau_b$ lbs/ft <sup>2</sup>	Point	y Coordinate ft.	$\tau_w$ lbs/ft <sup>2</sup>
1	0.0216	0.0643	1	0.0216	0.0621
2	0.0265	0.0688	2	0.0266	0.0917
3	0.0316	0.0827	3	0.0316	0.1196
4	0.0414	0.0825	4	0.0416	0.1216
5	0.0615	0.0981	5	0.0615	0.1329
6	0.0814	0.1231	6	0.0815	0.1906
7	0.1215	0.1198	7	0.1214	0.1873
8	0.2217	0.1792	8	0.1614	0.1739
9	0.3213	0.1251	9	0.2016	0.1856
10	0.5221	0.1742	10	0.3018	0.2344
11	1.0216	0.2173	11	0.5020	0.2397
12	1.5218	0.1382	12	0.6605	0.2085
13	2.0049	0.1510			

Using Equation B-11 with,  $h = 0.666$  feet and the data given in TABLE B-1,  $U_m = 3.745$  ft/sec. at  $z = 2.0049$  feet. Similarly the means for each profile were computed and stored. These values are presented in TABLE B-4.



TABLE B-4  
 MEAN VELOCITY FOR EACH VELOCITY PROFILE  
 NORMAL TO THE BED, TEST 3.60

Number	Average z Coordinate ft.	Mean Velocity, $U_m$ f.p.s.
1	0.0216	1.569
2	0.0265	1.588
3	0.0316	1.777
4	0.0414	2.042
5	0.0615	2.329
6	0.0814	2.619
7	0.1215	2.880
8	0.2217	3.325
9	0.3213	3.577
10	0.5221	3.813
11	1.0216	3.905
12	1.5218	3.595
13	2.0049	3.745

The mean value for the entire channel cross section was then computed using the normal means. Again symmetry about the channel centerline was assumed and the following equation used:

$$V_m = \frac{1}{z_n} \left( \frac{U_{m1}}{2} (z_1) + \frac{U_{m1} + U_{m2}}{2} (z_2 - z_1) + \dots \right. \\ \left. \dots + \frac{U_{m\ n-1} + U_{m\ n}}{2} (z_n - z_{n-1}) \right) \dots \dots \dots B-12$$



Using Equation B-12 with the values in TABLE B-4,  $V_m = 3.606$  ft/sec.

#### B.1.4. Maximum Velocity

The maximum extrapolated velocity for each of the normals to the bed was computed by extrapolating the regression line to the free surface. Rewriting Equation B-2,

$$u = \frac{1}{b} (\log y - a) \quad \dots\dots\dots B-13$$

and for the sample vertical, with  $y = h = 0.666$  feet,

$$u_{\max.} = \frac{1}{0.62303} (\log 0.666 + 3.00031) = 4.53 \text{ f.p.s.}$$

Similarly, extrapolated maximum velocities were computed and retained for each velocity profile.

#### B.1.5. Dimensionless Velocities

The dimensionless velocities  $u/u_*$  were calculated along with the dimensionless distances  $y/k$  and  $u_*y/\nu$  for each measured velocity. These values were retained for plotting.

The constant B in Equation 5-1 was calculated for each dimensionless velocity profile, using the regression equation with  $y = k$ , such that:

$$B = A (\log k - a) \quad \dots\dots\dots B-14$$

For the sample normal presented in TABLES B-1 and B-2

$$B = 5.75 (\log 0.0415 + 3.00031) = 9.31$$

These values were retained for averaging and plotting.



## B.2. Boundary Tube Data

The following sections describe computations carried out by the computer program for analysis of Preston tube data.

### B.2.1. Preliminary Processing

Preliminary processing of the 2529, 10 digit readings which formed Test 3.61 was similar to that described for the velocity distribution data of Test 3.60. The data was comprised of 20 scans of dynamic head along with the tubes y and z coordinates at each of 21 points on the bed and 21 points on the wall. Other readings were test number, discharge, temperature and x coordinate. TABLE B-5 presents the data set resulting from preliminary processing.

The z and y coordinates in TABLE B-5 are the averages of 20 readings. The datum planes for the bed and wall are exactly the same as for the velocity distribution measurements. The dynamic pressures are the average of 20 values calculated from the measured dynamic head indicated by the pressure transducer. The following conversion is required:

$$\Delta p = \rho g \Delta h \quad \dots\dots\dots B-15$$

where  $\Delta h$  is the dynamic head in feet of water.

### B.2.2. Preston Tube Calibration

A sub-program computed the pressure to shear ratio  $\Delta p/\tau_0$  and the parameter  $\Delta p_*$  for boundary tube measurements on the central portion of the bed at locations where velocity profiles were available. For this example,  $\Delta p$  at  $z = 2.0060$  feet is  $5.0535 \text{ lbs/ft}^2$  (TABLE B-5) and





TABLE B-5

DATA FROM BOUNDARY TUBE 1 AFTER PRELIMINARY PROCESSING

Test	Discharge c.f.s.	Temp. °F	x Coord. ft.	z Coord. ft.	y Coord. ft.	Pressure lbs/ft. <sup>2</sup>
3.61	9.01	71.1	32.0	0.0215	0.0217	1.4565
				0.0269	0.0218	1.4316
				0.0315	0.0219	1.4734
				0.0414	0.0218	1.6599
				0.0516	0.0217	2.0605
				0.0615	0.0218	2.3959
				0.0816	0.0217	2.9653
				0.1013	0.0218	3.3002
				0.1211	0.0215	3.6558
				0.1616	0.0211	3.9485
				0.2221	0.0215	4.1511
				0.3222	0.0214	4.4366
				0.4223	0.0215	4.6196
				0.5224	0.0218	5.2360
				0.6233	0.0220	5.2502
				0.8219	0.0216	5.0672
				1.0228	0.0216	4.2050
				1.3225	0.0214	4.5998
				1.5222	0.0215	4.2504
				1.8209	0.0214	4.4884
				2.0060	0.0213	5.0535
				0.0216	0.0214	1.2993
				0.0215	0.0265	1.5392
				0.0213	0.0316	1.7442
				0.0216	0.0417	2.1086
				0.0216	0.0514	2.4708
				0.0215	0.0616	2.7488
				0.0216	0.0816	3.0958
				0.0215	0.1015	3.5890
				0.0214	0.1213	3.7121
				0.0217	0.1413	4.1576
				0.0217	0.1615	4.2807
				0.0218	0.2011	4.3475
				0.0220	0.2515	4.4275
				0.0216	0.3017	4.1589
				0.0215	0.3519	4.1074
				0.0214	0.4027	3.9550
				0.0217	0.4522	3.8766
				0.0217	0.5020	3.6966
				0.0215	0.5520	3.8890
				0.0214	0.6013	4.0110
				0.0215	0.6621	1.9164



$\tau_o$  at nearly the same location ( $z = 2.0049$  feet) was given by Equation B-7. Therefore,

$$\frac{\Delta p}{\tau_o} = \frac{5.0535}{0.1510} = 33.5 \quad \dots\dots\dots \text{B-16}$$

$$\begin{aligned} \text{and } \Delta p_* &= \frac{\Delta p}{4} \frac{d^2}{\rho v^2} = \frac{5.053(0.0098)^2}{4 \times 1.937(1.038 \times 10^5)^2} \\ &= 5.81 \times 10^5 \quad \dots\dots\dots \text{B-17} \end{aligned}$$

These parameters provided one point for the Preston tube calibration which is presented in CHAPTER VI.

### B.2.3. Boundary Shear Stress from Preston Tube Readings

From the completed Preston tube calibration chart, a calibration curve was derived for each tube size on each roughness. For tube 1 and  $k_s = 0.0415$  feet, the following equations were used:

$$\text{for } \Delta p_* > 4 \times 10^5, \quad \frac{\Delta p}{\tau_o} = 29.0 \quad \dots\dots\dots \text{B-18}$$

$$\begin{aligned} \text{for } 4 \times 10^3 < \Delta p_* < 4 \times 10^5, \quad \frac{\Delta p}{\tau_o} &= 29.0 + \\ &8.5 \frac{4 \times 10^5 - \Delta p_*}{3.6 \times 10^5} \quad \dots\dots\dots \text{B-19} \end{aligned}$$

$$\text{for } \Delta p_* < 4 \times 10^3, \quad \text{Equation 2-23}$$

Using these equations in a sub-program with the data of TABLE B-5, the boundary shear stress was computed for each position. The results are presented in TABLE B-6.

The local shear stress values were then integrated to yield means for the bed, the wall and the entire boundary. Using Equation



TABLE B-6  
BOUNDARY SHEAR STRESSES AND COORDINATES  
FROM PRESTON TUBE DATA, TEST 3.61

ON BED			ON WALL		
Point	z Coordinate ft.	$\tau_b$ lbs/ft. <sup>2</sup>	Point	y Coordinate ft.	$\tau_w$ lbs/ft. <sup>2</sup>
1	0.0215	0.0422	1	0.0214	0.0372
2	0.0269	0.0414	2	0.0265	0.0449
3	0.0315	0.0428	3	0.0316	0.0517
4	0.0414	0.0489	4	0.0417	0.0644
5	0.0516	0.0627	5	0.0514	0.0778
6	0.0615	0.0750	6	0.0616	0.0887
7	0.0818	0.0976	7	0.0816	0.1030
8	0.1013	0.1119	8	0.1015	0.1238
9	0.1211	0.1261	9	0.1213	0.1280
10	0.1616	0.1362	10	0.1413	0.1434
11	0.2221	0.1431	11	0.1615	0.1476
12	0.3222	0.1530	12	0.2011	0.1499
13	0.4223	0.1593	13	0.2515	0.1527
14	0.5224	0.1805	14	0.3017	0.1434
15	0.6233	0.1810	15	0.3519	0.1416
16	0.8219	0.1747	16	0.4027	0.1364
17	1.0228	0.1450	17	0.4522	0.1337
18	1.3225	0.1586	18	0.5020	0.1274
19	1.5222	0.1466	19	0.5520	0.1341
20	1.8209	0.1548	20	0.6013	0.1383
21	2.0060	0.1743	21	0.6621	0.0576

B-8 with the data in TABLE B-6,  $\bar{\tau}_b = 0.1531$  lbs/ft.<sup>2</sup>. Using the wall data and Equation B-9,  $\bar{\tau}_w = 0.1246$  lbs/ft.<sup>2</sup>. With these results in Equation B-10,  $\bar{\tau}_o = 0.1459$  lbs/ft.<sup>2</sup>. These values were stored for



each test.

Other sub-programs calculated the dimensionless shear stress values and dimensionless distances and arranged the values for plotting in various forms.

### B.3. Error Estimates

TABLE B-7 lists an estimate of the error for each measured variable and each calculated parameter for the sample data of Tests 3.60 and 3.61.

TABLE B-7

ESTIMATED EXPERIMENTAL ERRORS FOR TESTS 3.60 AND 3.61

Parameter	Symbol	Value	Units	Error
coordinates	x	32.00	ft.	$\pm 0.01$
	y	0.0217 to 0.6507	ft.	$\pm 0.002$
	z	0.0216 to 2.0049	ft.	$\pm 0.002$
discharge	Q	9.00	c.f.s.	$\pm 0.1$
temperature	T	71.2	$^{\circ}\text{F}$	$\pm 0.1$
differential head	$\Delta h$	0 to 0.5	ft.	$\pm 0.001$
shear meter force	$F_x$	0.044	lbs.	$\pm 0.002$
average depth	h	0.67	ft.	$\pm 0.01$
water surface slope	S	0.0044		$\pm 0.0006$
roughness height	k	0.0415	ft.	$\pm 0.0002$
flume breadth	b	3.923	ft.	$\pm 0.002$
breadth/depth	b/h	5.90		$\pm 0.09$
depth/roughness	h/k	16.0		$\pm 0.25$





TABLE B-7 - (Cont'd.)

Parameter	Symbol	Value	Units	Error
tube diameter	d	0.0098	ft.	$\pm 0.0001$
wetted perimeter	P	5.26	ft.	$\pm 0.02$
section area	A	2.61	ft. <sup>2</sup>	$\pm 0.04$
hydraulic radius	R	0.497	ft.	$\pm 0.008$
point velocity	u	2.13 to 4.07	f.p.s.	$\pm 0.1$
shear velocity	$u_*$	0.28	f.p.s.	$\pm 0.03$
local shear stress	$\tau_0$	0.15	p.s.f.	$\pm 0.03$
integrated shear stress	$\overline{\tau_0}$	0.17	p.s.f.	$\pm 0.01$
local shear stress	$F_x/A_x$	0.084	p.s.f.	$\pm 0.005$
average shear stress	$\gamma_{RS}$	0.14	p.s.f.	$\pm 0.02$
mean velocity in vertical	$U_m$	3.75	f.p.s.	$\pm 0.1$
integrated mean velocities	$V_m$	3.61	f.p.s.	$\pm 0.1$
section mean	Q/A	3.44	f.p.s.	$\pm 0.07$
Froude number	$V^2/g h$	0.55		$\pm 0.02$
Reynolds number	$V R/\nu$	$171 \times 10^3$		$\pm 3 \times 10^3$
roughness Reynolds number	$\overline{u_*} k/\nu$	1060		$\pm 100$
Preston tube measurement	$\Delta p$	5.05	p.s.f.	$\pm 0.3$
pressure shear ratio	$\Delta p/\tau_0$	33.4		$\pm 7.0$
$\Delta p d^2/4 \rho \nu^2$	$p_*$	$5.80 \times 10^5$		$\pm 0.3 \times 10^5$
local shear stress from $\Delta p$	$\tau_0$	0.17	p.s.f.	$\pm 0.03$
integrated shear stress	$\overline{\tau_0}$	0.15	p.s.f.	$\pm 0.01$



## APPENDIX C

### EXPERIMENTAL DATA



SERIES 1

Rectangular Channel,  $b = 4.021$  feet  
Smooth Boundary

TABLE C-1  
EXPERIMENTAL DATA

Test Number	1	2	3	4	5	6
Slope	0.0100	0.0100	0.0100	0.0100	0.0100	0.0100
Discharge	2.65	0.75	2.25	2.25	3.75	1.00
Depth	0.162	0.070	0.135	0.135	0.186	0.081
Kinematic Viscosity						
$\nu \times 10^5$	1.140	1.105	1.104	1.100	1.093	1.088
Mean Velocity, Centerline Profile	4.78	3.03	4.40	4.46	5.07	3.25
Breadth/Depth	24.8	57.4	29.8	29.8	21.6	49.6
Wetted Perimeter	4.345	4.161	4.291	4.291	4.393	4.183
Hydraulic Radius	0.150	0.068	0.127	0.127	0.170	0.079
Mean Velocity	4.07	2.66	4.14	4.14	5.01	3.07
Froude Number	3.18	3.14	3.94	3.94	4.19	3.61
Reynolds Number	53600	16400	47500	47800	77700	22200
Friction Factor	0.0233	0.0248	0.0191	0.0191	0.0174	0.0216
Shear Stress	0.101	0.0436	0.0842	0.0842	0.116	0.0505
	0.0935	0.0424	0.0792	0.0792	0.106	0.0493
velocity profile on centerline						
$u^2$	0.107	0.0508	0.103	0.0990	0.119	0.0587
shear meter on centerline	0.0905	0.0454	0.0824	0.0824	0.112	0.0580



TABLE C-1 (continued)

Test Number		7	8	9	10	11	12
Slope	S	0.0100	0.0100	0.005	0.005	0.005	0.005
Discharge	Q	c.f.s.	7.25	4.85	2.50	1.00	0.50
Depth	h	ft.	0.305	0.270	0.172	0.102	0.068
Kinematic Viscosity	$\nu \times 10^5$	ft. <sup>2</sup> /sec.	1.100	1.096	1.092	1.088	1.062
Mean Velocity, Centerline Profile	$U_m$	f.p.s.	5.79	4.61	3.66	2.64	1.99
breadth/Depth	b/h		16.5	14.9	23.4	39.4	59.1
Wetted Perimeter	P	ft.	4.507	4.561	4.365	4.225	4.157
Hydraulic Radius	R	ft.	0.217	0.238	0.158	0.097	0.066
Mean Velocity	$V = Q/A$	f.p.s.	5.62	4.45	3.62	2.44	1.82
Froude Number	$V^2/gh$		4.02	2.28	2.36	1.81	1.52
Reynolds Number	$VR/\nu$		111000	96600	52300	21800	11300
Friction Factor	$f = 8gRS/V^2$		0.0177	0.0155	0.0155	0.0210	0.0256
Shear Stress	$\gamma$ lbs	lbs./ft. <sup>2</sup>	0.152	0.190	0.0536	0.0318	0.0212
	$\gamma$ RS	"	0.135	0.165	0.0493	0.0302	0.0206
velocity profile on centerline	$\rho u_*^2$	"	0.142	0.187	0.0508	0.0280	0.0186
shear meter on centerline	$F_s/A_s$	"	0.125	0.132	0.0656	0.0289	0.0217









TABLE C-3  
EXPERIMENTAL DATA

SERIES 3

Rectangular Channel,  $b = 3.923$  feet  
Rough Boundary,  $k = 0.0415$  feet

Test Number	1	2	3	4	5	6
Slope	0.0100	0.0097	0.0100	0.00465	0.00450	0.00440
Discharge	1.05	5.00	9.00	1.00	5.03	9.00
Depth	0.150	0.366	0.537	0.173	0.452	0.666
Kinematic Viscosity						
Mean Velocity, integrated	0.987	1.038	1.006	0.950	0.997	1.038
Breadth/Depth	1.44	3.21	4.36	1.56	2.90	3.61
Depth/Roughness	26.1	10.7	7.30	22.6	8.66	5.90
Wetted Perimeter	3.62	8.82	12.9	4.16	10.9	16.0
Hydraulic Radius	4.223	4.665	4.997	4.269	4.827	5.255
Mean Velocity	0.139	0.309	0.422	0.159	0.368	0.497
Froude Number	1.79	3.48	4.26	1.48	2.82	3.44
Reynolds Number	0.664	1.06	1.05	0.393	0.546	0.551
Friction Factor	25200	103500	179000	24800	104000	171000
Roughness Reynolds Number	0.112	0.0658	0.0659	0.0875	0.0539	0.0477
Shear Stress	890	1260	1520	673	961	1060
velocity profile on centerline	0.0936	0.229	0.335	0.0501	0.127	0.183
shear meter on centerline	0.0866	0.193	0.263	0.0460	0.104	0.136
	0.109	0.211	0.228	0.0442	0.118	0.151
	-	0.178	0.205	0.0641	0.0939	0.0838







TABLE C-4  
EXPERIMENTAL DATA

SERIES 4

Rectangular Channel,  $b = 4.021$  feet  
Rough Bed  $k = 0.0208$  feet

Test Number	1	2	3	4	5	6
Slope	0.0010	0.0010	0.0010	0.0030	0.0030	0.0030
Discharge	4.40	1.00	5.20	2.50	4.40	5.65
Depth	0.635	0.238	0.693	0.294	0.468	0.538
Kinematic Viscosity						
$\nu \times 10^5$	1.111	1.142	1.135	1.135	1.135	1.135
Mean Velocity on Centerline						
$U_m$	1.98	1.17	2.30	2.18	2.54	2.92
Breadth/Depth	6.33	16.9	5.80	13.7	8.59	7.48
Depth/Roughness	30.2	11.4	33.3	14.1	22.4	25.9
Wetted Perimeter	5.291	4.497	5.407	4.609	4.957	5.097
Hydraulic Radius	0.483	0.213	0.515	0.256	0.380	0.424
Mean Velocity	1.72	1.04	1.74	2.12	2.32	2.62
Froude Number	0.145	0.141	0.136	0.475	0.358	0.396
Reynolds Number	74600	19400	79000	47800	77600	97700
Friction Factor	0.0418	0.0507	0.0440	0.0440	0.0544	0.0478
Roughness Reynolds Number	234	210	236	288	351	371
Shear Stress						
$\tau_{hs}$	0.0397	0.0149	0.0432	0.0550	0.0880	0.101
$\tau_{RS}$	0.0302	0.0133	0.0322	0.0479	0.0712	0.0795
velocity profile on center-line						
$\rho u_*^2$	0.0401	0.0186	0.0472	0.0621	0.0945	0.103





TABLE C-4 (continued)

Test Number	S	7	8	9	10	11	12
Slope		0.0030	0.0050	0.0050	0.0050	0.0090	0.0090
Discharge	Q	1.25	2.00	3.90	0.85	4.85	2.25
Depth	h	0.205	0.231	0.363	0.125	0.350	0.220
Kinematic Viscosity	$\nu \times 10^5$	1.135	1.122	1.125	1.105	1.111	1.109
Mean Velocity, on centerline	$U_m$	1.67	2.26	2.72	1.64	4.04	2.82
Breadth/Depth	b/h	19.6	17.4	11.1	32.1	11.5	18.3
Depth/Roughness	h/k	9.95	11.1	17.5	6.00	16.8	10.6
Wetted Perimeter	P	4.431	4.483	4.747	4.271	4.721	4.461
Hydraulic Radius	R	0.186	0.207	0.308	0.118	0.298	0.198
Mean Velocity	$V = Q/A$	1.51	2.15	2.68	1.68	3.44	2.54
Froude Number	$V^2/gh$	0.345	0.621	0.613	0.700	1.05	0.912
Reynolds Number	$VR/\nu$	24600	39600	73400	17900	92100	45400
Friction Factor	$f = 8gRS/V^2$	0.0630	0.0577	0.0553	0.0539	0.0583	0.0711
Roughness Reynolds Number	$\bar{u}_* k/\nu$	244	338	418	258	540	448
Shear Stress	$\gamma_{RS}$	0.0384	0.0722	0.113	0.0390	0.197	0.124
	$\gamma_{RS}$	0.0348	0.0646	0.0961	0.0368	0.162	0.111
velocity profile on centerline	$\rho u_*^2$	0.0425	0.0776	0.106	0.0554	0.218	0.132



TABLE C-4 (continued)

Test Number		13	14	15	16	17	18	19
Slope	S	0.0090	0.0120	0.0120	0.0120	0.0005	0.0005	0.0005
Discharge	Q	1.00	0.50	2.00	5.50	4.00	5.40	1.50
Depth	h	0.140	0.100	0.200	0.320	0.750	0.830	0.380
Kinematic Viscosity	$\nu \times 10^5$	1.095	1.100	1.095	.095	1.111	1.175	1.145
Mean Velocity, on centerline	$U_m$	2.14	1.94	3.00	4.42	1.64	1.78	0.92
Breadth/Depth	b/h	28.7	40.2	20.1	12.5	5.36	4.85	10.6
Depth/Roughness	h/k	6.73	4.81	9.62	15.4	36.0	40.0	18.2
Wetted Perimeter	P	4.301	4.221	4.421	4.661	5.521	5.681	4.781
Hydraulic Radius	R	0.131	0.0953	0.182	0.276	0.547	0.588	0.320
Mean Velocity	$V = Q/A$	1.78	1.24	2.49	4.27	1.32	1.61	0.98
Froude Number	$V^2/gh$	0.705	0.477	0.962	1.77	0.0720	0.0975	0.0785
Reynolds Number	$VR/\nu$	21300	10700	41400	108000	65200	80600	27400
Friction Factor	$f = 8gRS/V^2$	0.0956	0.192	0.0907	0.0468	0.0405	0.0291	0.0430
Roughness Reynolds Number	$u_* k/\nu$	370	362	506	620	176	172	130
Shear Stress	$\gamma$ hS	0.0785	0.0750	0.150	0.240	0.0234	0.0259	0.0119
	$\gamma$ RS	0.0735	0.0714	0.137	0.207	0.0171	0.0184	0.0100
velocity profile on centerline	$\epsilon u_*^2$	0.0776	0.0856	0.150	0.283	0.0234	0.0298	0.0115



TABLE C-5  
EXPERIMENTAL DATA

SERIES 5

Rectangular Channel,  $b = 4.008$  feet  
Rough Boundary,  $k = 0.00183$  feet

Test Number	1	2
Slope	0.0120	0.0100
Discharge	5.40	2.00
Depth	0.286	0.163
Kinematic Viscosity		
Mean Velocity, integrated		
breadth/Depth		
Depth Roughness		
Wetted Perimeter		
Hydraulic Radius		
Mean Velocity		
Froude Number		
Reynolds Number		
Friction Factor		
Roughness Reynolds Number		
Shear Stress		
velocity profile on centerline		
from velocity profiles		
from Preston Tube #1		



TABLE C-6

## EXPERIMENTAL DATA

## SERIES 6

Rectangular Channel,  $b = 3.953$  feet  
 Rough Boundary,  $k = 0.0208$  feet

Test Number	1	2	3	4
Slope	0.0100	0.0100	0.0100	0.0100
Discharge	1.00	0.382	5.01	9.01
Depth	0.130	0.0729	0.335	0.485
kinematic Viscosity				
Mean Velocity, integrated				
Breadth/Depth				
Depth/Roughness				
Wetted Perimeter				
Hydraulic Radius				
Mean Velocity				
Froude Number				
Reynolds Number				
Friction Factor				
Roughness Reynolds Number				
Shear Stress				
velocity profile on centerline				





TABLE C-6 (continued)

Shear Stress		1	2	3	4
from velocity profiles	$\tau_b$	0.0614	0.0330	0.171	0.233
	$\tau_w$	0.0363	0.0130	0.102	0.197
	$\tau_o$	0.0598	0.0323	0.161	0.226
from Preston Tube #1	$\tau_b$ max.	0.0823	0.0493	0.193	0.278
	$\tau_w$ max.	0.0605	0.0242	0.161	0.256
	$\tau_o$	0.0563	0.0309	0.168	0.223
from Preston Tube #2	$\tau_b$	0.0198	0.0097	0.0897	0.136
	$\tau_w$	0.0540	0.0302	0.156	0.206
	$\tau_o$	0.0719	0.0347	0.211	0.263
from Preston Tube #3	$\tau_b$ max.	0.0265	0.0144	0.126	0.173
	$\tau_w$ max.	0.0541	0.0310	0.160	0.211
	$\tau_o$	0.0257	0.0120	0.0748	0.132
from Preston Tube #4	$\tau_b$	0.0524	0.0303	0.148	0.195
	$\tau_w$	0.0643	0.0346	0.197	0.246
	$\tau_o$	0.0346	0.0179	0.0993	0.173
from Preston Tube #5	$\tau_b$ max.	0.0555	0.0310	0.172	0.215
	$\tau_w$ max.	0.0295	0.0101	0.0902	0.171
	$\tau_o$	0.0539	0.0301	0.160	0.206
from Preston Tube #6	$\tau_b$	0.0614	0.0361	0.206	0.258
	$\tau_w$	0.0410	0.0168	0.117	0.202
	$\tau_o$	0.0561	0.0325	0.161	0.226
from Preston Tube #7	$\tau_b$ max.	0.0311	0.0081	0.0869	0.166
	$\tau_w$ max.	0.0545	0.0316	0.150	0.214
	$\tau_o$	0.0603	0.0387	0.193	0.274
from Preston Tube #8	$\tau_b$	0.0490	0.0157	0.115	0.215
	$\tau_w$				
	$\tau_o$				



TABLE C-7  
EXPERIMENTAL DATA

SERIES 7

Trapezoidal Channel, 1:2 side slope,  $b = 1.974$  feet  
Rough Boundary,  $k = 0.0415$  feet

Test Number	1	2	3	4
Slope	0.01	0.01	0.01	0.01
Discharge	Q	1.50	2.50	3.50
Depth	h	0.251	0.325	0.378
Kinematic Viscosity	$\nu \times 10^5$	0.956	1.018	1.039
Mean Velocity, integrated	$V_m$	2.61	3.12	3.43
Breadth/Depth	$b/h$	12.7	6.07	5.23
Depth/Roughness	$h/k$	3.74	7.83	9.10
Wetted Perimeter	$P$	2.66	3.43	3.66
Hydraulic Radius	$R$	0.132	0.249	0.281
Mean Velocity	$V = Q/A$	1.56	2.92	3.40
Froude Number	$V^2/gh$	0.487	0.815	0.950
Reynolds Number	$VR/\nu$	21500	71500	91800
Friction Factor	$f = 8gRS/V^2$	0.140	0.0880	0.0627
Roughness Reynolds Number	$\bar{u}_* k/\nu$	895	1090	1200
Shear Stress	$\gamma_{hs}$	0.0965	0.203	0.236
	$\gamma_{RS}$	0.0824	0.125	0.175
	$\rho u_*^2$	0.1058	0.193	0.245
velocity profile on centerline	$\bar{u}_b$	0.106	0.184	0.233
from velocity profiles	$\bar{u}_w$	0.0502	0.0898	0.149
	$\bar{u}_b$	0.123	0.198	0.266
	$\bar{u}_b$ max.	0.118	0.148	0.256
	$\bar{u}_w$ max.	0.107	0.180	0.229
	$\bar{u}_b$	0.0415	0.0848	0.115
from Preston Tube #1	$\bar{u}_w$	0.0897	0.146	0.181
	$\bar{u}_b$ max.	0.117	0.195	0.295
	$\bar{u}_w$ max.	0.0871	0.134	0.239
	$\bar{u}_b$	0.119	0.157	0.220
from Preston Tube #2	$\bar{u}_b$	0.0414	0.0809	0.131
	$\bar{u}_w$	0.0992	0.130	0.190
	$\bar{u}_b$ max.	0.133	0.168	0.276
	$\bar{u}_w$ max.	0.0858	0.136	0.190



TABLE C-8  
EXPERIMENTAL DATA

SERIES 8

Trapezoidal Channel, 1:2 side slope,  $b = 1.550$  feet  
Rough Boundary,  $k = 0.0208$  feet

Test Number	1	2	3	4
Slope	0.010	0.010	0.010	0.010
Discharge	0.27	0.80	1.50	2.50
Depth	0.101	0.175	0.247	0.326
Kinematic Viscosity	$\nu \times 10^5$	1.034	1.041	1.079
Mean Velocity, integrated	$V_m$	2.47	3.05	3.48
Breadth/Depth	$b/h$	8.88	6.27	4.75
Depth/Roughness	$h/k$	8.41	11.9	15.7
Wetted Perimeter	$P$	2.33	2.66	3.01
Hydraulic Radius	$R$	0.143	0.198	0.238
Mean Velocity	$V = Q/A$	2.41	2.96	3.48
Froude Number	$V^2/gh$	1.03	1.10	1.15
Reynolds Number	$VR/\nu$	3300	56300	76800
Friction Factor	$f = 8gRS/V^2$	0.0634	0.0582	0.0507
Roughness Reynolds Number	$\bar{u}_* k/\nu$	339	515	535
Shear Stress	$\gamma$ $hS$	0.0630	0.154	0.204
	$\gamma$ $RS$	0.0552	0.129	0.149
	$\rho u_*^2$	0.0951	0.208	0.243
velocity profile on centerline	$\tau_b$	0.0799	0.172	0.216
from velocity profiles	$\tau_w$	0.0495	0.125	0.157
	$\tau_o$	0.0730	0.152	0.187
	$\tau_b$ max.	0.0951	0.208	0.243
	$\tau_w$ max.	0.0764	0.223	0.256
from Preston Tube #1	$\tau_b$	0.0873	0.182	0.234
	$\tau_w$	0.0371	0.125	0.159
	$\tau_o$	0.0760	0.158	0.198
	$\tau_b$ max.	0.114	0.202	0.263
	$\tau_w$ max.	0.0518	0.178	0.222
from Preston Tube #2	$\tau_b$	0.0890	0.194	0.224
	$\tau_w$	0.0422	0.136	0.167
	$\tau_o$	0.0783	0.170	0.197
	$\tau_b$ max.	0.101	0.209	0.251
	$\tau_w$ max.	0.0575	0.182	0.235



TABLE C-9  
EXPERIMENTAL DATA

SERIES 9

Trapezoidal Channel, 1:2 side slope,  $b = 1.581$  feet  
Rough Boundary,  $k = 0.00183$  feet

Test Number	1	2	3	4
Slope	0.010	0.010	0.010	0.010
Discharge	Q	c.f.s.	2.50	3.50
Depth	h	ft.	0.279	0.342
Kinematic Viscosity	$\nu \times 10^5$	ft. <sup>2</sup> /sec.	1.105	1.092
Mean Velocity, integrated	$V_m$	f.p.s.	4.31	4.72
Breadth/Depth	b/h	20.4	5.65	4.62
Depth/Roughness	h/k	42.4	153	187
Wetted Perimeter	P	ft.	2.83	3.11
Hydraulic Radius	R	ft.	0.211	0.244
Mean Velocity	$V = Q/A$	f.p.s.	4.18	4.60
Froude Number	$V^2/gh$	1.97	1.94	1.92
Reynolds Number	$VR/\nu$	13400	79800	102500
Friction Factor	$f = 8gRS/V^2$	0.0366	0.0345	0.0297
Roughness Reynolds Number	$\bar{u}_* k/\nu$	23.8	43.2	46.9
Shear Stress	$\gamma$ hS	lbs./ft. <sup>2</sup>	0.174	0.214
velocity profile on centerline from velocity profiles	$\gamma$ RS	"	0.132	0.152
	$\rho u_*^2$	"	0.143	0.183
	$\bar{t}_b$	"	0.145	0.164
	$\bar{t}_w$	"	0.104	0.114
	$\bar{t}_o$	"	0.127	0.140
	$\bar{t}_b$ max.	"	0.168	0.197
	$\bar{t}_w$ max.	"	0.154	0.194
	$\bar{t}_b$	"	0.143	0.155
	$\bar{t}_w$	"	0.0990	0.109
	$\bar{t}_o$	"	0.124	0.133
from Preston Tube #1	$\bar{t}_b$ max.	"	0.156	0.172
	$\bar{t}_w$ max.	"	0.134	0.156
	$\bar{t}_b$	"	0.142	0.163
	$\bar{t}_w$	"	0.0982	0.119
	$\bar{t}_o$	"	0.123	0.141
	$\bar{t}_b$ max.	"	0.155	0.176
	$\bar{t}_w$ max.	"	0.133	0.157
	$\bar{t}_b$	"		
	$\bar{t}_w$	"		
	$\bar{t}_o$	"		
from Preston Tube #2	$\bar{t}_b$ max.	"		
	$\bar{t}_w$ max.	"		
	$\bar{t}_b$	"		
	$\bar{t}_w$	"		
	$\bar{t}_o$	"		
	$\bar{t}_b$ max.	"		
	$\bar{t}_w$ max.	"		
	$\bar{t}_b$	"		
	$\bar{t}_w$	"		
	$\bar{t}_o$	"		





## APPENDIX D

### VELOCITY MEASUREMENTS



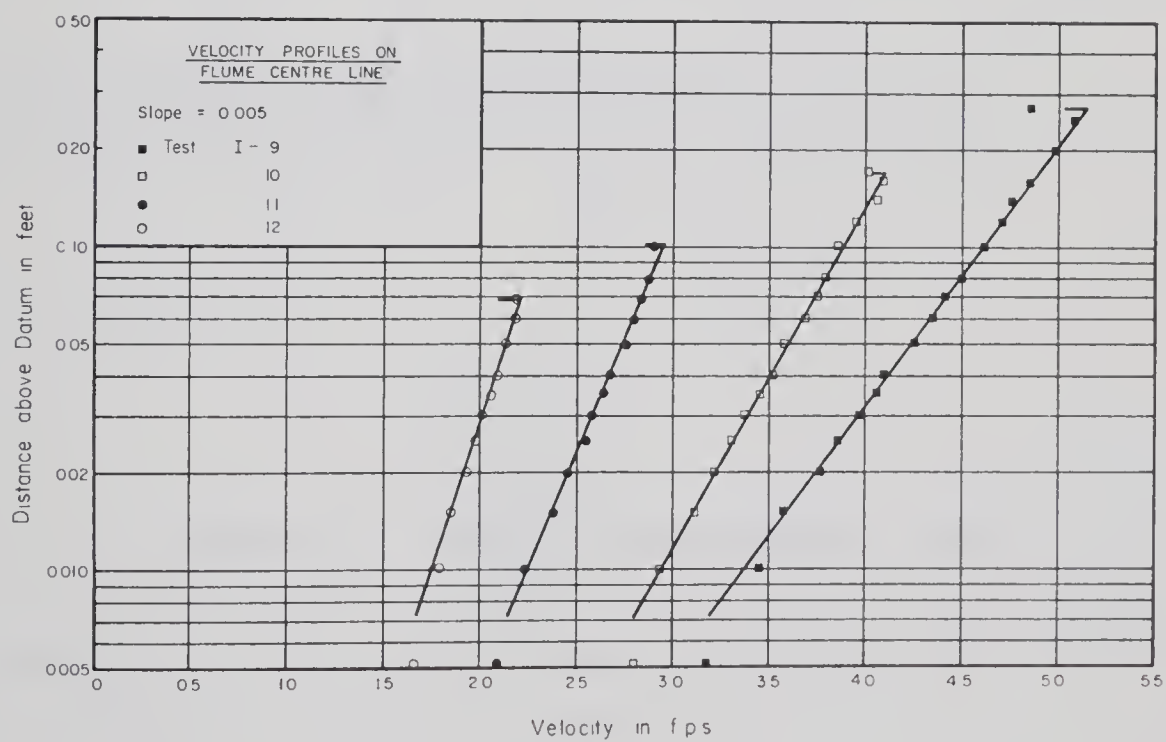
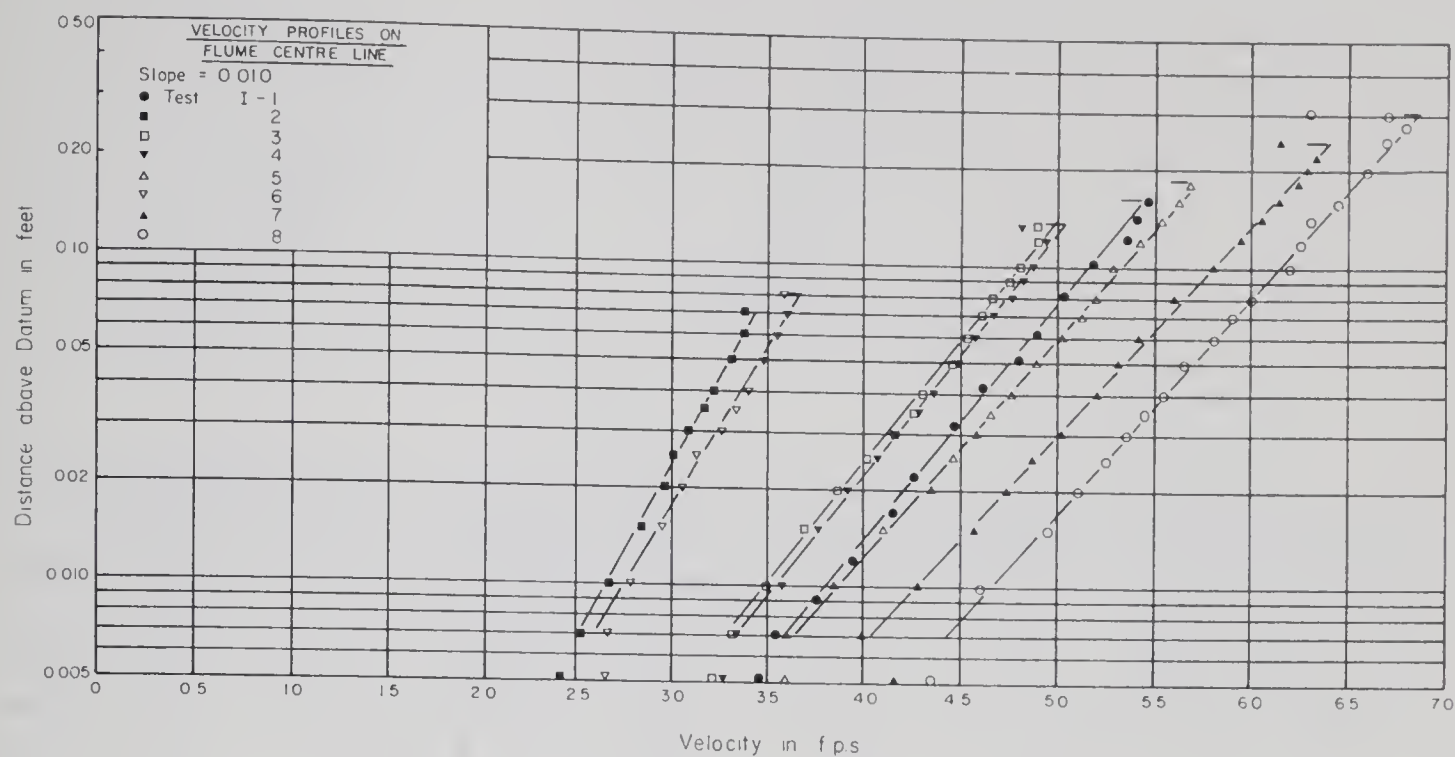


FIGURE D-1. VELOCITY MEASUREMENTS, SERIES 1



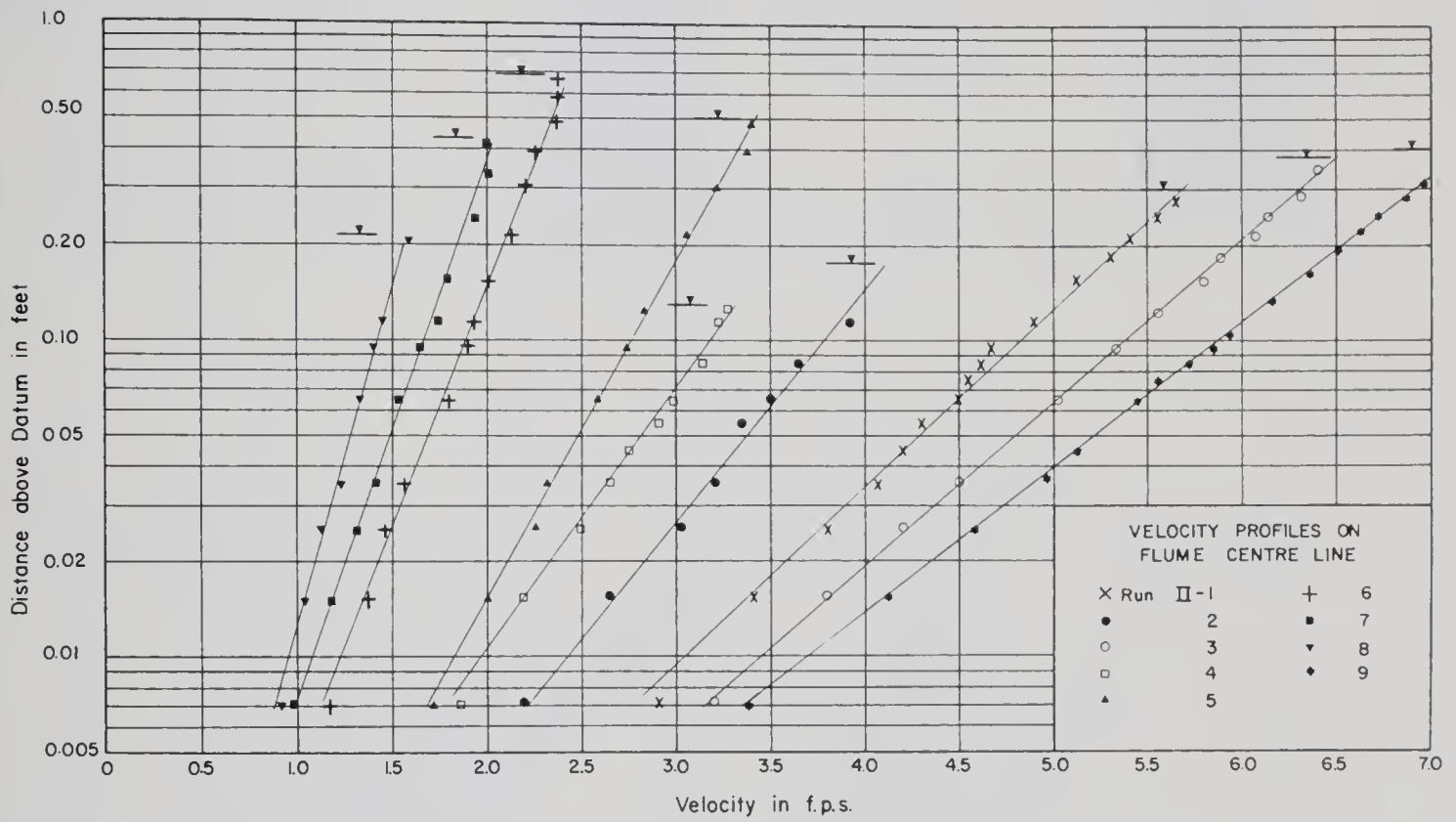


FIGURE D-2. VELOCITY MEASUREMENTS, SERIES 2



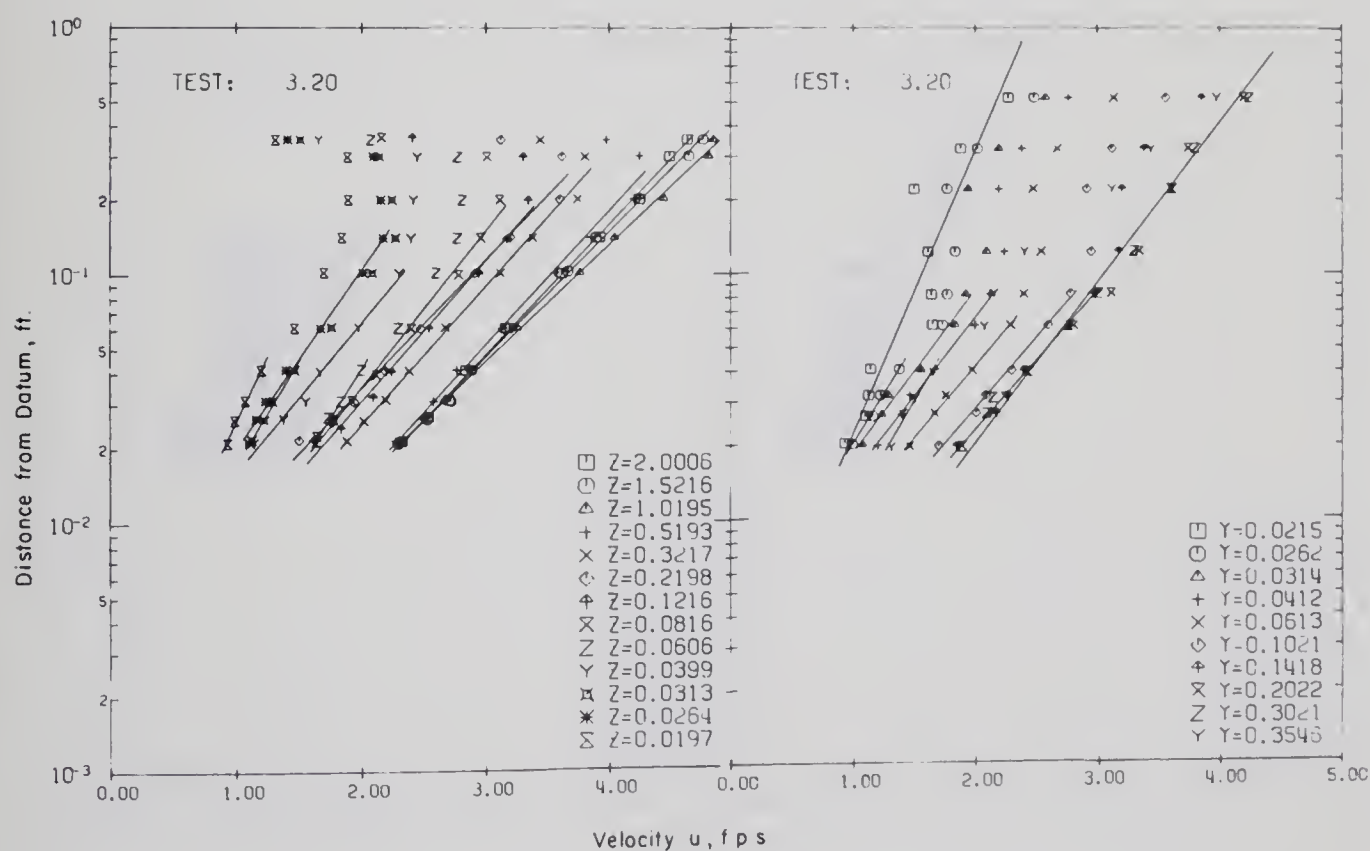
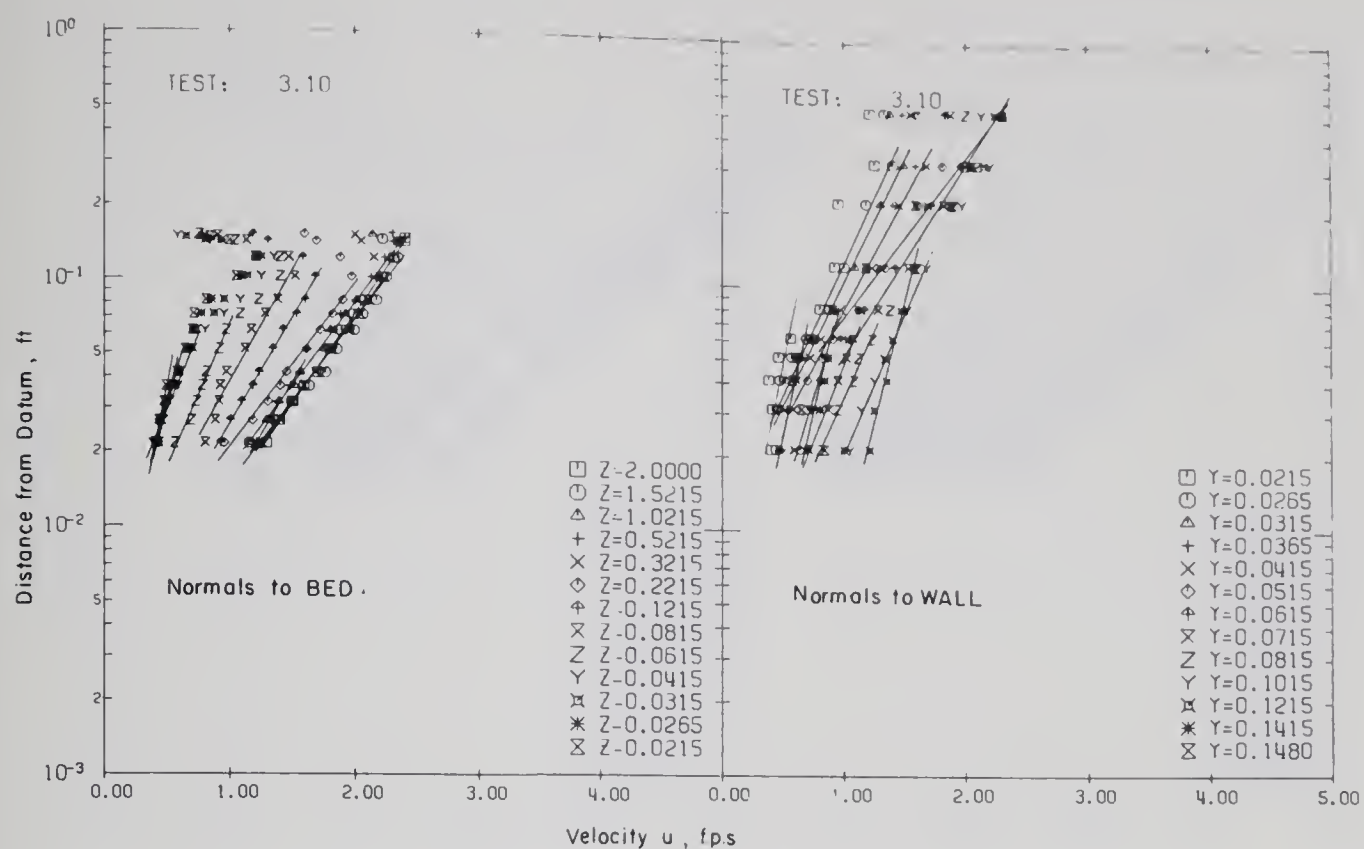


FIGURE D-3. VELOCITY MEASUREMENTS, SERIES 3





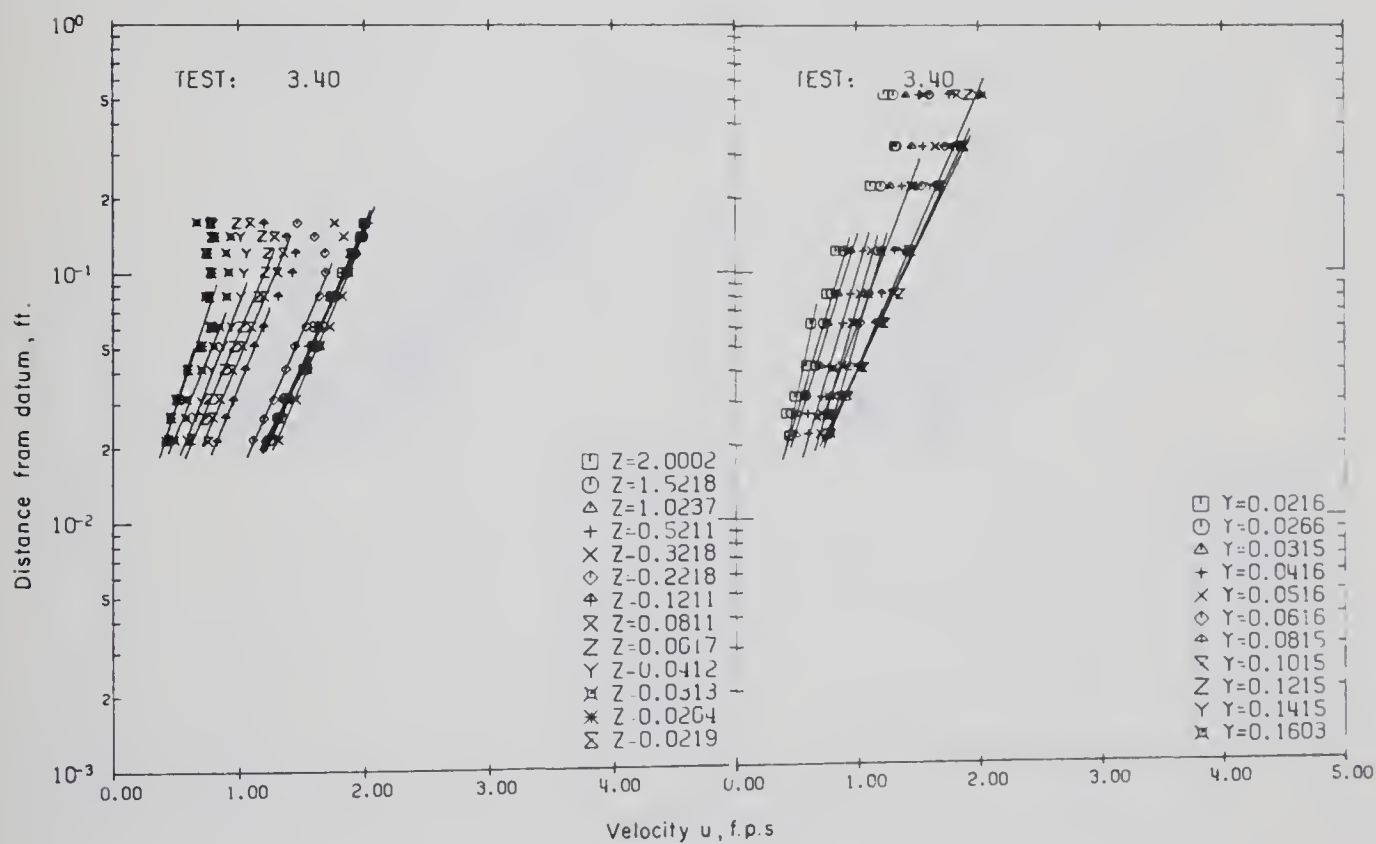
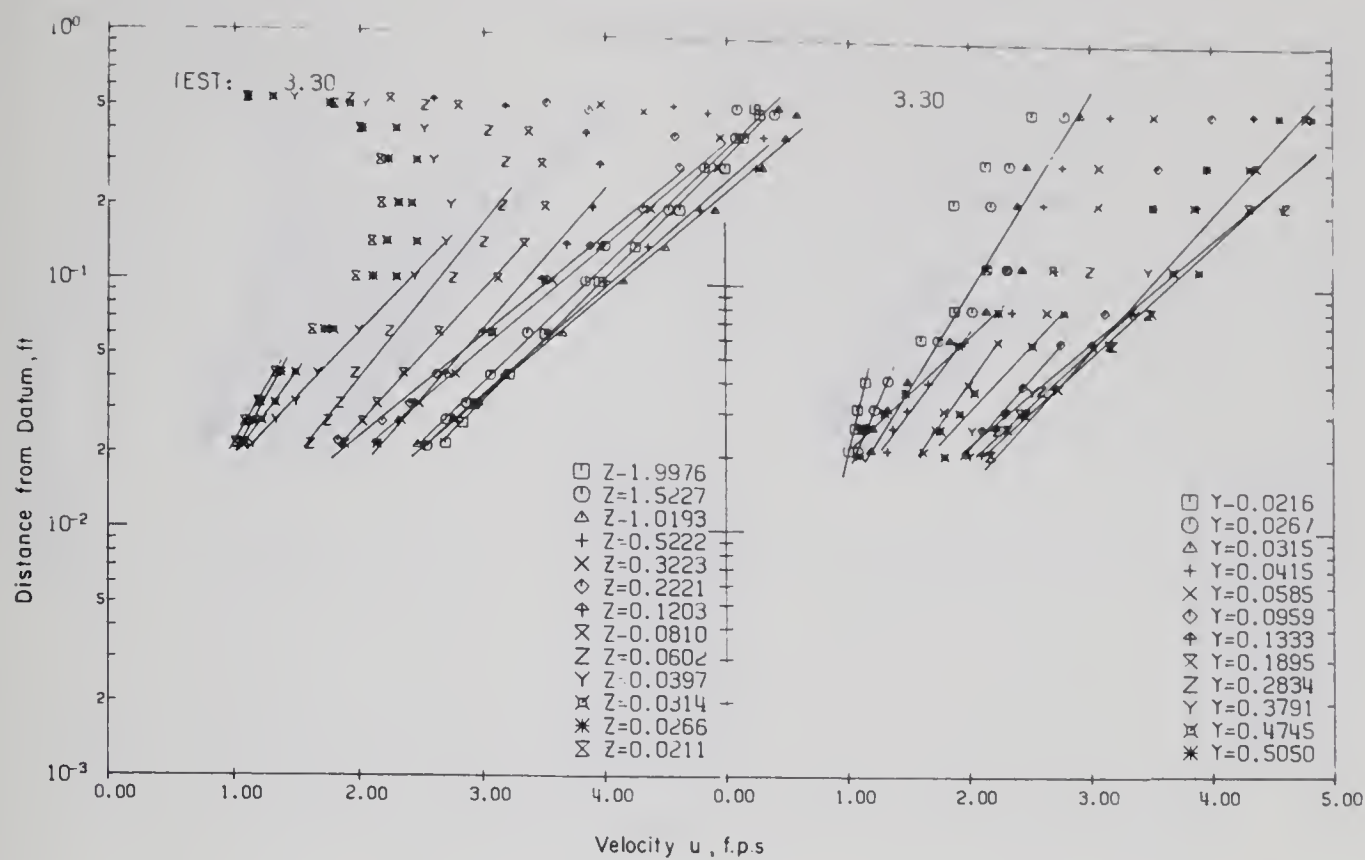


FIGURE D-3 - (Continued)



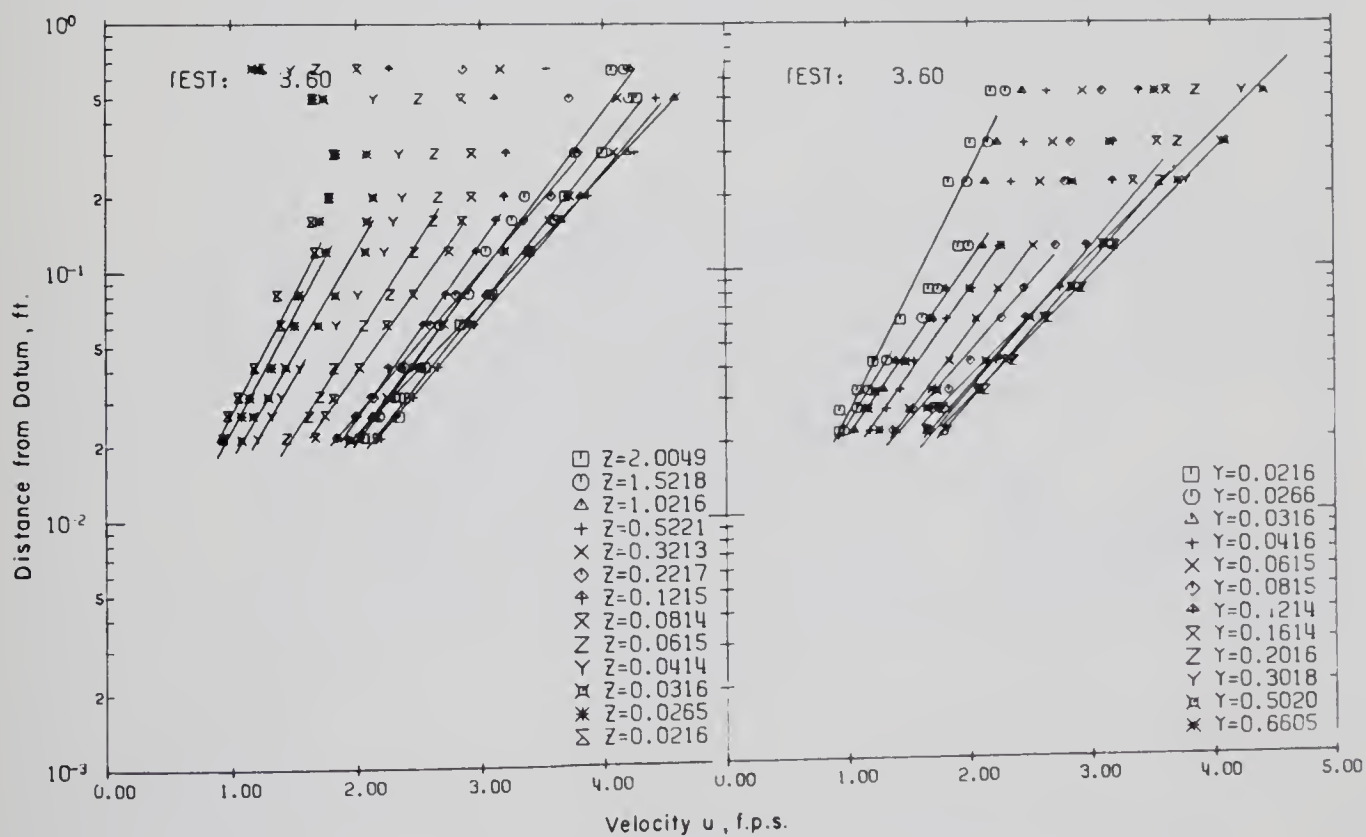
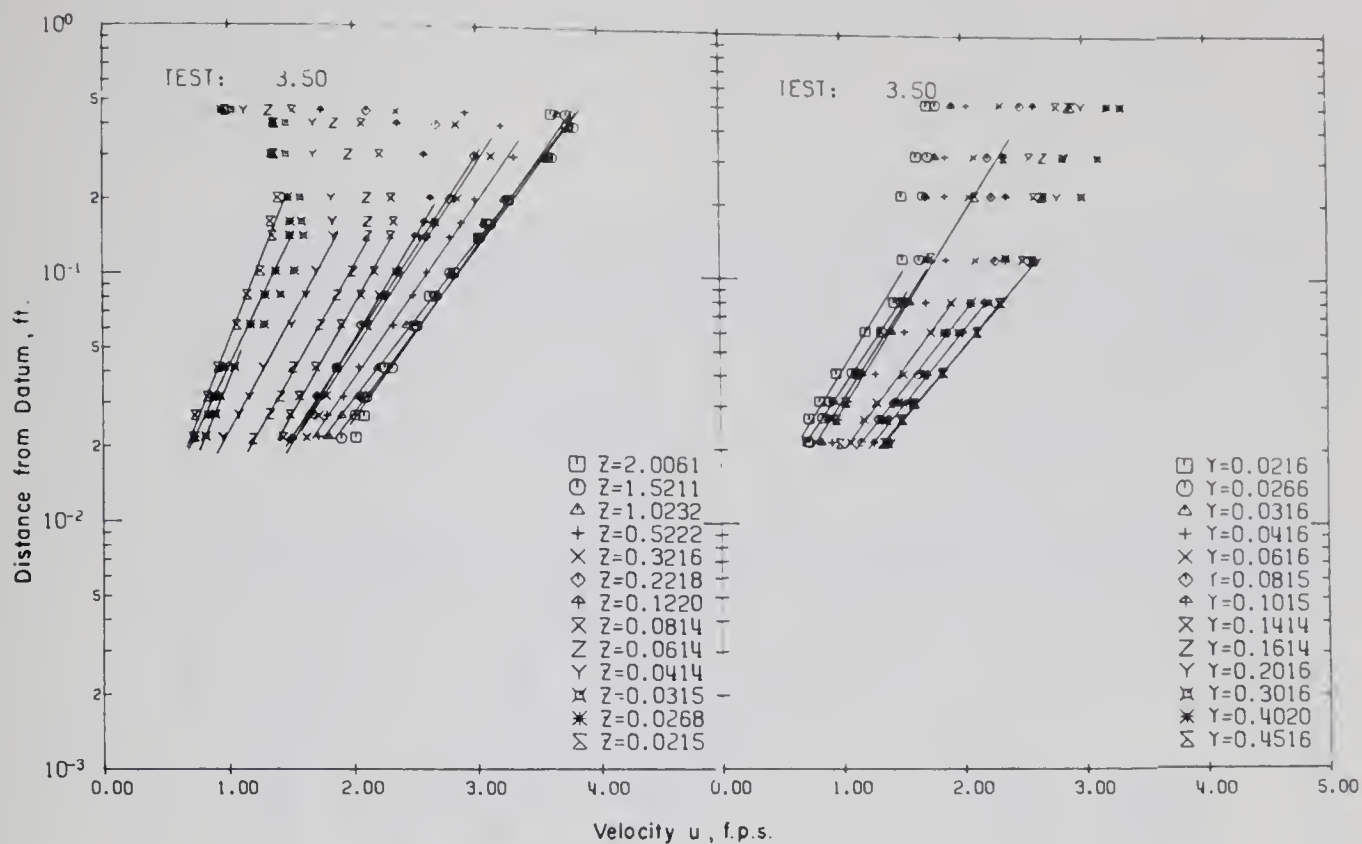


FIGURE D-3 - (Continued)



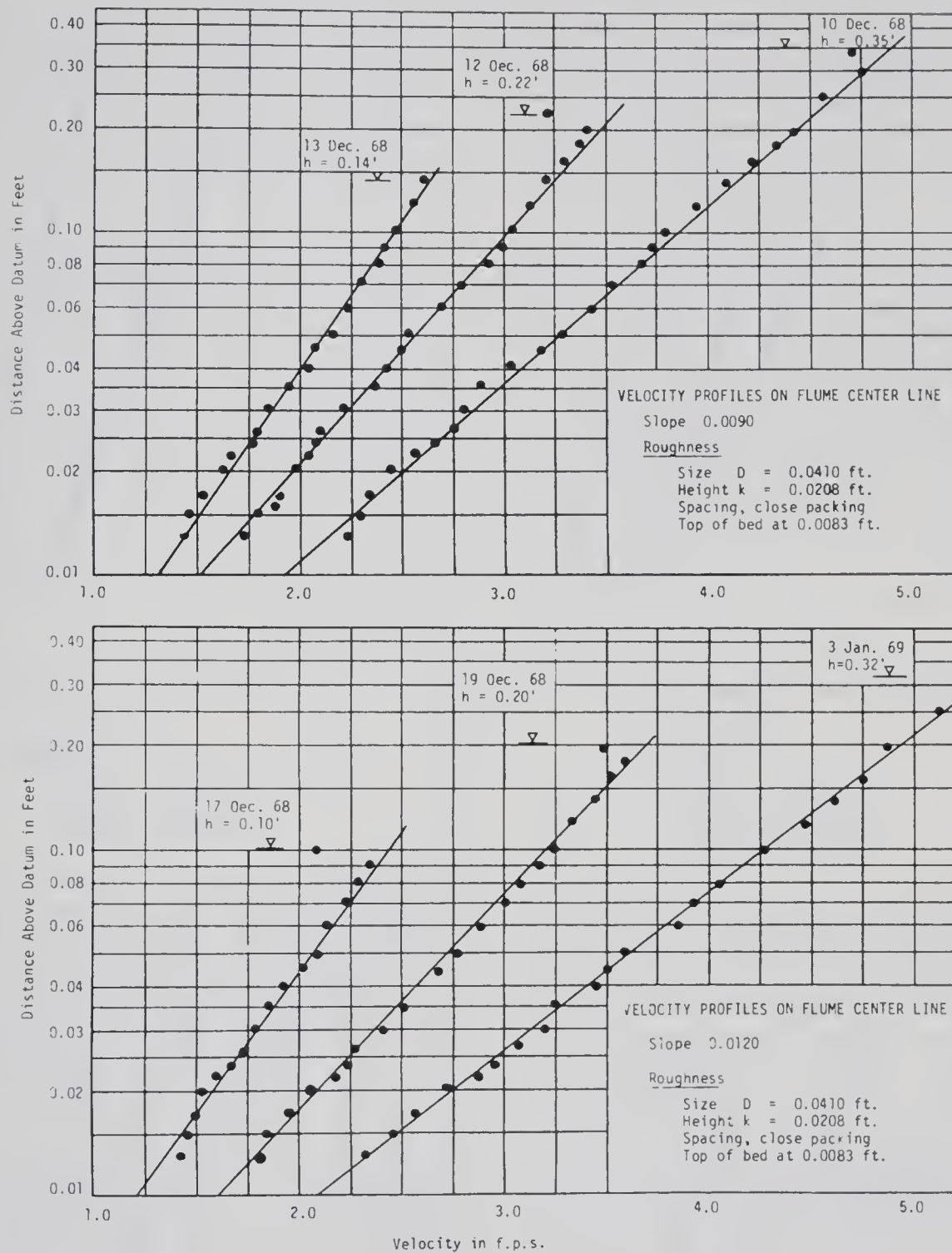


FIGURE D-4. VELOCITY MEASUREMENTS, SERIES 4



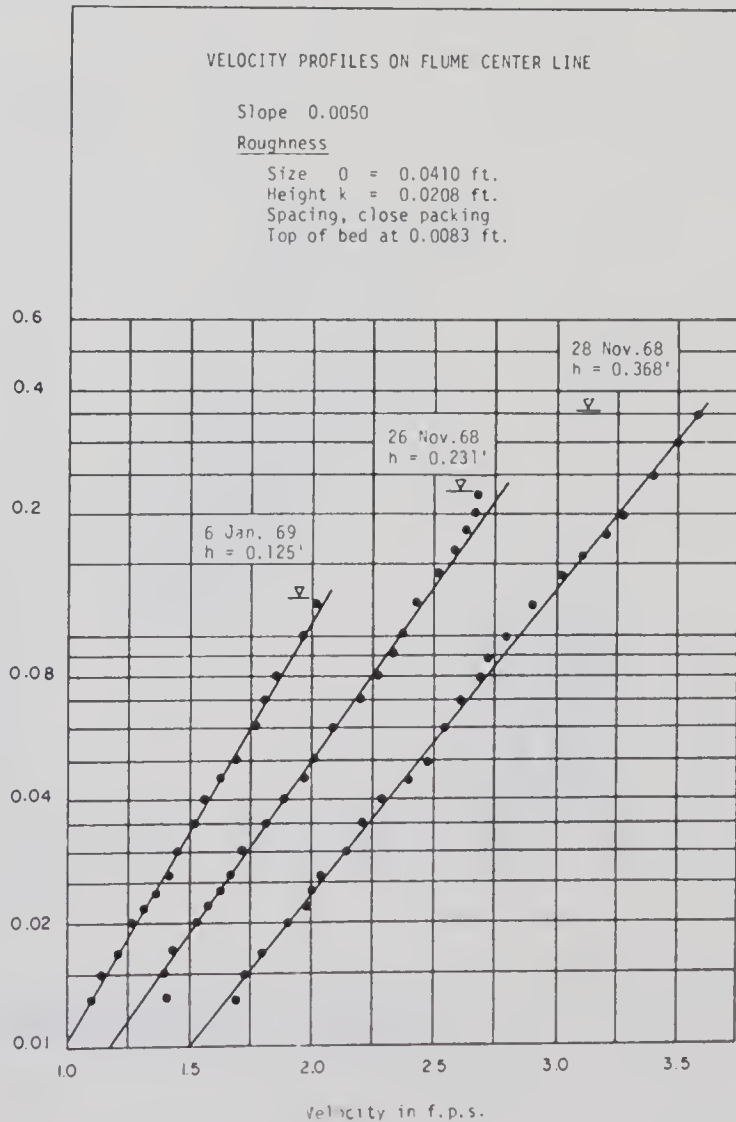
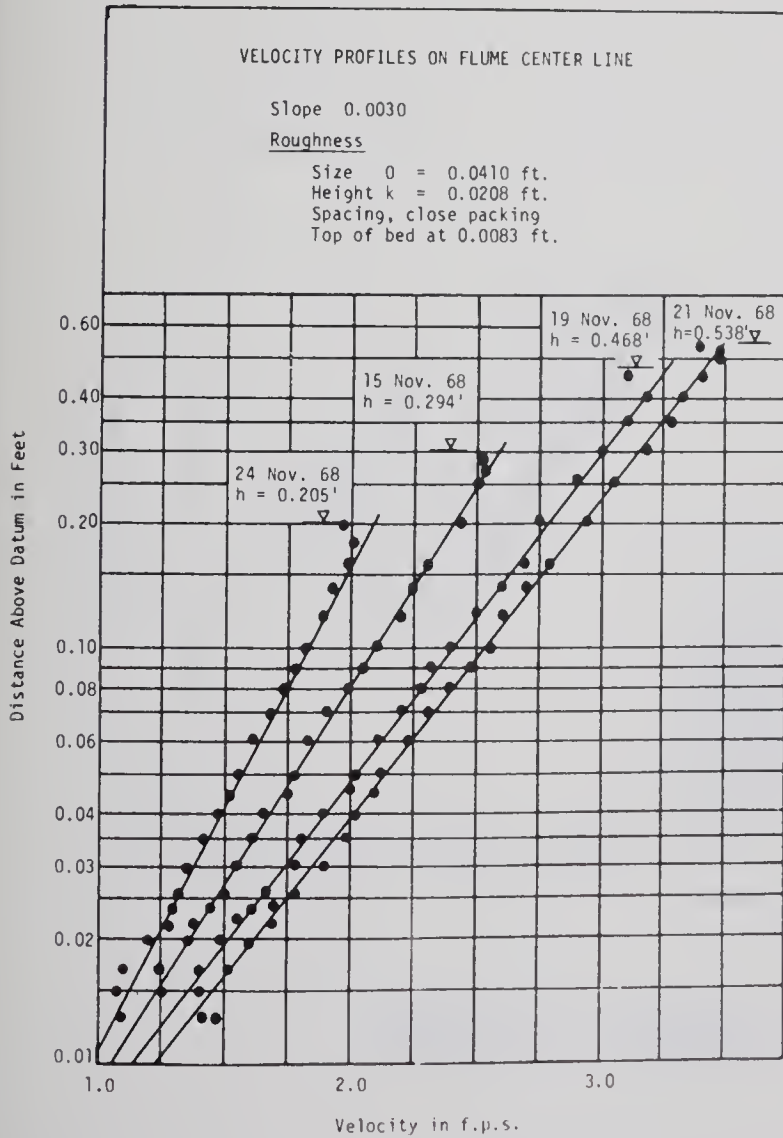
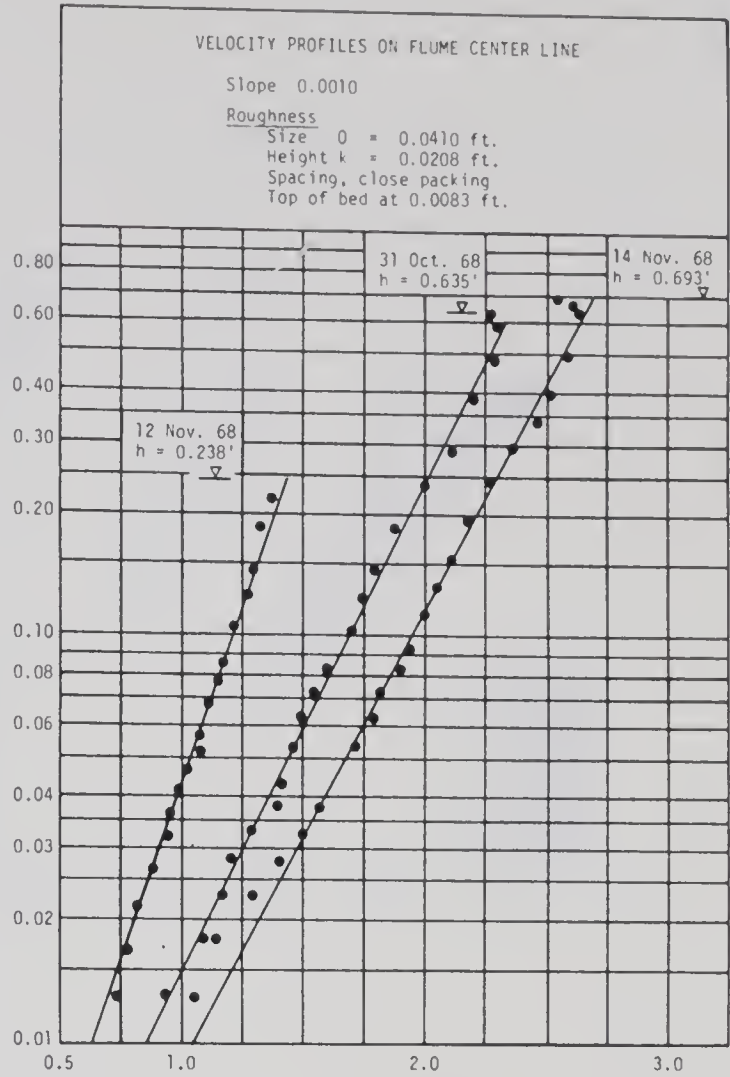
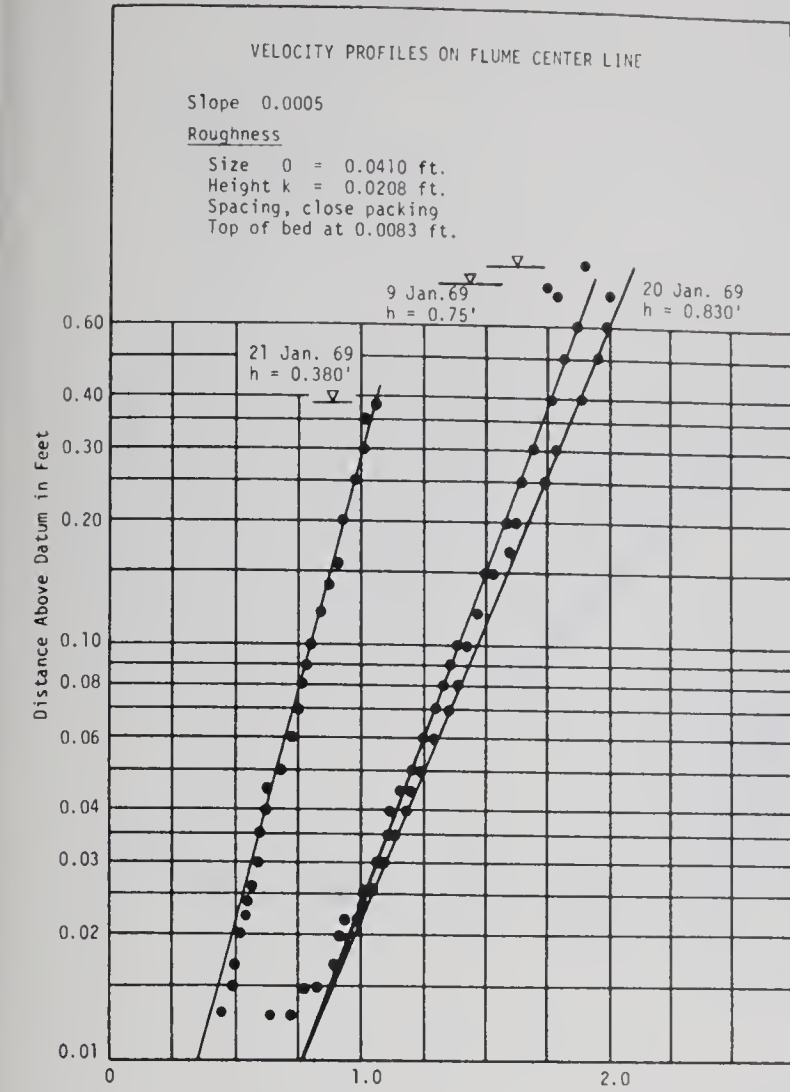


FIGURE D-4 - (Continued)







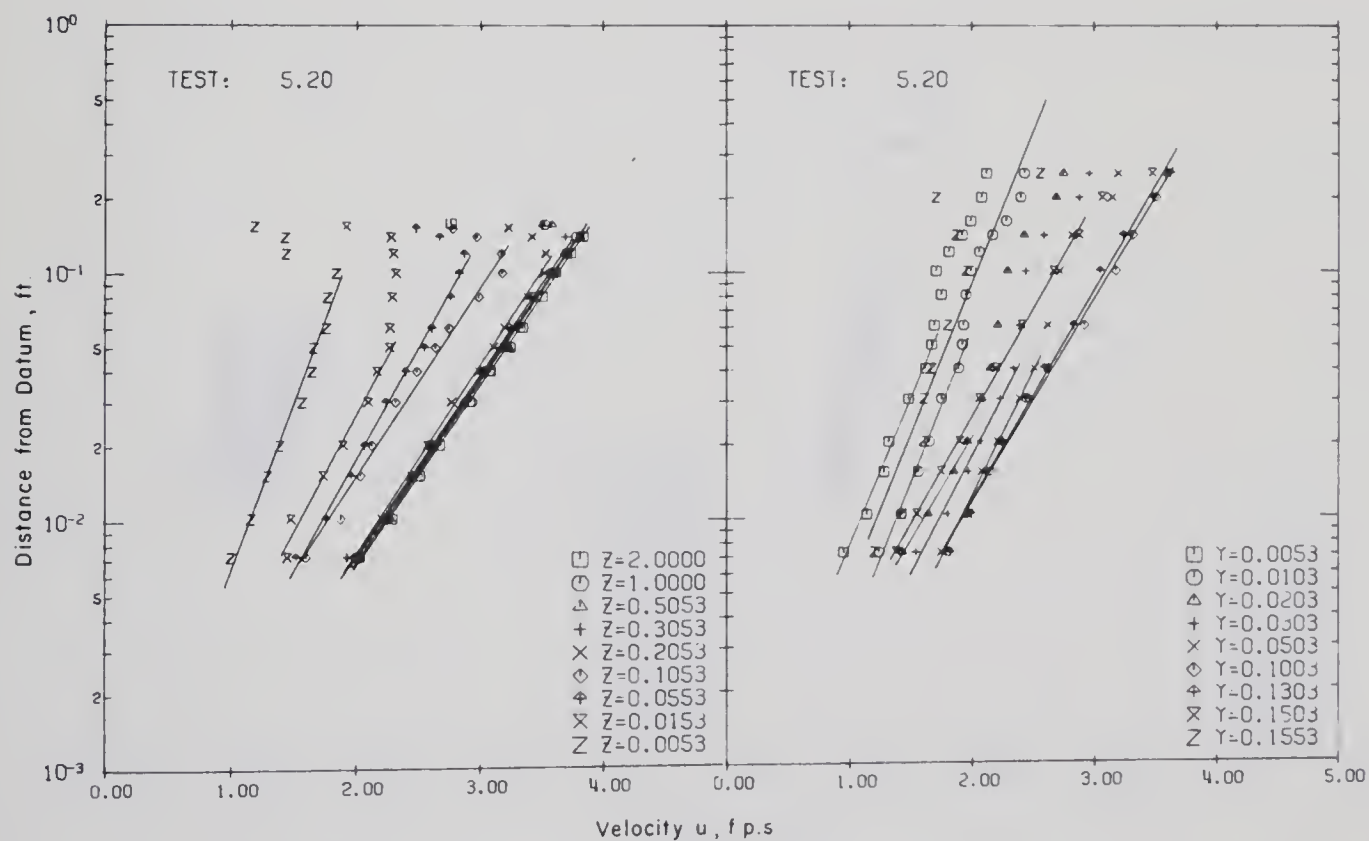
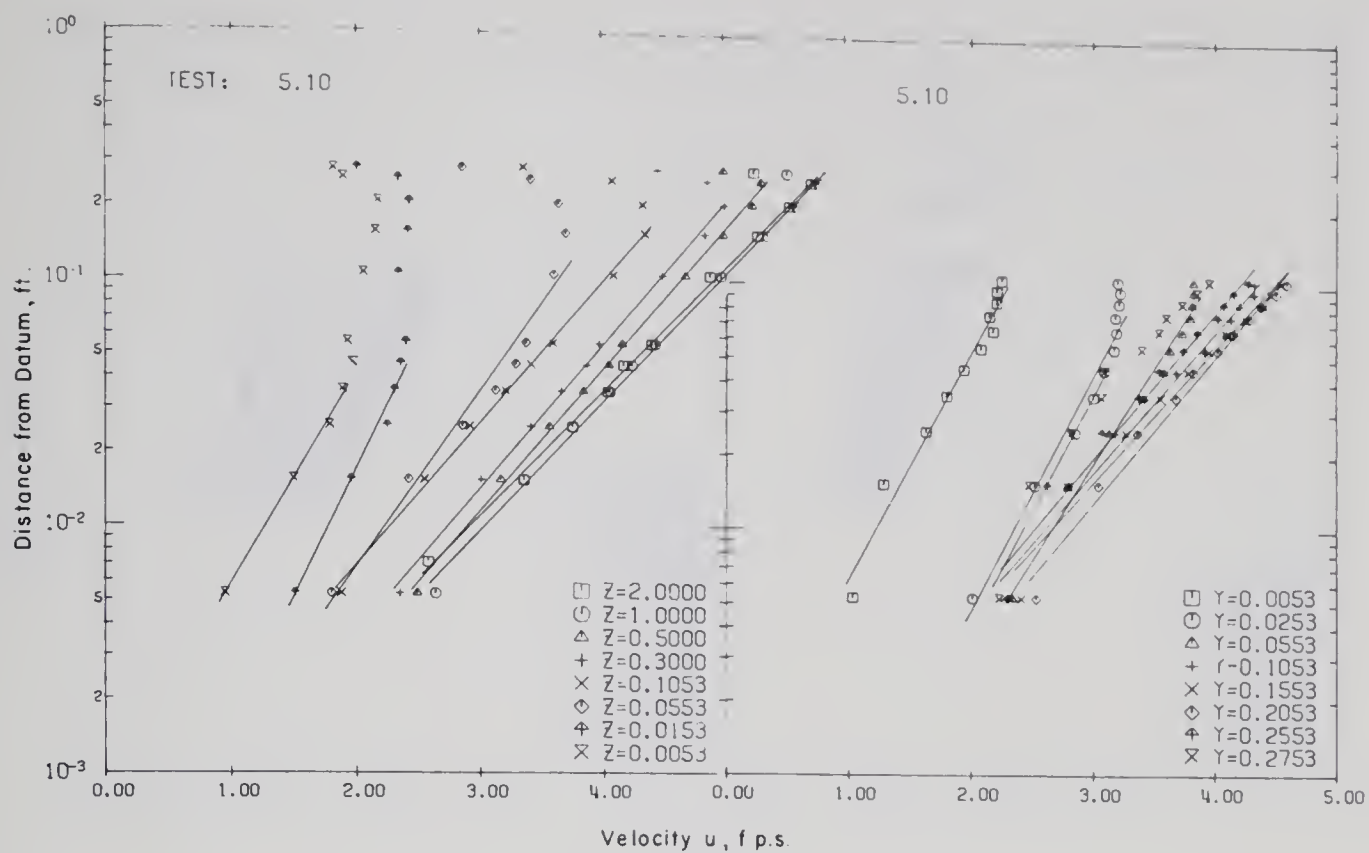


FIGURE D-5. VELOCITY MEASUREMENTS, SERIES 5



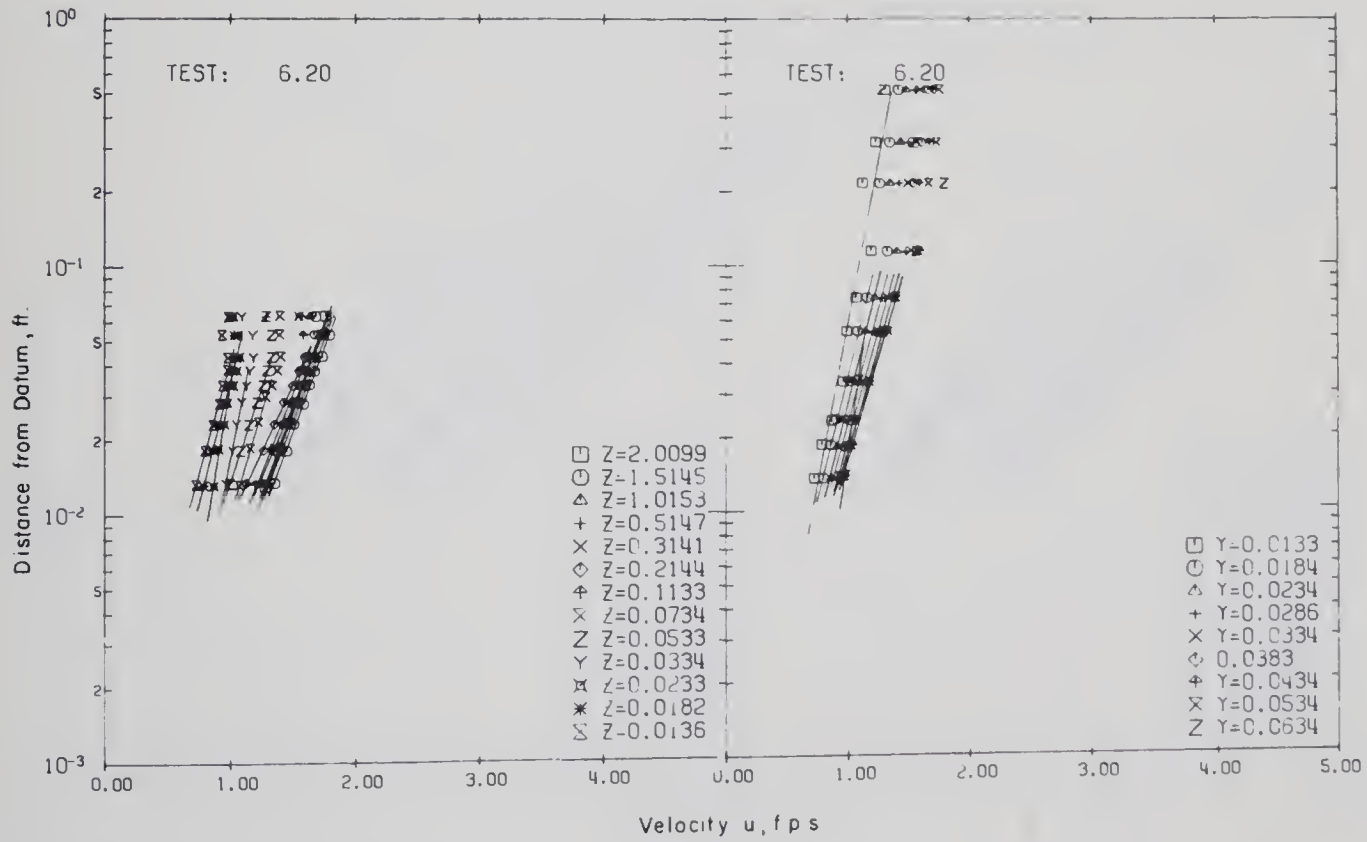
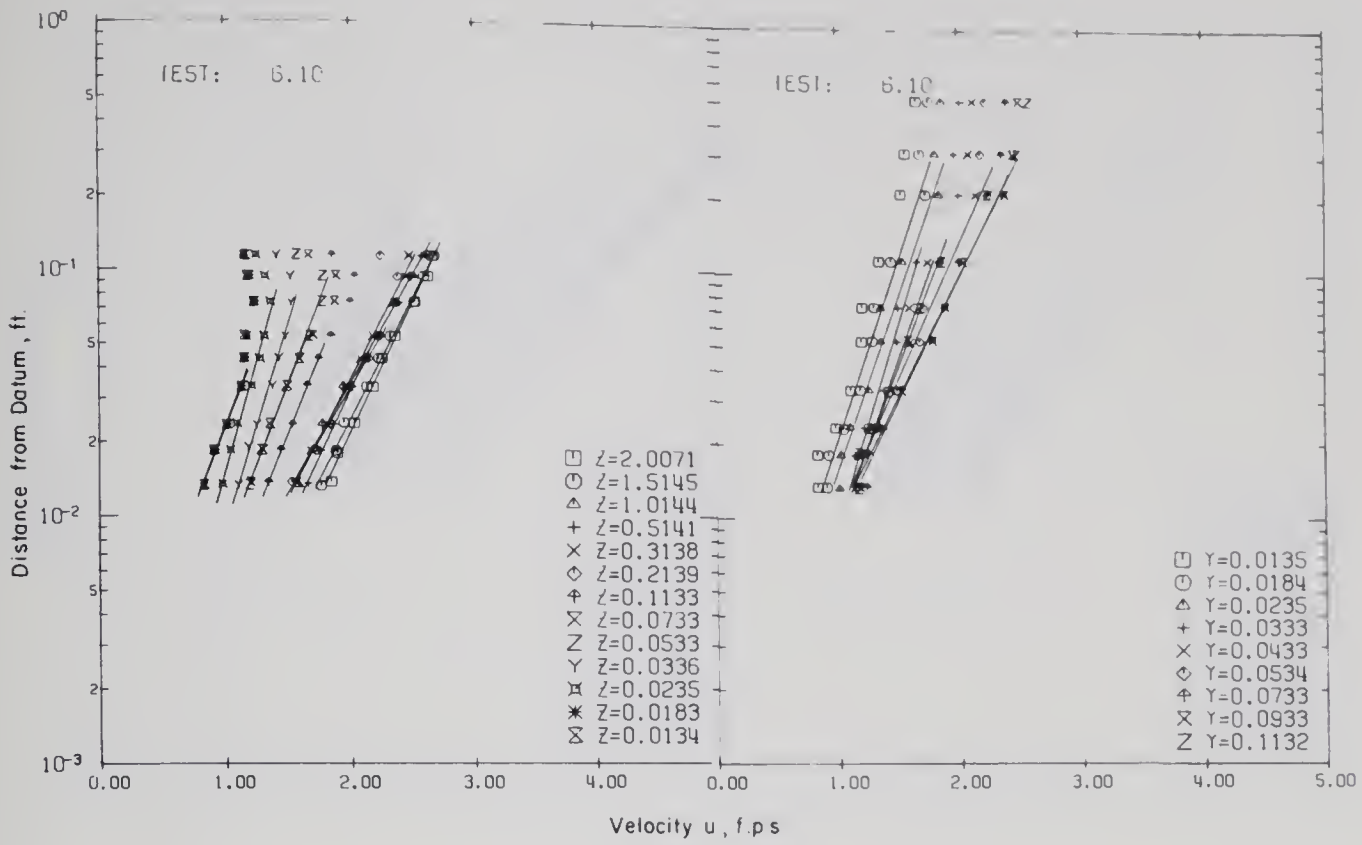


FIGURE D-6. VELOCITY MEASUREMENTS, SERIES 6



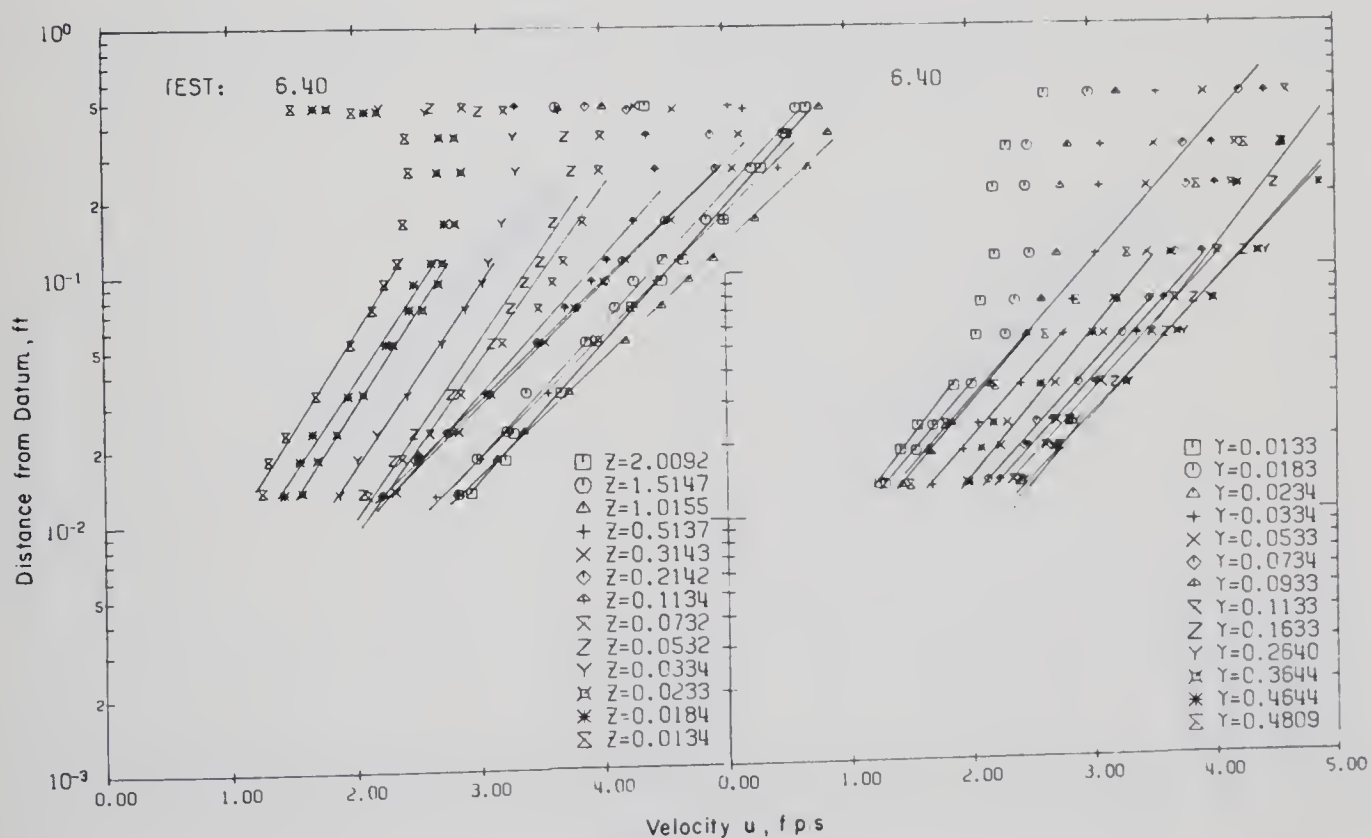
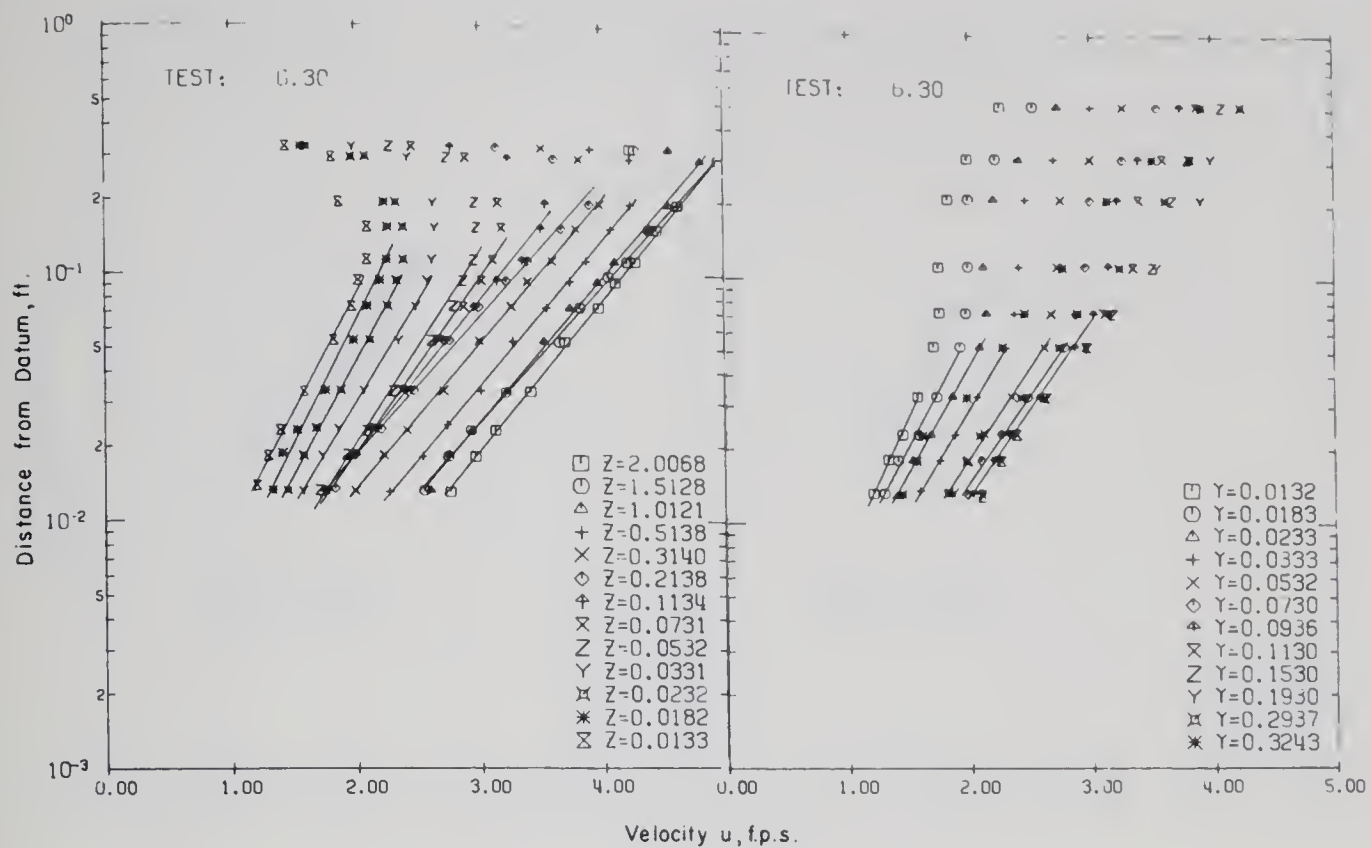


FIGURE D-6 - (Continued)



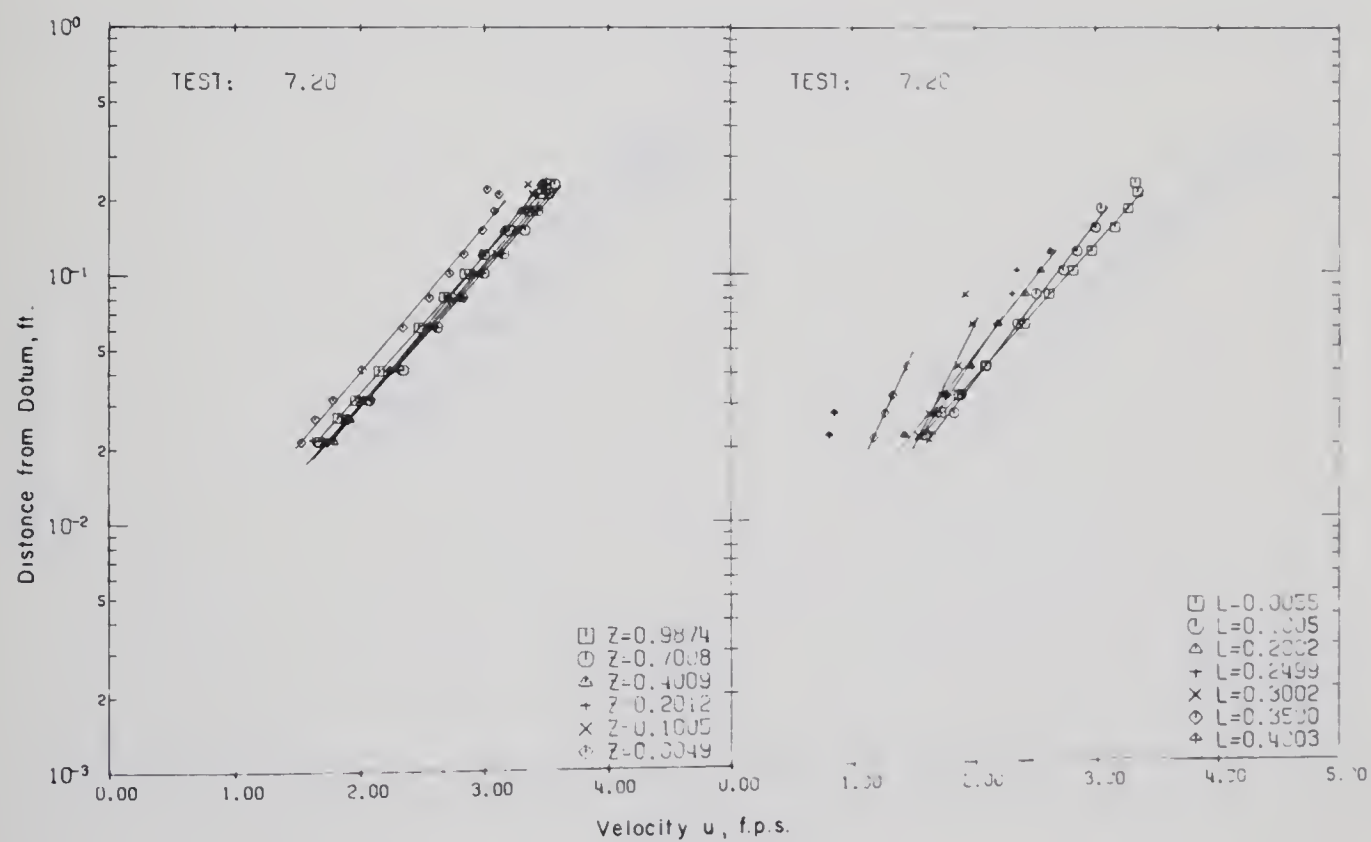
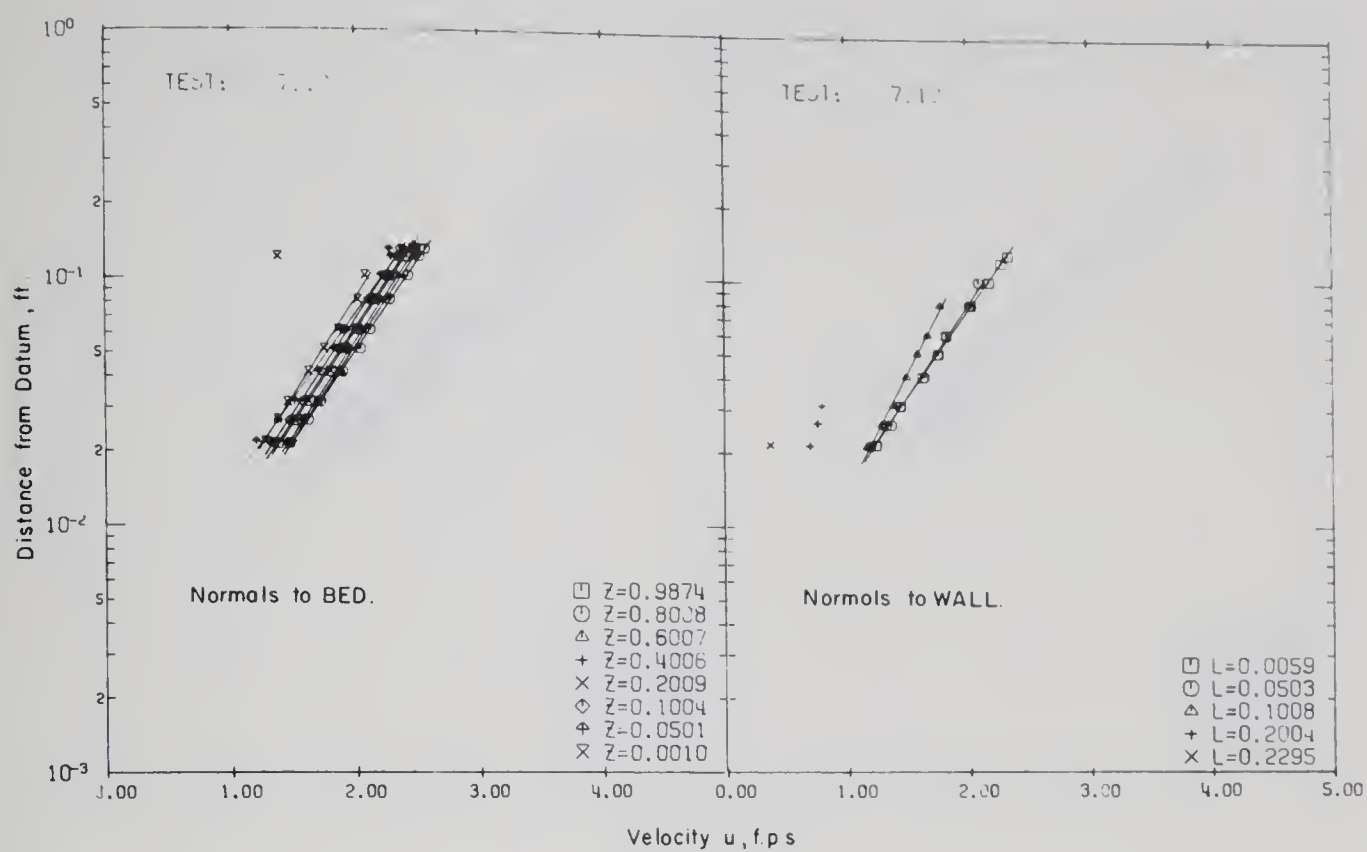


FIGURE D-7. VELOCITY MEASUREMENTS, SERIES 7





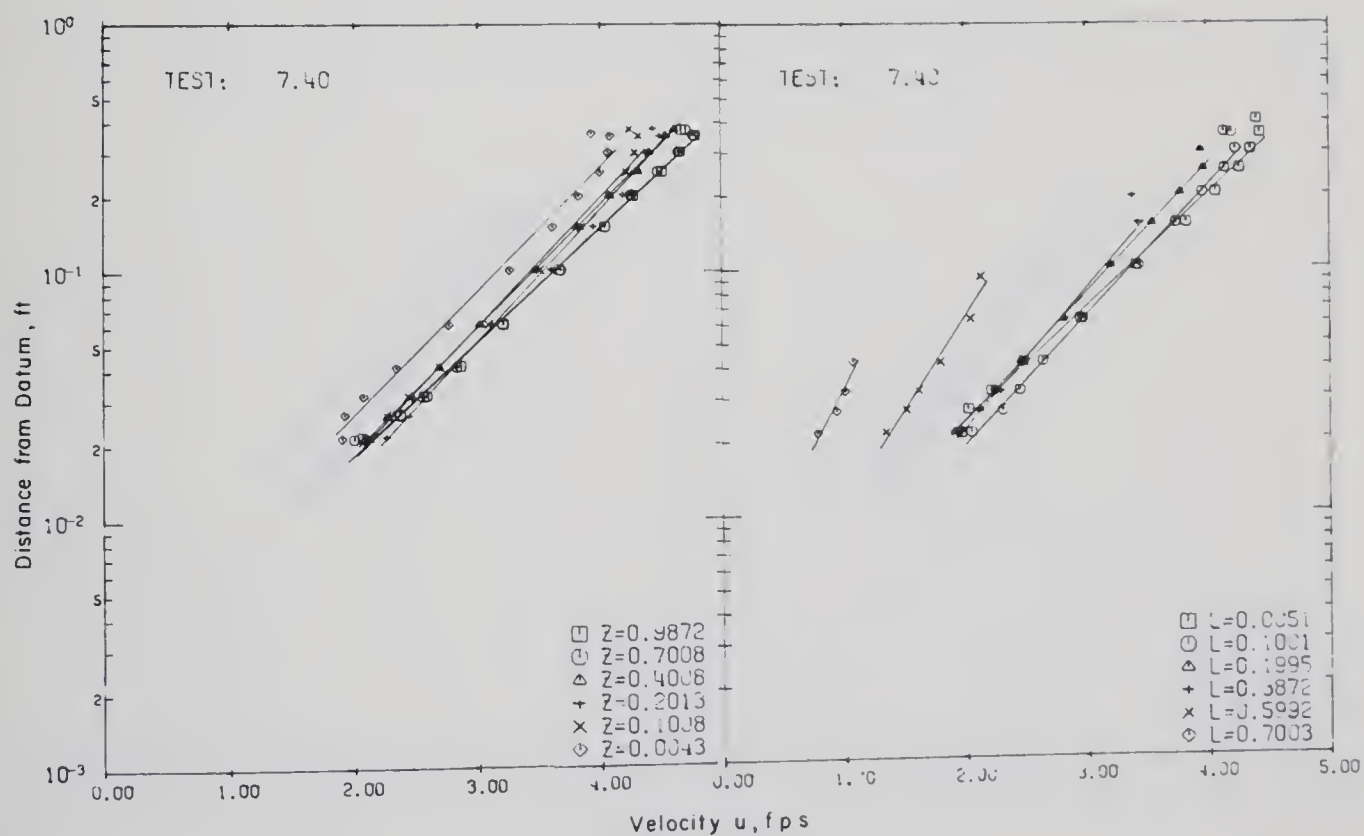
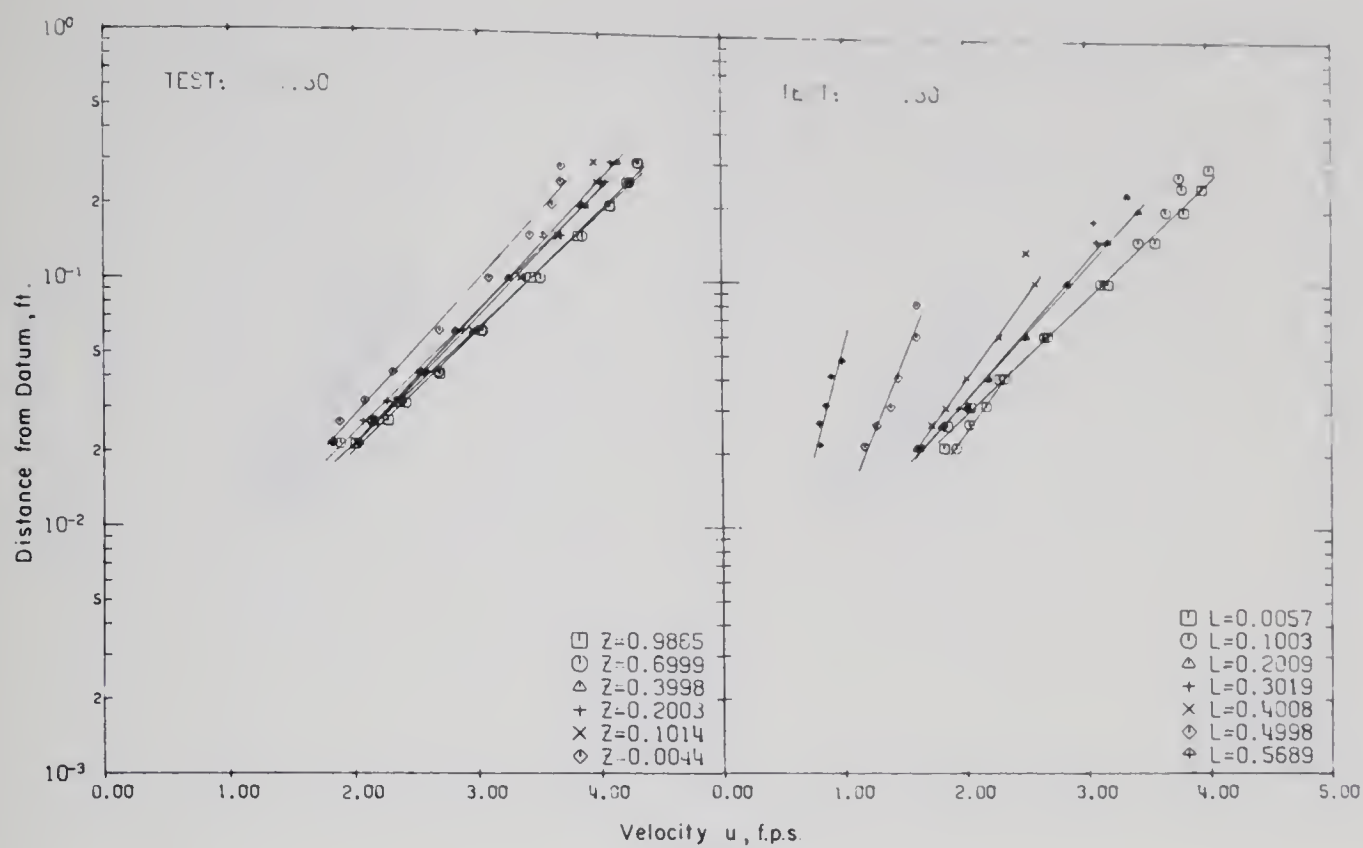


FIGURE D-7 - (Continued)



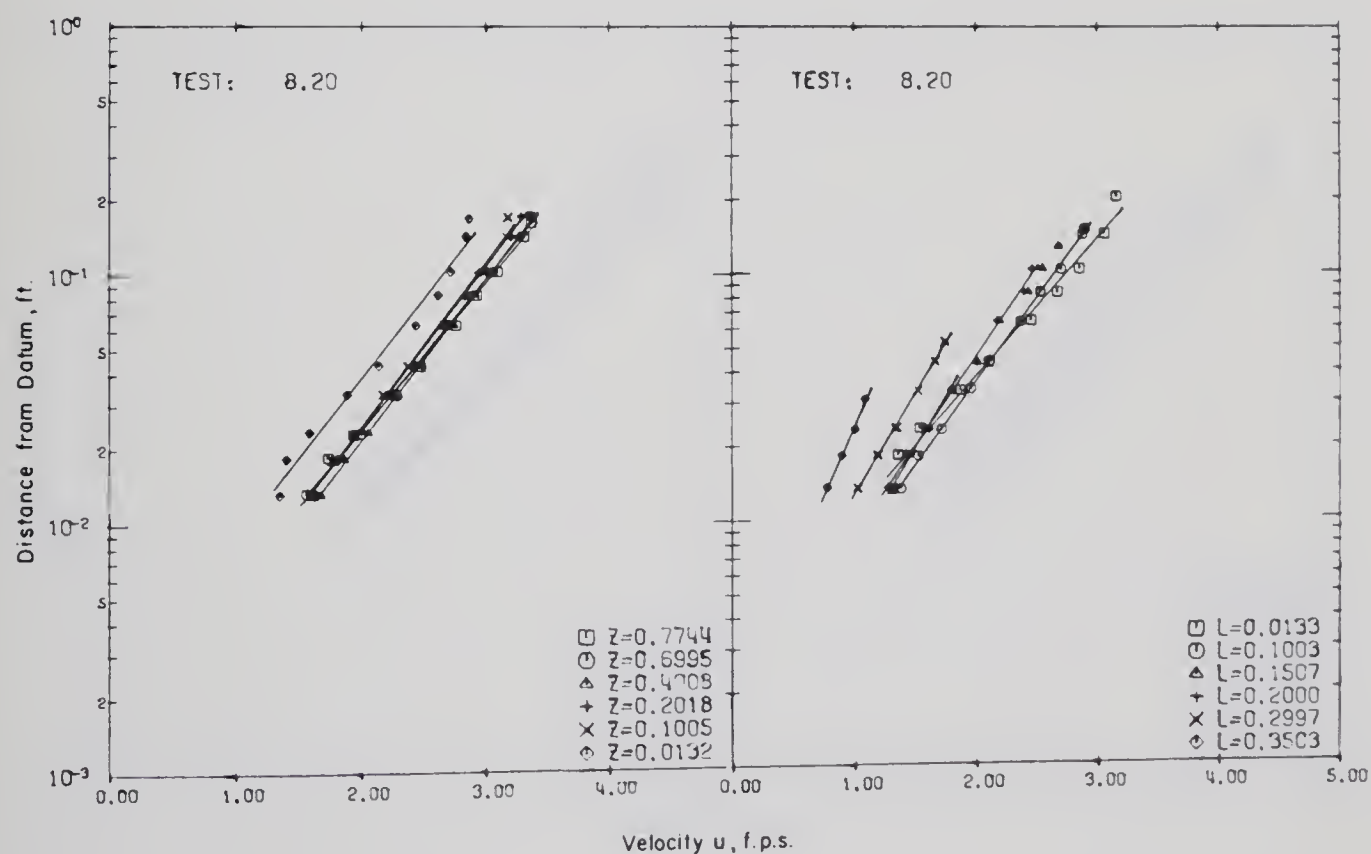
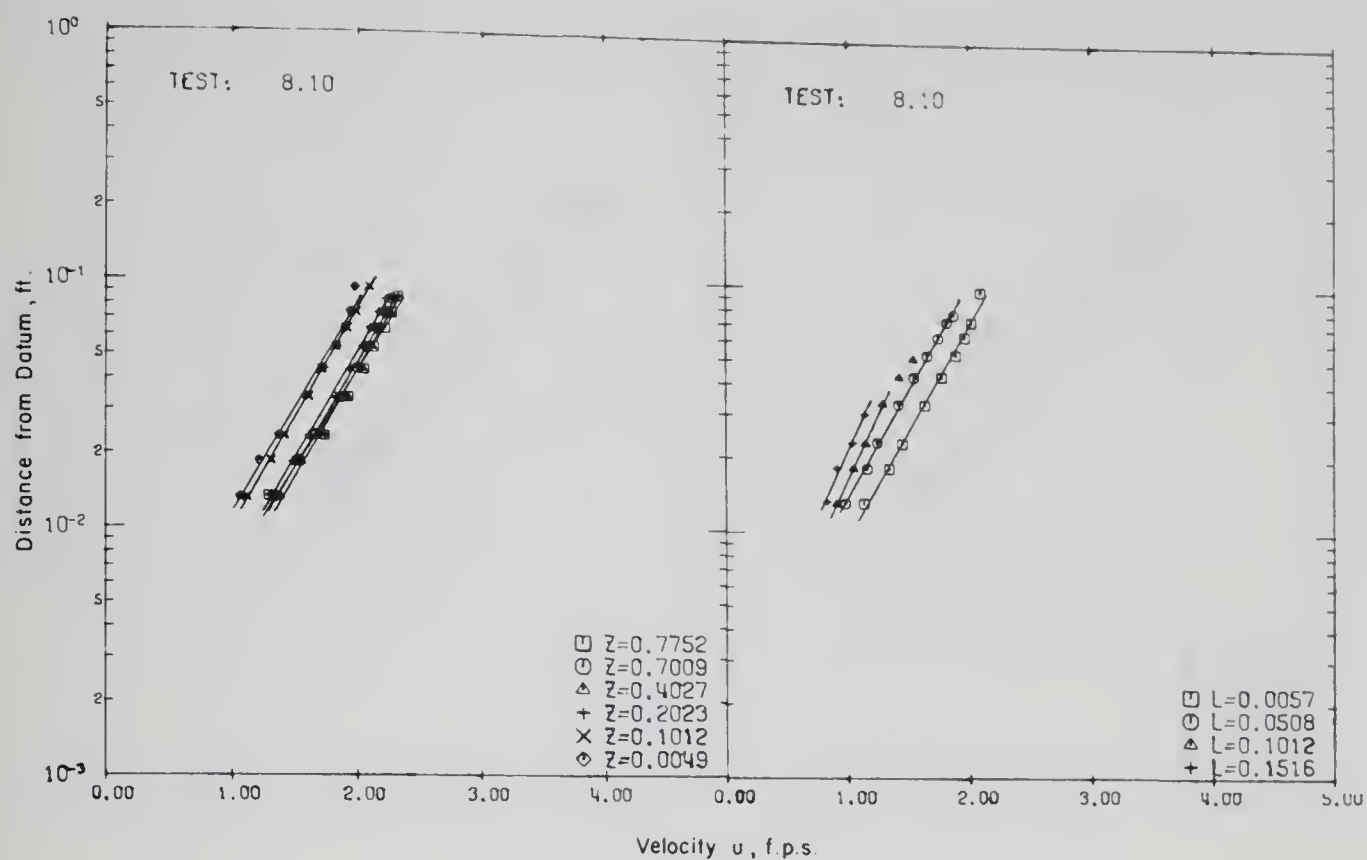


FIGURE D-8. VELOCITY MEASUREMENTS, SERIES 8



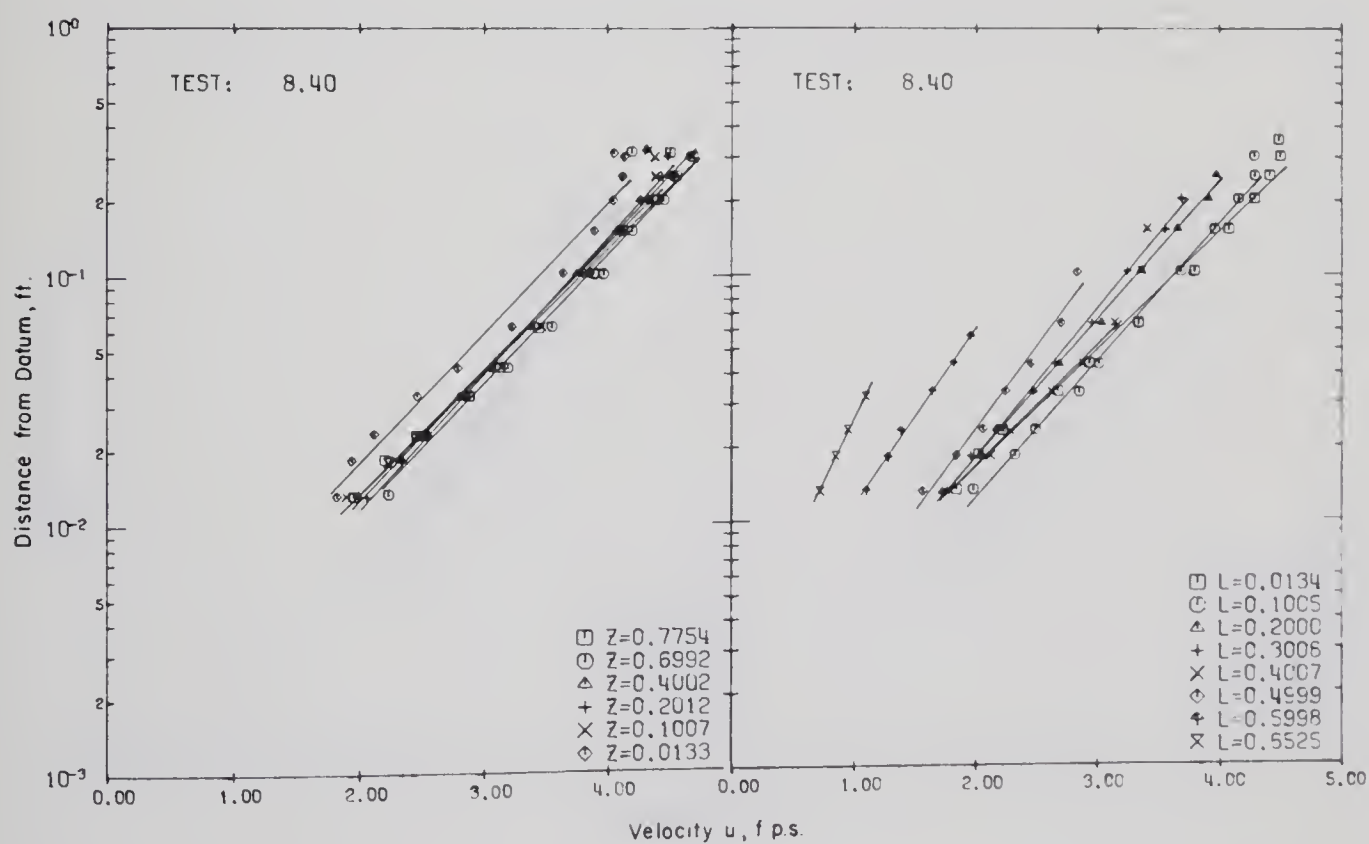
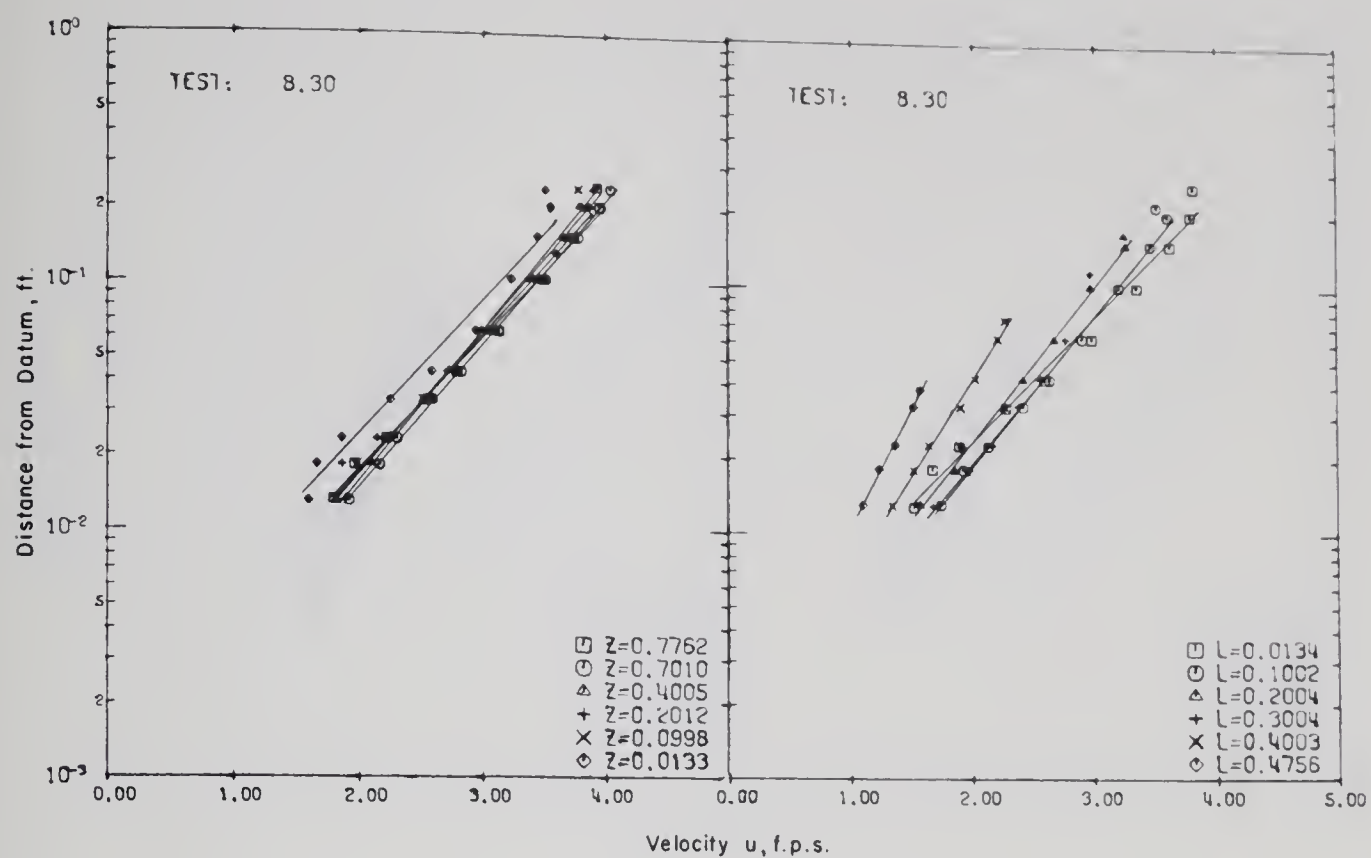


FIGURE D-8 - (Continued)



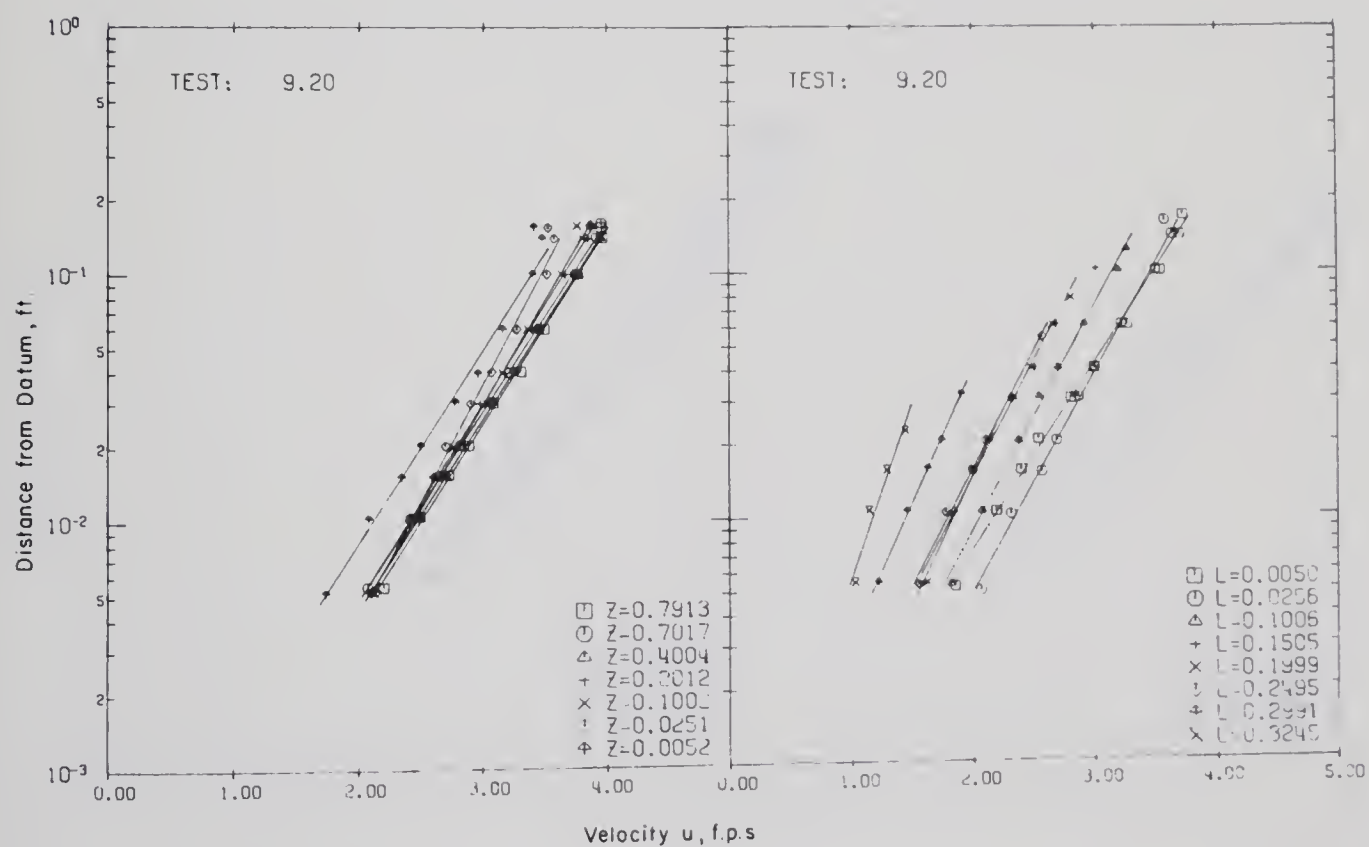
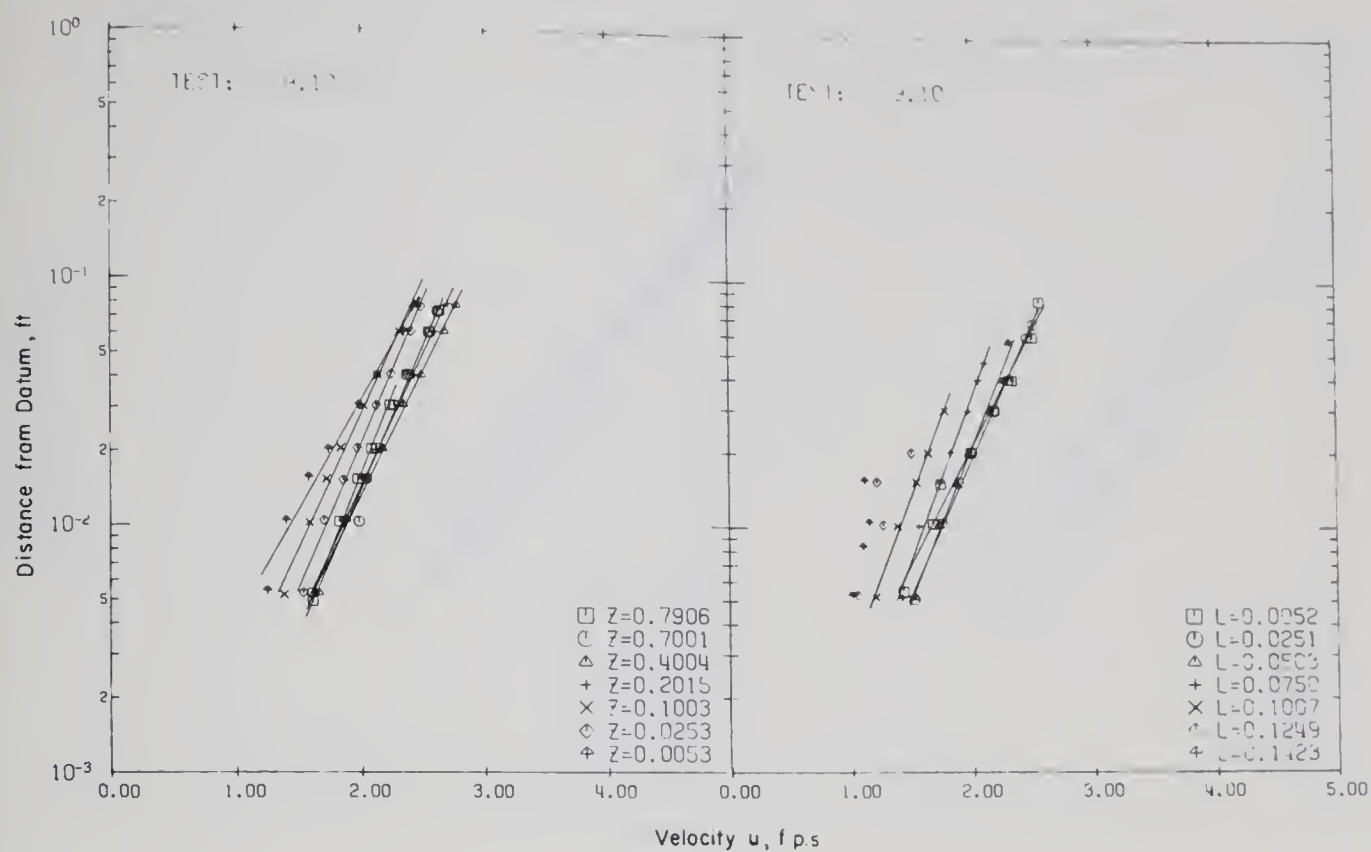


FIGURE D-9. VELOCITY MEASUREMENTS, SERIES 9





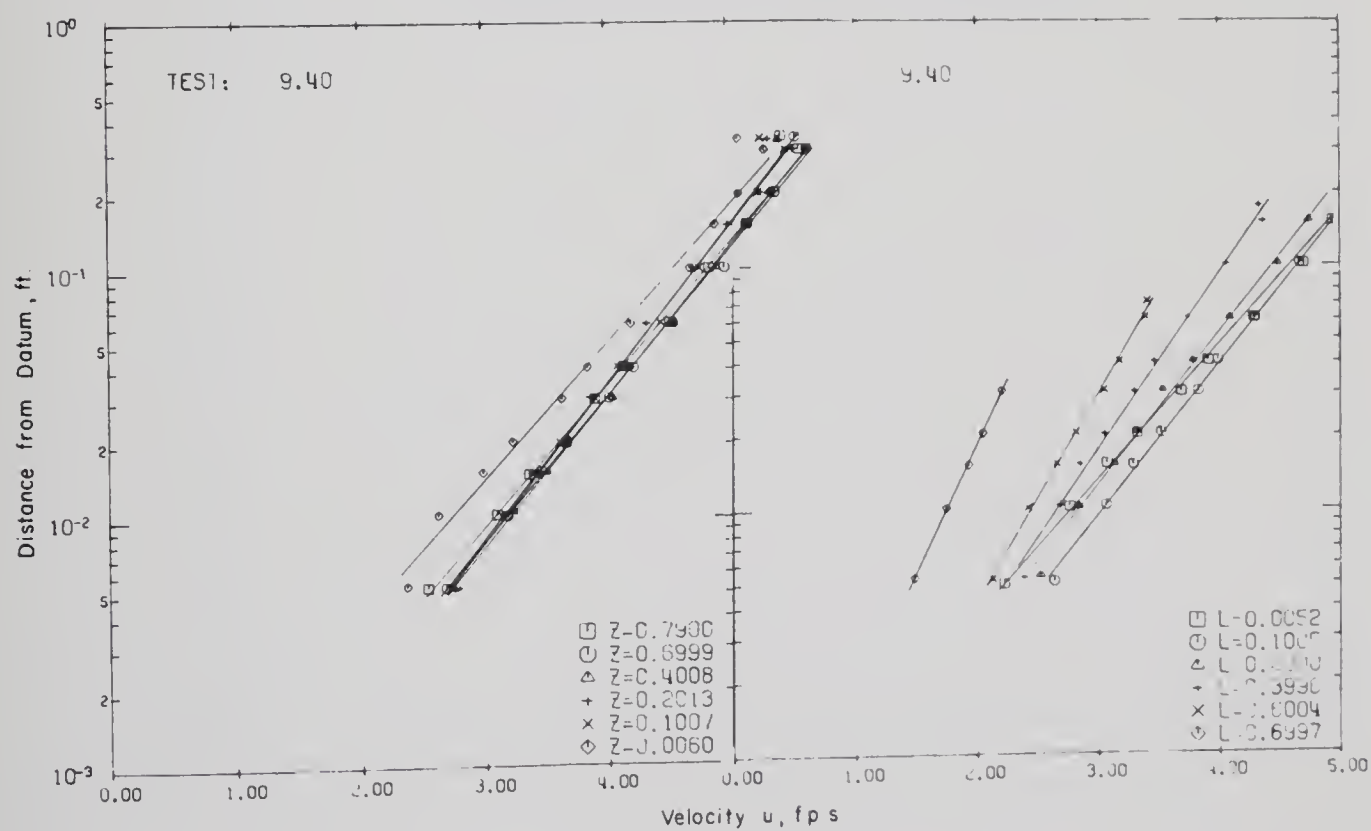
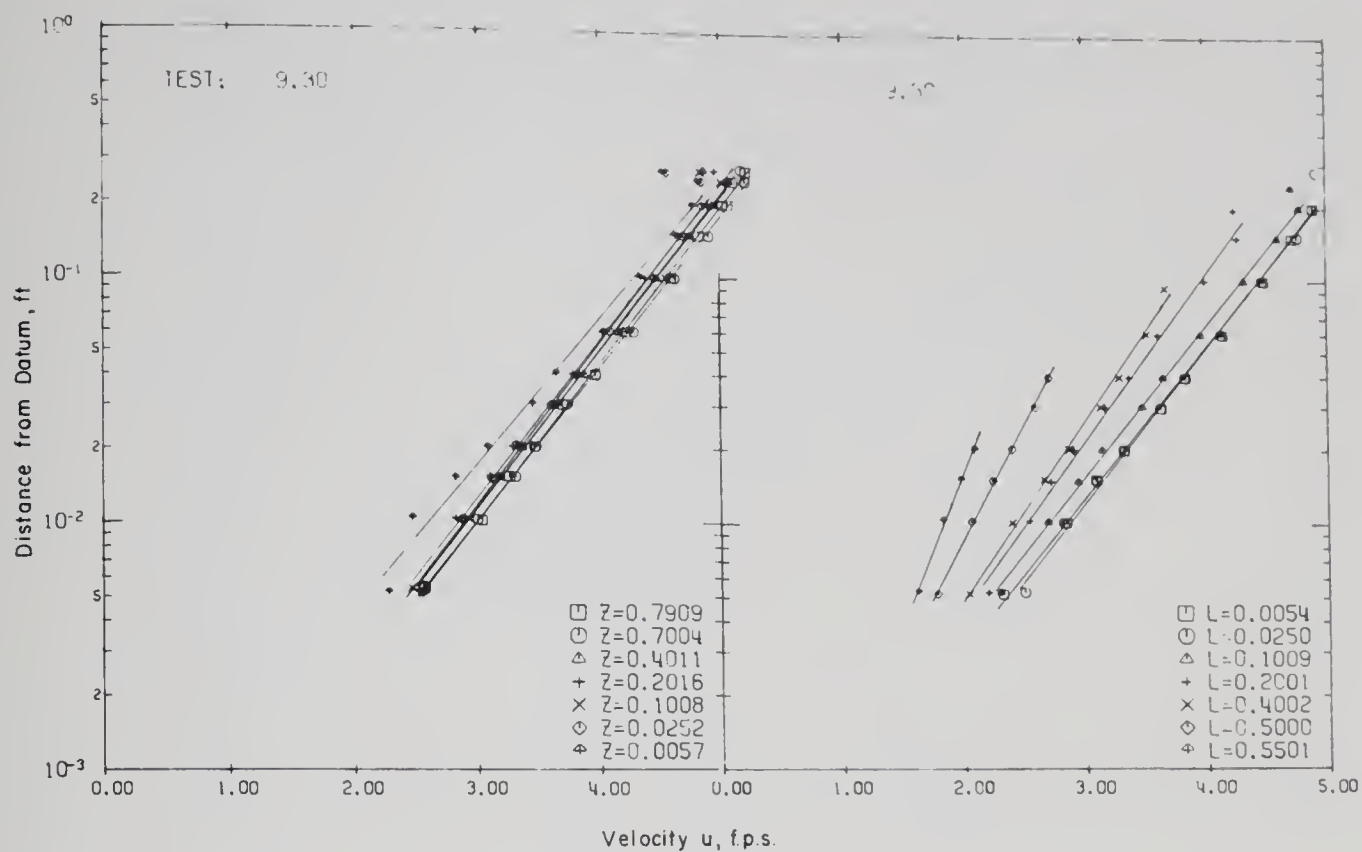


FIGURE D-9 - (Continued)



## APPENDIX E

### DIMENSIONLESS VELOCITY PROFILES



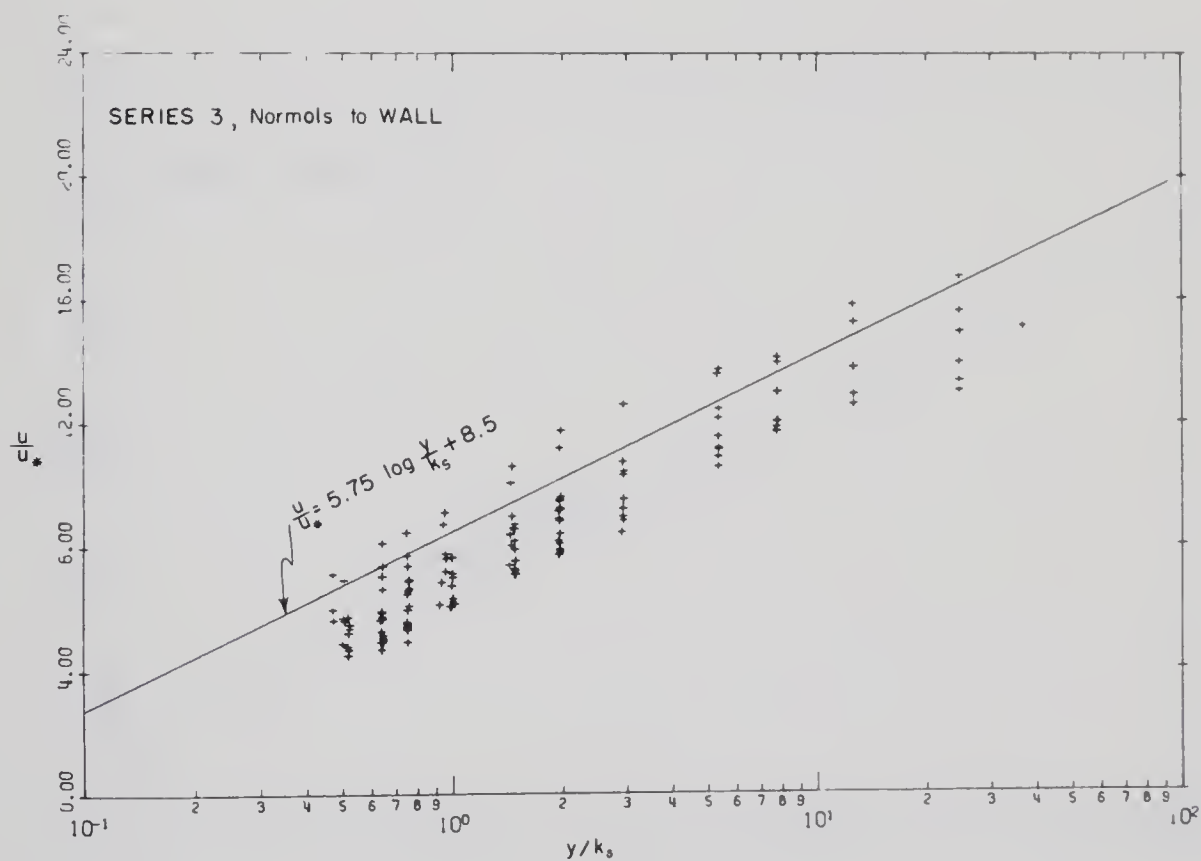
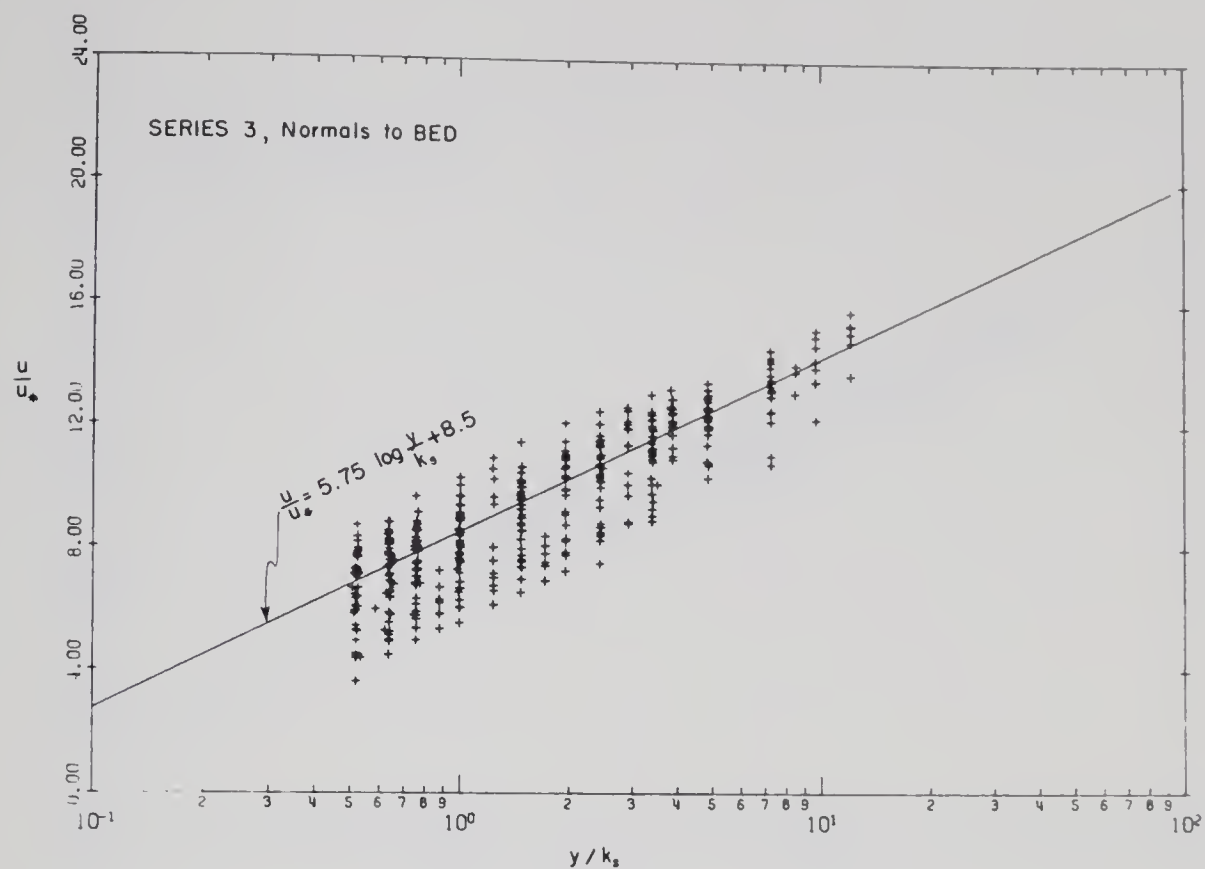


FIGURE E-1. DIMENSIONLESS VELOCITY PROFILES, SERIES 3



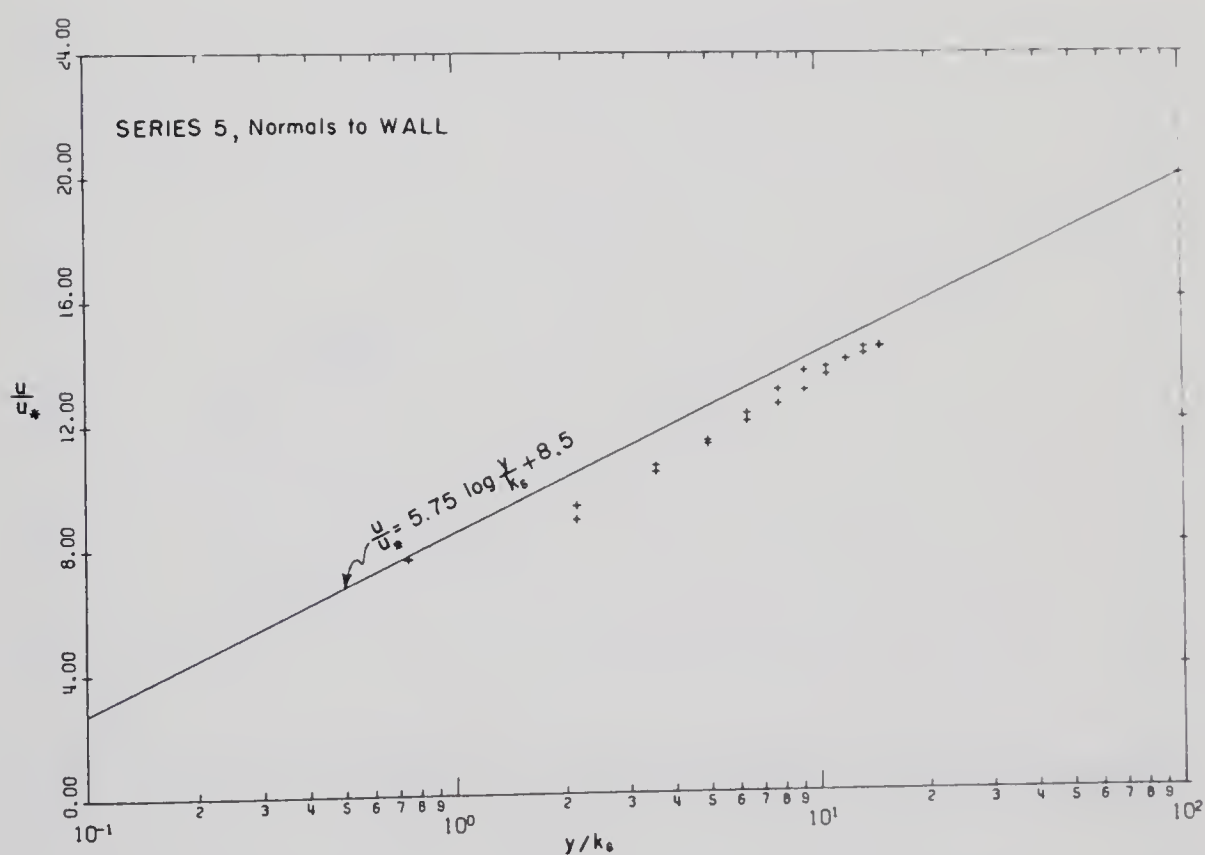
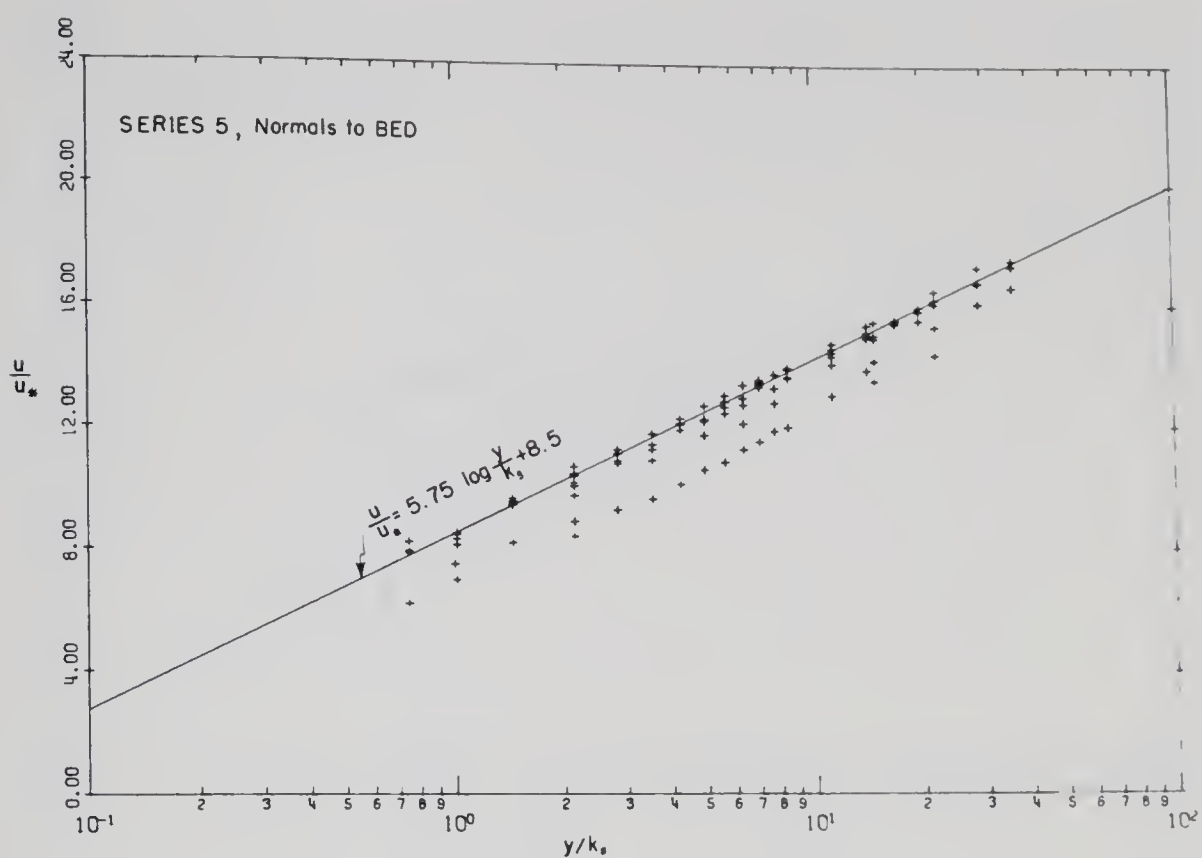


FIGURE E-2. DIMENSIONLESS VELOCITY PROFILES, SERIES 5





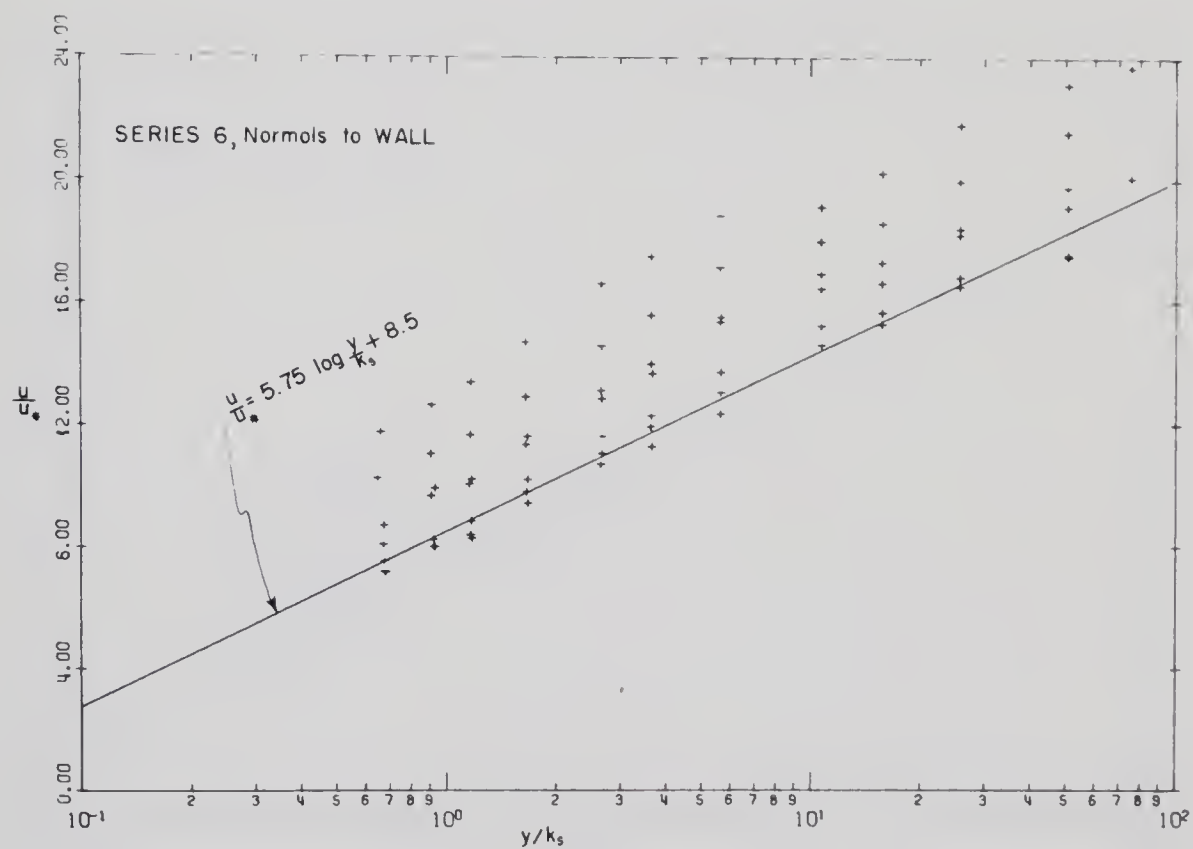
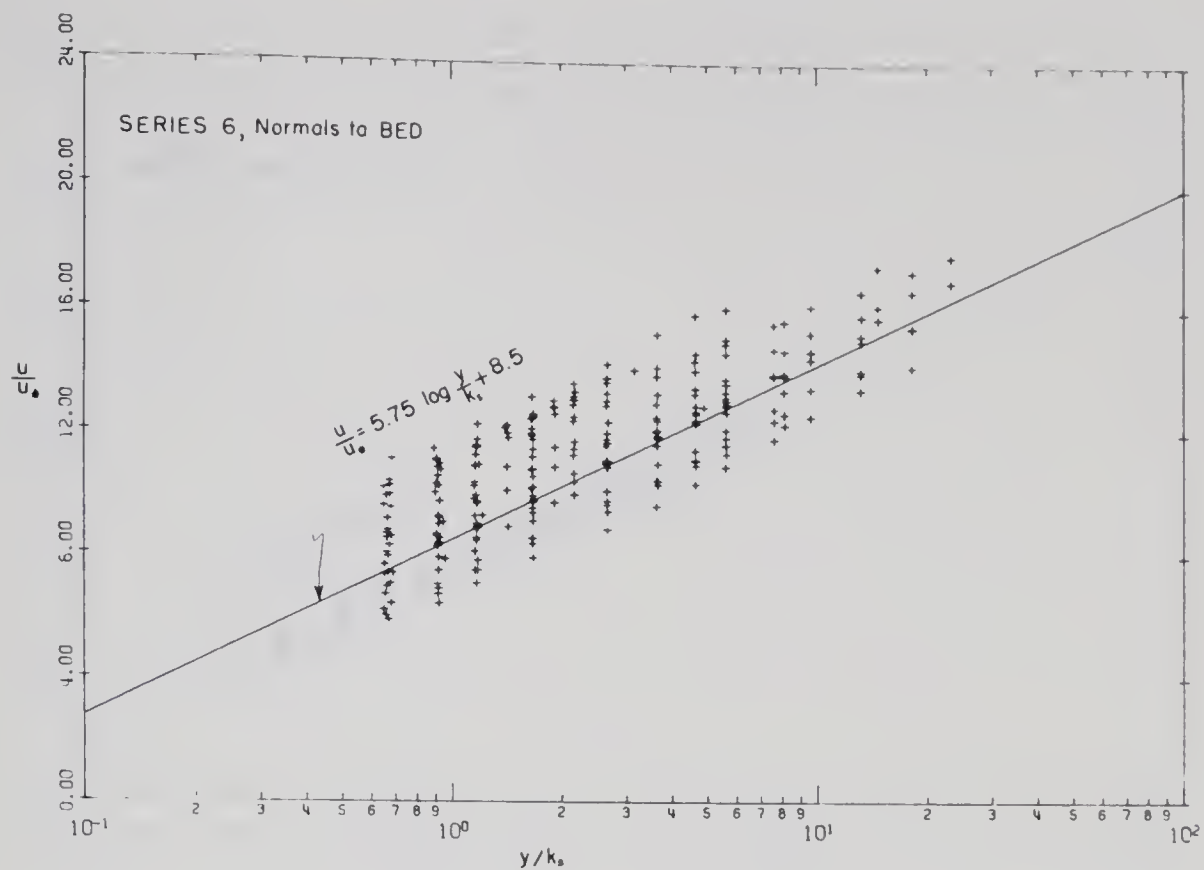


FIGURE E-3. DIMENSIONLESS VELOCITY PROFILES, SERIES 6



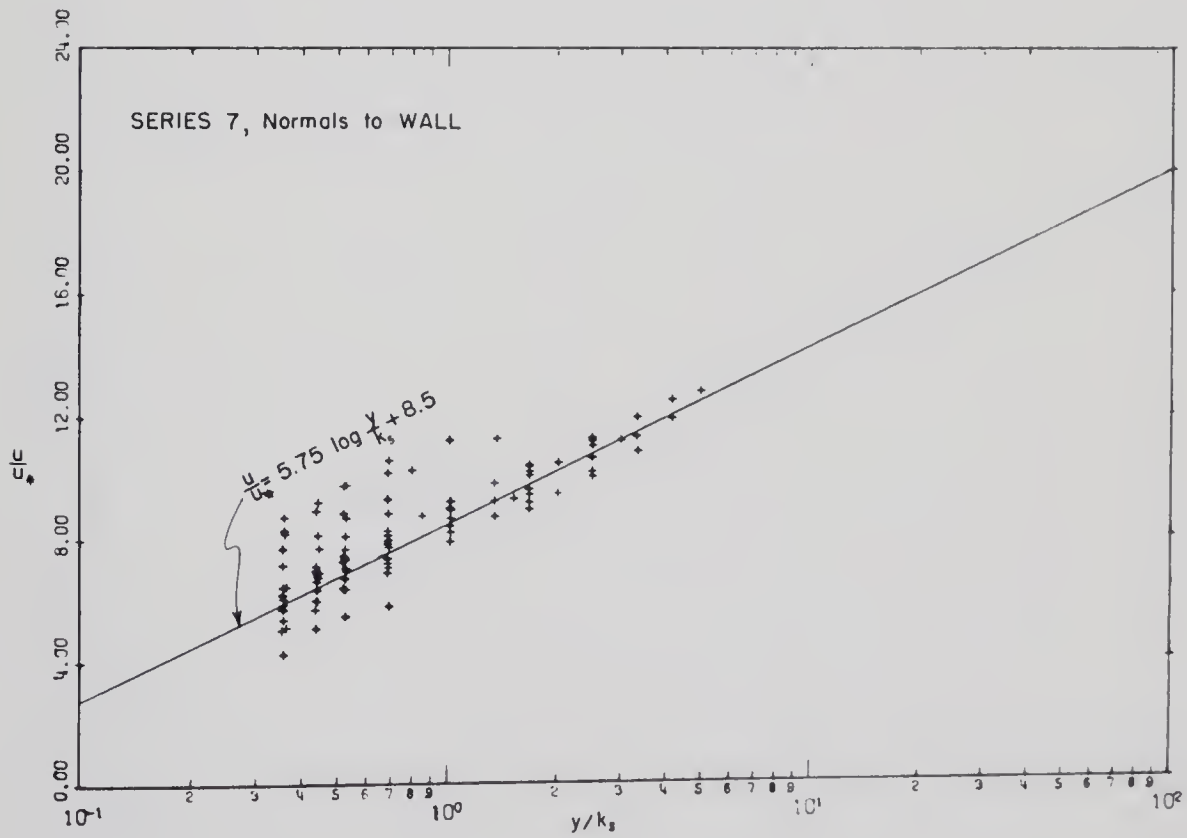
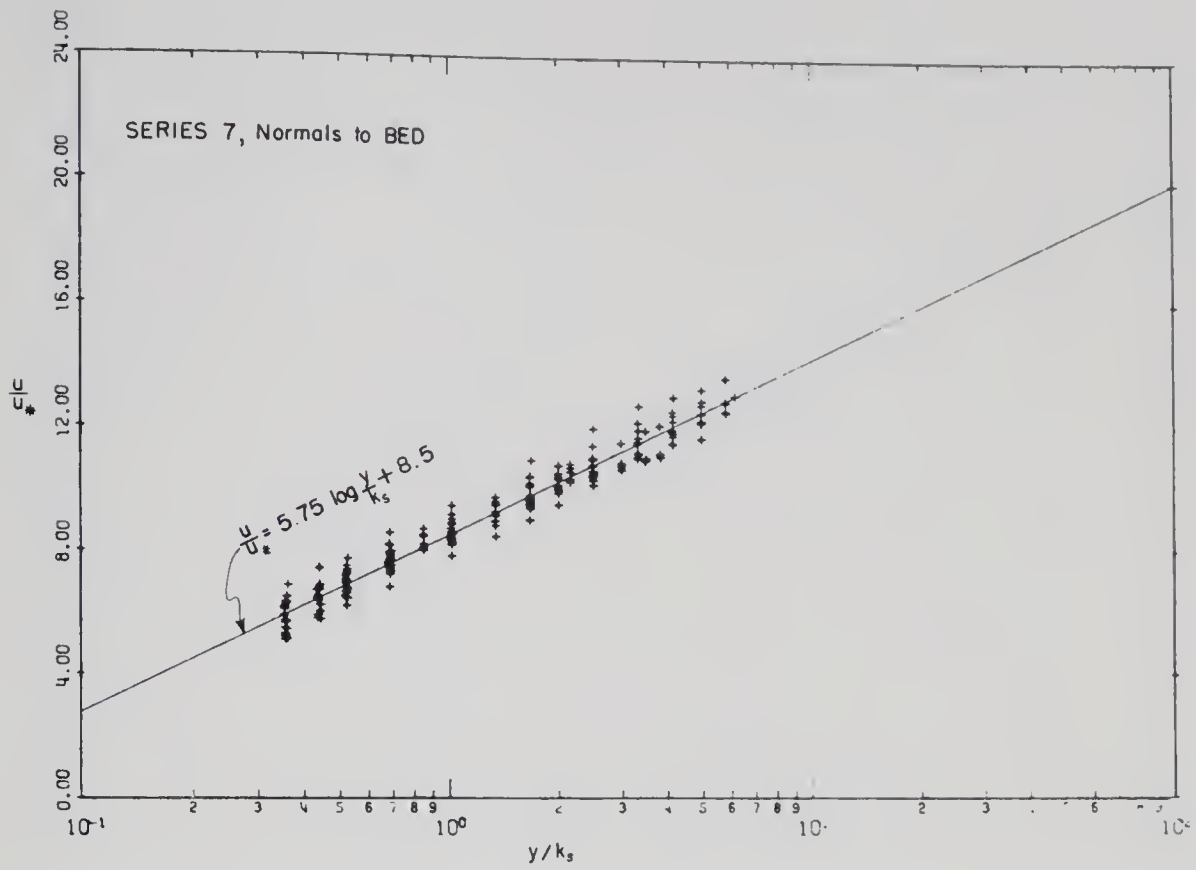


FIGURE E-4. DIMENSIONLESS VELOCITY PROFILES, SERIES 7



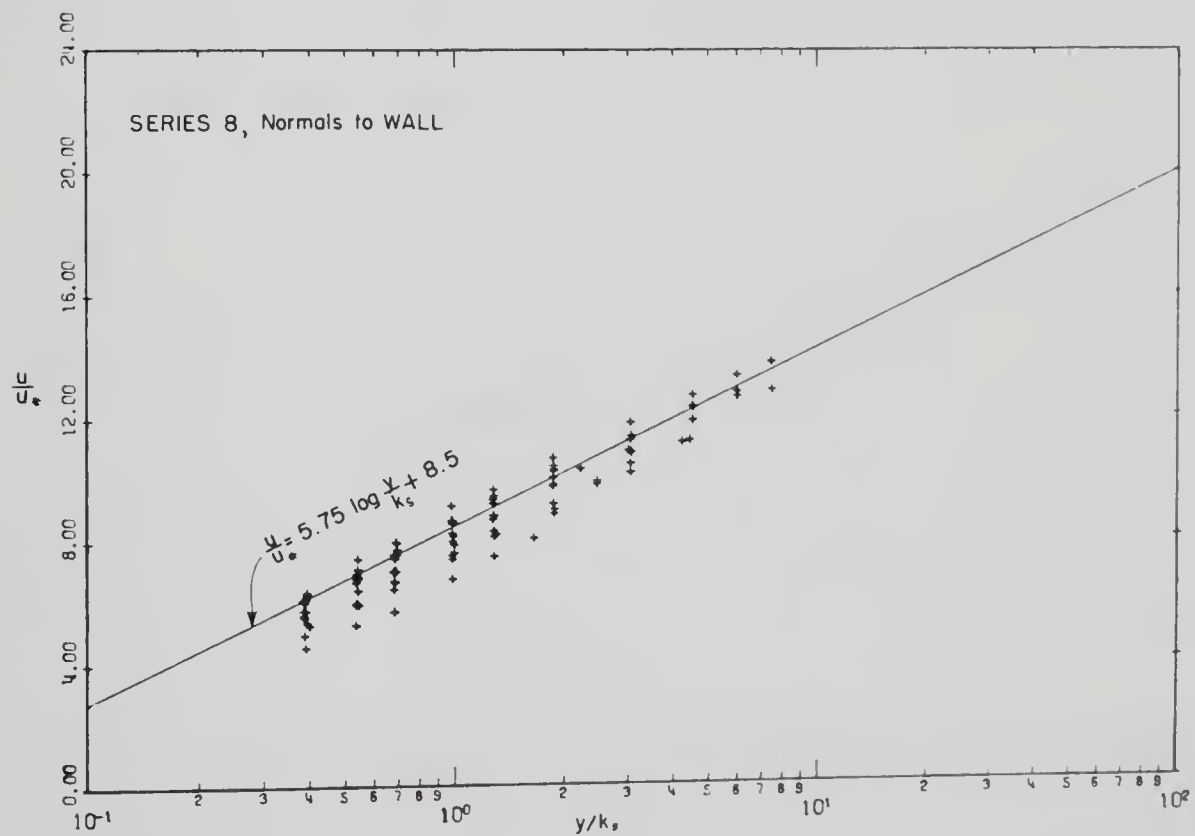
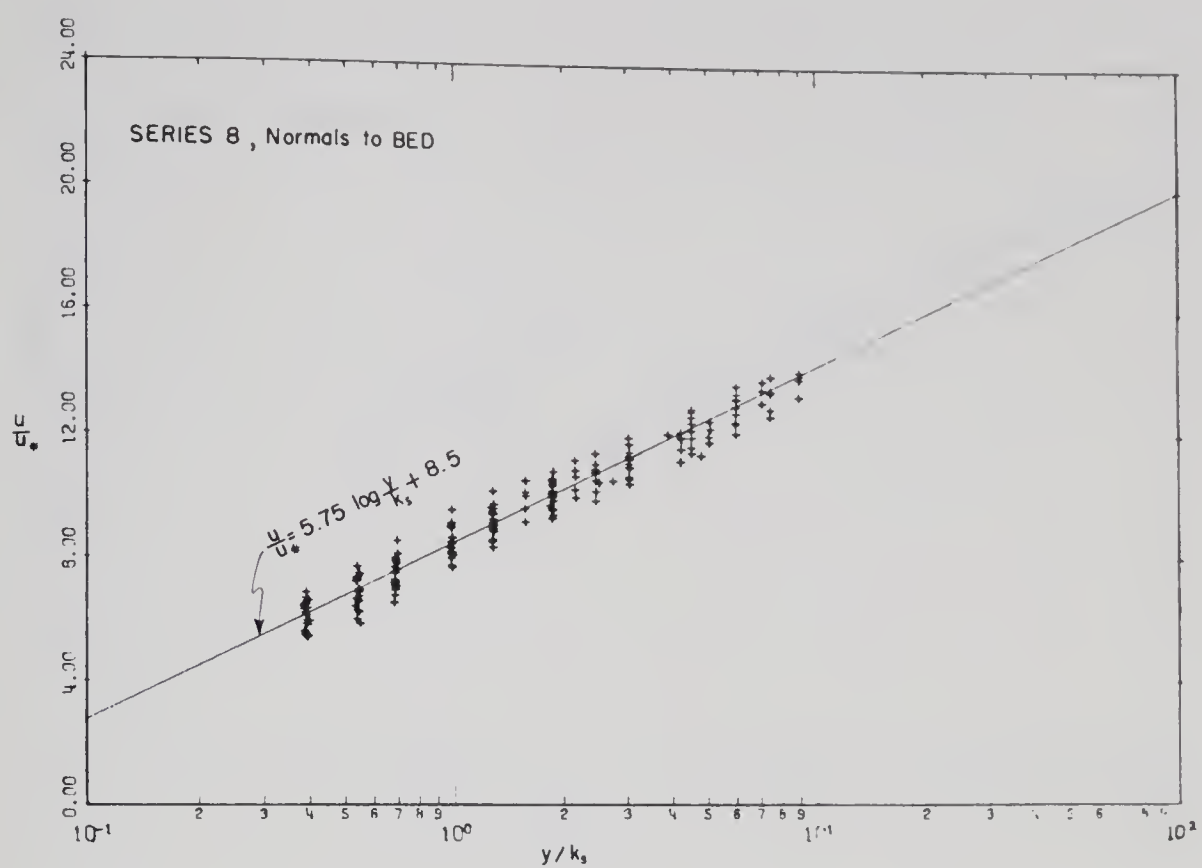


FIGURE E-5. DIMENSIONLESS VELOCITY PROFILES, SERIES 8



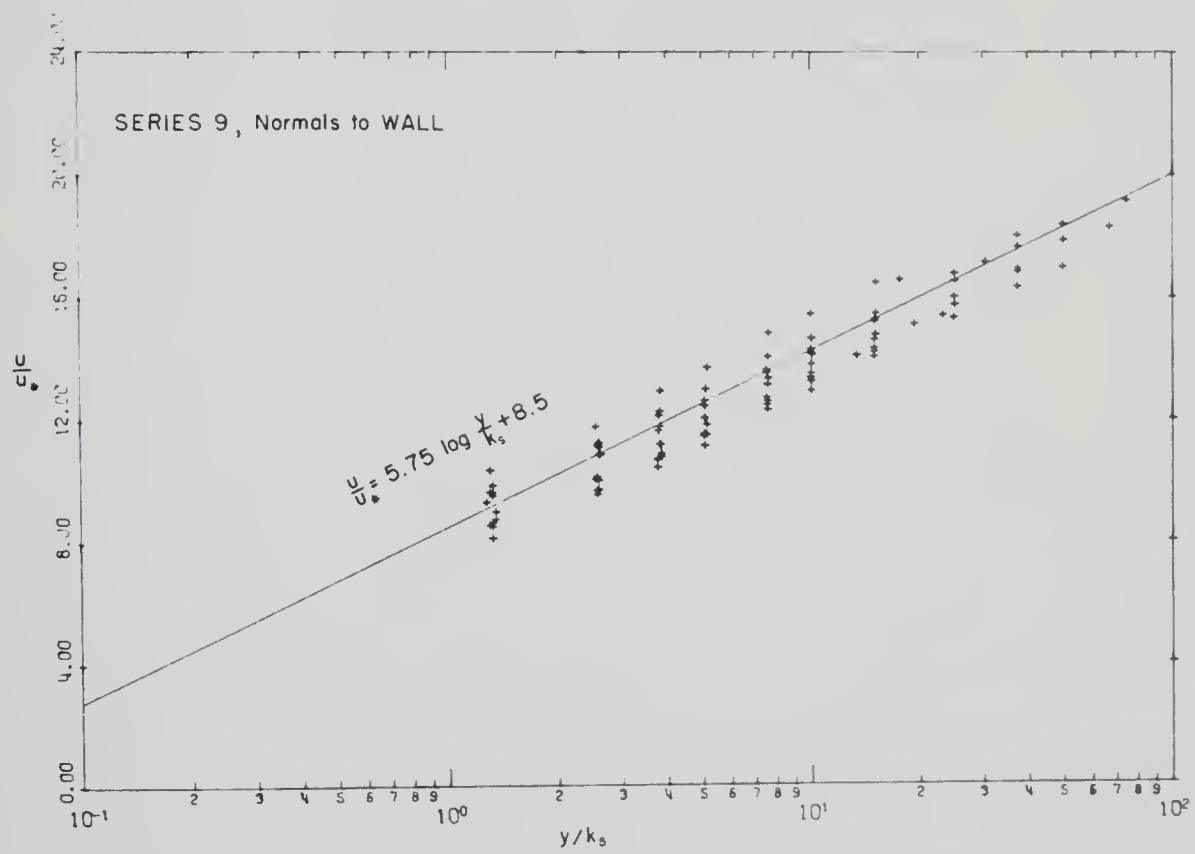
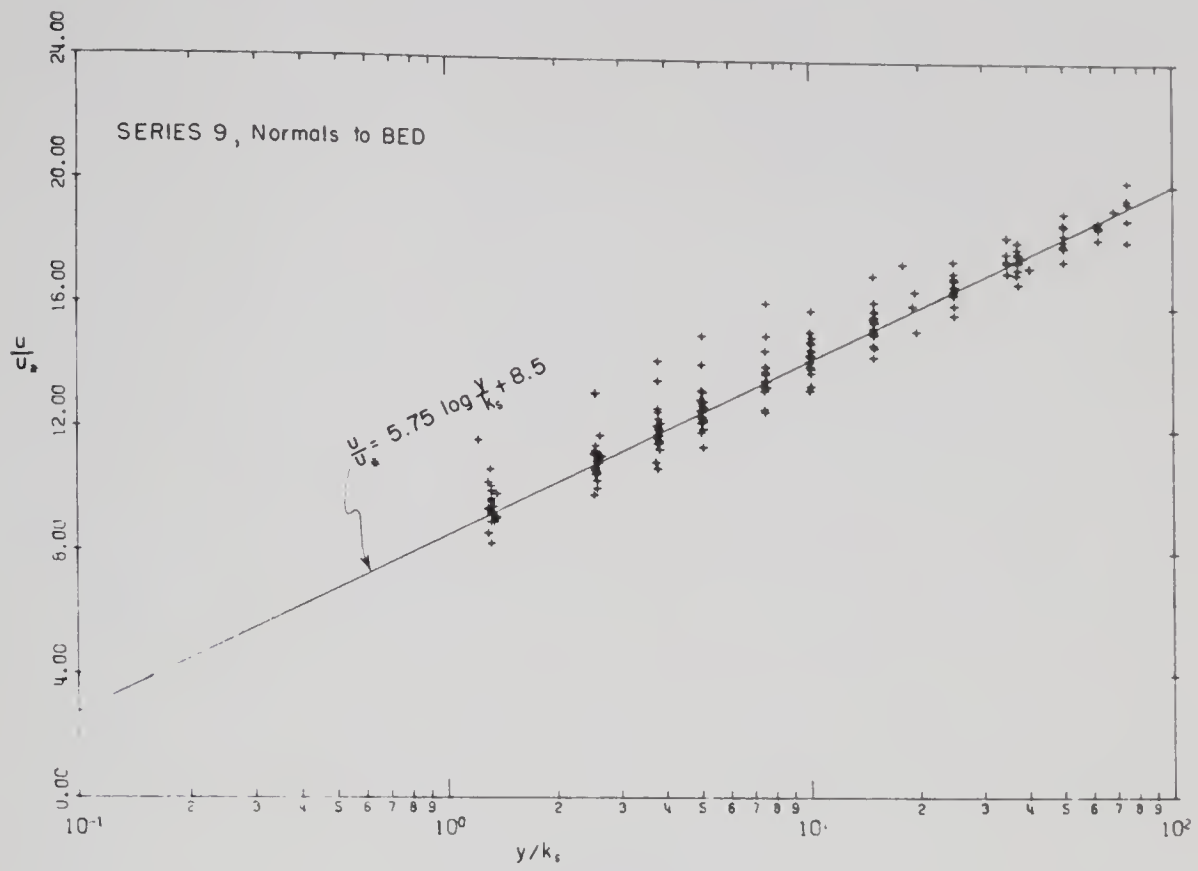


FIGURE E-6. DIMENSIONLESS VELOCITY PROFILES, SERIES 9





## APPENDIX F

### SHEAR STRESS DISTRIBUTIONS



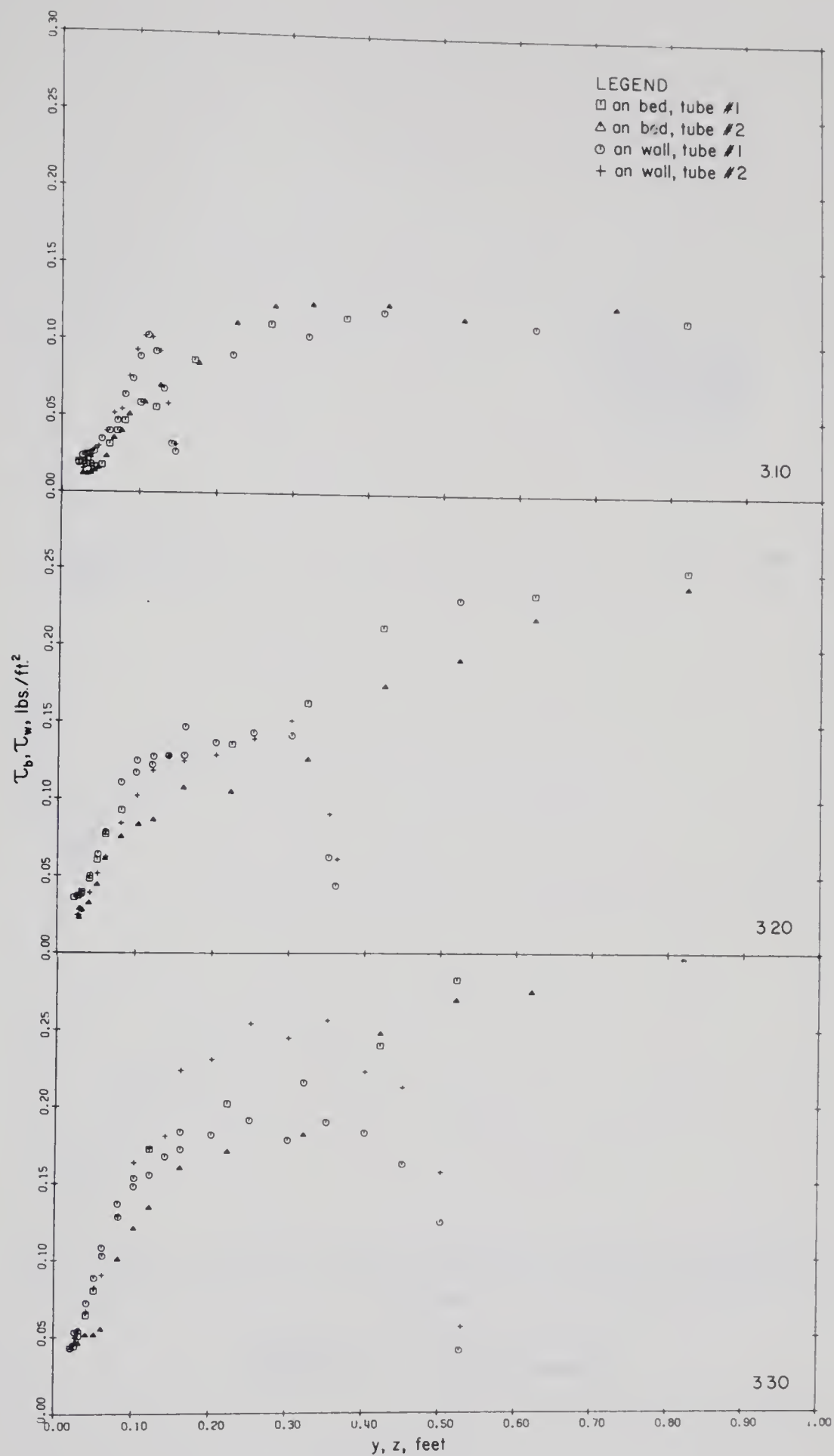


FIGURE F-1. SHEAR STRESS DISTRIBUTIONS, SERIES 3



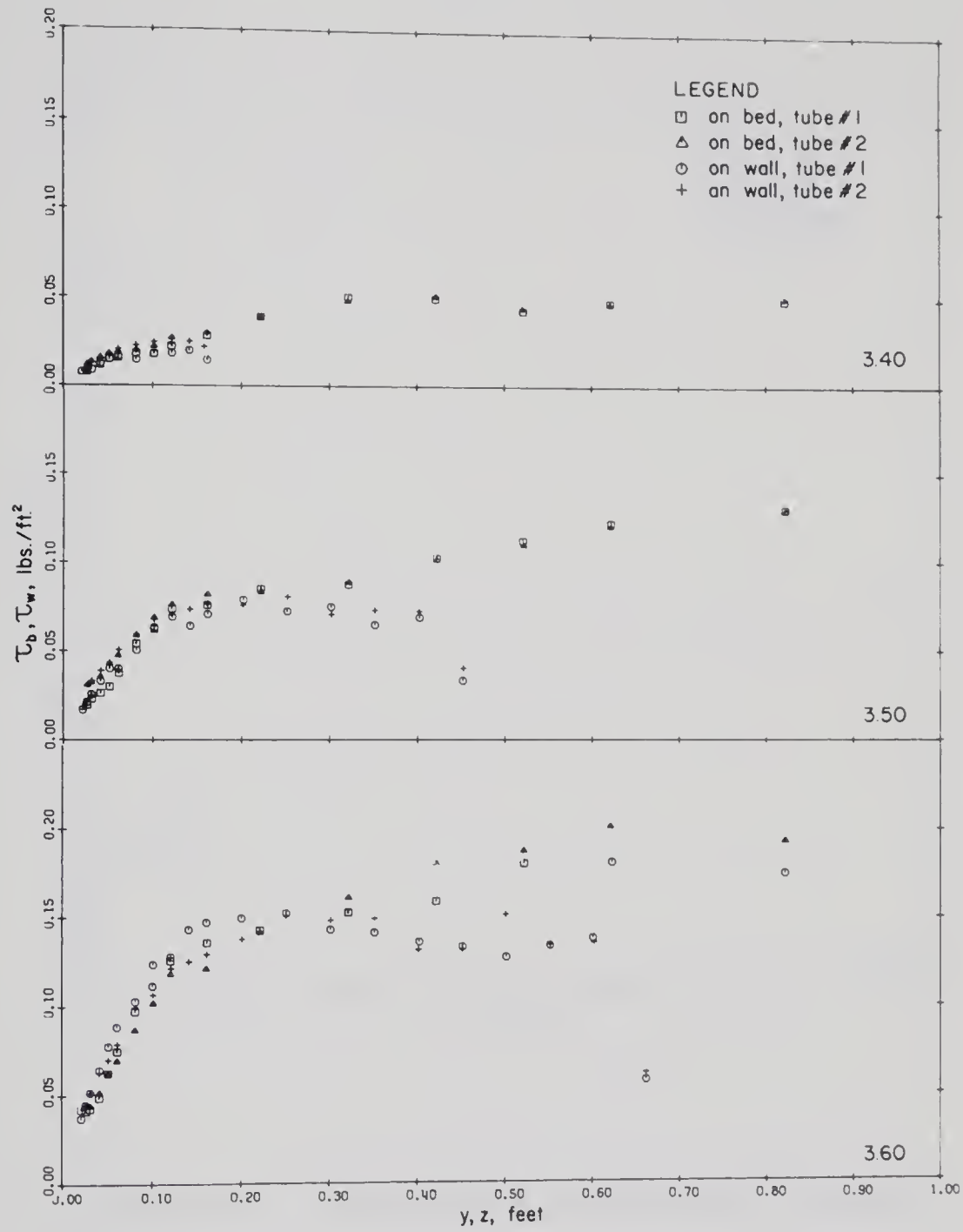


FIGURE F-1 - (Continued)



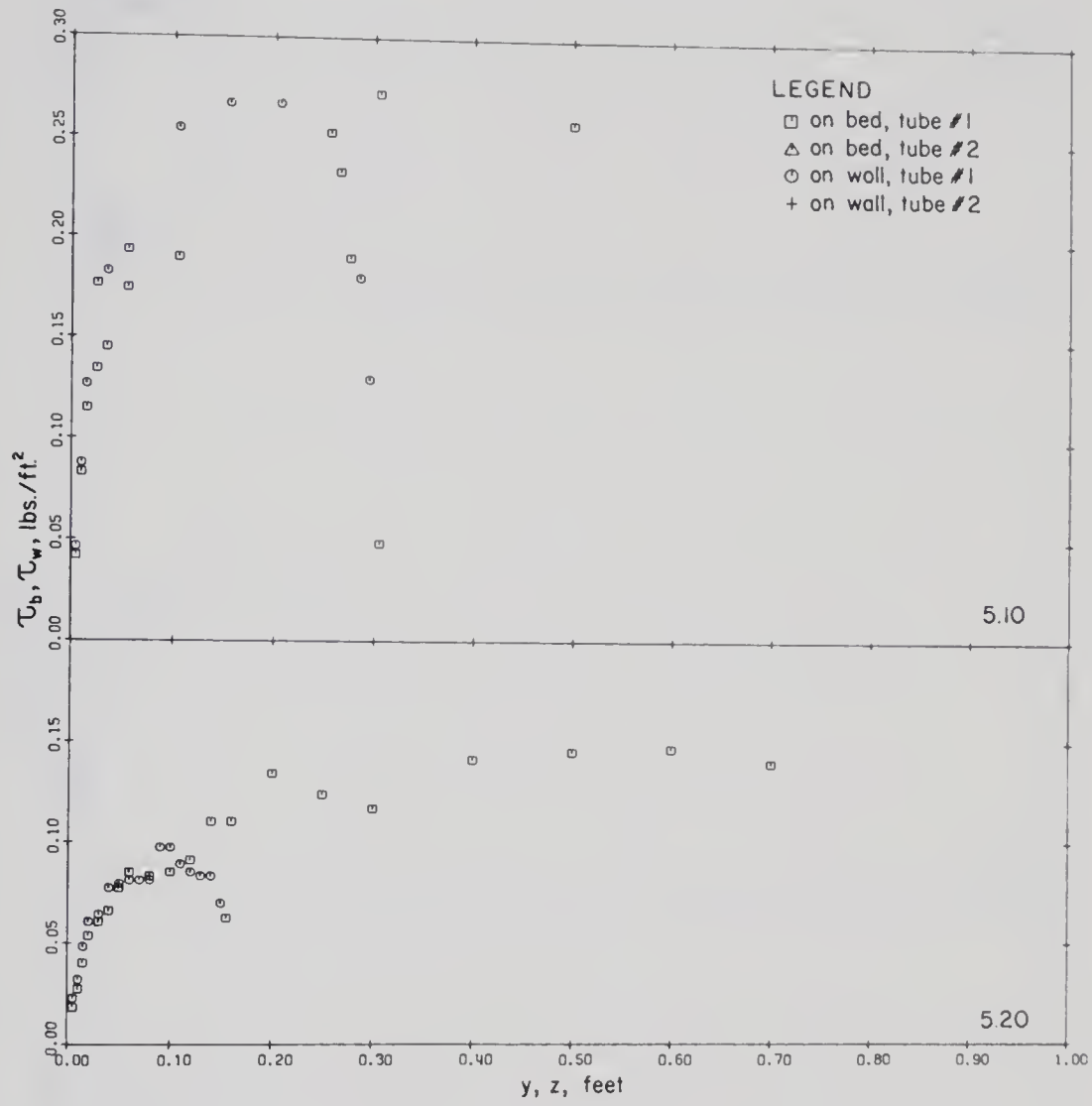


FIGURE F-2. SHEAR STRESS DISTRIBUTIONS, SERIES 5





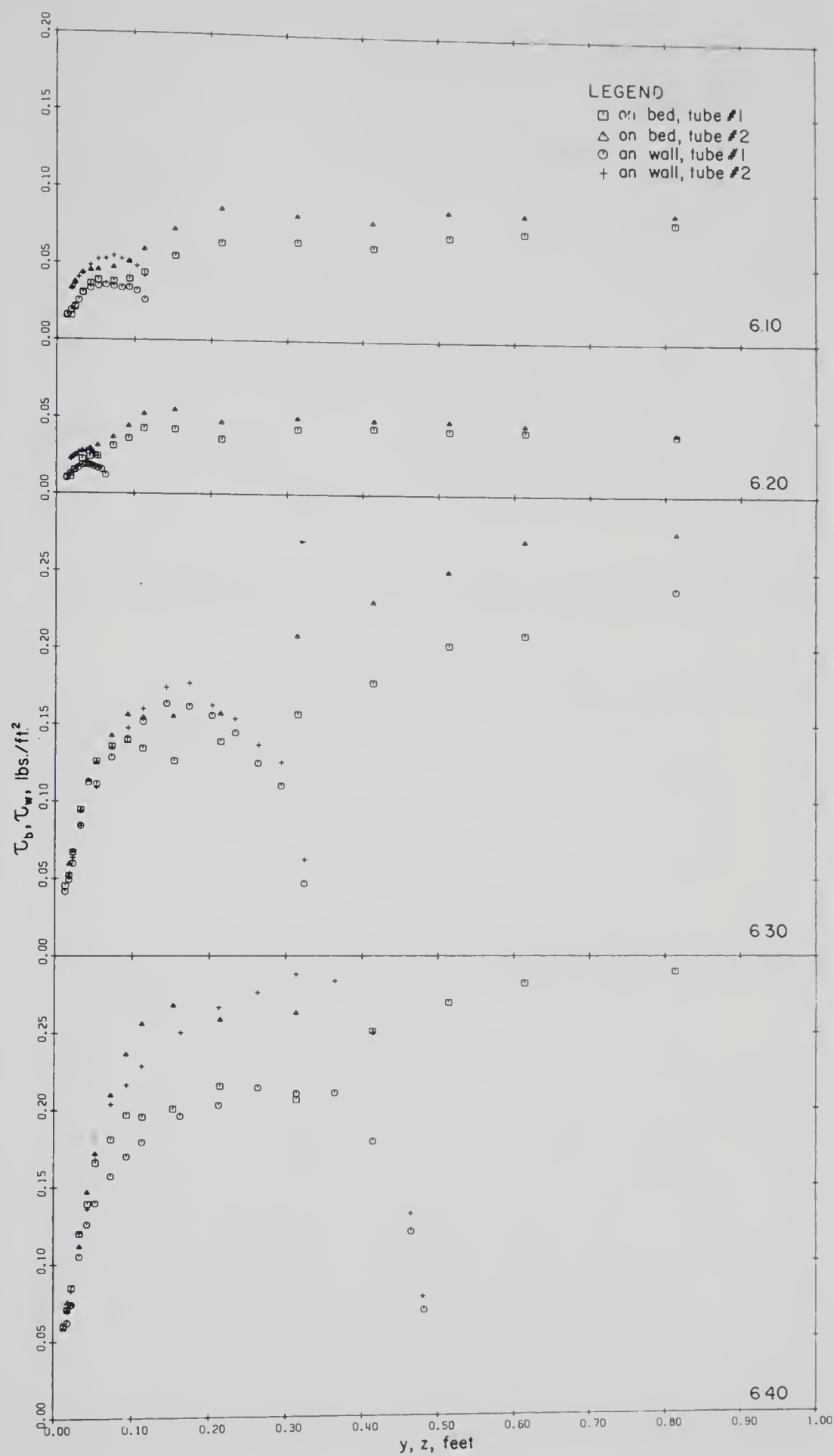


FIGURE F-3. SHEAR STRESS DISTRIBUTIONS, SERIES 6



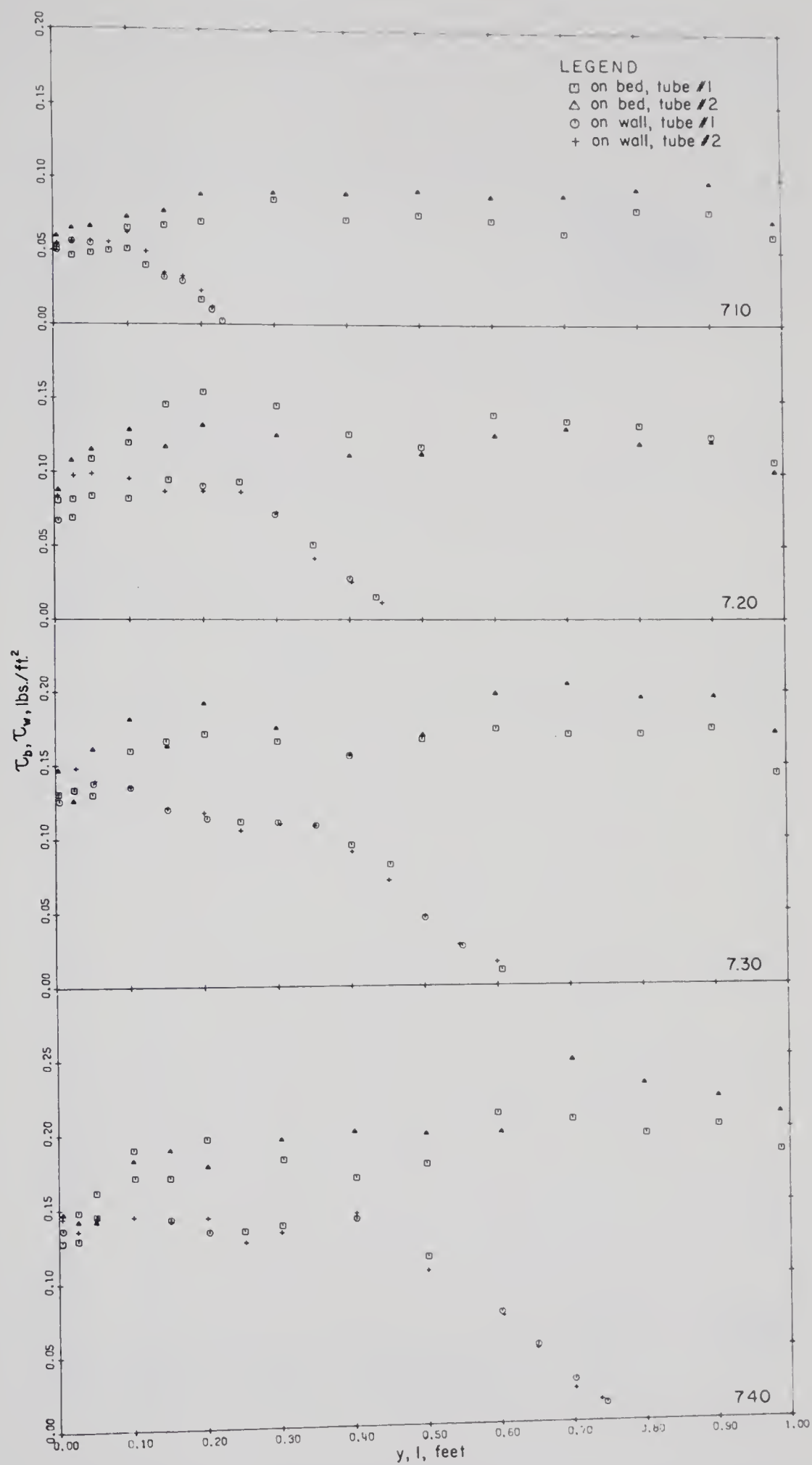


FIGURE F-4. SHEAR STRESS DISTRIBUTIONS, SERIES 7



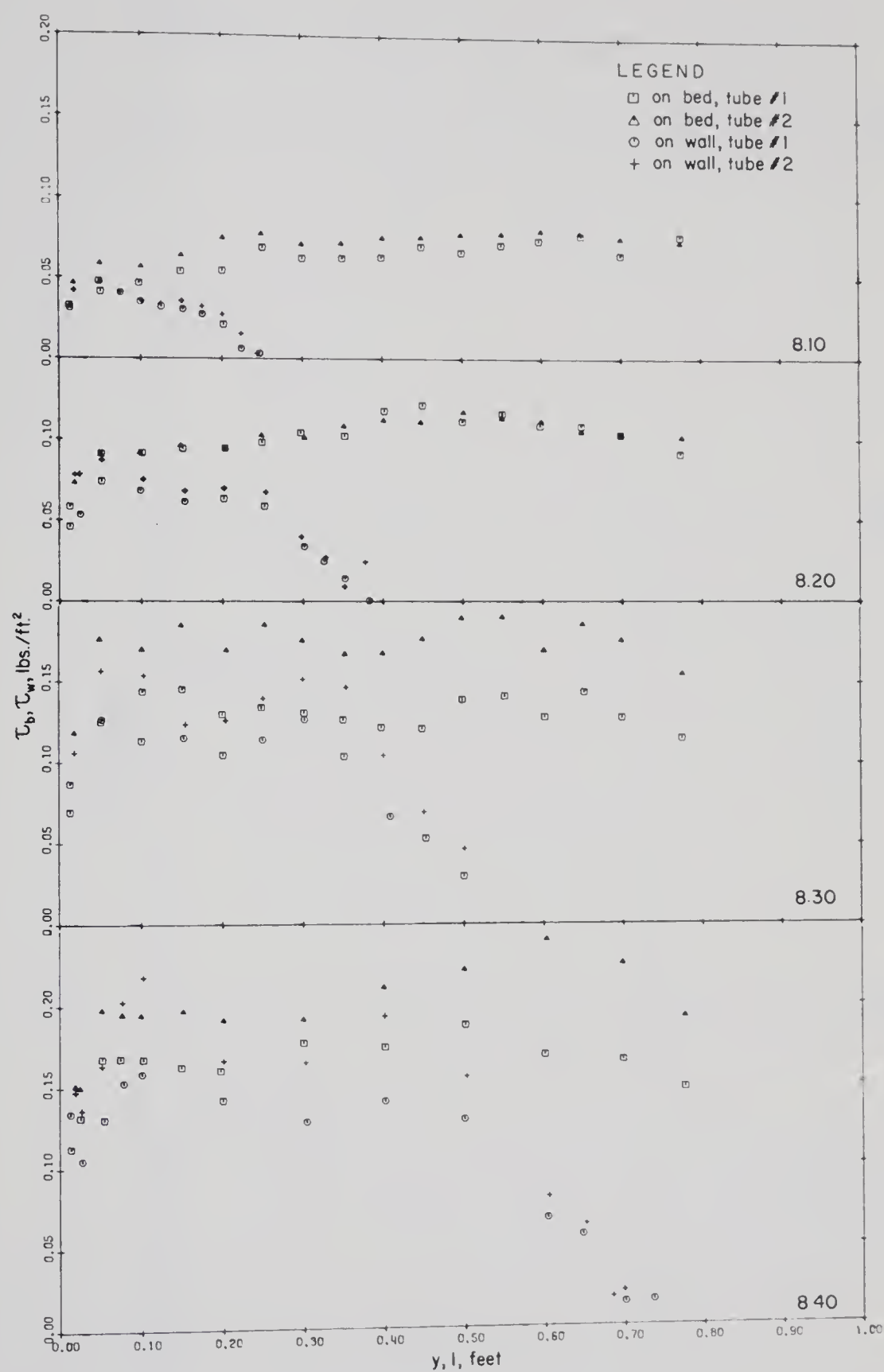


FIGURE F-5. SHEAR STRESS DISTRIBUTIONS, SERIES 8



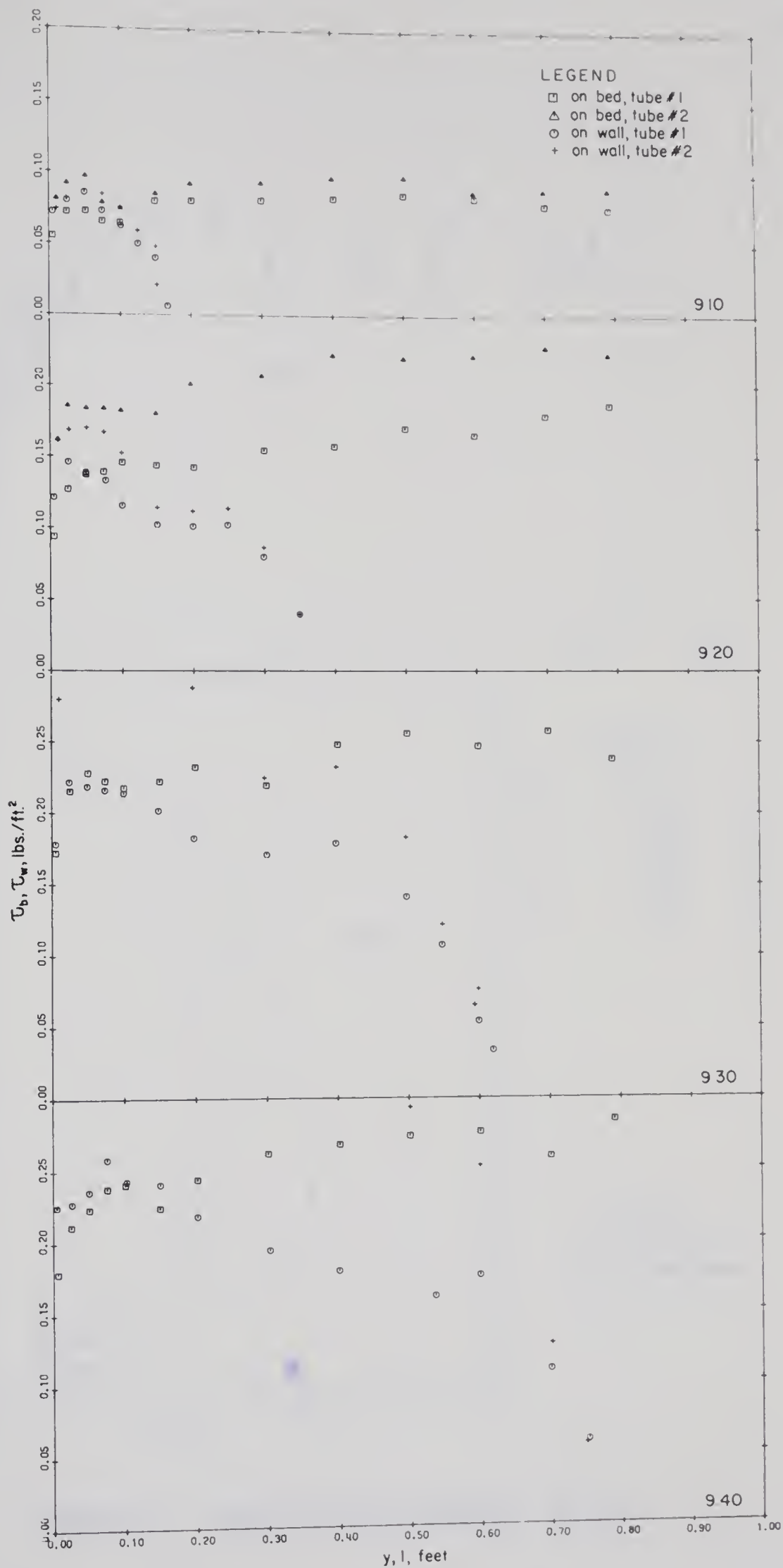


FIGURE F-6. SHEAR STRESS DISTRIBUTIONS, SERIES 9





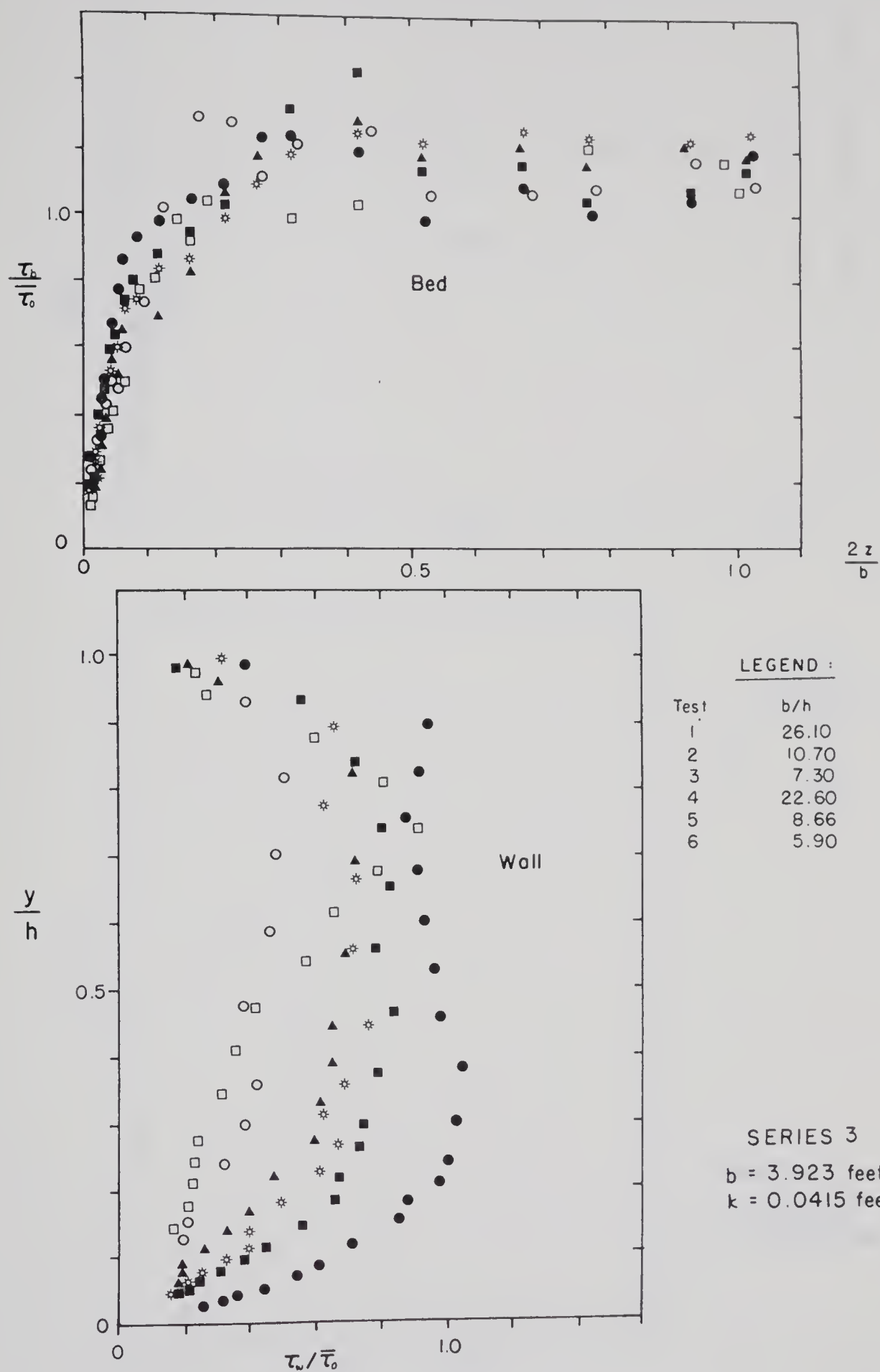


FIGURE F-7. SHEAR STRESS DIAGRAMS, SERIES 3



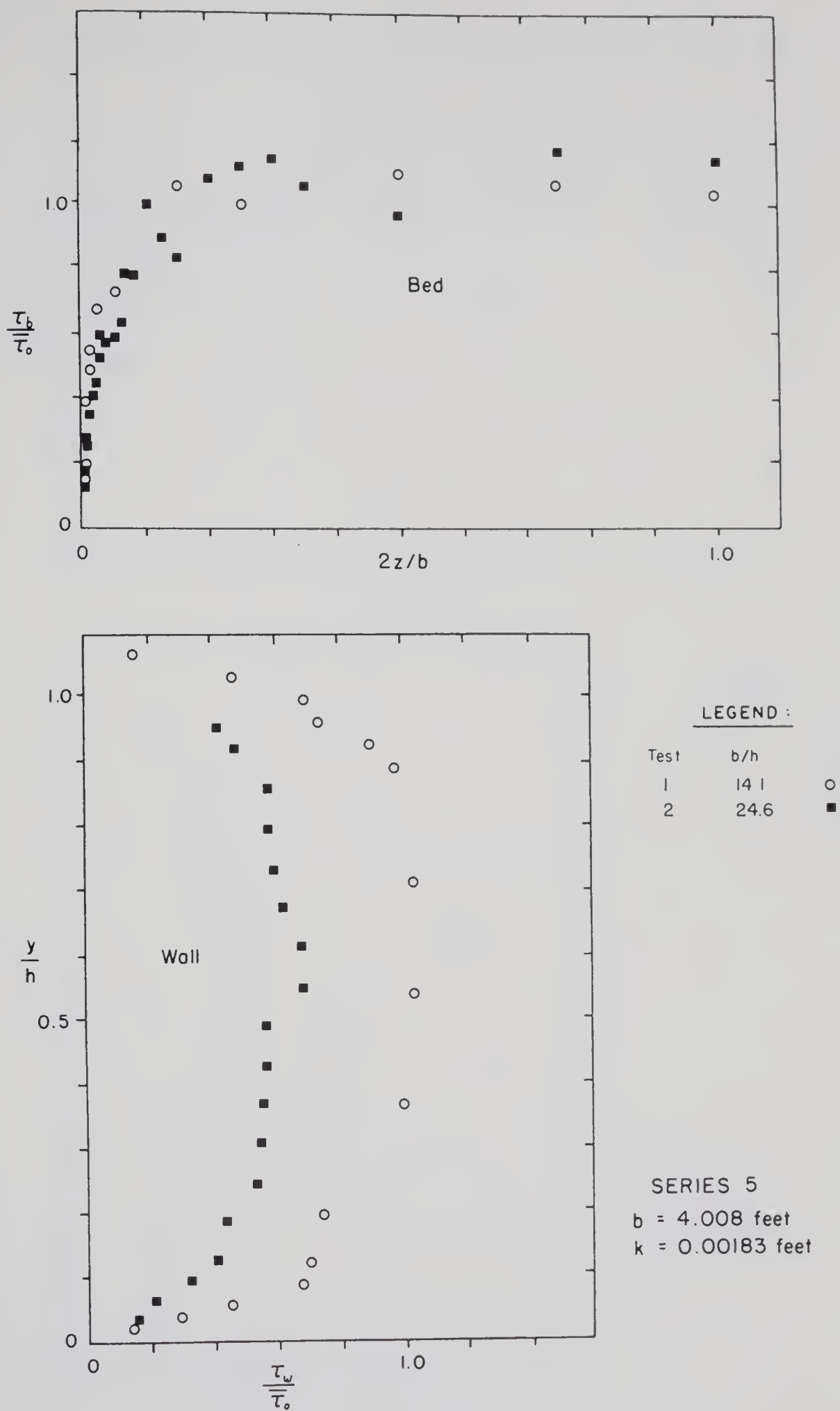


FIGURE F-8. SHEAR STRESS DIAGRAMS, SERIES 5



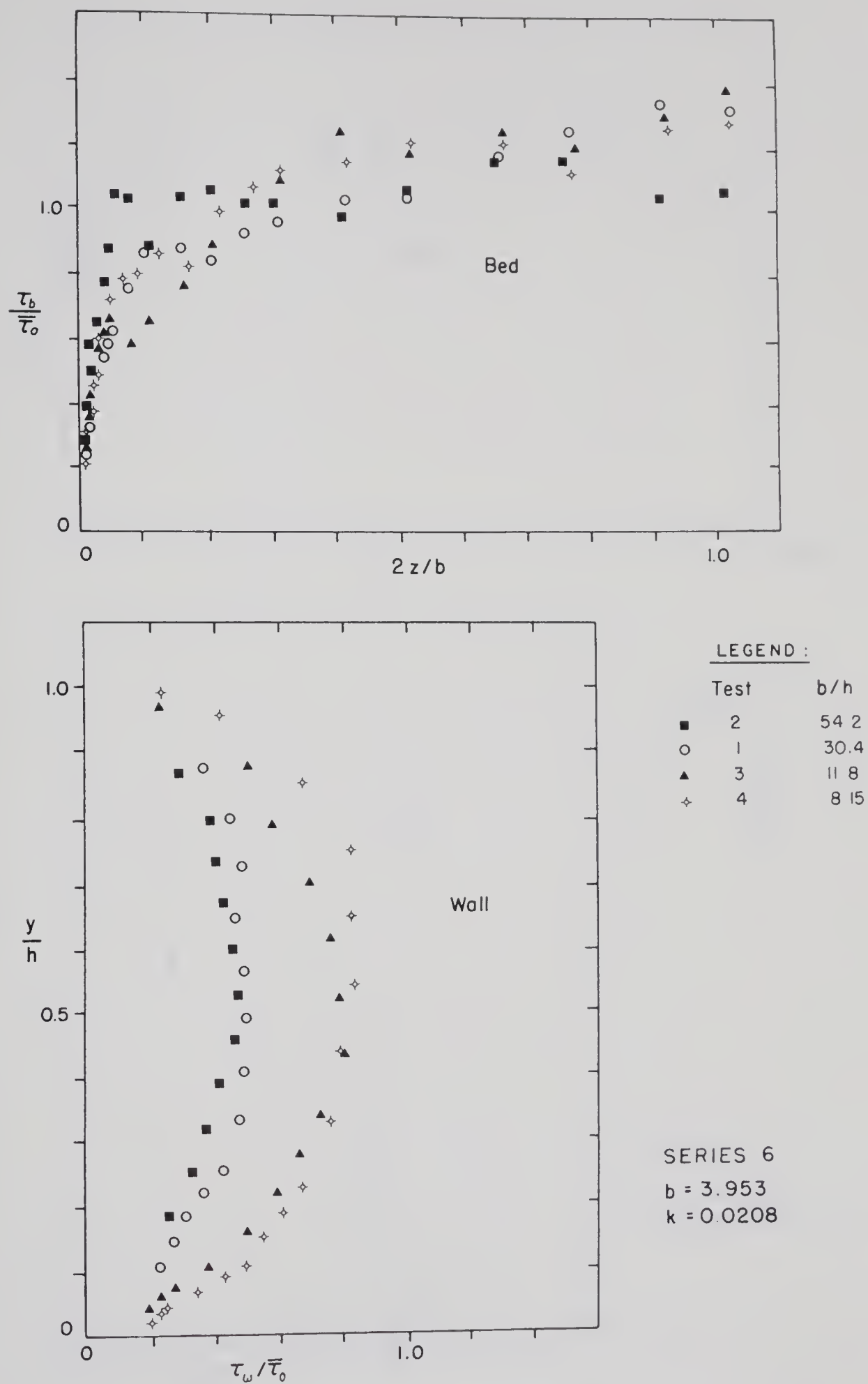


FIGURE F-9. SHEAR STRESS DIAGRAMS, SERIES 6



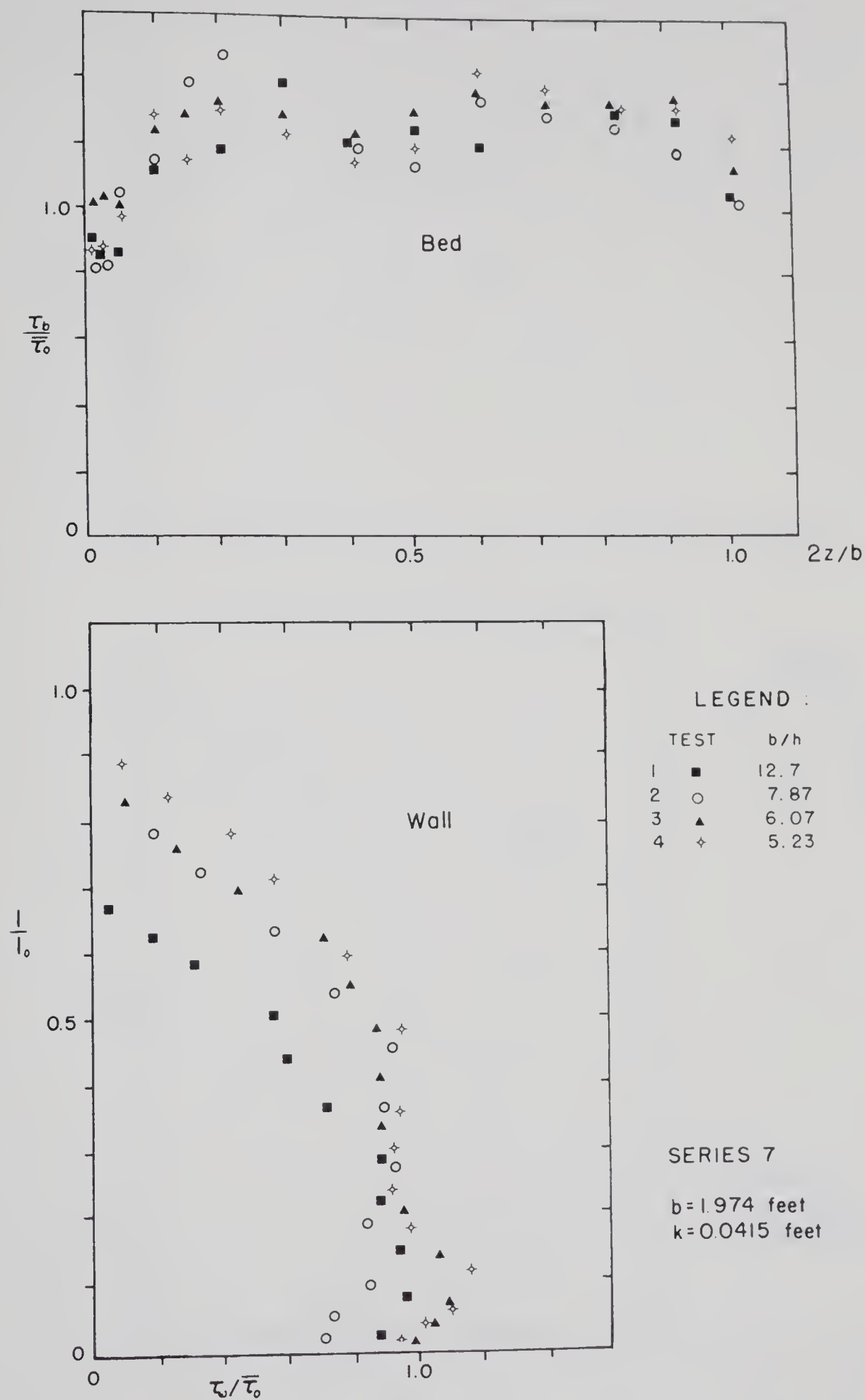


FIGURE F-10. SHEAR STRESS DIAGRAM, SERIES 7





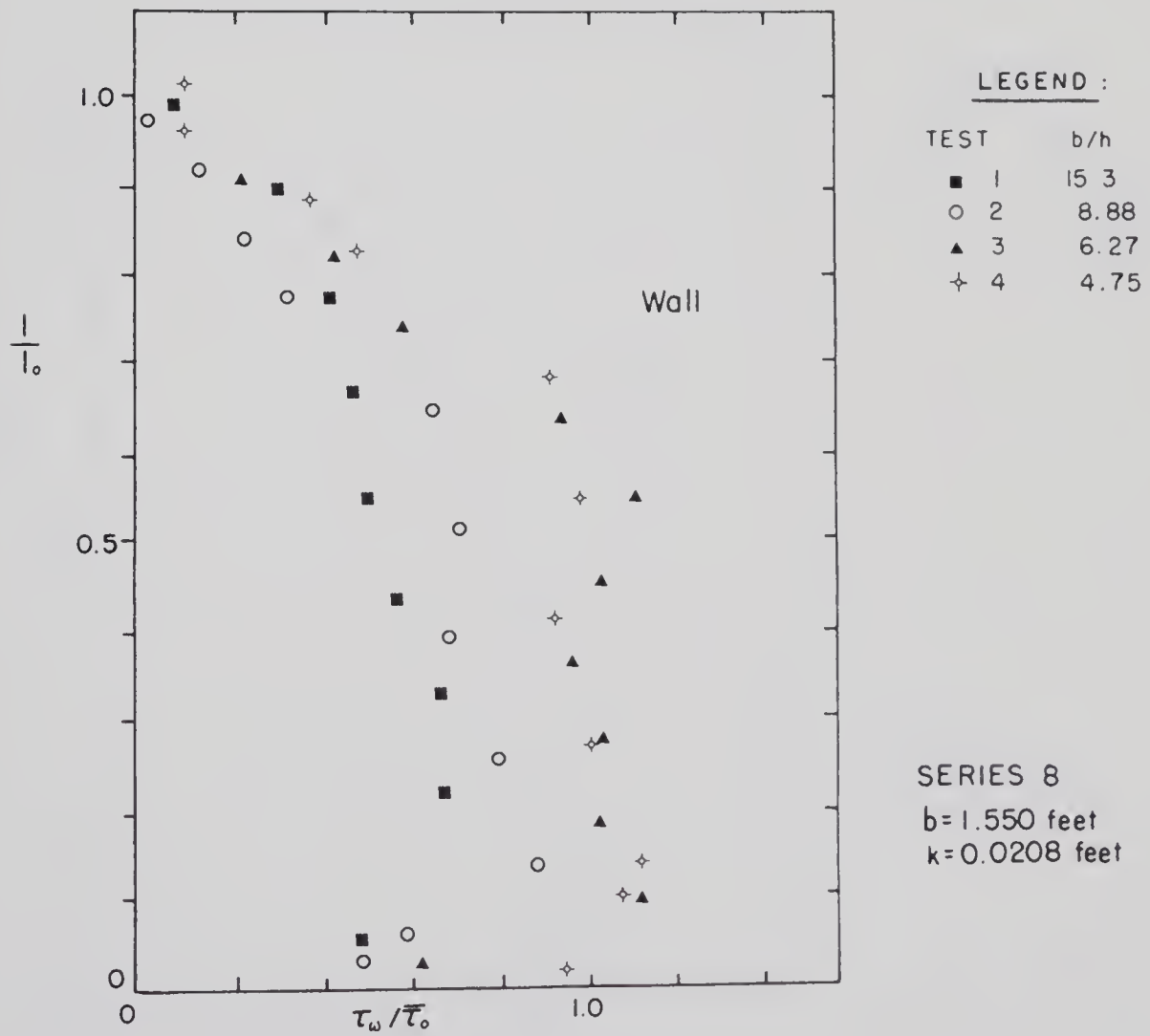
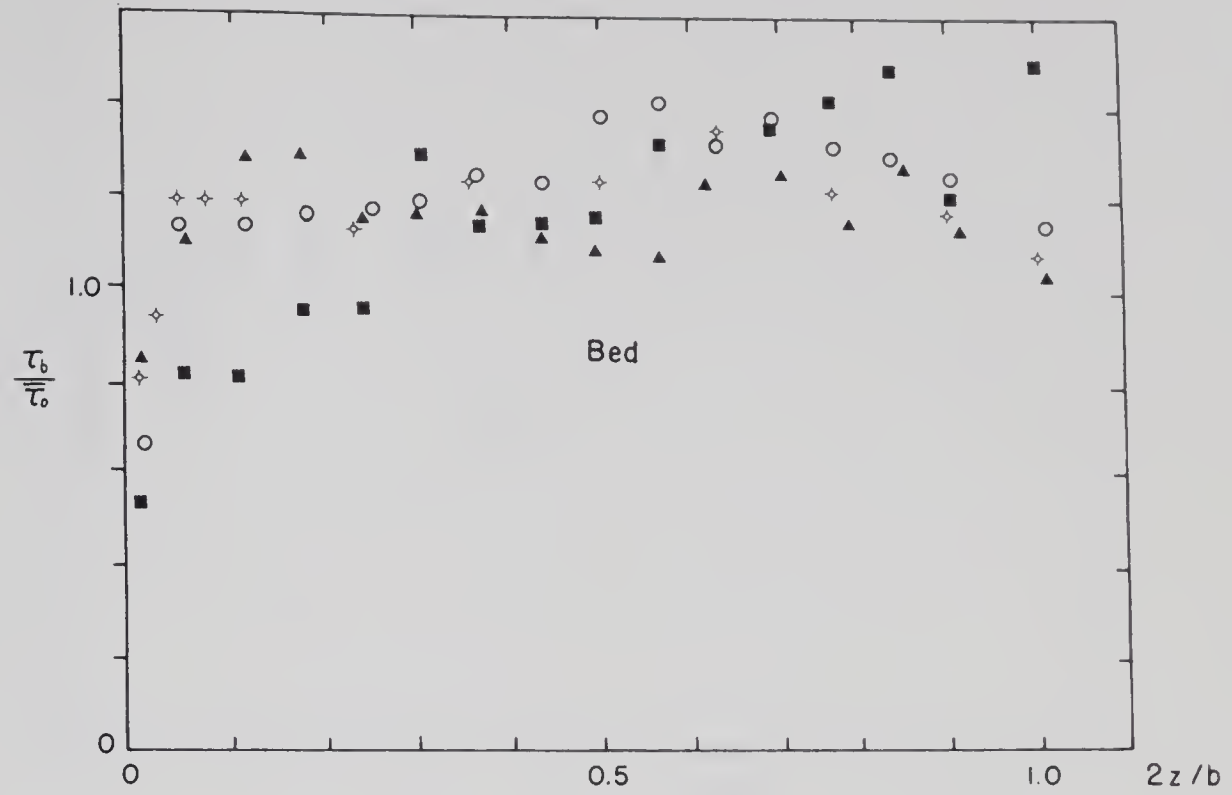


FIGURE F-11. SHEAR STRESS DIAGRAMS, SERIES 8



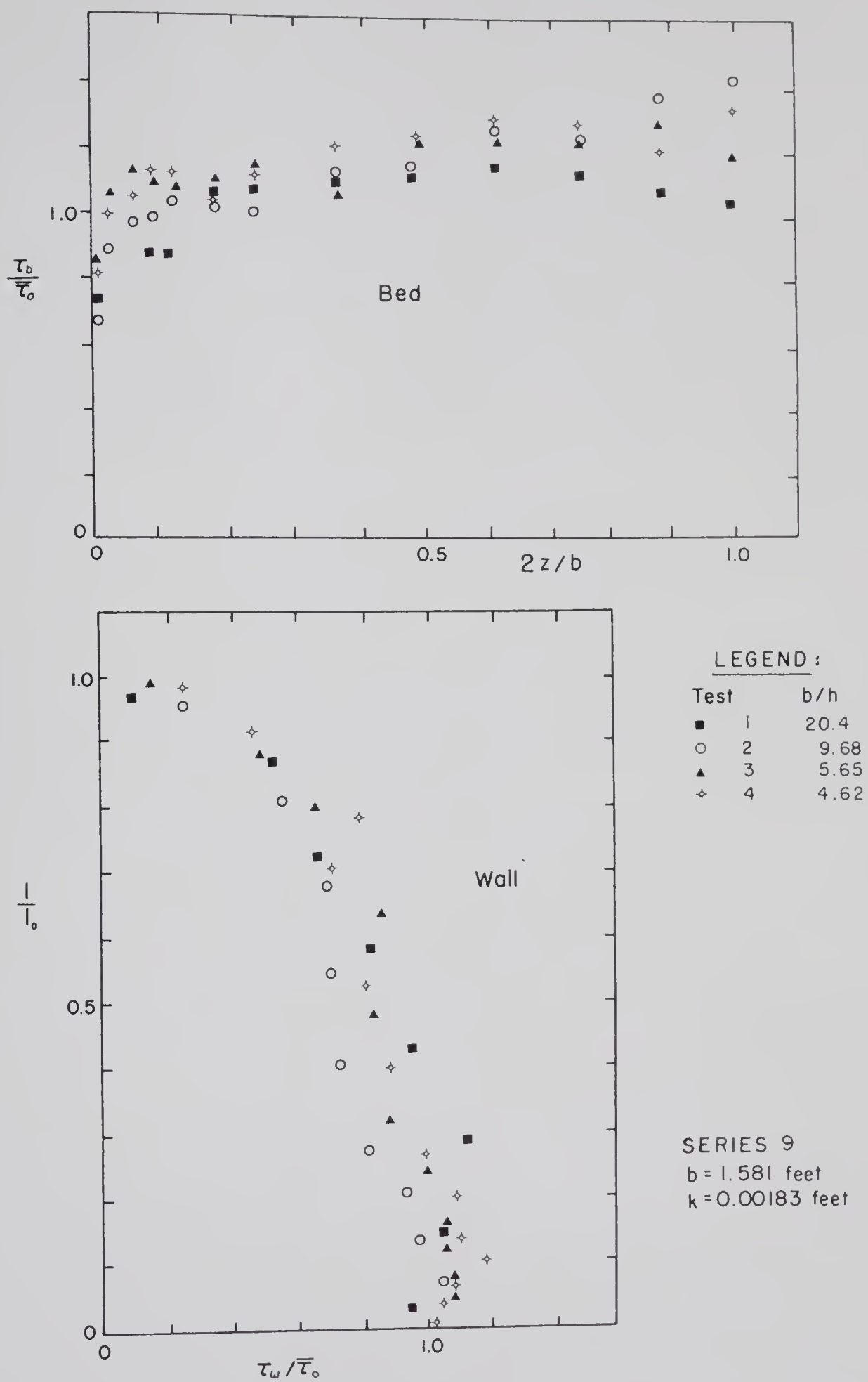


FIGURE F-12. SHEAR STRESS DIAGRAMS, SERIES 9















**B30020**